Loss-of-Coolant Accident Evaluation Model

December 2016

Revision 0

Docket: PROJ0769

NuScale Power, LLC

1100 NE Circle Blvd., Suite 200

Corvallis, Oregon 97330

www.nuscalepower.com

© Copyright 2016 by NuScale Power, LLC

© Copyright 2016 by NuScale Power, LLC

COPYRIGHT NOTICE

This report has been prepared by NuScale Power, LLC and bears a NuScale Power, LLC, copyright notice. No right to disclose, use, or copy any of the information in this report, other than by the U.S. Nuclear Regulatory Commission (NRC), is authorized without the express, written permission of NuScale Power, LLC.

The NRC is permitted to make the number of copies of the information contained in this report that is necessary for its internal use in connection with generic and plant-specific reviews and approvals, as well as the issuance, denial, amendment, transfer, renewal, modification, suspension, revocation, or violation of a license, permit, order, or regulation subject to the requirements of 10 CFR 2.390 regarding restrictions on public disclosure to the extent such information has been identified as proprietary by NuScale Power, LLC, copyright protection notwithstanding. Regarding nonproprietary versions of these reports, the NRC is permitted to make the number of copies necessary for public viewing in appropriate docket files in public document rooms in Washington, DC, and elsewhere as may be required by NRC regulations. Copies made by the NRC must include this copyright notice and contain the proprietary marking if the original was identified as proprietary.

Department of Energy Acknowledgement and Disclaimer

This material is based upon work supported by the Department of Energy under Award Number DE-NE0000633.

This report was prepared as an account of work sponsored by an agency of the United States Government. Neither the United States Government nor any agency thereof, nor any of their employees, makes any warranty, express or implied, or assumes any legal liability or responsibility for the accuracy, completeness, or usefulness of any information, apparatus, product, or process disclosed, or represents that its use would not infringe privately owned rights. Reference herein to any specific commercial product, process, or service by trade name, trademark, manufacturer, or otherwise does not necessarily constitute or imply its endorsement, recommendation, or favoring by the United States Government or any agency thereof. The views and opinions of authors expressed herein do not necessarily state or reflect those of the United States Government or any agency thereof.

© Copyright 2016 by NuScale Power, LLC

CONTENTS

Abstract **1**

Executive Summary **3**

1.0 Introduction **6**

1.1 Purpose 6

1.2 Scope 6

1.3 Abbreviations and Definitions 7

2.0 Background **10**

2.1 Loss-of-Coolant Accident Evaluation Model Roadmap 10

2.2 Regulatory Requirements 14

2.2.1 10 CFR 50.46 Loss-of-Coolant Accident Acceptance Criteria 14

2.2.2 10 CFR 50 Appendix K 15

2.2.3 Other Requirements 34

3.0 NuScale Power Module Description and Operations **35**

3.1 General Plant Design 35

3.2 Plant Operation 38

3.3 Safety-Related System Operation 39

3.3.1 Emergency Core Cooling System 40

3.3.2 Decay Heat Removal System 40

4.0 Phenomena Identification and Ranking **42**

4.1 Phenomena Identification and Ranking Process 42

4.2 Loss-of-Coolant Accident Scenarios 43

4.3 Figures of Merit 44

4.4 Definitions of Importance and Knowledge Level Rankings 44

4.5 Systems, Structures, and Components 45

4.6 High-Ranked Phenomena 45

4.6.1 Discussion of Phenomena Ranked High Importance 48

4.7 Phenomena Identification and Ranking Table Summary 52

5.0 Evaluation Model Description **53**

5.1 NRELAP5 Loss-of-Coolant Accident Model for the NuScale Power Module 53

5.1.1 General Model Nodalization 53

5.1.2 Reactor Coolant System 55

5.1.3 Helical Coil Steam Generators 60

© Copyright 2016 by NuScale Power, LLC

5.1.4 Containment Vessel and Reactor Pool 60
5.1.5 Chemical and Volume Control System 61
5.1.6 Secondary System 62
5.1.7 Decay Heat Removal System 62
5.1.8 NRELAP5 Modeling Options 62
5.1.9 Time Step Size Control 65
5.2 Analysis Setpoints and Trips 66
5.3 Initial Plant Conditions 69
5.4 Loss-of-Coolant Accident Break Spectrum 70
5.4.1 Break Location 70
5.4.2 Break Configuration and Size 71
5.4.3 Single Failures 72
5.4.4 Loss of Power 73
5.4.5 Decay Heat Removal System Availability 74
5.5 Sensitivity Studies 74
6.0 NRELAP5 Code Description 76
6.1 Quality Assurance Requirements 77
6.2 NRELAP5 Hydrodynamic Model 78
6.2.1 Field Equations 78
6.2.2 State Relations 81
6.2.3 Flow Regime Maps 82
6.2.4 Momentum Closure Relations 84
6.2.5 Heat Transfer 90
6.3 Heat Structure Models 92
6.4 Point Reactor Kinetics Model 94
6.5 Trips and Control System Models 96
6.6 Special Solution Techniques 97
6.6.1 Choked Flow 97
6.6.2 Abrupt Area Change 100
6.6.3 Counter Current Flow Limitation 101
6.7 Helical Coil Steam Generator Component 103
6.7.1 Helical Coil Tube Friction 104
6.7.2 Helical Coil Tube Heat Transfer 105

© Copyright 2016 by NuScale Power, LLC

6.8 Wall Condensation 107
6.9 Interfacial Drag in Large Diameter Pipes 110
6.10 Fission Decay Heat and Actinide Models 110
6.11 Critical Heat Flux Models 113
6.11.1 {{ }}2(a),(c) 114
6.11.2 Implementation of Critical Heat Flux correlations 116
6.11.3 {{ }}2(a),(c) 116
6.11.4 {{ }}2(a),(c) 120
7.0 NRELAP5 Assessments 122
7.1 Assessment Methodology 122
7.2 Legacy Test Data 124
7.2.1 Ferrell-McGee 124
7.2.2 GE Level Swell (1 ft) 128
7.2.3 GE Level Swell (4 ft) 136
7.2.4 KAIST 141
7.2.5 FRIGG 148
7.2.6 FLECHT-SEASET 155
7.2.7 SemiScale (S-NC-02 and S-NC-10) 164
7.2.8 Wilson Bubble Rise 169
7.2.9 Marviken Jet Impingement Test (JIT) 11 174
7.2.10 Bankoff Perforated Plate 177
7.2.11 Marviken Critical Flow Test 22 and 24 179
7.3 NuScale Stern Critical Heat Flux Tests 188
7.3.1 Facility Description 189
7.3.2 Experimental Procedure 190
7.3.3 Phenomenon Addressed 191
7.3.4 Parameter Ranges Assessed 191
7.3.5 Special Analysis Techniques 192
7.3.6 Assessment Results 192
7.4 NuScale SIET Steam Generator Tests 193
7.4.1 SIET Tests 194
7.4.2 SIET Fluid-Heated Test 203
7.4.2.2 Phenomenon Addressed 204

© Copyright 2016 by NuScale Power, LLC

7.5 NuScale NIST-1 Test Assessment Cases 213
7.5.1 Test Facility Description 214
7.5.2 Facility NRELAP5 Model 220
7.5.3 Facility Test Matrix 220
7.5.4 Separate Effect High Pressure Condensation Tests 221
7.5.5 Natural Circulation Test at Power 235
7.5.6 Chemical and Volume Control System Loss-of-Coolant Accident Integral Effects Tests 240
7.5.7 Pressurizer Spray Supply Line Loss-of-Coolant Accident Integral Effects Test 260
7.5.8 Spurious Reactor Vent Valve Opening Test 268
8.0 Assessment of Evaluation Model Adequacy 277
8.1 Adequacy Demonstration Overview 277
8.2 Evaluation of Models and Correlations (Bottom-Up Assessment) 277
8.2.1 Important Models and Correlations 279
8.2.2 {{ }}2(a),(c) 288
8.2.3 {{ }}2(a),(c) 293
8.2.4 {{ }}2(a),(c) 296
8.2.5 {{ }}2(a),(c) 299
8.2.6 {{ }}2(a),(c) 300
8.2.7 {{ }}2(a),(c) 305
8.2.8 {{ }}2(a),(c) 306
8.2.9 {{ }}2(a),(c) 309
8.2.10 Flashing 310
8.2.11 {{ }}2(a),(c) 311
8.2.12 {{ }}2(a),(c) 315
8.2.13 {{ }}2(a),(c) 316
8.2.14 {{ }}2(a),(c) 317
8.2.15 {{ }}2(a),(c) 321
8.2.16 {{ }}2(a),(c) 321
8.2.17 {{ }}2(a),(c) 322

© Copyright 2016 by NuScale Power, LLC

8.2.18 {{ }}2(a),(c) 325
8.2.19 {{ }}2(a),(c) 327
8.2.20 {{ }}2(a),(c) 330
8.2.21 {{ }}2(a),(c) 331
8.2.22 {{ }}2(a),(c) 333
8.3 Evaluation of Integral Performance (Top-Down Assessment) 334
8.3.1 Review of Code Governing Equations and Numerics 335
8.3.2 NuScale Facility Scaling 337
8.3.3 Assessment of NuScale Facility Integral Effects Test Data 350
8.3.4 Evaluation of NuScale Facility Distortions and NRELAP5 Scalability 351
8.4 Summary of Adequacy Findings 361
8.4.1 Findings from Bottom-Up Evaluation 361
8.4.2 Findings from Top-Down Evaluation 368
8.4.3 Summary of Biases and Uncertainties 372
9.0 Loss-of-Coolant Accident Calculations 373
9.1 Loss-of-Coolant Accident Progression in the NuScale Power Module 373
9.1.1 Liquid Space Break 373
9.1.2 Steam Space Break 381
9.2 Break Size 385
9.3 Decay Heat Removal System Availability 389
9.4 Power Availability 391
9.5 Single Failure 391
9.6 Sensitivity Studies 393
9.6.1 Model Nodalization 393
9.6.2 Time-Step Size Selection 397
9.6.3 Counter Current Flow Limitation Behavior on Pressurizer Baffle Plate 399
9.6.4 Emergency Core Cooling System Valve Parameters 400
9.6.5 Initial Reactor Pool Temperature 402
9.6.6 Core Power Distribution 404
9.7 Loss-of-Coolant Accident Calculation Summary 407
10.0 Conclusions 409
11.0 References 412

© Copyright 2016 by NuScale Power, LLC

Appendix A. Input for NuScale Power Module Loss-of-Coolant Accident Model 418

TABLES

Table 1-1. Abbreviations.....7
Table 1-2. Definitions.....9
Table 2-1. Evaluation model development and assessment process steps and the associated sections in this document.....12
Table 2-2. 10 CFR 50 Appendix K required and acceptable features compliance 18
Table 4-1. Importance rankings.....45
Table 4-2. Knowledge levels 45
Table 4-3. Systems, structures, and components 45
Table 4-4. High-ranked phenomena.....47
Table 5-1. Default junction options for the NRELAP5 loss-of-coolant accident model.....63
Table 5-2. Default volume options for the NRELAP5 loss-of-coolant accident model.....64
Table 5-3. NuScale Power Module safety-related system measurement parameters.....66
Table 5-4. Safety-related system actuation signals.....67
Table 5-5. Safety-related analysis signal delays 68
Table 5-6 Plant initial conditions.....70
Table 5-7. Summary of analyzed break sizes.....72
Table 5-8. NuScale Power Module valve fail-safe positions with loss of DC power.....74
Table 6-1. Dimensionless vapor velocity transition criteria for condensation 109
Table 6-2. Regime Nusselt relations for condensation.....109
Table 6-3. ANS 1973 11-group fission decay constants..... 111
Table 6-4. ANS-79 actinide model constants. 113
Table 6-5. Coefficient of revised pressure correction term in Equation 6-102..... 118
Table 6-6. {{ }}2(a),(c) critical heat flux correlation application range120
Table 7-1. NRELAP5 loss-of-coolant accident assessment matrix 123
Table 7-2. Summary of Ferrell-McGee experimental test data range.....126
Table 7-3. Summary of GE 1 ft. vessel level swell experiments.....130
Table 7-4. Range of KAIST test data.....144
Table 7-5. Range of Stern steady state critical heat flux data 192
Table 7-6. Facility high priority tests for NRELAP5 code validation.....221
Table 8-1. Dominant NRELAP5 models and correlations.....280
Table 8-2. NuScale Power Module range of process parameters.....283
Table 8-3. Range of NuScale Power Module geometric parameters 285
Table 8-4. Marviken range of parameters compared to the NuScale Power Module.....291
Table 8-5. Ferrell-McGee range of parameters compared to the NuScale Power Module.295
Table 8-6. Dimensions of NuScale Power Module, NIST-1 and Bankoff pressurizer plate 298
Table 8-7. Range of riser interphase friction - separate effects tests and NuScale Power Module 303
Table 8-8. Ranges of key parameters for core interphase friction - separate effects tests and plant 323
Table 8-9. Range of key parameters for core flow – separate effects tests and plant.....326
Table 8-10. Range of key parameters for core boiling - separate effects tests and plant 328
Table 8-11. Range of key parameters for subcooling boiling and separate effects tests and plant 333
Table 8-12. Scaling factors for NIST-1 facility 343
Table 8-13. Summary of bottom-up evaluation of NRELAP5 models and correlations.....362

© Copyright 2016 by NuScale Power, LLC

Table 8-14. Applicability summary for high-ranked phenomena 369
Table 9-1. Event table for 100 percent reactor coolant system injection line break 375
Table 9-2. Event table for {{ }}2(a),(c) 382
Table 9-3. Number of volumes in reactor pressure vessel and containment vessel nodalization 394
Table A-1. Core input parameters 419
Table A-2. Initial conditions for loss-of-coolant accident analysis 421
Table A-3. Safety signal actuation setpoints and delays 422
Table A-4. Break spectrum parameters 424

FIGURES

Figure 2-1. Evaluation model development and assessment process 11
Figure 3-1. A single NuScale Power Module during normal operation 36
Figure 3-2. Schematic of NuScale Power Module decay heat removal system and emergency core cooling system during operation 38
Figure 5-1. Noding diagram of NRELAP5 loss-of-coolant accident input model for NuScale Power Module 55
Figure 6-1. Schematic of vertical flow-regime map indicating transitions 83
Figure 6-2. NRELAP5 boiling and condensing curves 92
Figure 6-3. NRELAP5 ANS 1973 implemented fission decay heat curve 112
Figure 6-4. NRELAP5 ANS-79 implemented actinide heat curve 113
Figure 6-5. {{ }}2(a),(c) 115
Figure 6-6. {{ }}2(a),(c) 119
Figure 7-1. Schematic of the Ferrell-McGee test section 125
Figure 7-2. Predicted versus measured pressure drop for selected contraction tests 128
Figure 7-3. Schematic of the GE 1 ft. blowdown vessel 129
Figure 7-4. GE level swell 1 ft. vessel pressure versus time 132
Figure 7-5. GE level swell 1 ft. vessel void fraction versus elevation at 10 seconds 133
Figure 7-6. GE level swell 1 ft. vessel void fraction versus elevation at 40 seconds 134
Figure 7-7. GE level swell 1 ft. vessel void fraction versus elevation at 100 seconds 135
Figure 7-8. GE level swell 1 ft. vessel void fraction versus elevation at 160 seconds 136
Figure 7-9. Schematic of the GE 4 ft. blowdown vessel 137
Figure 7-10. GE level swell 4-ft vessel pressure versus time 139
Figure 7-11. GE level swell 4-ft vessel void fraction versus elevation at 5 seconds 139
Figure 7-12. GE level swell 4-ft vessel void fraction versus elevation at 10 seconds 140
Figure 7-13. GE level swell 4-ft vessel void fraction versus elevation at 20 seconds 140
Figure 7-14. Schematic of KAIST test facility 142
Figure 7-15. Schematic of the KAIST test section 143
Figure 7-16. Measured versus predicted heat transfer coefficient 145
Figure 7-17. KAIST and NRELAP5 axial heat transfer coefficient 146
Figure 7-18. KAIST and NRELAP5 axial inner wall temperature 147
Figure 7-19. KAIST and NRELAP5 axial liquid mass flow rate 148
Figure 7-20. FRIGG-4 experimental loop 150
Figure 7-21. FRIGG-4 36 rod test section 151
Figure 7-22. FRIGG-4 zones for evaluation of radial void distribution 152
Figure 7-23. FRIGG mean void data of NRELAP5 versus Test 613123 data 153
Figure 7-24. FRIGG mean void data of NRELAP5 versus Test 613130 data 154
Figure 7-25. FRIGG mean void data of NRELAP5 versus Test 613010 data 154

© Copyright 2016 by NuScale Power, LLC

Figure 7-26. FRIGG mean void data of NRELAP5 versus Test 613118 data 155
Figure 7-27. FLECHT-SEASET experimental facility 156
Figure 7-28. FLECHT-SEASET level 1 void fraction versus time – Test 35557 157
Figure 7-29. FLECHT-SEASET level 2 void fraction versus time – Test 35557 158
Figure 7-30. FLECHT-SEASET level 3 void fraction versus time – Test 35557 159
Figure 7-31. FLECHT-SEASET level 4 void fraction versus time – Test 35557 160
Figure 7-32. FLECHT-SEASET level 1 collapsed water level versus time – Test 35557 161
Figure 7-33. FLECHT-SEASET level 2 collapsed water level versus time – Test 35557 162
Figure 7-34. FLECHT-SEASET level 3 collapsed water level versus time – Test 35557 163
Figure 7-35. FLECHT-SEASET level 4 collapsed water level versus time – Test 35557 164
Figure 7-36. Semiscale Mod-2A single (intact) loop test facility configuration 165
Figure 7-37. S-NC-2 30 kW average mass flow rate versus percent inventory 167
Figure 7-38. S-NC-2 60 kW average mass flow rate versus percent inventory 168
Figure 7-39. S-NC-10 100 kW average mass flow rate versus percent inventory 169
Figure 7-40. Schematic of Wilson bubble rise test facility 170
Figure 7-41. NRELAP5 and Wilson void fraction versus superficial velocity at 600 psig (4.14 MPa) 171
Figure 7-42. NRELAP5 and Wilson void fraction versus superficial velocity 1,000 psig (6.89 MPa) 172
Figure 7-43. NRELAP5 and Wilson void fraction versus superficial velocity 2,000 psig (13.8 MPa) 173
Figure 7-44. Predicted versus measured area averaged void fraction (all cases) 174
Figure 7-45. Marviken jet impingement test facility 175
Figure 7-46. Marviken jet impingement test 11 flowrate 176
Figure 7-47. Marviken jet impingement test 11 density 177
Figure 7-48. Schematic of Bankoff counter current flow apparatus (from Reference 68) 178
Figure 7-49. Superficial vapor velocity versus superficial liquid velocity 179
Figure 7-50. Schematic of the Marviken pressure vessel 180
Figure 7-51. Discharge pipe dimensions and instrument locations 181
Figure 7-52. Measured versus calculated mass flow rate for Marviken critical flow test 22 184
Figure 7-53. Marviken critical flow test 22 comparison to calculated mixture density 185
Figure 7-54. Measured versus calculated mass flow rate for Marviken critical flow test 24 187
Figure 7-55. Marviken critical flow test 24 mixture density and calculated mixture density 188
Figure 7-56. U1 & C1 (left) versus U2 (right) radial layout 189
Figure 7-57. Stern test section axial layout 190
Figure 7-58. Predicted versus measured Stern power 193
Figure 7-59. SIET electrically-heated test instrumentation diagram 195
Figure 7-60. Time averaged wall temperature profile for coil 2 test TD0015 197
Figure 7-61. Time averaged wall temperature profile for coil 2 test TD0003 198
Figure 7-62. SIET electrically-heated test differential pressure for all coil 1 diabatic tests 199
Figure 7-63. SIET electrically-heated test differential pressure for all coil 2 diabatic tests 200
Figure 7-64. SIET electrically-heated test differential pressure for all coil 3 diabatic tests 201
Figure 7-65. SIET electrically-heated test fluid temperatures for all coil 1 diabatic tests 202
Figure 7-66. SIET electrically-heated test wall temperature for all coil 1 diabatic tests 203
Figure 7-67. SIET fluid-heated test adiabatic primary differential pressure 206
Figure 7-68. SIET fluid-heated test diabatic test primary differential pressure 207
Figure 7-69. SIET fluid-heated test diabatic test primary temperature 208
Figure 7-70. Comparison of wall temperatures in TD0001 (Case 1) 209
Figure 7-71. Comparison of wall temperatures in TD0007 (Case 1) 210

© Copyright 2016 by NuScale Power, LLC

Figure 7-72. Comparison of wall temperatures in TD0002 (Case 1) 211
Figure 7-73. Comparison of secondary side fluid temperatures Row 3 (Case 1) 212
Figure 7-74. Comparison of secondary side fluid temperatures in TD0002 (Case 1) 213
Figure 7-75. Schematic of NuScale integral test facility and NRELAP5 nodalization 215
Figure 7-76. HP-02 Run 1 containment vessel pressure response 224
Figure 7-77. HP-02 Run 1 containment vessel collapsed level response 225
Figure 7-78. HP-02 Run 1 upper containment vessel fluid temperature response (in vapor space) 226
Figure 7-79. HP-02 Run 1 upper cooling pool vessel temperature response 227
Figure 7-80. HP-02 Run 2 containment vessel pressure response 228
Figure 7-81. HP-02 Run 2 containment vessel collapsed level response 229
Figure 7-82. HP-02 Run 2 upper containment vessel fluid temperature response (in vapor space) 230
Figure 7-83. HP-02 Run 2 upper cooling pool temperature response 231
Figure 7-84. HP-02 Run 3 containment vessel pressure response 232
Figure 7-85. HP-02 Run 3 containment vessel collapsed level response 233
Figure 7-86. HP-02 Run 3 upper containment vessel fluid temperature response (in vapor space) 234
Figure 7-87. HP-02 Run 3 upper cooling pool temperature response 235
Figure 7-88. HP-05 NIST-1 averaged mass flowrate and NRELAP5 results 238
Figure 7-89. HP-05 NIST-1 averaged core inlet temperature and NRELAP5 results 239
Figure 7-90. HP-05 NIST-1 averaged core outlet temperature and NRELAP5 results 240
Figure 7-91. NIST-1 HP-06 NRELAP5 chemical and volume control system discharge line break mass flow rate 243
Figure 7-92. NIST-1 HP-06 break orifice differential pressure 244
Figure 7-93. NIST-1 HP-06 primary mass flow rate 245
Figure 7-94. NIST-1 HP-06 pressurizer level comparison 246
Figure 7-95. NIST-1 HP-06 reactor pressure vessel level comparison 247
Figure 7-96. NIST-1 HP-06 containment vessel level comparison 248
Figure 7-97. NIST-1 HP-06 containment vessel pressure comparison 249
Figure 7-98. NIST-1 HP-06 containment vessel pressure comparison 250
Figure 7-99. NIST-1 HP-06 primary pressure comparison 251
Figure 7-100. Comparison of core power in HP-06 and HP-06b tests with the NuScale Power Module decay power after reactor trip (scaled) 252
Figure 7-101. NIST-1 HP-06b primary pressure comparison 253
Figure 7-102. NIST-1 HP-06b containment vessel pressure comparison 254
Figure 7-103. NIST-1 HP-06b reactor pressure vessel level comparison 255
Figure 7-104. NIST-1 HP-06b containment vessel level comparison 256
Figure 7-105. Comparison of NIST-1 HP-06 and HP-06b reactor pressure vessel pressure 257
Figure 7-106. Comparison of NIST-1 HP-06 and HP-06b containment vessel pressure 258
Figure 7-107. Comparison of NIST-1 HP-06 and HP-06b reactor pressure vessel level 259
Figure 7-108. Comparison of NIST-1 HP-06 and HP-06b containment vessel level 260
Figure 7-109. Comparison of core power in HP-07 with the NuScale Power Module power (fission and decay) after reactor trip (scaled) 262
Figure 7-110. NIST-1 HP-07 pressurizer spray supply line break discharge mass flow rate 263
Figure 7-111. NIST-1 HP-07 primary mass flow rate 264
Figure 7-112. NIST-1 HP-07 reactor pressure vessel level response comparison with data 265
Figure 7-113. NIST-1 HP-07 containment vessel level response 266
Figure 7-114. NIST-1 HP-07 containment vessel pressure comparison 267

© Copyright 2016 by NuScale Power, LLC

Figure 7-115. NIST-1 HP-07 primary pressure comparison....268
Figure 7-116. Comparison of HP-09 core power with the scaled NuScale Power Module fission and decay power....270
Figure 7-117. NIST-1 HP-09 valve mass flow rate....271
Figure 7-118. NIST-1 HP-09 pressurizer pressure comparison....272
Figure 7-119. NIST-1 HP-09 pressurizer pressure comparison....272
Figure 7-120. NIST-1 HP-09 containment vessel pressure comparison....273
Figure 7-121. NIST-1 HP-09 containment vessel pressure comparison....274
Figure 7-122. NIST-1 HP-09 pressurizer level comparison....275
Figure 7-123. NIST-1 HP-09 reactor pressure vessel level comparison....275
Figure 7-124. NIST-1 HP-09 reactor pressure vessel level comparison....276
Figure 8-1. Transient void fraction in node 5 for the GE 4-ft level swell test....313
Figure 8-2. Transient void fraction in node 4 for the GE 4-ft level swell test....313
Figure 8-3. Transient void fraction in node 6 for the GE 1-ft level swell test....314
Figure 8-4. Transient void fraction in node 5 for the GE 1-ft level swell test....314
Figure 8-5. Hot leg riser flow for NIST-1 chemical and volume control system discharge line break integral effects test HP-06....320
Figure 8-6. Hot leg riser flow for NIST-1 pressurizer spray supply line break integral effects test HP-07....320
Figure 8-7. General design framework for the NuScale Integral System Test facility....338
Figure 8-8. Flow diagram for the hierarchical, two-tiered scaling analysis (NUREG/CR-5809)....340
Figure 8-9. NuScale system breakdown into hierarchical levels and primary operational modes to be scaled....341
Figure 8-10. Scaling analysis flow diagram for single-phase primary loop natural circulation....344
Figure 8-11. Scaling analysis flow diagram for reactor coolant system depressurization....345
Figure 8-12. Scaling analysis flow diagram for containment pressurization....346
Figure 8-13. Scaling analysis flow diagram for long-term recirculation cooling mode....347
Figure 8-14. Scaling analysis flow diagram for Reactor Building pool heat-up....348
Figure 8-15. Comparison of HP-05 feedwater flow to test data....353
Figure 8-16. Comparison of HP-05 reactor pressure vessel flow to test data....354
Figure 8-17. Comparison of HP-05 core exit subcooling to test data....355
Figure 8-18. Comparison of HP-05 core inlet temperature to test data....355
Figure 8-19. Comparison of HP-06 primary pressure to test data....358
Figure 8-20. Comparison of HP-06 containment vessel pressure to test data....359
Figure 8-21. Comparison to HP-06 primary liquid level to test data....360
Figure 8-22. Comparison of HP-06 containment vessel liquid level to test data....361
Figure 9-1. Break and emergency core cooling system valve flows to the containment vessel for injection line break....376
Figure 9-2. Integrated energy for injection line break....376
Figure 9-3. Reactor pressure vessel and containment vessel pressure for injection line break....377
Figure 9-4. Comparison of collapsed liquid levels in reactor pressure vessel, containment vessel, and pressurizer....378
Figure 9-5. Core flow for injection line break....379
Figure 9-6. Core minimum critical heat flux ratio during injection line break....380
Figure 9-7. Peak cladding and fuel centerline temperature during injection line break....380
Figure 9-8. Comparison of pressure for injection line and high point vent line breaks....383

© Copyright 2016 by NuScale Power, LLC

Figure 9-9. Break and emergency core cooling system valve flow during high point vent line break 384
Figure 9-10. Collapsed liquid levels during high point vent line break 384
Figure 9-11. Minimum critical heat flux ratio during high point vent line break 385
Figure 9-12. Peak containment vessel pressure and collapsed level above top of active fuel for different reactor coolant system injection line break sizes 386
Figure 9-13. Peak containment vessel pressure and collapsed level above top of active fuel for different reactor coolant system discharge line break sizes 387
Figure 9-14. Peak containment vessel pressure and collapsed level above top of active fuel for different high point vent line break sizes 387
Figure 9-15. Peak containment vessel pressure and minimum collapsed liquid level as a function of break location and size 388
Figure 9-16. Minimum critical heat flux ratio for injection line (left) and high point vent line (right) breaks 389
Figure 9-17. Reactor coolant system injection line pressure without decay heat removal system (left) and with decay heat removal system (right) 390
Figure 9-18. Collapsed liquid level for reactor coolant system injection line break without decay heat removal system (left) and with decay heat removal system (right) 390
Figure 9-19. Effect of power availability on peak containment vessel pressure for injection line (left) and high point vent (right) line breaks 391
Figure 9-20. The effect of single failure on peak containment vessel pressure for reactor coolant system injection line (left) and high point vent (right) line breaks 392
Figure 9-21. The effect of single failure on minimum collapsed level for reactor coolant system injection line (left) and high point vent line (right) breaks 393
Figure 9-22. Reactor pressure vessel and containment vessel pressure (left) and collapsed level above top of active fuel (right) for reactor coolant system injection line break 395
Figure 9-23. Reactor pressure vessel and containment vessel pressure (left) and collapsed level above top of active fuel (right) for 10 percent reactor coolant system injection line break 395
Figure 9-24. Reactor pressure vessel and containment vessel pressure (left) and collapsed level above top of active fuel (right) for high point vent line break 396
Figure 9-25. Hot channel core flow (left) and core critical heat flux ratio (right) during 100 percent reactor coolant system injection line break 397
Figure 9-26. Time-step size sensitivity on reactor and containment vessel pressures and reactor pressure vessel collapsed liquid level for 100 percent reactor coolant system injection line break. 398
Figure 9-27. Time-step size sensitivity on hot assembly flow and minimum critical heat flux ratio for 100 percent reactor coolant system injection line break 398
Figure 9-28. Time-step size sensitivity on reactor and containment vessel pressures and reactor pressure vessel collapsed liquid level for high point vent line break 399
Figure 9-29. Time-step size sensitivity on hot assembly flow and minimum critical heat flux ratio for high point vent break 399
Figure 9-30. Effect of counter current flow limitation line slope on levels for high point vent line break 400
Figure 9-31. Effect of inadvertent actuation block release pressure on peak containment vessel pressure and minimum collapsed liquid level above top of active fuel as a function of break size for reactor coolant system injection line break 401

© Copyright 2016 by NuScale Power, LLC

Figure 9-32. Effect of reactor recirculation valve size on peak containment vessel pressure and minimum collapsed liquid level for reactor coolant system injection line break 402
Figure 9-33. Effect of reactor vent valve size on peak containment vessel pressure and minimum collapsed liquid level for reactor coolant system injection line break 402
Figure 9-34. Effect of initial reactor pool temperature on peak containment vessel pressure and minimum collapsed liquid level above top of active fuel for reactor coolant system injection line break 403
Figure 9-35. Containment vessel to pool energy transfer at different initial pool temperatures for 100 percent (left) and 10 percent (right) reactor coolant system injection line break 404
Figure 9-36. Generic normalized axial power shapes 405
Figure 9-37. Effect of axial power shape on reactor pressure vessel and containment pressures and collapsed liquid level above top of active fuel for reactor coolant system injection line break 406
Figure 9-38. Effect of axial power shape on peak containment vessel pressure and minimum collapsed liquid level above top of active fuel for reactor coolant system injection line break 406
Figure 9-39. Effect of axial power shape on hot assembly flow and minimum critical heat flux ratio during reactor coolant system injection line break 407

© Copyright 2016 by NuScale Power, LLC

Abstract

NuScale Power, LLC (NuScale) has developed a small modular reactor (SMR) that supports operation of up to 12 NuScale Power Modules (NPM) at a specific site. Each NPM is an advanced, light-water, integrated pressurized water reactor (PWR) using natural circulation for primary coolant flow. Each NPM has an independent nuclear steam supply system (NSSS), a standard steam power conversion system, and a compact steel containment vessel (CNV). In the NPM design, all primary components are integral to the reactor pressure vessel (RPV), which eliminates most of the reactor piping found on conventional PWRs, thereby reducing the possibility of a pipe rupture that would result in a loss-of-coolant accident (LOCA).

NuScale is requesting Nuclear Regulatory Commission (NRC) review and approval to use the LOCA evaluation model (EM) described in this report for analyses of design-basis LOCA events in the NPM. The NuScale LOCA EM has been developed using the evaluation model development and assessment process (EMDAP) of “Transient and Accident Analysis Methods,” Regulatory Guide (RG) 1.203 (Reference 1), and it adheres to the applicable requirements of “ECCS Evaluation Models,” 10 CFR 50 Appendix K (Reference 2), and “Acceptance Criteria for Emergency Core Cooling Systems for Light-Water Nuclear Power Reactors,” 10 CFR 50.46 (Reference 3). This topical report is not intended to provide final design values or results; rather, example values for the various evaluations are provided for illustrative purposes in order to aid the reader’s understanding of the context of the application of the NuScale LOCA EM.

The LOCA EM uses the proprietary NRELAP5 systems analysis computer code as the computational engine, derived from the Idaho National Laboratory (INL) RELAP5-3D© computer code. The models and correlations used by NRELAP5 were reviewed and, where appropriate, modified for use within the NuScale LOCA EM.

Validation and verification of the LOCA EM and NRELAP5 code has been performed in accordance with the EMDAP. A phenomena identification and ranking table (PIRT), which identifies the important phenomena and processes occurring in the NPM during a LOCA, was developed by gathering and ranking expert evaluations of phenomena that could occur in the NPM during a LOCA. Twenty-one (21) phenomena were identified as important to capture in the NuScale LOCA EM.

Extensive NRELAP5 code validation was performed to ensure that the LOCA EM is applicable for important phenomena and processes over the range encountered in the NPM LOCA. The validation suite includes many legacy separate effects tests (SETs) and integral effects tests (IETs), as well as many SETs and IETs developed and run specifically for the NPM application.

The EMDAP requires an applicability demonstration of the NRELAP5 code and tests. A unique aspect of the demonstration provided for the NPM is the comparison of NRELAP5 simulations of LOCA to NuScale Integral System Test Facility (NIST-1) test data and NRELAP5 simulation of the same LOCA in the NPM. The reasonable-to-excellent agreement obtained by these comparisons establishes the applicability of NRELAP5 to accurately predict LOCA phenomena at both the NIST-1 and NPM scales.

This topical report provides an example application of the LOCA EM in order to aid the reader’s understanding of the context of the application of the NuScale LOCA EM. These calculations are

© Copyright 2016 by NuScale Power, LLC

presented for break spectra that cover a range of break locations, break sizes, single failures, equipment unavailability, and initial and boundary conditions.

© Copyright 2016 by NuScale Power, LLC

Executive Summary

NuScale Power, LLC (NuScale) has developed a small modular reactor that supports operation of up to 12 NuScale Power Modules (NPMs) at a specific site. Each NPM is an advanced, light-water, integral pressurized water reactor (PWR) that uses a high-pressure containment vessel (CNV) immersed in a reactor pool coupled with simple, redundant, passive safety-related systems. The design ensures safe plant shutdown and cooldown in the event of a loss-of-coolant accident (LOCA). Each NPM has an independent nuclear steam supply system (NSSS) that includes a nuclear core, helical-coil steam generator (SG), integral pressurizer, and a compact, high-pressure steel CNV that contains the NSSS. The secondary system includes a traditional steam-power conversion system including a steam turbine generator, condenser, and feedwater system. The integral PWR design eliminates most of the reactor piping found on conventional PWRs, thereby reducing the possibility of a pipe rupture that would result in a LOCA. Piping in the NPM containment that potentially can break is limited to the reactor coolant system (RCS) injection line, RCS discharge line, pressurizer spray supply line, and pressurizer high point vent line. The RCS injection line is supplied by the chemical and volume control system (CVCS) and the discharge line returns to the CVCS. The NPM is designed to reduce the consequences of design basis LOCAs by using redundant, simplified, passive safety-related systems that eliminate the need for emergency core cooling system (ECCS) pumps, accumulators, and water storage tanks found on conventional PWRs. During operation, flow through the reactor is driven by natural circulation resulting from the thermal driving head produced by the temperature difference between the core and the heat sink afforded by the SG. Natural circulation flow increases reliability by eliminating primary coolant pumps that can fail or lock up.

The purpose of this topical report is to present the NuScale evaluation model (EM) used to evaluate ECCS performance in the NPM for design basis LOCAs. This LOCA EM was developed following the guidelines in the evaluation model development and assessment process (EMDAP) of “Transient and Accident Analysis Methods,” Regulatory Guide (RG) 1.203 (Reference1), and adheres to the applicable requirements of “ECCS Evaluation Models,” 10 CFR 50 Appendix K (Reference 2) and “Acceptance Criteria for Emergency Core Cooling Systems for Light-Water Nuclear Power Reactors,” 10 CFR 50.46 (Reference 3). Multiple layers of conservatism are incorporated in the NuScale LOCA EM to ensure that a conservative analysis result is obtained. These conservatisms stem from application of the modeling requirements of 10 CFR 50 Appendix K and through a series of conservative modeling features.

The LOCA EM uses the proprietary NRELAP5 systems analysis computer code as the computational engine, derived from the Idaho National Laboratory (INL) RELAP5-3D© computer code. RELAP5-3D© was procured and as part of the procurement process commercial grade dedication was performed by NuScale to establish the baseline NRELAP5 code for development. Subsequently, features were added and changes made to NRELAP5 to address the unique aspects of the NPM design and licensing methodology. NRELAP5 includes all of the necessary models for characterization of the NPM hydrodynamics, heat transfer between structures and fluids, modeling of fuel, reactor kinetics models, and control systems. The models and correlations used by NRELAP5 have been reviewed and, where appropriate, modified for use within the NuScale LOCA methodology. Code changes for the NuScale application include new helical coil SG heat transfer and pressure drop models, core critical heat flux (CHF) models, and interfacial drag models for large-diameter pipes. The fuel CHF models were selected based on full-scale fuel bundle performance tests.

© Copyright 2016 by NuScale Power, LLC

Validation and verification of the EM and NRELAP5 code were conducted in accordance with the EMDAP process. A phenomena identification and ranking table (PIRT), which identifies the important phenomena and processes occurring in the NPM during a LOCA event, was developed by gathering and ranking expert evaluations of phenomena that could occur in the NPM during a LOCA. Phenomena and process ranking was performed in relation to specified figures of merit (FOMs) as described by RG 1.203. The PIRT also established a knowledge ranking for each phenomenon identified. Using these FOMs, 21 phenomena were identified as important to capture in the NuScale LOCA EM.

Extensive NRELAP5 code validation was performed to ensure that the LOCA EM is applicable for all important phenomena and processes over the range encountered in the NPM LOCA. The validation suite includes many legacy separate effects tests (SETs) and integral effects tests (IETs), as well as many SETs and IETs developed and run specifically for the NPM application. The SETs run for the NPM application were performed at the Società Informazioni Esperienze Termoidrauliche (SIET) facility on a model helical coil SG, and at the Stern facility to obtain CHF data on a full-scale rod bundle test section. The IETs were performed at the Oregon State University NuScale Integral System Test -1 (NIST-1) facility, a scaled representation of the complete NPM primary and secondary systems, as well as the reactor pool.

The EMDAP requires an applicability demonstration of the NRELAP5 code and tests. A unique aspect of the demonstration provided for the NPM is the comparison of NRELAP5 simulations of LOCA events to NIST-1 test data and NRELAP5 simulation of the same LOCA event in the NPM. In the comparisons, the NPM results are scaled down to the NIST-1 size using the scaling ratios used to design the NIST-1 facility. The reasonable-to-excellent agreement obtained by these comparisons establishes the applicability of NRELAP5 to accurately predict LOCA phenomena at both the NIST-1 and NPM scales.

This topical report provides example applications of the LOCA EM in order to aid the reader's understanding of the context of the application of the NuScale LOCA EM. These calculations are presented for break spectra that cover a range of break locations, break sizes, single failures, equipment unavailability and initial and boundary conditions. Nodalization and time-step sensitivity required by 10 CFR 50 Appendix K are also performed. The analyses conducted show that the NPM retains sufficient water inventory in the primary system that the core does not uncover or experience a CHF condition during a LOCA and that containment design pressure is not challenged. Peak cladding temperature (PCT) is shown to occur at the beginning of the LOCA event and cladding temperature decreases as the transient evolves. Because no fuel heat-up occurs for any design-basis LOCA, the following regulatory acceptance criteria from 10 CFR 50.46 are met:

(1) Peak cladding temperature remains below 2,200 degrees Fahrenheit (1,204 degrees Celsius).

(2) Maximum fuel oxidation is less than 0.17 times total cladding thickness.

(3) Maximum hydrogen generation is less than 0.01 times that generated if all cladding were to react.

(4) Coolable geometry is retained.

© Copyright 2016 by NuScale Power, LLC

NuScale requests Nuclear Regulatory Commission (NRC) review and approval to use the LOCA EM described in this report for analyses of design basis LOCA events in the NPM. The NuScale LOCA EM includes the following components:

- LOCA PIRT
- NRELAP5 code with NuScale-specific modifications
- assessment of the NRELAP5 code against experimental data
- demonstration of the applicability of the NRELAP5 code to LOCA analysis
- input model of the NPM

This LOCA EM uses a conservative bounding approach to analyzing LOCA transients that follows the guidance provided in RG 1.203 and satisfies the applicable requirements of 10 CFR 50 Appendix K. Results show that its application to the NPM demonstrates acceptable performance based upon the acceptance criteria of 10 CFR 50.46.

© Copyright 2016 by NuScale Power, LLC

1.0 Introduction

1.1 Purpose

The purpose of this report is to present the NuScale evaluation model (EM) used to evaluate emergency core cooling system (ECCS) performance in the NuScale Power Module (NPM) for design-basis loss-of-coolant accidents (LOCAs). The LOCA EM follows the guidance provided in "Transient and Accident Analysis Methods," Regulatory Guide (RG) 1.203 (Reference 1) and satisfies the applicable requirements of "ECCS Evaluation Models," 10 CFR 50 Appendix K (Reference 2). NuScale requests U.S. Nuclear Regulatory Commission (NRC) approval to use the EM described in this report for analyses of design-basis LOCA events in the NPM.

1.2 Scope

This report summarizes the following:

- NPM design and operation
- NuScale LOCA phenomena identification and ranking table (PIRT)
- NRELAP5 input model for the NPM
- NRELAP5 code features and modifications
- assessment of NRELAP5 against separate effects tests (SETs) and integral effects tests (IETs)
- applicability evaluation to determine the adequacy of NRELAP5 for NPM LOCA analyses

This report also provides LOCA analysis at several locations and over a spectrum of break sizes to demonstrate the application of the EM to the NPM design. Additionally, the results of sensitivity calculations performed in accordance with the applicable requirements of 10 CFR 50 Appendix K are summarized.

The scope of the NuScale LOCA EM is as follows:

- The EM is applicable to a nuclear power plant that follows the general description of the NuScale Power Plant design in Section 3.0. Applicability of the EM is based on the NuScale LOCA PIRT, which identifies and ranks those phenomena the EM must be qualified to model during a LOCA in an NPM.
- The EM does not have restrictions concerning operating setpoints or loss of offsite-power conditions as long as the phenomena that occur during the progression of a LOCA have been identified by the PIRT process.
- The EM is qualified for thermal-hydraulic conditions that span normal operating conditions down to atmospheric pressure. Initially, the containment is at low absolute pressure conditions (subatmospheric). During a LOCA, the containment response depends primarily on the mass and energy release and, secondarily, on heat transfer

© Copyright 2016 by NuScale Power, LLC

processes on and within the containment shell. The mass and energy release does not depend on downstream (containment) conditions until the containment pressure is above atmospheric pressure. Hence, the lower limit for models and correlations used in the LOCA analysis is atmospheric pressure.

- The EM requires that certain checks be made and conservative assumptions be taken when building the model. This includes the generation and application of a bounding power shape and the selection of a set of thermal-mechanical properties that bounds all times in cycle.
- Application of the EM demonstrates that fuel does not experience CHF conditions, collapsed water level remains above the top of the active fuel, and containment remains intact and pressure and temperature remain below design limits. This assures that no fuel failure occurs and the acceptance criteria of 10 CFR 50.46 (Reference 3), excluding long-term cooling, are satisfied.
- The EM described in this document addresses ECCS performance in the NPM up to the time when a recirculation flow is established. Recirculation flow is considered established when pressure and level in containment and the RPV approach a stable equilibrium condition {i.e., flow is recirculating through the reactor recirculation valves [RRVs]), core heat is removed by boiling in the core, and steam exits through the reactor vent valves (RVVs). This EM does not assess radiological impacts, boron precipitation, or boron dilution. These aspects are assessed by separate methodologies. Long term cooling is addressed in the NuScale technical report, “Long Term Cooling,” TR-0916-51299 (Reference 11).
- Pipe breaks inside containment are considered to be LOCA. Pipe breaks outside containment and failures in reactor pressure vessel (RPV) appurtenances, e.g., control rod drive mechanism housings and RPV nozzles and flanges, are not evaluated as part of the LOCA definition. Inadvertent opening of valves on the RPV leading to a decrease in reactor coolant system (RCS) inventory are not included in the LOCA definition per 10 CFR 50.46, although the EM may be used to evaluate such transients.

1.3 Abbreviations and Definitions

Table 1-1. Abbreviations

Term	Definition
AC	alternating current
BOL	beginning-of-life
BWR	boiling water reactor
CCFL	counter current flow limitation
CFT	critical flow test
CHF	critical heat flux
CHFR	critical heat flux ratio
CPV	cooling pool vessel
CVCS	chemical and volume control system
CNV	containment vessel
DACS	data acquisition and control system

© Copyright 2016 by NuScale Power, LLC

Term	Definition
DC	direct current
DHRS	decay heat removal system
DSM	direct substitution method
ECCS	emergency core cooling system
EM	evaluation model
EMDAP	evaluation model development and assessment process
EOL	end-of-life
FLECHT	full length emergency cooling heat transfer
FOM	figure of merit
GDF	general design framework
HBM	heat balance method
HTFS	heat transfer and fluid flow service
HTP	heat transfer plate
H2TS	hierarchical two-tiered scaling
IAB	inadvertent actuation block
ID	inner diameter
IET	integral effects test
INL	Idaho National Laboratory
JIT	jet impingement test
L/D	length-to-diameter
LOCA	loss-of-coolant accident
LP	lower plenum
MASLWR	Multi-Application Small Light Water Reactor
MCHFR	minimum critical heat flux ratio
MPS	module protection system
NIST-1	NuScale Integral System Test -1
NRC	U.S. Nuclear Regulatory Commission
NSSS	nuclear steam supply system
NPM	NuScale Power Module
PCT	peak cladding temperature
PIRT	phenomena identification and ranking table
PWR	pressurized water reactor
QAPD	Quality Assurance Program Description
RCS	reactor coolant system
RG	Regulatory Guide
RPV	reactor pressure vessel
RRV	reactor recirculation valve
RSV	reactor safety valve
RVV	reactor vent valve
SET	separate effects test
SG	steam generator
SIET	Società Informazioni Esperienze Termoidrauliche
SSC	Structures, Systems and Components
TAF	top of active fuel

© Copyright 2016 by NuScale Power, LLC

Term	Definition
UCP	upper core plate

Table 1-2. Definitions

Term	Definition
Figure of merit	A parameter selected to characterize the plant accident response.
“Excellent” agreement	One of the acceptance criteria defined in RG 1.203. “Excellent” agreement applies when the code exhibits no deficiencies in modeling a given behavior. Major and minor phenomena and trends are correctly predicted. The calculated results are judged to agree closely with the data. The calculation will, with few exceptions, lay within the specified or inferred uncertainty bands of the data. The code may be used with confidence in similar applications.
“Reasonable” agreement	One of the acceptance criteria defined in RG 1.203. “Reasonable” agreement applies when the code exhibits minor deficiencies. Overall, the code provides an acceptable prediction. All major trends and phenomena are correctly predicted. Differences between calculation and data are greater than deemed necessary for excellent agreement. The calculation will frequently lie outside but near the specified or inferred uncertainty bands of the data. However, the correct conclusions about trends and phenomena would be reached if the code was used in similar applications.
“Minimal” agreement	One of the acceptance criteria defined in RG 1.203. “Minimal” agreement applies when the code exhibits significant deficiencies. Overall, the code provides a prediction that is only conditionally acceptable. Some major trends or phenomena are not predicted correctly and some calculated values lie considerably outside the specified or inferred uncertainty bands of the data. Incorrect conclusions about trends and phenomena may be reached if the code were to be used in similar applications and an appropriate warning needs to be issued to users. Selected code models and facility model noding need to be reviewed, modified, and assessed before the code can be used with confidence in similar applications.

© Copyright 2016 by NuScale Power, LLC

2.0 Background

This topical report provides a description of the NuScale LOCA EM, developed following the guidelines in the EMDAP of RG 1.203.

Six basic principles are identified in RG 1.203 as important in the process of developing and assessing an EM. Four of the principles (corresponding to the 20 steps identified in the EMDAP process) are addressed in this report. They include

- determining the requirements for the EM.
- developing an assessment base consistent with the determined requirements.
- developing the EM.
- assessing the adequacy of the EM.

The remaining principles related to establishing an appropriate quality assurance program and providing comprehensive, accurate, up-to-date documentation) are addressed outside this report as part of "NuScale Topical Report: Quality Assurance Program Description for the NuScale Power Plant," NP-TR-1010-859-NP-A (Reference 4).

The NuScale LOCA EM specifically addresses the application of the EM to the NPM and how the EM meets the applicable requirements of 10 CFR 50 Appendix K. This report also demonstrates how the NuScale LOCA EM can be applied to evaluate ECCS performance to meet 10 CFR 50.46 acceptance criteria.

This EM uses the NRELAP5 code that was developed from the Idaho National Laboratory (INL) RELAP5-3D© computer code. This report discusses the code modifications and modeling requirements needed to address the unique features and phenomena of the NPM design, as well as those required to comply with the applicable requirements of 10 CFR 50 Appendix K.

The EM developed in this report is consistent with the applicable TMI Action Items (Reference 5) as described in the Design-Specific Review Standard for NuScale, Section 15.6.5 (Reference 6).

2.1 Loss-of-Coolant Accident Evaluation Model Roadmap

Figure 2-1 shows various elements of the EMDAP as defined in RG 1.203 and provides a roadmap that relates the sections of this report to the elements and steps of the EMDAP. The EMDAP establishes the adequacy of a methodology for evaluating complex events that are postulated to occur in nuclear power plant systems. The EMDAP described here has been developed for analyzing postulated LOCAs in the NPM.

© Copyright 2016 by NuScale Power, LLC

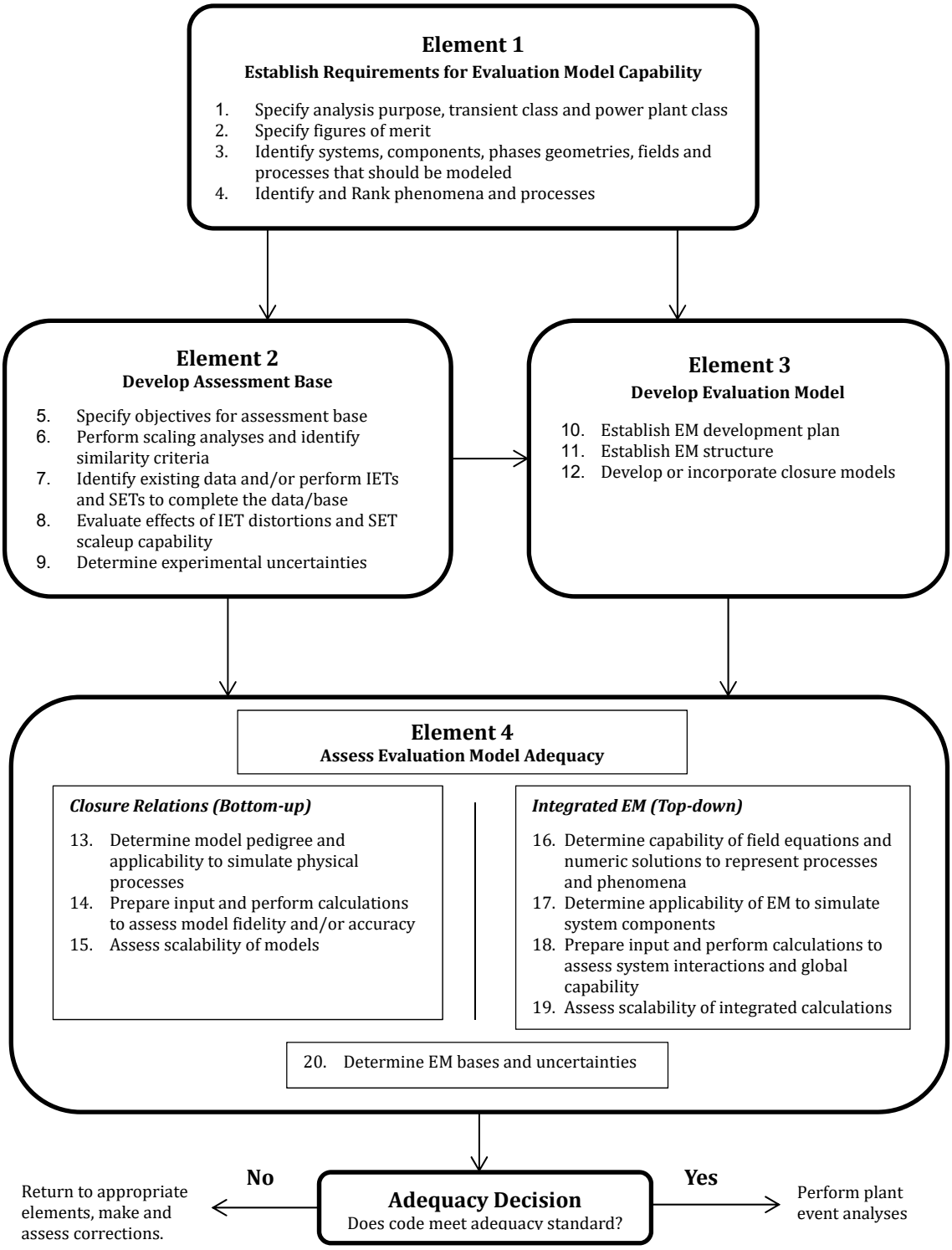

Figure 2-1. Evaluation model development and assessment process

© Copyright 2016 by NuScale Power, LLC

Table 2-1. Evaluation model development and assessment process steps and the associated sections in this document

EMDAP Step	Description	EM Section
Element 1, Establish Requirements for Evaluation Model Capability		
1	Specify analysis purpose, transient class, and power plant class.	The purpose of the LOCA EM is described in Section 1.1. Section 2.0 briefly describes the background of the process followed to develop the LOCA EM and the principal software used. Section 3.0 provides an overview of the NPM design and operation. This includes the safety-related systems, the system logic, and operational phases that could occur in the NPM. The regulatory requirements with which the EM is designed to comply are described in Section 2.2.
2	Specify figures of merit (FOMs).	Section 4.3 discusses the FOMs which are used for the development of the NuScale LOCA PIRT.
3	Identify systems, components, phases, geometries, fields, and processes that should be modeled.	Systems, components, phases, and processes are identified as a part of the NuScale LOCA PIRT discussed in Section 4.0.
4	Identify and rank phenomena and processes.	Section 4.0 summarizes the PIRT that has been established for this EM.
Element 2, Develop Assessment Base		
5	Specify objectives for assessment base.	Section 7.0 describes objectives of the benchmarks selected for the assessment of NRELAP5 against SETs and IETs.
6	Perform scaling analysis and identify similarity criteria.	A scaling analysis has been performed for the NPM based on the NuScale Integral System Test -1 (NIST-1) facility. The results of the scaling analysis are discussed in Section 8.3.2 to address the EM applicability to the NPM LOCA analysis.
7	Identify existing data and perform IETs and SETs to complete database.	Sections 7.2 through 7.5 provide the results of the NRELAP5 validation against the SETs and IETs. In Section 8.0 these results are evaluated relative to NRELAP5 modeling of the high-ranked phenomena identified in the NuScale LOCA PIRT.

© Copyright 2016 by NuScale Power, LLC

EMDAP Step	Description	EM Section
8	Evaluate effects of IET distortions and SET scale-up capability.	The SET scale-up capability is evaluated in Section 8.2. NIST-1 IET distortions are evaluated in Section 8.3. These results justify the applicability of the EM to NPM LOCA analysis.
9	Determine experimental uncertainties.	Section 7 covers experimental uncertainties for NRELAP5 assessments against the SETs and IETs.
Element 3, Develop Evaluation Model		
10	Establish EM development plan.	The NRELAP5 development plan includes programming standards and procedures, quality assurance procedures, and configuration control, which are summarized in Section 6.1.
11	Establish EM structure.	The final structure of the LOCA EM is described in Section 5.0. The NRELAP5 code description and new model features are discussed in Section 6.0.
12	Develop or incorporate closure models.	A full description of the closure models and the associated equations used in the LOCA EM is provided in the NRELAP5 theory and users manuals. Section 6.2 provides a summary of NRELAP5 models and correlations. The applicability evaluation in Section 8.0 also provides further discussion of the NRELAP5 code models and correlations.
Element 4, Assess Evaluation Model Adequacy Closure Relations (Bottom-up)		
13	Determine model pedigree and applicability to simulate physical processes.	Bottom-up assessments presented in Section 8.2 include discussion of pedigree and applicability of dominant NRELAP5 models and correlations that are essential to simulate high-ranked PIRT phenomena.
14	Prepare input and perform calculations to assess model fidelity and accuracy.	Sections 7.2 through 7.5 summarize the results of comparison of NRELAP5 against the selected SETs and IETs, including evaluation of code fidelity and accuracy. These results are considered in Section 8.2 to address the applicability of the EM to NPM LOCA analysis.
15	Assess scalability of models.	Section 8.2 includes discussion of scalability of dominant NRELAP5 models and correlations that are essential to simulate high-ranked PIRT phenomena.
Element 4, Assess Evaluation Model Adequacy Integrated EM (Top-down)		
16	Determine capability of field equations and numeric solutions to represent processes and phenomena.	NRELAP5 field equations and the numeric solution scheme are discussed in Section 6.2 and evaluated for their applicability to NPM LOCA in Section 8.0.

© Copyright 2016 by NuScale Power, LLC

EMDAP Step	Description	EM Section
17	Determine applicability of EM to simulate system components.	The applicability of the EM to simulate the NPM system and components is demonstrated by assessment of NRELAP5 against NuScale design-specific SETs and IETs in Section 8.3.1.
18	Prepare input and perform calculations to assess system interactions and global capability.	Section 7.0 summarizes the results of the assessment of NRELAP5 against NIST-1 IET data. These results are considered in Section 8.3 to address the applicability of the EM to NPM LOCA analysis.
19	Assess scalability of integrated calculations and data for distortions.	Section 8.3 provides an evaluation of scaling distortions between the NIST-1 IET data and the NPM design. The scalability of EM to represent NPM LOCA phenomena and processes is presented.
20	Determine EM biases and uncertainties.	This step is not required per RG 1.203 for safety analyses that implement 10 CFR 50 Appendix K.

2.2 Regulatory Requirements

This section discusses the regulatory acceptance criteria for ECCS performance and the manner in which they are satisfied by application of the NuScale LOCA EM.

2.2.1 10 CFR 50.46 Loss-of-Coolant Accident Acceptance Criteria

10 CFR 50.46 requires that light water nuclear reactors fueled with uranium oxide pellets within cylindrical zircaloy cladding be provided with an ECCS that is designed in such a way that their calculated core cooling performance after a postulated LOCA conforms to certain criteria specified in 10 CFR 50.46(b). The five acceptance criteria are the following:

1. The calculated maximum fuel element cladding temperature shall not exceed 2200 degrees Fahrenheit (1,204 degrees Celsius).

2. The calculated total oxidation of the cladding shall nowhere exceed 0.17 times the total cladding thickness before oxidation.

3. The calculated total amount of hydrogen generated from the chemical reaction of the cladding with water or steam shall not exceed 0.01 times the hypothetical amount that would be generated if all the metal in the cladding cylinders surrounding the fuel, excluding the cladding surrounding the plenum volume, were to react.

4. Calculated changes in core geometry shall be such that the core remains amenable to cooling.

5. After any calculated successful initial operation of the ECCS, the calculated core temperature shall be maintained at an acceptably low value and decay heat shall be

© Copyright 2016 by NuScale Power, LLC

removed for the extended period of time required by the long-lived radioactivity remaining in the core.

The NuScale LOCA EM addresses the first four criteria. The EM described in this document addresses ECCS performance in the NPM up to the time when a recirculation flow is established, pressures and levels in containment and the RPV approach a stable equilibrium condition (i.e., flow is recirculating in through the RRVs), core heat is removed by boiling in the core, and steam exits through the RVVs.

The NPM is designed so that there is no core uncovery or heatup for a design-basis LOCA. As a result, peak cladding temperature (PCT) will be well within the acceptance criterion of 2,200 degrees Fahrenheit (1,204 degrees Celsius). The parameters of interest are the collapsed liquid water level above the top of active fuel (TAF) and minimum critical heat flux ratio (MCHFR). These two criteria are more sensitive than PCT in the NPM design. Maintaining primary inventory and ensuring the core does not go into post-critical heat flux (CHF) heat transfer ensures that the 10 CFR 50.46(b) limitations for PCT, oxidation, and hydrogen production are protected.

There is no oxidation of the cladding as a result of a LOCA. There is no hydrogen generated from the chemical reaction of the cladding with water or steam because fuel temperatures are not high enough to initiate this chemical reaction. There are no changes in core geometry resulting from a LOCA that would prevent the core from being amenable to cooling. Therefore, the first four acceptance criteria are met when the collapsed liquid level is above the top of the active fuel and MCHFR is greater than the safety limit for the entire time period covered by this EM (see Section 7.3.6).

The fifth criterion is also met during the shorter period this EM addresses. The longer-term evaluation for the fifth criteria is addressed by other NuScale methodologies (Reference11).

2.2.2 10 CFR 50 Appendix K

The ECCS performance is calculated in conformance with the required and acceptable features of ECCS EMs specified in 10 CFR 50 Appendix K, and is calculated for a number of cases to provide assurance that the most severe postulated LOCAs are identified. 10 CFR 50.46 provides two options for an acceptable LOCA EM. Paragraph 50.46(a)(i) allows for a best-estimate approach to be followed and Paragraph 50.46.(a)(ii) allows for the conservative deterministic approach detailed in 10 CFR 50 Appendix K. In view of the large safety margins in the NPM, the deterministic bounding approach in Paragraph 50.46(a)(ii) is used by NuScale.

The NPM is designed to reduce the consequences of design-basis LOCAs compared to existing light water reactors for which 10 CFR 50 Appendix K was developed. Consequently, many of the phenomena that are the subject of 10 CFR 50 Appendix K requirements are not encountered in design-basis NPM LOCAs in the NPM. That is, certain phenomena have been designed out of the NPM and, therefore, a number of requirements are satisfied by design rather than by analysis. Examples of phenomena

© Copyright 2016 by NuScale Power, LLC

and processes that can occur during a typical pressurized water reactor (PWR) LOCA that do not occur during an NPM LOCA include:

- loop seal clearing
- pump coastdown
- two-phase pump performance
- entry of significant amounts of non-condensable gases into the system
- core uncovery
- core refilling
- core reflooding
- cladding swelling and rupture
- metal-water reaction
- post-CHF heat transfer
- cladding rewet
- ECCS bypass

Hence, only a subset of the phenomena that are addressed in 10 CFR 50 Appendix K is encountered in the design-basis NPM LOCAs and thus relevant to the NuScale LOCA EM. Table 2-2 lists each required and acceptable feature of the EM specified in 10 CFR 50 Appendix K and describes the manner in which the NuScale LOCA EM addresses each feature. The NuScale LOCA EM includes model features required by Appendix K that are relevant to the NPM. Features required by 10 CFR 50 Appendix K that are not relevant to the NuScale LOCA EM are identified in Table 2-2 as either “satisfied by design” or “excluded from model.”

A feature “satisfied by design” means that a 10 CFR 50 Appendix K required feature is expressly or impliedly conditional on the presence of process or phenomena in the design or analysis. Because such process or phenomena does not exist for the NuScale design, the required feature is not applicable and not included in the NuScale LOCA EM. For example, there are no reactor coolant pumps in the NPM. Therefore the phenomena that are the subject of 10 CFR 50 Appendix K Requirement I.C.6 “Pump Modeling” are not encountered because of the design of the NPM, and thus the required model features are “satisfied by design.”

A feature “excluded” from the EM means that 10 CFR 50 Appendix K directly requires the feature, without condition on the presence of a process or phenomena, but that the feature is not relevant to the NuScale LOCA EM. Table 2-2 technically justifies the exclusion of such feature from the model. However, an applicant or licensee referencing this report will be required to address regulatory compliance with 10 CFR 50.46 and 10 CFR 50 Appendix K (e.g., by seeking an exemption from that required feature). Similarly, an “acceptable alternative” model feature is technically justified by Table 2-2, but does not strictly meet the 10 CFR 50 Appendix K required feature, and thus an applicant or licensee referencing

© Copyright 2016 by NuScale Power, LLC

this report will be required to address regulatory compliance. Historically, RELAP5 has been applied to evaluate post-CHF fuel conditions for events in LWRs. While these features have been retained in NRELAP5, the application of the LOCA EM to predict fuel temperature response is limited to pre-CHF heat transfer regimes.

In the NuScale LOCA EM, applicable closure models or correlations required by 10 CFR 50 Appendix K are used. The NuScale LOCA EM also uses appropriate closure models or correlations in addition to those required in 10 CFR 50 Appendix K. All closure models and correlations are verified and validated for use within their range of applicability.

© Copyright 2016 by NuScale Power, LLC

Table 2-2. 10 CFR 50 Appendix K required and acceptable features compliance

10 CFR 50 Appendix K Required and Acceptable Feature	NuScale LOCA EM
I.A Sources of heat during the LOCA: For the heat sources listed in paragraphs I.A.1 to 4 of this appendix, it must be assumed that the reactor has been operating continuously at a power level at least 1.02 times the licensed power level (to allow for instrumentation error) with the maximum peaking factor allowed by the technical specifications. An assumed power level lower than the level specified in this paragraph (but not less than the licensed power level) may be used provided the proposed alternative value has been demonstrated to account for uncertainties due to power level instrumentation error. A range of power distribution shapes and peaking factors representing power distributions that may occur over the core lifetime must be studied. The selected combination of power distribution shape and peaking factor should be the one that results in the most severe calculated consequences for the spectrum of postulated breaks and single failures that are analyzed.	The initial power level is set at 102 percent of rated power. The maximum radial peaking factor is used in the hot assembly to bound all possible power peaking. (See Section 9.6.6). Sensitivity calculations were performed with different axial power shapes that bound maximum axial power peaking. Further discussion on core power distribution is provided in Section 5.1.2.2.3. Therefore, the required features of I.A are included in the NuScale LOCA EM.
I.A.1 The Initial Stored Energy in the Fuel: The steady-state temperature distribution and stored energy in the fuel before the hypothetical accident shall be calculated for the burn-up that yields the highest calculated cladding temperature (or, optionally, the highest calculated stored energy.) To accomplish this, the thermal conductivity of the UO_2 shall be evaluated as a function of burn-up and temperature, taking into consideration differences in initial density, and the thermal conductance of the gap between the UO_2 and the cladding shall be evaluated as a function of the burn-up, taking into consideration fuel densification and expansion, the composition and pressure of the gases within the fuel rod, the initial cold gap dimension with its tolerances, and cladding creep.	Based on the burn-up dependent fuel performance analysis, it was determined that choosing end-of-life (EOL) fuel thermal conductivity and beginning-of-life (BOL) volumetric heat capacity and fuel-cladding gap conductance maximizes the initial stored energy in the fuel. An additional 15 percent bias is applied to both volumetric heat capacity and thermal conductivity to maximize the initial stored energy. Further discussion on selection of fuel rod mechanical property input is provided in Section 5.1.2.2.4. Therefore, the required features of I.A.1 are included in the NuScale LOCA EM.

© Copyright 2016 by NuScale Power, LLC

10 CFR 50 Appendix K Required and Acceptable Feature	NuScale LOCA EM
I.A.2 Fission Heat: Fission heat shall be calculated using reactivity and reactor kinetics. Shutdown reactivities resulting from temperatures and voids shall be given their minimum plausible values, including allowance for uncertainties, for the range of power distribution shapes and peaking factors indicated to be studied above. Rod trip and insertion may be assumed if they are calculated to occur.	A point kinetics model is used to calculate fission power. Credit is taken for reactor trip. A conservative control rod insertion curve is used along with a minimum rod worth and conservative delay in initiation of rod insertion. The most reactive control rod is assumed to be stuck out of the core. Doppler and moderator density coefficients are calculated conservatively (Section 5.1.2.2.5). Therefore, the required features of I.A.2 are included in the NuScale LOCA EM.
I.A.3 Decay of Actinides: The heat from the radioactive decay of actinides, including neptunium and plutonium generated during operation, as well as isotopes of uranium, shall be calculated in accordance with fuel cycle calculations and known radioactive properties. The actinide decay heat chosen shall be that appropriate for the time in the fuel cycle that yields the highest calculated fuel temperature during the LOCA.	The 1979 ANS actinide decay heat standard is applied which includes the decay of neptunium and plutonium (Sections 5.1.2.2.5). The actinide decay heat assumes infinite operating time to maximize actinide concentration. This assumption results in the highest calculated fuel temperature during the LOCA. Therefore, the required features of I.A.3 are included in the NuScale LOCA EM.
I.A.4 Fission Product Decay: The heat generation rates from radioactive decay of fission products shall be assumed to be equal to 1.2 times the values for infinite operating time in the ANS Standard (Proposed American Nuclear Society Standards--"Decay Energy Release Rates Following Shutdown of Uranium-Fueled Thermal Reactors." Approved by Subcommittee ANS-5, ANS Standards Committee, October 1971). This standard has been approved for incorporation by reference by the Director of the Federal Register. A copy of the standard is available for inspection at the NRC Library, 11545 Rockville Pike, Rockville, Maryland 20852-2738. The fraction of the locally generated gamma energy that is deposited in the fuel (including the cladding) may be different from 1.0; the value used shall be justified by a suitable calculation.	The 1973 ANS decay heat standard (Reference 44) is used with a 20 percent uncertainty added to the base value. A bounding form of the 1973 ANS standard in NRELAP5 meets the intent of the 10 CFR 50 Appendix K requirement (Section 5.1.2.2.5). Therefore, the NuScale LOCA EM includes an acceptable alternative to the requirement of I.A.4.

© Copyright 2016 by NuScale Power, LLC

10 CFR 50 Appendix K Required and Acceptable Feature	NuScale LOCA EM
I.A.5 Metal-Water Reaction Rate: The rate of energy release, hydrogen generation, and cladding oxidation from the metal-water reaction shall be calculated using the Baker-Just equation (Baker, L., Just, L.C., "Studies of Metal Water Reactions at High Temperatures, III. Experimental and Theoretical Studies of the Zirconium-Water Reaction," ANL-6548, page 7, May 1962). This publication has been approved for incorporation by reference by the Director of the Federal Register. A copy of the publication is available for inspection at the NRC Library, 11545 Rockville Pike, Two White Flint North, Rockville, Maryland 20852-2738. The reaction shall be assumed not to be steam limited. For rods whose cladding is calculated to rupture during the LOCA, the inside of the cladding shall be assumed to react after the rupture. The calculation of the reaction rate on the inside of the cladding shall also follow the Baker-Just equation, starting at the time when the cladding is calculated to rupture, and extending around the cladding inner circumference and axially no less than 1.5 inches each way from the location of the rupture, with the reaction assumed not to be steam limited.	Calculated cladding temperatures for design basis LOCAs are well below the level where cladding oxidation occurs on a time scale of a LOCA event for the NPM (see the results of LOCA break spectrum calculations in Section 9.0). Therefore, this requirement is not relevant to the NuScale design, which precludes fuel temperature reaching CHF and any significant fuel cladding heatup. For the NuScale LOCA EM, core coverage and an MCHFR greater than the safety limit (see Section 7.3.6) precludes the occurrence of cladding oxidation. Therefore, the required features of I.A.5 are excluded from the NuScale LOCA EM.
I.A.6 Reactor Internals Heat Transfer: Heat transfer from piping, vessel walls, and non-fuel internal hardware shall be taken into account.	The NRELAP5 plant model explicitly represents all major reactor internal heat structures. Heat structures are also included for the primary and secondary system pressure boundary materials. See Section 5.1.2 for details of the internal heat structures represented in the NuScale LOCA EM. Therefore, the required features of I.A.6 are included in the NuScale LOCA EM.
I.A.7 Pressurized Water Reactor Primary-to-Secondary Heat Transfer: Heat transferred between primary and secondary systems through heat exchangers (steam generators) shall be taken into account. (Not applicable to boiling water reactors (BWRs).)	Heat transfer through the steam generator (SG) tubes is included in the EM. The model is validated using experimental data from Società Italiana Esperienze Termoidrauliche (SIET) tests (see Section 7.4) and NIST-1 tests (see Section 7.5). Therefore, the required features of I.A.7 are included in the NuScale LOCA EM.

© Copyright 2016 by NuScale Power, LLC

10 CFR 50 Appendix K Required and Acceptable Feature	NuScale LOCA EM
I.B Swelling and Rupture of the Cladding and Fuel Rod Thermal Parameters: Each evaluation model shall include a provision for predicting cladding swelling and rupture from consideration of the axial temperature distribution of the cladding and from the difference in pressure between the inside and outside of the cladding, both as functions of time. To be acceptable the swelling and rupture calculations shall be based on applicable data in such a way that the degree of swelling and incidence of rupture are not underestimated. The degree of swelling and rupture shall be taken into account in calculations of gap conductance, cladding oxidation and embrittlement, and hydrogen generation. The calculations of fuel and cladding temperatures as a function of time shall use values for gap conductance and other thermal parameters as functions of temperature and other applicable time-dependent variables. The gap conductance shall be varied in accordance with changes in gap dimensions and any other applicable variables.	Calculated cladding temperatures for design basis LOCAs in the NPM are well below the threshold for cladding swelling and rupture (see the results of LOCA break spectrum calculations in Section 9.0). Peak cladding temperatures in the NPM occur at steady state normal operation. Because swelling and rupture do not occur during normal operation, they will not occur in a NPM LOCA event. Therefore, this requirement is not relevant for the NuScale LOCA EM as core coverage precludes the occurrence of cladding swelling and rupture. Therefore, the required features of I.B are excluded from the NuScale LOCA EM.
I.C Blowdown Phenomena	
I.C.1.a Break Characteristics and Flow: In analyses of hypothetical LOCAs, a spectrum of possible pipe breaks shall be considered. This spectrum shall include instantaneous double-ended breaks ranging in cross-sectional area up to and including that of the largest pipe in the primary coolant system. The analysis shall also include the effects of longitudinal splits in the largest pipes, with the split area equal to the cross-sectional area of the pipe.	A complete spectrum of break sizes and locations is analyzed up to the largest penetrations in the RPV including the double-ended guillotine break where appropriate. The size of the pipes precludes the impact of longitudinal split breaks in the NPM design. Therefore, the requirement for analyzing the effect of longitudinal split break is not relevant to the NuScale LOCA EM. Further discussion of break spectrum analysis is provided in Section 5.4. The break spectrum calculation results are available in Section 9.0. Therefore, the required features of I.C.1.a are included or satisfied by design in the NuScale LOCA EM.

© Copyright 2016 by NuScale Power, LLC

10 CFR 50 Appendix K Required and Acceptable Feature	NuScale LOCA EM
I.C.1.b Discharge Model: For all times after the discharging fluid has been calculated to be two-phase in composition, the discharge rate shall be calculated by use of the Moody model (F.J. Moody, "Maximum Flow Rate of a Single Component, Two-Phase Mixture," Journal of Heat Transfer, Trans American Society of Mechanical Engineers, 87, No. 1, February, 1965).. The calculation shall be conducted with at least three values of a discharge coefficient applied to the postulated break area, these values spanning the range from 0.6 to 1.0. If the results indicate that the maximum cladding temperature for the hypothetical accident is to be found at an even lower value of the discharge coefficient, the range of discharge coefficients shall be extended until the maximum cladding temperatures calculated by this variation has been achieved.	The required Moody critical flow is used when the break flow is calculated to be two-phase flow and the {{ }}$^{2(a),(c)}$ model is used to calculate single-phase choked flow {{ }}$^{2(a),(c)}$ For the NPM, single phase flow through the break may recur after the transition to two-phase flow. The {{ }}$^{2(a),(c)}$ model is conservative for single-phase break flow. See Section 6.6.1 for details. The range of postulated break sizes in the break analysis covers the 10 CFR 50 Appendix K required range of discharge coefficient, as discussed in Section 5.4. Therefore, the required features of I.C.1.b, including an acceptable alternative feature, are included in the NuScale LOCA EM.

© Copyright 2016 by NuScale Power, LLC

10 CFR 50 Appendix K Required and Acceptable Feature	NuScale LOCA EM
I.C.1.c End of Blowdown. (Applies Only to Pressurized Water Reactors): For postulated cold leg breaks, all emergency cooling water injected into the inlet lines or the reactor vessel during the bypass period shall in the calculations be subtracted from the reactor vessel calculated inventory. This may be executed in the calculation during the bypass period, or as an alternative the amount of emergency core cooling water calculated to be injected during the bypass period may be subtracted later in the calculation from the water remaining in the inlet lines, downcomer, and reactor vessel lower plenum after the bypass period. This bypassing shall end in the calculation at a time designated as the "end of bypass," after which the expulsion or entrainment mechanisms responsible for the bypassing are calculated not to be effective. The end-of-bypass definition used in the calculation shall be justified by a suitable combination of analysis and experimental data. Acceptable methods for defining "end of bypass" include, but are not limited to, the following: (1) Prediction of the blowdown calculation of downward flow in the downcomer for the remainder of the blowdown period; (2) Prediction of a threshold for droplet entrainment in the upward velocity, using local fluid conditions and a conservative critical Weber number.	For the NuScale design, there are no cold legs and hence no cold leg breaks. All of the coolant that exits the break remains in the containment and is available to return when the RRVs are opened. Emergency core cooling system bypass cannot occur in the NPM, so this requirement is not relevant to the NuScale LOCA EM. Therefore, the required features of I.C.1.c are satisfied by design.
I.C.1.d Noding Near the Break and the ECCS Injection Points: The noding in the vicinity of and including the broken or split sections of pipe and the points of ECCS injection shall be chosen to permit a reliable analysis of the thermodynamic history in these regions during blowdown.	Noding sensitivity studies have been conducted to demonstrate that the calculated conditions in the vicinity of the break locations, RVVs, and RRVs are reliable. The results of the noding sensitivity studies are discussed in Section 9.6.1. Therefore, the required features of I.C.1.d are included in the NuScale LOCA EM.

© Copyright 2016 by NuScale Power, LLC

10 CFR 50 Appendix K Required and Acceptable Feature	NuScale LOCA EM
I.C.2 Frictional Pressure Drops: The frictional losses in pipes and other components including the reactor core shall be calculated using models that include realistic variation of friction factor with Reynolds number, and realistic two-phase friction multipliers that have been adequately verified by comparison with experimental data, or models that prove at least equally conservative with respect to maximum cladding temperature calculated during the hypothetical accident. The modified Baroczy correlation (Baroczy, C. J., "A Systematic Correlation for Two-Phase Pressure Drop," Chem. Enging. Prog. Symp. Series, No. 64, Vol. 62, 1965) or a combination of the Thom correlation (Thom, J.R.S., "Prediction of Pressure Drop During Forced Circulation Boiling of Water," Int. J. of Heat & Mass Transfer, 7, 709-724, 1964) for pressures equal to or greater than 250 psia and the Martinelli-Nelson correlation (Martinelli, R. C. Nelson, D.B., "Prediction of Pressure Drop During Forced Circulation Boiling of Water," Transactions of ASME, 695-702, 1948) for pressures lower than 250 psia is acceptable as a basis for calculating realistic two-phase friction multipliers.	Friction losses in pipes and components are calculated using Reynolds number-dependent friction factors. The NRELAP5 wall friction model is based on a two-phase multiplier approach (see Section 6.2.4). The models used in NRELAP5 have been validated for the range of conditions encountered in design-basis LOCAs as shown by assessment against SETs and IETs in Section 7.0. Therefore, the required features of I.C.2 are included in the NuScale LOCA EM.
I.C.3 Momentum Equation: The following effects shall be taken into account in the conservation of momentum equation: (1) temporal change of momentum, (2) momentum convection, (3) area change momentum flux, (4) momentum change due to compressibility, (5) pressure loss resulting from wall friction, (6) pressure loss resulting from area change, and (7) gravitational acceleration. Any omission of one or more of these terms under stated circumstances shall be justified by comparative analyses or by experimental data.	All of the momentum equation effects required by Section I.C.3 are included in NRELAP5 (see Sections 6.2.1 and 6.2.4). Benchmarks for the NIST-1 facility and other assessments show that simulations made by NRELAP5 are acceptable, based on reasonable-to- excellent agreement with experimental data (see Section 7.0). Therefore, the required features of I.C.3 are included in the NuScale LOCA EM.

© Copyright 2016 by NuScale Power, LLC

10 CFR 50 Appendix K Required and Acceptable Feature	NuScale LOCA EM
I.C.4.a (Critical Heat Flux): Correlations developed from appropriate steady-state and transient-state experimental data are acceptable for use in predicting the CHF during LOCA transients. The computer programs in which these correlations are used shall contain suitable checks to ensure that the physical parameters are within the range of parameters specified for use of the correlations by their respective authors.	Two CHF correlations are used to monitor for CHF occurrence, {{ }}[2(a),(c)] See Sections 6.10.3 and 6.10.4 for description of the correlations. Section 7.3 describes the assessment against the NuScale CHF data that bounds the range of LOCA parameters.. The NuScale LOCA EM checks to ensure that the physical parameters are within the range of parameters specified for use of the correlations. Therefore, the required features of I.C.4.a are included in the NuScale LOCA EM.
I.C.4.b (Critical Heat Flux): Steady-state CHF correlations acceptable for use in LOCA transients include, but are not limited to, the following: [six acceptable CHF correlations are identified in 10 CFR 50 Appendix K, I.C.4.b].	I.C.4.b identifies acceptable, but not required, EM features. The NuScale LOCA EM includes an acceptable steady-state CHF correlation as addressed by I.C.4.a.
I.C.4.c (Critical Heat Flux): Correlations of appropriate transient CHF data may be accepted for use in LOCA transient analyses if comparisons between the data and the correlations are provided to demonstrate that the correlations predict values of CHF which allow for uncertainty in the experimental data throughout the range of parameters for which the correlations are to be used. Where appropriate, the comparisons shall use statistical uncertainty analysis of the data to demonstrate the conservatism of the transient correlation.	I.C.4.c identifies acceptable, but not required, EM features. The NuScale LOCA EM does not use a transient CHF correlation. See I.C.4.a.
I.C.4.d (Critical Heat Flux): Transient CHF correlations acceptable for use in LOCA transients include, but are not limited to, the following: (GE transient CHF correlation is listed in 10 CFR 50 Appendix K, I.C.4.d.)	I.C.4.d identifies acceptable, but not required, EM features. The NuScale LOCA EM does not use a transient CHF correlation. See I.C.4.a.

© Copyright 2016 by NuScale Power, LLC

10 CFR 50 Appendix K Required and Acceptable Feature	NuScale LOCA EM
I.C.4.e (Critical Heat Flux): After CHF is first predicted at an axial fuel rod location during blowdown, the calculation shall not use nucleate boiling heat transfer correlations at that location subsequently during the blowdown even if the calculated local fluid and surface conditions would apparently justify the reestablishment of nucleate boiling. Heat transfer assumptions characteristic of return to nucleate boiling (rewetting) shall be permitted when justified by the calculated local fluid and surface conditions during the reflood portion of a LOCA.	The break analysis in Section 9.0 demonstrates that CHF does not occur in the NPM for LOCAs. Heat transfer beyond CHF is not a phenomenon encountered during a design-basis LOCA. The NuScale LOCA methodology does not calculate heat transfer beyond CHF in the core. Therefore, this requirement is satisfied by a design that has a margin to CHF for LOCA events.
I.C.5.a (Post-CHF Heat Transfer Correlations): Correlations of heat transfer from the fuel cladding to the surrounding fluid in the post-CHF regimes of transition and film boiling shall be compared to applicable steady-state and transient-state data using statistical correlation and uncertainty analyses. Such comparison shall demonstrate that the correlations predict values of heat transfer co-efficient equal to or less than the mean value of the applicable experimental heat transfer data throughout the range of parameters for which the correlations are to be used. The comparisons shall quantify the relation of the correlations to the statistical uncertainty of the applicable data.	The break analysis in Section 9.0 demonstrates that CHF does not occur in the NPM for LOCAs. Heat transfer beyond CHF is not a phenomenon encountered during a design-basis LOCA. Therefore, this requirement is not relevant to the NuScale LOCA EM. Therefore, the required features of I.C.5.a are excluded from the NuScale LOCA EM.

© Copyright 2016 by NuScale Power, LLC

10 CFR 50 Appendix K Required and Acceptable Feature	NuScale LOCA EM
I.C.5.b (Post-CHF Heat Transfer Correlations): The Groeneveld flow film boiling correlation (equation 5.7 of D.C. Groeneveld, "An Investigation of Heat Transfer in the Liquid Deficient Regime," AECL-3281, revised December 1969) and the Westinghouse correlation of steady-state transition boiling ("Proprietary Redirect/Rebuttal Testimony of Westinghouse Electric Corporation," USNRC Docket RM-50-1, page 25-1, October 26, 1972) are acceptable for use in the post-CHF boiling regimes. In addition, the transition boiling correlation of McDonough, Milich, and King (J.B. McDonough, W. Milich, E.C. King, "An Experimental Study of Partial Film Boiling Region with Water at Elevated Pressures in a Round Vertical Tube," Chemical Engineering Progress Symposium Series, Vol. 57, No. 32, pages 197-208, (1961) is suitable for use between nucleate and film boiling. Use of all these correlations is restricted as follows: (1) The Groeneveld correlation shall not be used in the region near its low-pressure singularity, (2) The first term (nucleate) of the Westinghouse correlation and the entire McDonough, Milich, and King correlation shall not be used during the blowdown after the temperature difference between the cladding and the saturated fluid first exceeds 300°F, (3) Transition boiling heat transfer shall not be reapplied for the remainder of the LOCA blowdown, even if the cladding superheat returns below 300°F, except for the reflood portion of the LOCA when justified by the calculated local fluid and surface conditions.	I.C.5.b identifies acceptable, but not required, EM features. The NuScale LOCA methodology does not calculate heat transfer beyond CHF in the core. Therefore, these acceptable correlations are not relevant to the EM. See I.C.5.a.

© Copyright 2016 by NuScale Power, LLC

10 CFR 50 Appendix K Required and Acceptable Feature	NuScale LOCA EM
I.C.5.c (Post-CHF Heat Transfer Correlations): Evaluation models approved after October 17, 1988, which make use of the Dougall-Rohsenow flow film boiling correlation (R.S. Dougall and W.M. Rohsenow, "Film Boiling on the Inside of Vertical Tubes with Upward Flow of Fluid at Low Qualities," MIT Report Number 9079 26, Cambridge, Massachusetts, September 1963) may not use this correlation under conditions where nonconservative predictions of heat transfer result. Evaluation models that make use of the Dougall-Rohsenow correlation and were approved prior to October 17, 1988, continue to be acceptable until a change is made to, or an error is corrected in, the evaluation model that results in a significant reduction in the overall conservatism in the evaluation model. At that time continued use of the Dougall-Rohsenow correlation under conditions where nonconservative predictions of heat transfer result will no longer be acceptable. For this purpose, a significant reduction in the overall conservatism in the evaluation model would be a reduction in the calculated peak fuel cladding temperature of at least 50°F from that which would have been calculated on October 17, 1988, due either to individual changes or error corrections or the net effect of an accumulation of changes or error corrections.	I.C.5.c identifies acceptable, but not required, EM features. The NuScale LOCA methodology does not calculate heat transfer beyond CHF in the core. Therefore, these acceptable correlations are not relevant to the EM. See I.C.5.a.
I.C.6 Pump Modeling: The characteristics of rotating primary system pumps (axial flow, turbine, or centrifugal) shall be derived from a dynamic model that includes momentum transfer between the fluid and the rotating member, with variable pump speed as a function of time. The pump model resistance used for analysis should be justified. The pump model for the two-phase region shall be verified by applicable two-phase pump performance data. For BWRs after saturation is calculated at the pump suction, the pump head may be assumed to vary linearly with quality, going to zero for one percent quality at the pump suction, so long as the analysis shows that core flow stops before the quality at pump suction reaches one percent.	There are no primary system coolant pumps, so the requirements related to pump models are not relevant to the NuScale LOCA EM, as shown in Section 3.0. Therefore, the required features of I.C.6 are satisfied by design.

© Copyright 2016 by NuScale Power, LLC

10 CFR 50 Appendix K Required and Acceptable Feature	NuScale LOCA EM
I.C.7.a Core Flow Distribution During Blowdown. (Applies only to pressurized water reactors): The flow rate through the hot region of the core during blowdown shall be calculated as a function of time. For the purpose of these calculations the hot region chosen shall not be greater than the size of one fuel assembly. Calculations of average flow and flow in the hot region shall take into account cross flow between regions and any flow blockage calculated to occur during blowdown as a result of cladding swelling or rupture. The calculated flow shall be smoothed to eliminate any calculated rapid oscillations (period less than 0.1 seconds).	The core is represented by three non-interacting channels: hot channel represents hot assembly, average channel represents rest of the core assemblies, and total core bypass. The assumption of no crossflow between the core regions results in conservative flow distribution. Cladding swelling or rupture does not occur because the fuel does not encounter a CHF event and because the core remains covered throughout the LOCA event. Therefore, cross flows will not be impacted by geometrical changes in the fuel during the transient. Due to the mild nature of natural circulation flow during blowdown, rapid oscillations during the LOCA transient with a period less than 0.1 second do not occur. Therefore, smoothing is not necessary. Therefore, the required features of I.C.7.a are included in the NuScale LOCA EM, except that cross-flow is conservatively excluded from the model.
I.C.7.b Core Flow Distribution During Blowdown. (Applies only to pressurized water reactors)]: A method shall be specified for determining the enthalpy to be used as input data to the hot channel heatup analysis from quantities calculated in the blowdown analysis, consistent with the flow distribution calculations.	The intention of the I.C.7.b requirement was to ensure that LOCA EMs that assessed the hot channel separately would use the correct thermal-hydraulic boundary conditions. For the NuScale LOCA EM, the active core is represented by {{ }}$^{2(a),(c)}$ The hot channel is not analyzed in a separate code, but is included in the NPM model. (See Section 5.1.2.2 for core nodalization.) Therefore, the required features of I.C.7.b are included in the NuScale LOCA EM.

© Copyright 2016 by NuScale Power, LLC

10 CFR 50 Appendix K Required and Acceptable Feature	NuScale LOCA EM
I.D Post-Blowdown Phenomena; Heat Removal by the ECCS	
I.D.1 Single Failure Criterion: An analysis of possible failure modes of ECCS equipment and of their effects on ECCS performance must be made. In carrying out the accident evaluation the combination of ECCS subsystems assumed to be operative shall be those available after the most damaging single failure of ECCS equipment has taken place.	Safety-related system single failures considered for break spectrum calculations are discussed in Section 5.4.3. An evaluation of ECCS failure modes has been performed. Sensitivity studies were conducted to determine the limiting single failure for each type of LOCA. The results of break spectrum calculations are discussed in Section 9.0. Therefore, the required features of I.D.1 are included in the NuScale LOCA EM.
I.D.2 Containment Pressure: The containment pressure used for evaluating cooling effectiveness during reflood and spray cooling shall not exceed a pressure calculated conservatively for this purpose. The calculation shall include the effects of operation of all installed pressure-reducing systems and processes.	The NPM containment design is intended to equilibrate RCS and containment vessel (CNV) pressure when ECCS has been actuated. Condensed effluent will then be returned to the RCS in natural circulation flow. Although there are no active pressure-reducing systems, the CNV is immersed in the reactor pool, resulting in significant condensation and cooling of effluent prior to returning to the RPV. Therefore, the required features of I.D.2 are satisfied by design.

© Copyright 2016 by NuScale Power, LLC

10 CFR 50 Appendix K Required and Acceptable Feature	NuScale LOCA EM
I.D.3 Calculation of Reflood Rate for Pressurized Water Reactors: The refilling of the reactor vessel and the time and rate of reflooding of the core shall be calculated by an acceptable model that takes into consideration the thermal and hydraulic characteristics of the core and of the reactor system. The primary system coolant pumps shall be assumed to have locked impellers if this assumption leads to the maximum calculated cladding temperature; otherwise the pump rotor shall be assumed to be running free. The ratio of the total fluid flow at the core exit plane to the total liquid flow at the core inlet plane (carryover fraction) shall be used to determine the core exit flow and shall be determined in accordance with applicable experimental data (for example, "PWR FLECHT (Full Length Emergency Cooling Heat Transfer) Final Report," Westinghouse Report WCAP-7665, April 1971; "PWR Full Length Emergency Cooling Heat Transfer (FLECHT) Group I Test Report," Westinghouse Report WCAP-7435, January 1970; "PWR FLECHT (Full Length Emergency Cooling Heat Transfer) Group II Test Report," Westinghouse Report WCAP-7544, September 1970; "PWR FLECHT Final Report Supplement," Westinghouse Report WCAP-7931, October 1972). The effects on reflooding rate of the compressed gas in the accumulator which is discharged following accumulator water discharge shall also be taken into account.	Refilling or reflooding is not required for the NuScale design as in a conventional PWR, because there is no core uncovery (see the results of LOCA break spectrum calculations in Section 9.0). This requirement is not relevant to the NuScale LOCA EM. There are no primary system coolant pumps, so the requirements related to pump models are satisfied by the NuScale design. Also, there are no accumulators, so requirements related to accumulator discharge are satisfied by being designed out of the NPM.

© Copyright 2016 by NuScale Power, LLC

10 CFR 50 Appendix K Required and Acceptable Feature	NuScale LOCA EM
I.D.4 Steam Interaction with Emergency Core Cooling Water in Pressurized Water Reactors: The thermal-hydraulic interaction between steam and all emergency core cooling water shall be taken into account in calculating the core reflooding rate. During refill and reflood, the calculated steam flow in unbroken reactor coolant pipes shall be taken to be zero during the time that accumulators are discharging water into those pipes unless experimental evidence is available regarding the realistic thermal-hydraulic interaction between the steam and the liquid. In this case, the experimental data may be used to support an alternate assumption.	Refilling or reflooding is not required for the NuScale design as in a conventional PWR, because there is no core uncovery (see the results of LOCA break spectrum calculations in Section 9.0). Traditional concerns regarding steam interaction with injected ECCS water are not a factor in the NuScale design, although the phenomenon of non-equilibrium conditions existing between steam and subcooled liquid does occur. For the NuScale design, such interactions could occur in either the CNV or in the downcomer when subcooled containment liquid enters from the RRVs. While I.D.4 is not relevant to the NuScale LOCA EM, the intent of this requirement is addressed by the capability of NRELAP5 to model thermal non-equilibrium states and by the NPM design which minimizes these phenomena. Therefore, the required features of I.D.4 are satisfied by design.

© Copyright 2016 by NuScale Power, LLC

10 CFR 50 Appendix K Required and Acceptable Feature	NuScale LOCA EM
I.D.5.a (Refill and Reflood Heat Transfer for Pressurized Water Reactors): For reflood rates of one inch per second or higher, reflood heat transfer coefficients shall be based on applicable experimental data for unblocked cores including FLECHT results ("PWR FLECHT (Full Length Emergency Cooling Heat Transfer) Final Report," Westinghouse Report WCAP-7665, April 1971). The use of a correlation derived from FLECHT data shall be demonstrated to be conservative for the transient to which it is applied; presently available FLECHT heat transfer correlations ("PWR Full Length Emergency Cooling Heat Transfer (FLECHT) Group I Test Report," Westinghouse Report WCAP-7544, September 1970; "PWR FLECHT Final Report Supplement," Westinghouse Report WCAP-7931, October 1972) are not acceptable. Westinghouse Report WCAP-7665 has been approved for incorporation by reference by the Director of the Federal Register. A copy of this report is available for inspection at the NRC Library, 11545 Rockville Pike, Rockville, Maryland 20852-2738. New correlations or modifications to the FLECHT heat transfer correlations are acceptable only after they are demonstrated to be conservative, by comparison with FLECHT data, for a range of parameters consistent with the transient to which they are applied.	Refilling or reflooding is not required for the NuScale design as in a conventional PWR, because there is no core uncovery (see the results of LOCA break spectrum calculations in Section 9.0). This requirement is not relevant to the NuScale LOCA EM. Therefore, the required features of I.D.5.a are satisfied by design.
I.D.5.b (Refill and Reflood Heat Transfer for Pressurized Water Reactors): During refill and during reflood when reflood rates are less than one inch per second, heat transfer calculations shall be based on the assumption that cooling is only by steam, and shall take into account any flow blockage calculated to occur as a result of cladding swelling or rupture as such blockage might affect both local steam flow and heat transfer.	Refilling or reflooding is not required for the NuScale design as in a conventional PWR, because there is no core uncovery (see the results of LOCA break spectrum calculations in Section 9.0). This requirement is not relevant to the NuScale LOCA EM. Therefore, the required features of D.5.b are satisfied by design.
I.D.6.Convective Heat Transfer Coefficients for Boiling Water Reactor Fuel Rods Under Spray Cooling.	The NuScale plant is not a BWR and does not have core spray cooling. Therefore, this requirement is not applicable to the NuScale LOCA EM.

© Copyright 2016 by NuScale Power, LLC

10 CFR 50 Appendix K Required and Acceptable Feature	NuScale LOCA EM
I.D.7 The Boiling Water Reactor Channel Box Under Spray Cooling.	The NuScale plant is not a BWR and does not have channel boxes. Therefore, this requirement is not applicable to the NuScale LOCA EM.

2.2.3 Other Requirements

Per the Design-Specific Review Standard for NuScale SMR Design, Section 4.4 (Reference 7), the thermal-hydraulic design should account for the effects of crud in the CHF calculations in the core or in the pressure drop throughout the RCS. NuScale will require that the fuel supplied for the NPM be supported with a qualified and approved product that supports this regulatory requirement. It is, however, acknowledged that crud deposition is driven by factors beyond fuel design, such as operating conditions and RCS chemistry. In order to evaluate the impact of crud on the LOCA FOMs, NuScale has evaluated the effect of the changes in thermal properties of the maximum credible crud thickness on fuel centerline and cladding temperatures during a LOCA. This evaluation determined that while the initial stored energy did increase as a result of crud, there was no significant impact on the LOCA response.

© Copyright 2016 by NuScale Power, LLC

3.0 NuScale Power Module Description and Operations

3.1 General Plant Design

The NuScale Power Plant consists of one or more Reactor Modules (RXM), each of which is a small, passive PWR. The RXM consists of the nuclear steam supply system (NSSS), which includes the nuclear core, the helical coil SGs and the pressurizer, within a single pressure vessel and the compact steel CNV that houses the NSSS.

Unique features of the NuScale plant design include the following:

- reduced core size
- natural circulation reactor coolant flow (i.e., no reactor coolant pumps)
- integrated SG and a pressurizer inside the RPV. As a result, there is no piping connecting the SG or pressurizer with the reactor
- simplified passive safety-related systems that do not rely on ECCS pumps, accumulators, and water storage tanks (e.g., core makeup tank, in-containment refueling water storage tank)
- high-pressure steel containment
- containment immersed in a water-filled pool providing an effective passive heat sink for emergency cooling

The NPM is designed to operate efficiently at full-power conditions using natural circulation as the means of providing core coolant flow, eliminating the need for reactor coolant pumps. As shown in Figure 3-1, the reactor core is located inside a shroud connected to the hot leg riser. The reactor core heats reactor coolant, decreasing its density, causing the coolant to flow upward through the riser. When the heated reactor coolant exits the riser, it passes across the tubes of the helical coil SG, which acts as a heat sink. As the reactor coolant passes over the SG tubes, it cools, increases in density, and naturally circulates down the downcomer to the reactor core where the cycle begins again.

The NPMs are immersed in a reactor pool and protected by passive safety-related systems. Each NPM has a dedicated ECCS, chemical and volume control system (CVCS), and decay heat removal system (DHRS).

NuScale has achieved a substantial improvement in safety over existing plants through simplicity of design, reliance on passive safety-related systems, and small fuel inventory. The definition of a LOCA in 10 CFR 50.46(c)(1) addresses the geometry of a typical PWR, in which reactor coolant piping connects the RPV to primary system components external to the RPV. In the NuScale Power Plant design, all primary components are integral to the RPV, eliminating external coolant loops and pressurizer piping, which significantly reduces the number of possible LOCA scenarios.

© Copyright 2016 by NuScale Power, LLC

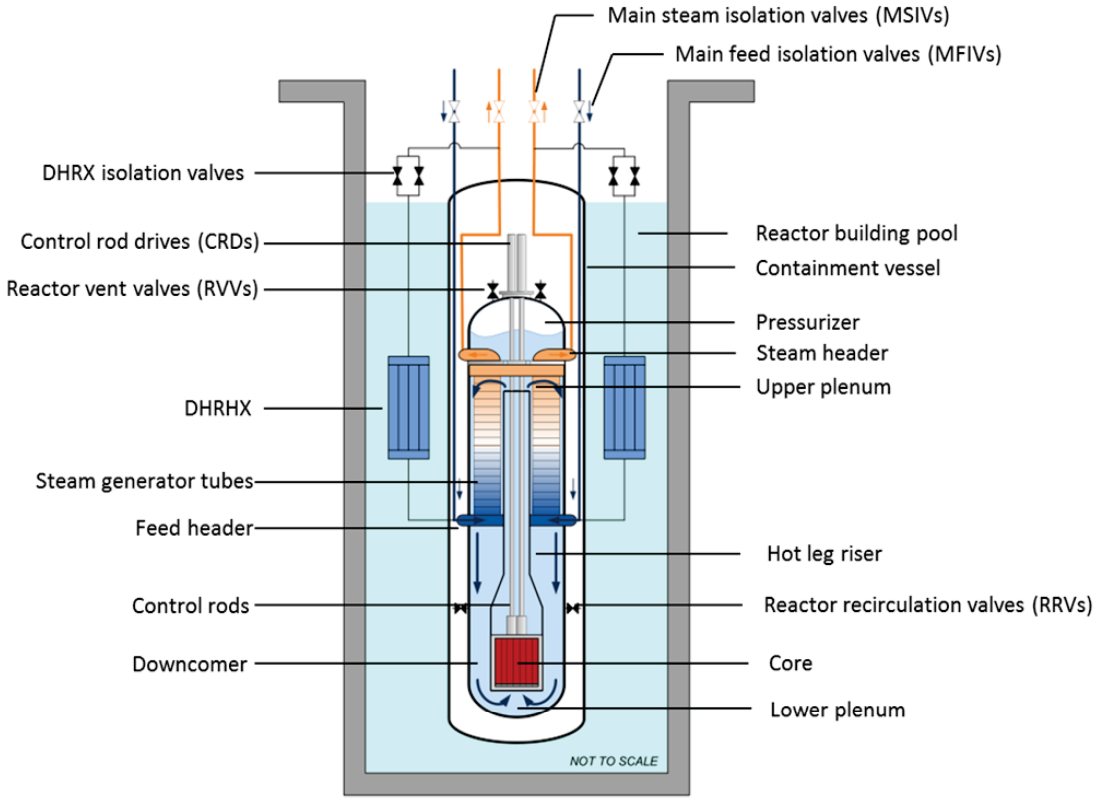

Figure 3-1. A single NuScale Power Module during normal operation

The potential break sizes included in the LOCA EM include the possible spectrum of breaks that can result in a break flow that exceeds the capability of the CVCS.

The NPM piping break locations are few (when compared to conventional PWR designs), and consist of the RCS injection and discharge lines, pressurizer spray supply line, and pressurizer high point vent line. These connections can be grouped into penetrations that are high on the RPV (pressurizer steam space) and low on the RPV (penetrate into an area which is normally in a liquid condition). All of the penetrations in the NPM design are at an elevation above the top of the core.

The NPM was designed with the intent of reducing the impact of a LOCA event. All LOCAs result in the actuation of both the ECCS and the DHRS. As shown in Figure 3-2, the ECCS consists of independent RVVs and independent RRVs.

The ECCS is initiated by opening the RVVs exiting the top of the RPV and the RRVs entering the RPV in the downcomer region (above the core elevation). Opening the valves allows the RPV and the CNV pressure to equalize which creates a natural circulation path to remove decay heat from the core. Water that is vaporized in the core leaves as steam through the RVVs, is condensed and collected in the CNV, and is then returned to the downcomer region inside the RPV through the RRVs by natural circulation.

© Copyright 2016 by NuScale Power, LLC

The CNV is sized such that the displacement of liquid from the RPV into containment will result in the liquid level being above the RRVs (which are located above the core) establishing a natural circulation loop. By the time the natural circulation pattern forms, the outside of the RPV will be cool enough that boiling on the outside of the RPV is relatively limited and the liquid level in the containment will have minimum swelling. The natural circulation loop removes decay heat from the core and RPV, and deposits it in containment. Heat deposited in containment is transferred by conduction and convection to the water in the reactor pool.

Following actuation of the ECCS, heat removal through the CNV rapidly reduces reactor and containment pressures and temperatures, and maintains them at acceptably low levels for extended periods of time. Because the CNV is evacuated to a low absolute pressure during normal operation (i.e., vacuum), only a small amount of non-condensable gas will be present inside the CNV at the beginning of the event.

The DHRS provides additional capacity to remove decay heat during the initial blowdown period of a LOCA, but it is neither required nor credited for such events. The DHRS provides secondary-side reactor cooling when normal feedwater is not available. The system, as shown in Figure 3-1, is a closed-loop, two-phase natural circulation cooling system. Two trains of decay heat removal equipment are provided, one attached to each SG loop. Each train is independently capable of removing 100 percent of the decay heat load and can cool the reactor primary-side inventory. Each train has a passive condenser submerged in the reactor pool. The condensers are maintained with sufficient water inventory for stable operation.

Analyses using the EM described in this report show that LOCAs do not challenge the safety of an NPM (see the results of LOCA break spectrum calculations in Section 9.0).

© Copyright 2016 by NuScale Power, LLC

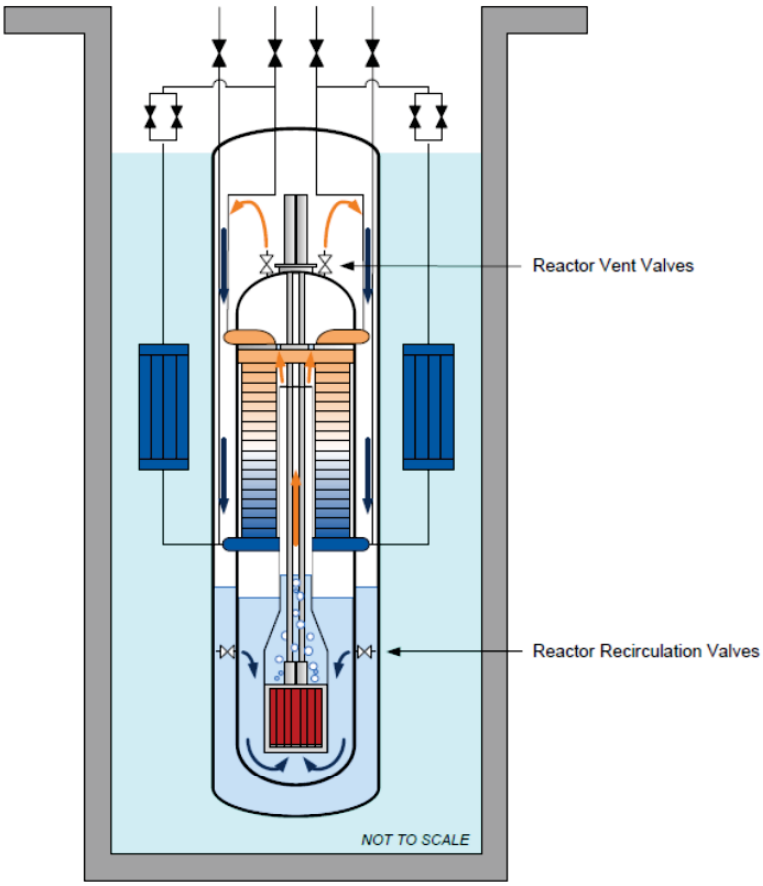

Figure 3-2. Schematic of NuScale Power Module decay heat removal system and emergency core cooling system during operation

3.2 Plant Operation

This LOCA EM initiates the analyses of an NPM with 102 percent full-rated power operation (as required by 10 CFR 50 Appendix K). This assumption represents the uncertainty in the initial power.

Pressurizer heaters and a spray system are used to maintain nominal operating pressure similar to conventional PWRs. The reactor coolant is driven by natural circulation. At nominal full-power conditions, the flow rate is dependent on the fluid density differences through the loop, the losses incurred along the loop, and the elevation difference between the core and the SG.

During nominal full-power conditions, the control rods are retracted up to or above their insertion limits. Borated water is used as the primary coolant and the CVCS regulates the boron concentration to maintain criticality. The CVCS provides reactor inventory make-up through the RCS injection line in the riser and inventory let-down through a separate RCS discharge line in the downcomer region.

© Copyright 2016 by NuScale Power, LLC

The secondary side is operated such that the SGs remove the heat generated by the reactor core. The DHRS heat exchangers are isolated from the steam line and do not remove heat during normal operation.

The containment is evacuated during normal operation to provide an insulated barrier between the reactor and containment; no physical RPV insulation is present inside containment.

3.3 Safety-Related System Operation

The NuScale Module Protection System (MPS) is composed primarily of the reactor trip system and the engineered safety features actuation system. The MPS protection functions are limited to automated safety responses to off-normal conditions. The MPS functional response to an initiating event is a reactor trip; isolation (as necessary) of main feedwater, main steam, CVCS, and containment; followed by an integrated safety actuation of one or more of the passive safety-related systems (DHRS and ECCS). Containment isolation is achieved by closing of the following containment isolation valves:

- CVCS isolation valves
  - CVCS makeup line
  - CVCS letdown line
  - CVCS pressurizer spray supply line
  - CVCS high point degasification line,
- reactor component cooling water system isolation valves
- main steam system isolation valves
- feedwater system isolation valves
- containment flood and drain system isolation valves
- containment evacuation system isolation valves

Dual safety-related isolation valves are installed on piping for the CVCS, containment evacuation system, containment flood and drain system, and reactor component cooling water system. There is one safety-related containment isolation valve in the main steam and feedwater piping penetrating containment with a redundant nonsafety-related isolation valve for each safety-related valve.

The reactor trip system consists of four independent separation groups with independent measurement channels to monitor plant parameters that can generate a reactor trip. Each measurement channel trips when the parameter exceeds a predetermined setpoint.

The engineered safety features actuation system also consists of four independent separation groups with independent measurement channels that monitor plant parameters that activate the operation of the engineered safety features.

© Copyright 2016 by NuScale Power, LLC

3.3.1 Emergency Core Cooling System

The ECCS is a two-phase natural circulation system that maintains a liquid water supply to the core during its operation in a LOCA scenario. This results in a collapsed liquid level in the RPV that is above the top of the core.

The ECCS consists of three independent RVVs and two independent RRVs. It is initiated by simultaneously actuating the RVVs on the top of the RPV in the pressurizer region and the RRVs on the side of the RPV in the downcomer region. The RRVs are designed to provide a low-resistance flow path for coolant to flow from the CNV into the RPV. The RVVs are designed to equalize pressure between the two vessels allowing steam from the reactor to vent to the containment and to provide hydrostatic equalization that allows coolant flow through the RRVs back into the reactor.

The ECCS actuation creates a steam flow path from the pressurizer to the containment and an RPV downcomer flow path to and from containment.

The RPV depressurizes due to liquid and steam exiting the ECCS valves. Steam entering containment is condensed on the containment wall, which in turn is cooled by the reactor pool. Initially, the containment pressure will increase to a peak, and then decrease as flow from the RPV decreases and heat is transferred from the CNV to the reactor pool. The RPV water inventory decreases while the containment level increases due to inventory transferred from the RPV.

As the pressure between the two vessels reach a near-equilibrium condition, the collapsed liquid level in the containment rises to a level higher than the RRV elevation, creating enough static head to overcome the pressure difference between the RPV and CNV. At this point, the condensed liquid in containment enters the RPV through the RRVs while steam exits the RPV through the RVVs. This stable process continues maintaining a collapsed water level above the top of the active fuel.

All ECCS valves are equipped with an inadvertent actuation block (IAB), the feature that prevents spurious opening of the ECCS valves at full operating pressure. The IAB prevents the valves from opening when the differential pressure between the RPV and CNV is greater than the IAB threshold pressure setpoint. After the IAB has blocked a spurious opening of the ECCS valve, it allows the valve to open only after the differential pressure between the RPV and CNV has decreased below the IAB release pressure setpoint.

3.3.2 Decay Heat Removal System

The DHRS is a passive safety-related system that relies on natural circulation to remove heat from the RCS through the SG and reject heat to the reactor pool through the DHRS condenser. The DHRS is composed of two DHRS trains associated with one of the two NPM SGs. Each DHRS train is capable of independently removing 100 percent of decay heat. The DHRS piping connects to the main steam and feedwater lines specific to the associated SG. During normal operation, the DHRS condenser and piping are isolated by

© Copyright 2016 by NuScale Power, LLC

valves on the steam side of the SG. The condensate side of the DHRS is open to the feedwater piping supplying the associated SG.

Upon actuation of the DHRS, the SG feedwater and steam isolation valves close and the DHRS isolation valves open, creating a closed loop between the SG and DHRS condenser. Both liquid and vapor are contained in the DHRS on system actuation. Because the DHRS is a closed system, the total water mass remains constant during the system operation.

For successful operation, liquid water enters the SG through the feedwater line and is boiled by heat from the RCS. The vapor exits the SG through the steam line and is directed to the DHRS condenser where it condenses back to liquid before return to the SG. Thus, the loop transfers heat from the RCS to the DHRS fluid and then from the DHRS to the reactor pool water.

The bottom of the DHRS condenser is located above the bottom of the SG providing the static head to drive natural circulation.

The DHRS provides additional capacity to remove decay heat during the initial blowdown period of a LOCA. However, the break spectrum calculation (see Section 5.4) includes sampling conditions where both the DHRS trains are excluded. Not crediting DHRS operation provides results that cover the full range of possible DHRS performance conditions (including full failure).

© Copyright 2016 by NuScale Power, LLC

4.0 Phenomena Identification and Ranking

4.1 Phenomena Identification and Ranking Process

The purpose of the NuScale LOCA PIRT is to provide an assessment of the relative importance of phenomena and processes that may occur in the NPM during LOCA conditions in relation to specified FOMs. The PIRT assessment is part of the EMDAP process prescribed by RG 1.203.

The initial NuScale LOCA PIRT was developed in 2008. This PIRT was subsequently updated in 2013 and 2015 to address the design changes. The initial PIRT and the PIRT updates have been developed by a panel of recognized industry experts and NuScale subject matter experts, and are built upon the state-of-knowledge at the time of their development. The panel members of the initial LOCA PIRT were

- Dr. Brent Boyack (Los Alamos National Laboratory, retired)
- Dr. Larry Hochreiter (Pennsylvania State University)
- Dr. Mujid Kazimi (Massachusetts Institute of Technology)
- Dr. Jose Reyes (NuScale Power, Inc.)
- Dr. Kord Smith (Studsvik Scandpower, Inc.)
- Dr. Graham Wallis, Chair (Darthmouth University, Creare, Inc.)

The panel members for the 2013 NuScale LOCA were

- Mr. Steve Congdon (GE Nuclear Energy, retired)
- Dr. Tom George (Zachry Nuclear Engineering)
- Mr. Craig Peterson (Computer Simulation and Analysis)
- Dr. Jose Reyes (NuScale Power, Inc.)
- Mr. Gregg Swindlehurst (GS Nuclear Consulting, LLC)
- Dr. Graham Wallis, Chair (Darthmouth University, Creare, Inc.)

The panel members for the 2015 NuScale LOCA were

- Mr. Steve Congdon (GE Nuclear Energy, retired)
- Dr. Tom George (Zachry Nuclear Engineering)
- Dr. Jose Reyes (NuScale Power, Inc.)
- Mr. Gregg Swindlehurst (Chair, GS Nuclear Consulting, LLC)
- Dr. Graham Wallis, Chair (Darthmouth University, Creare, Inc.)

The 2015 NuScale LOCA PIRT incorporates lessons learned from testing and insights gained from computer code simulations of many LOCA scenarios.

© Copyright 2016 by NuScale Power, LLC

The PIRT panel received an in-depth briefing on the NPM design, LOCA sequence of events, and computer code predictions of the response of the NPM to LOCA scenarios. The panel then followed the PIRT process by first identifying the structures, systems, and components (SSC) of the NPM that were associated with the LOCA scenario. The LOCA scenario was then separated into phases with each phase representing a distinct process-dominated time period. Then FOMs were selected for each phase. Specifically, the FOMs were chosen to be quantifiable measures of the systems potential to meet regulatory safety limits. Phenomena were identified for each SSC for each phase, and the phenomena were ranked considering their level of importance relative to the FOMs. The panel also established a knowledge ranking for each of the phenomena.

The first NuScale LOCA PIRT was developed in 2008. This PIRT was subsequently updated in 2013 and 2015, primarily to address the changes in NPM design and operation. The PIRT panel was reconvened for each PIRT update and was presented with the changes in NPM design and their impact on progression of LOCA. The biographical information for each PIRT panel member is included with each PIRT release. The 2015 NuScale LOCA PIRT is used for the development of LOCA EM.

The following section provides a brief description of the LOCA scenarios and the accident phases considered for the PIRT developed. The definitions of the selected FOMs and the importance and knowledge ranking categories are summarized. Finally, the list of phenomena that were ranked as high importance by the PIRT panel in at least one of the phases of the NuScale LOCA scenarios is provided along with the brief description of the rational for assigned importance and knowledge level rankings. The rankings for all the identified phenomena and detailed description of the rationale are available in the 2015 NuScale LOCA PIRT report.

4.2 Loss-of-Coolant Accident Scenarios

Loss-of-coolant accidents are postulated breaks in the reactor coolant pressure boundary that result in leakage of reactor coolant at a rate exceeding the capability of the normal reactor coolant makeup system, as defined in 10 CFR 50.46(c)(1).

Breaks of various sizes, types, and orientations are postulated to occur in piping connected to the RPV. With the elimination of most primary coolant piping in the NPM design, breaks are limited to RCS injection and discharge lines, pressurizer spray supply line, and pressurizer high point vent line.

Two types of LOCA scenarios were addressed in the PIRT development process. The first type of LOCA scenarios were {{

}}2(a),(c) Section 9.1 provides further description of the progression of each LOCA scenario.

© Copyright 2016 by NuScale Power, LLC

The PIRT panel divided the NPM LOCA scenarios into two phases for the phenomena identification:

LOCA blowdown (Phase 1a)

Phase 1a begins with a postulated breach in the RCS pressure boundary that initiates the blowdown of the RCS into the CNV and ends when the MPS actuates ECCS to open the RVVs and RRVs.

ECCS actuation (Phase 1b)

Phase 1b begins when the MPS actuates ECCS to open the RVVs and RRVs and ends when the recirculation flow is established. The pressures and levels in containment and RPV approach a stable condition (i.e., initiation of long-term cooling).

4.3 Figures of Merit

The safe operation of the NPM was considered in the primary design phase. This produced a reactor system that protects the fuel using simple passive safety features. The NPM retains sufficient water in the RPV that the core will not be uncovered. For such a system, the LOCA PCT occurs at time zero (normal operating temperature). There is no heatup due to CHF or uncovering the core after event initiation; PCT remains below the 10 CFR 50.46 acceptance criterion of 2,200 degrees Fahrenheit (1,204 degrees Celsius) throughout the event. Hence, PCT is not an FOM for the NuScale PIRT process.

The critical heat flux ratio (CHFR) is an important FOM as it demonstrates there is no significant heatup of the cladding. One of the primary design fundamentals of the NPM is to protect the fuel from a CHF event. Therefore, an assessment of CHF becomes important.

Collapsed liquid level above the core is an additional FOM as it demonstrates there is an adequate supply of liquid water available to the core. Heatup of the fuel will not occur under LOCA conditions as long as the core is covered with coolant and CHF conditions do not exist.

To ensure ECCS performance, the containment must be intact and remain below pressure and temperature design limits. Consequently, peak containment pressure and temperature are evaluated to ensure compliance with 50.46 criteria. However, the peak containment pressure and temperature for containment performance are calculated with a different methodology.

4.4 Definitions of Importance and Knowledge Level Rankings

Each phenomenon identified in the PIRT was assigned an importance ranking and knowledge level ranking. Table 4-1 and Table 4-2 describe the importance rankings and knowledge level rankings developed by the PIRT panel.

© Copyright 2016 by NuScale Power, LLC

Table 4-1. Importance rankings

Importance Ranking	Definition
High (H)	Significant influence on FOM
Medium (M)	Moderate influence on FOM
Low (L)	Small influence on FOM
Inactive (I)	Phenomenon not present or negligible

Table 4-2. Knowledge levels

Knowledge Level	Definition
4	Well known/small uncertainty
3	Known/moderate uncertainty
2	Partially known/large uncertainty
1	Very limited knowledge/uncertainty cannot be characterized

4.5 Systems, Structures, and Components

To aid in the identification of phenomena, the PIRT panel divided the NPM into the SSC presented in Table 4-3. Phenomena were then identified in each SSC and for two of the LOCA phases.

Table 4-3. Systems, structures, and components

Containment Vessel	Reactor Pressure Vessel	Decay Heat Removal System	Reactor Building Pool
• RPV heat source • Containment vessel heat sink • RRVs • RVVs • Break	• Reactor core • Hot leg riser • Pressurizer • RRVs • RVVs • Break • Upper plenum • Downcomer • SG shell side (primary) • SG tube side (secondary) • LP	• Decay heat removal heat exchanger • DHRS isolation valves • SG	Reactor Building pool

4.6 High-Ranked Phenomena

Separate PIRTs were developed for the two types of LOCA scenarios defined in Section 4.2. More than 80 phenomena were identified and ranked in each PIRT. Only a few differences were identified between the two LOCA scenarios with respect to the

© Copyright 2016 by NuScale Power, LLC

phenomena that might occur and their associated ranking. Table 4-4 summarizes the phenomena that were ranked as high importance by the PIRT panel in at least one of the two phases of the LOCA Scenarios 1 and 2. The knowledge level assigned by the PIRT panel is also included. These high-ranked phenomena are addressed in the development of NuScale LOCA EM. These phenomena and the rationale for their ranking are briefly described below.

© Copyright 2016 by NuScale Power, LLC

Table 4-4. High-ranked phenomena

{{

}}2(a),(c)

© Copyright 2016 by NuScale Power, LLC

{{

}}2(a),(c)

4.6.1 Discussion of Phenomena Ranked High Importance

{{

}}2(a),(c)

© Copyright 2016 by NuScale Power, LLC

{{

}}2(a),(c)

© Copyright 2016 by NuScale Power, LLC

{{

}}2(a),(c)

© Copyright 2016 by NuScale Power, LLC

{{

}}2(a),(c)

© Copyright 2016 by NuScale Power, LLC

{{

}}2(a),(c)

4.7 Phenomena Identification and Ranking Table Summary

Some of the high-ranked phenomena identified in the NuScale PIRT are also important for existing reactors and have been the subject of considerable model development, testing, and analysis. Other phenomena are more unique to the NPM design due to the natural circulation coolant flow, integral RCS design, helical coil SG, unique passive ECCS and DHRS, reactor pool as the ultimate heat sink, and high-pressure containment. Phenomena associated with the helical coil SG and the DHRS are not ranked high importance because these systems do not play a significant role in determining the LOCA response with the assumptions used in this EM. {{

}}2(a),(c) However, the LOCA break analysis in Section 9.3 shows that not crediting the DHRS adds significant conservativism for these breaks. Since DHRS is assumed not available the phenomena are not ranked high importance.

Some of the unique phenomena have a more developed knowledge base due to occurrence of the phenomena in other designs with different geometries, e.g., natural circulation. The PIRT identified the phenomena within the specified components as the high-importance phenomena that have a low-knowledge level. These high importance, low knowledge phenomena are given the greatest focus in the development of the LOCA EM. {{

}}2(a),(c)

© Copyright 2016 by NuScale Power, LLC

5.0 Evaluation Model Description

This section provides a detailed description of the NPM LOCA model. The nodalization and modeling options selected for each NPM component are discussed along with the rationale for each choice. Justification is provided for the boundary and initial conditions selected for the model. A description of a break spectrum consistent with the requirements of 10 CFR 50 Appendix K is also provided.

The NPM LOCA model is consistent with the SET and IET assessments used to validate NRELAP5 (see Section 7). The model follows the recommended best practices for the preparation of a RELAP5-3D© input (Reference 8) that are applicable to the NRELAP5 LOCA model, as well as the NuScale-specific LOCA guidelines summarized in this report. The model conforms to the applicable requirements of 10 CFR 50 Appendix K, as described in Section 2. The results of the break spectrum calculations and the sensitivity studies (i.e., nodalization, time step, initial and boundary conditions, and selected model parameters) that supported the development of the LOCA EM are summarized in Section 9. Specific initial and boundary condition values and the inputs for other key model parameters are specified in Appendix A.

5.1 NRELAP5 Loss-of-Coolant Accident Model for the NuScale Power Module

The unique design features of the NPM permit a simple and reliable approach to evaluate and mitigate the consequences of postulated LOCAs by:

- ensuring that all LOCAs are contained within the containment pressure vessel by designing the NPM such that the isolation of the CNV is a safety-related system.
- actuating the ECCS valves, which depressurizes the RPV into the CNV to establish pressure equalization to allow return of discharged fluid back into the RPV to cool the core.
- maintaining stable natural circulation flow through the ECCS valves with the reactor pool acting as the ultimate heat sink.

In the event of a LOCA, these design features result in a simple, predictable transient progression, that can be explained by a standard mass and energy balance over the RPV and CNV considering:

- choked or unchoked flow through the break and ECCS valves between RPV and CNV.
- core decay heat generation and RCS stored energy release, heat transfer between CNV and reactor pool that is characterized by steam condensation at the CNV inside surface and free convection at the CNV outside surface to reactor pool.

5.1.1 General Model Nodalization

The NRELAP5 model for analyzing a NPM LOCA is developed by reviewing the postulated scenarios and the key phenomena described in the NuScale LOCA PIRT, summarized in Section 4. The model describes the key components of the NPM participating in a LOCA, as follows:

© Copyright 2016 by NuScale Power, LLC

- RPV with internals
  - LP
  - reactor core
  - riser including the riser upper plenum
  - upper and lower downcomer
  - pressurizer
- CNV
- SG secondary side with DHRS condensers
- reactor pool
- ECCS valves
- postulated break locations
- RPV internal heat structures and heat structures between components (i.e., RPV to CNV to reactor pool)

The nodalization diagram of these key components is shown in Figure 5-1. The details of the NRELAP5 NPM model are described in the following sections.

© Copyright 2016 by NuScale Power, LLC

{{

}}2(a),(c)

Figure 5-1. Noding diagram of NRELAP5 loss-of-coolant accident input model for NuScale Power Module

5.1.2 Reactor Coolant System

The RCS model is composed of the LP, reactor core, riser (lower, transition, and upper sections), riser plenum, downcomer (upper section containing the helical coil SGs and lower section), and pressurizer.

© Copyright 2016 by NuScale Power, LLC

5.1.2.1 Lower Plenum

{{

}}2(a),(c)

5.1.2.2 Reactor Core

5.1.2.2.1 General Model

The reactor core assembly is modeled with {{

}}2(a),(c)

Various passive heat structures inside the reactor core are also considered to increase the release of the stored energy accumulated in non-heat-generating structures with appreciable metal mass. These structures include:

- core support assembly including core barrel, reflector, upper support blocks, and lower core plate,

© Copyright 2016 by NuScale Power, LLC

- additional mass in fuel assemblies including top and bottom nozzles, upper and lower end caps, spacer grids, control rod assembly, instrument guide tubes, and springs.

5.1.2.2.2 Initial Power

In accordance with 10 CFR 50 Appendix K, Section I.A, the initial reactor power level is set to 102 percent of the rated thermal power to account for two percent measurement uncertainty. With a rated thermal power of 160 MWt, the initial reactor power before the initiation of a postulated LOCA is 163.2 MWt.

5.1.2.2.3 Core Power Distribution

The power distribution {{

}}[2(a),(c)] The sensitivity calculations presented in Section 9.6.6 show that axial power shape has negligible impact on LOCA FOMs.

5.1.2.2.4 Fuel Stored Energy

The fuel rods are initialized at the maximum initial stored energy condition as required by 10 CFR 50 Appendix K, Section I.A.1. The UO_2 fuel thermal conductivity, volumetric heat capacity, and fuel-cladding gap conductance are considered to be the key thermo-physical properties defining the stored energy in the fuel, as the amount of stored energy is inversely proportional to the thermal diffusivity of the fuel and fuel-cladding gap conductance. Based on the burnup-dependent fuel performance analysis provided by the fuel vendor, choosing {{

}}[2(a),(c)] Additional details regarding the specification of thermal properties are provided in Appendix A.

All reactor core power is deposited into the fuel pellet directly, conservatively neglecting direct moderator heating and heat deposition to in-core materials. This approach is conservative as it maximizes the initial stored energy of the fuel.

5.1.2.2.5 Point Kinetics Model and Decay Heat

The reactor kinetics model accounts for fission power due to prompt and delayed neutrons, decay power due to fission products, and actinides.

The reactivity equations are solved using a point kinetics model with the ‘separable’ option (see Section 6.4) to calculate the fission power. This model simulates reactivity changes due to reactor trip and feedback reactivity due to Doppler and moderator density effects. The reactivity change due to the insertion of control rods is modeled using a scram reactivity table as a function of time after the reactor trip. The table reflects conservative representations for the onset of rod motion, the rod position as a function of time after trip

© Copyright 2016 by NuScale Power, LLC

and the inserted reactivity as a function of rod position. The scram rod total worth considers that the most reactive rod remains stuck and does not insert into the core following reactor trip. Sensing signal delays are accounted for based on the instrument type (e.g., pressure and temperature) to determine if a reactor trip should be initiated and an additional delay is added to account for the initiation of rod insertion.

The Doppler and moderator density feedback input parameters depend on the average fuel burn-up. The weighted average fuel temperature and moderator density for the feedback reactivity calculations consider the given core power (flux) distribution to be consistent with the point kinetics model. {{

}}2(a),(c)

Six groups of delayed neutron precursors are considered based on the SIMULATE analysis for different cycles, beginning-of-cycle, middle-of-cycle, and end-of-cycle. Beginning-of-cycle kinetic parameters are used as bounding for point kinetic input with the smallest prompt neutron lifetime to maximize initial energy inventory by prolonging the fission power transient. The variation in precursor decay constants is insensitive to the time in cycle. Additional biasing is introduced to all kinetic parameters to account for uncertainty in calculated values in such a way that the prompt lifetime is decreased and the decay constants for each precursor group are increased. The objective is to maximize the delayed neutron contribution to the total fission power.

The ‘gamma-ac’ option in the NRELAP5 point kinetics model activates the models for the transient effects of decay heat and actinides. Use of the actinides model complies with 10 CFR 50 Appendix K, Section I.A.3. The ANS71 option represents an explicit implementation of four time-dependent exponentials detailed in the draft ANS 73 decay heat standard and includes a built-in 1.2 multiplier. Activation of a trip associated with this option initiates evaluation of the power decay as a function of time. However, this time-evaluation of power does not account for post-trip prompt and delayed fissions that can add additional decay heat precursors and increase the integral heat release.

The ANS73 model represents an 11 group exponential fit of production and decay constants of the decay heat defined in the standard. User input of a 1.2 multiplier addresses 10 CFR 50 Appendix K requirements for addressing prediction uncertainties (10 CFR 50 Appendix K, Section I.A.4). Decay heat is predicted by the behavior of the 11 precursor groups, and no explicit reactor trip is applied. Instead the model predicts precursor concentrations from the prompt and delayed fissions rate, and so naturally follows fission power.

Sensitivities have determined that the ANS71 option requires careful selection of an additional delay time beyond a reactor trip before activating the power decay to account for post-trip prompt and delayed fissions. This delay time, which depends on control rod insertion speed and reactivity, can be more than {{ }}2(a),(c) seconds. Once the delay is accounted for, both options are consistent for short term LOCA through the first 1000 seconds. Considering the correct response of the ANS73 option without any special evaluation of delay times, the ANS73 option was chosen as the standard choice in the LOCA guideline.

© Copyright 2016 by NuScale Power, LLC

The best-estimate ANS79 actinides model is used to account for heat deposition from actinide decay. The actinide model includes the decay energies from the production and decay of ^{239}U, ^{239}Np, and ^{239}Pu.

5.1.2.3 Riser

{{

}}2(a),(c)

5.1.2.4 Downcomer

{{

}}2(a),(c)

5.1.2.5 Pressurizer

{{

}}2(a),(c)

© Copyright 2016 by NuScale Power, LLC

- {{ }}2(a),(c)

5.1.3 Helical Coil Steam Generators

Two helical coil SGs are represented using an NRELAP5-specific helical SG component that models the component-specific internal pressure drop and heat transfer effects, as described in Section 6.7. The independent SGs are thermally connected to the upper downcomer to transfer heat to the steam turbine during normal operation. During off-normal operations, each SG transfers energy to an independent safety-related DHRS (see Section 5.1.7) to discharge energy to the reactor pool.

The tube-to-coil diameter ratio is specific to the SG geometry. {{ }}2(a),(c)

5.1.4 Containment Vessel and Reactor Pool

{{ }}2(a),(c)

© Copyright 2016 by NuScale Power, LLC

The reactor pool represents the ultimate heat sink in the NuScale design. The reactor pool volume corresponding to an individual NPM is represented by a {{ }}2(a),(c) The upper portion of the reactor pool is thermally connected to the DHRS condensers while {{ }}2(a),(c) A wide range of initial reactor pool temperatures is exercised to show the effect of the pool conditions on the LOCA behavior.

{{ }}2(a),(c)

5.1.5 Chemical and Volume Control System

The entirety of the CVCS is not explicitly included in the LOCA model. The CVCS, a nonsafety-related system, is not automatically actuated. {{ }}2(a),(c)

Continued operation of the CVCS through operator action would add cold water that is non-conservative. The only CVCS piping represented in the model is the injection line from the RPV wall, through the downcomer and into the riser. It connects the charging line break to the containment vessel at the correct elevation and accounts for a small loss through the line. The discharging line connection at the downcomer, and the two spray supply line and high point vent line connections at the top of the pressurizer are used as break locations with no attached piping included. The volumes corresponding to removed CVCS piping constitute a small fraction of the total RPV and CNV volume.

{{ }}2(a),(c)

© Copyright 2016 by NuScale Power, LLC

5.1.6 Secondary System

The model represents the secondary feedwater and steam lines with two helical coil SGs, described in Section 5.1.3. {{ }}2(a),(c) The secondary side also contains the DHRS, described in Section 5.1.7.

{{ }}2(a),(c)

5.1.7 Decay Heat Removal System

Both DHRS trains are included in the NPM LOCA model. The two independent trains of the DHRS are safety-related systems; however, no credit is taken for operation of the DHRS in the LOCA methodology. The break spectrum calculation results discussed in Section 9.3 confirm that this assumption is highly conservative for LOCA analysis.

5.1.8 NRELAP5 Modeling Options

The NPM LOCA analysis is performed with the latest released version of NRELAP5. {{ }}2(a),(c)

5.1.8.1 Junction Options

{{ }}2(a),(c)

© Copyright 2016 by NuScale Power, LLC

Table 5-1. Default junction options for the NRELAP5 loss-of-coolant accident model

{{

}}2(a),(c)

© Copyright 2016 by NuScale Power, LLC

5.1.8.2 Volume Options

{{
}}2(a),(c) This format is described by Table 5-2.

Table 5-2. Default volume options for the NRELAP5 loss-of-coolant accident model

{{

}}2(a),(c)

5.1.8.3 Heat Structure Options

{{

}}2(a),(c)

© Copyright 2016 by NuScale Power, LLC

- {{

}}2(a),(c)

5.1.9 Time Step Size Control

The NuScale LOCA EM uses the NRELAP5 semi-implicit scheme for the solution of the hydrodynamics. The heat structure solution is implicitly coupled to the hydrodynamic solution. With given user-specified minimum and maximum time step sizes, the code determines the appropriate time step in such a way that

- the current time step cannot be larger than the courant-time step size determined based on the limiting volume.
- no significant mass error accumulation occurs during the solution and halving of the current time step when it is deemed necessary.

NRELAP5 provides the capability of providing the user-defined maximum time step size through the definition of control variable. A control variable that defines the fraction of the current courant time-step size during the solution is used to set the user-defined maximum time step size. This approach has the advantage of taking larger time steps when larger courant time step sizes exist during the solution; therefore, the code takes larger time steps when the solution indicates smooth transient progression. The maximum time-step size of {{ }}2(a),(c) of the problem courant time step size is used in the evaluation of the NPM LOCA break spectrum. A sensitivity study is performed on the fraction specified to demonstrate that the selected maximum time-step size has no or insignificant impact on the LOCA figures of merit such as peak containment pressure and collapsed liquid level in the RPV riser above the TAF.

© Copyright 2016 by NuScale Power, LLC

5.2 Analysis Setpoints and Trips

A number of safety-related measurements exist in the NPM to detect off-normal conditions. Table 5-3 shows the measurements relevant to LOCA analysis along with their functions.

Table 5-4 presents the list of actuation signals for the NPM safety-related systems and identifies the signals that are credited and not credited in the LOCA EM. The table footnotes provide important definitions for containment isolation and DHRS actuation. {{

}}2(a),(c)

Not crediting these and other measurements for the associated safety-related signals would delay the activation of reactor trip and the DHRS under certain conditions, which is conservative for LOCA analysis.

Table 5-3. NuScale Power Module safety-related system measurement parameters

{{

}}2(a),(c)

© Copyright 2016 by NuScale Power, LLC

Table 5-4. Safety-related system actuation signals

{{

}}2(a),(c)

The safety analysis analytical limits specify the setpoints (or range of setpoints) and the sensing delay for each safety-related signal. Table A-3 shows the setpoint values and the

© Copyright 2016 by NuScale Power, LLC

signal actuation delays used for the LOCA break spectrum calculation and the sensitivity calculations presented in Section 9.0. Table 5-5 shows the basis for the selection of the safety-related signal delays in the NuScale LOCA EM. Signals not credited either do not play a role in LOCA {{ }}2(a),(c) or act to provide additional conservatism in the delay of actuating safety-related systems that are only beneficial to the LOCA progression.

Table 5-5. Safety-related analysis signal delays

{{

}}2(a),(c)

© Copyright 2016 by NuScale Power, LLC

{{

}}2(a),(c)

{{

}}2(a),(c)

The mixture level detection uses a simple approximation of the mixture level based on {{

}}2(a),(c)

5.3 Initial Plant Conditions

Table 5-6 provides the basis for conservatively biasing the initial conditions for LOCA analysis. Table A-3 of Appendix A provides the specific ranges of NPM primary and secondary side initial or operational conditions. These ranges are intended to account for both the normal control system deadband and the system/sensor measurement uncertainty without specifically quantifying the portion of the range applied to either uncertainty.

© Copyright 2016 by NuScale Power, LLC

Table 5-6 Plant initial conditions

{{

}}2(a),(c)

5.4 Loss-of-Coolant Accident Break Spectrum

10 CFR 50 Appendix K describes the break spectrum as a set of LOCA scenarios that are uniquely defined based on location, configuration and size. Additional sensitivity studies were performed on availability of DHRS, availability of power, and postulated single failures. The break spectrum for the NuScale LOCA EM is summarized in this section.

5.4.1 Break Location

The postulated break locations in the NPM design are the RCS injection and discharge lines, the pressurizer spray supply line, and high point vent lines. These break locations establish a flow path between RPV and CNV leading to CNV pressurization during the early phase of LOCA (i.e., Phase 1a):

- The injection line enters the RPV through a shell penetration and piping internal to the RPV that passes through the downcomer and terminates at an upwardly-oriented nozzle in the riser.
- The discharge line is connected to a RPV penetration to the downcomer.

© Copyright 2016 by NuScale Power, LLC

- The pressurizer spray supply line is connected to the top of the pressurizer at two separate penetrations. At each penetration there is a nozzle within the RPV wall. Outside the RPV wall (but within the CNV), the pressurizer spray supply lines connect to a tee which in turn connects to isolation valves on the CNV wall.
- The high point vent line connects to the top of the pressurizer.

All of the connections to the RPV are normally open, except for the high point vent. Each connection can be isolated by two independent safety-related isolation valves in series that close on the containment isolation signal. As a result, all discharged break fluid is retained within the CNV for eventual return to the RPV when ECCS actuates.

5.4.2 Break Configuration and Size

Table 5-8 summarizes the size and location of the breaks considered as part of the break spectrum of the NuScale LOCA EM. {{

}}2(a),(c),ECI

© Copyright 2016 by NuScale Power, LLC

{{

}}2(a),(c),ECI

Table 5-7. Summary of analyzed break sizes

{{

}}2(a),(c),ECI

5.4.3 Single Failures

10 CFR 50 Appendix K requires that single failures be considered within the break spectrum. This includes analyzing a system/component classified as nonsafety related if the inclusion of that system/component would introduce a more limiting condition. The following scenarios are considered:

- no single failure
- failure of a single RVV to open
- failure of a single RRV to open
- failure of one ECCS division (i.e., one RVV and one RRV)

The ECCS valves are held closed with direct current (DC) power and operate on two independent divisions. Each division controls one RRV and one RVV. The third RVV is connected to both Division 1 and 2. Removal of DC power from any division will cause the solenoid to release for this third RVV (ready to open pending dropping below the IAB release pressure). Two modes of failure can be postulated: (1) failure to actuate a division upon actuation request and (2) inadvertent actuation of a division.

In the event of failure of the actuation of a division, the DC power from one division is not removed when it should be removed. The result is one RRV and two RVVs actuating, with

© Copyright 2016 by NuScale Power, LLC

one RRV and one RVV not actuating. This scenario is explicitly analyzed within the LOCA EM.

In the event of an inadvertent actuation of a division (removal of DC power from that division) two RVVs and one RRV will be available to open immediately. The IAB setpoint will prevent the opening of these valves until the differential pressure between RCS and CNV falls below the IAB release pressure. If DC power is not available, all ECCS valves will open at the IAB release pressure. This case is covered as discussed in Section 5.4.4. If DC power is available the other division will still actuate on the level signal creating a staggered release. This is a non-limiting case as a staggered release has a smaller impact on system pressures, levels, and core coolability relative to the immediate opening of all ECCS valves at the IAB release pressure.

5.4.4 Loss of Power

Coincident with a postulated LOCA, two scenarios for loss of power are considered within the LOCA methodology:

- complete loss of normal alternating current (AC) and DC power and
- complete loss of only AC power with DC power availability.

The loss of DC power can impact the LOCA progression by immediately triggering valves to go to their fail-safe position. Table 5-8 presents the valves along with their fail-safe state.

© Copyright 2016 by NuScale Power, LLC

Table 5-8. NuScale Power Module valve fail-safe positions with loss of DC power

{{

}}2(a),(c)

For the ECCS valves after loss of DC power, the IAB arming valves close because the valve differential pressure is greater than the threshold setpoint, thereby preventing the immediate opening of the ECCS valves. As the RPV pressure decreases and the CNV pressure increases, the valves open as soon as the differential pressure drops below the IAB release pressure setpoint.

When normal AC power is lost, the feedwater pumps coast down and the turbine trip is initiated. Upon loss of normal AC power (with a time delay) the reactor trip, containment isolation, and DHRS actuation signals are generated (see Table 5-4 and Table 5-5). The ECCS does not receive an actuation signal based on loss of AC power until the 24 hour time delay is surpassed. The ECCS is still available to actuate based on its normal actuation signals (Table 5-4).

5.4.5 Decay Heat Removal System Availability

When the SG tubes are uncovered within the RPV, operation of the DHRS results in condensation of steam on the external surface of the helical coil SGs and retains liquid inventory in the RPV instead of releasing it to the CNV through vaporization. The RPV pressure is reduced for cases with DHRS available and there is a higher minimum inventory in the RPV.

There is no single failure that can prevent a single DHRS train from actuating; however, to account for uncertainties in modeling of the DHRS, the DHRS performance is considered in a sensitivity study. Specifically, consideration is given to full availability and full loss of both DHRS trains and is included in the LOCA break spectrum calculations presented in Section 9.3. The crediting of DHRS is not required for the LOCA EM to meet acceptance criteria.

5.5 Sensitivity Studies

The sensitivity calculations described in Section 9.6 are performed in three categories:

© Copyright 2016 by NuScale Power, LLC

- sensitivies required by 10 CFR 50 Appendix K, (e.g., nodalization and time-step size to demonstrate the stability and consistency of the numerical scheme used by the NRELAP5 code),
- sensitivities related to key phenomena and design input parameters considered to be important to the LOCA progression and LOCA FOMs (e.g., CCFL at pressurizer baffle plate, ECCS parameters, etc.).
- sensitivities to determine input parameters to ensure conservativism (e.g., reactor pool initial temperature, core power distribution, etc.).

© Copyright 2016 by NuScale Power, LLC

6.0 NRELAP5 Code Description

The NuScale LOCA EM is based on the NRELAP5 system thermal-hydraulics code. The NRELAP5 code includes models for characterization of hydrodynamics, heat transfer between structures and fluids, modeling of fuel, reactor kinetics models, and control systems. NRELAP5 uses a two-fluid, non-equilibrium, non-homogenous model to simulate system thermal-hydraulic responses. This section provides a general overview of the code structure, models, and correlations. This section also addresses the LOCA-specific code models and improvements implemented to address unique design features and phenomena for the NPM. The adequacy of code models and correlations essential for modeling all high-ranked PIRT phenomena is discussed in Section 8.0. The full details of the models and correlations that makeup NRELAP5 can be found in the NRELAP5 Theory Manual (Reference 9).

RELAP5-3D©, version 4.1.3, was used as the baseline development platform for the NRELAP5 code. RELAP5-3D© was procured and as part of the procurement process commercial grade dedication was performed by NuScale to establish the baseline NRELAP5 code. Subsequently, features were added and changes made to NRELAP5 to address the unique aspects of the NPM design and licensing methodology. Those aspects of NRELAP5 that are new or revised specifically for the NPM application include:

- {{

}}2(a),(c)

The previous RELAP5 series of codes were developed at the INL under sponsorship of the DOE, the U.S. NRC, members of the International Code Assessment and Applications Program, members of the Code Applications and Maintenance Program, and members of the International RELAP5 Users Group. Specific applications of the code have included simulations of transients in light water reactor systems, such as LOCAs, anticipated transients without scram, and anticipated operational occurrences, such as loss of feedwater, loss of offsite power, station blackout, and turbine trip.

The RELAP5 code, including the RELAP5-3D© version that was used as the development platform for NRELAP5, has an extensive record of usage and acceptable performance for nuclear safety analysis. RELAP5-3D© is the latest version of the RELAP5 code that has been under continuous development since 1975, first under NRC sponsorship and then with additional DOE sponsorship beginning in the early 1980s. While NRC sponsorship ended in 1997, the DOE continued sponsorship of RELAP5-3D© to meet its own reactor safety assessment needs. The RELAP5 code was chosen by DOE as the thermal-hydraulic analysis tool because of its widespread acceptance.

© Copyright 2016 by NuScale Power, LLC

Systematic safety analyses were carried out for the DOE that included the N reactor at Hanford, the K and L reactors at Savannah River, the Advanced Test Reactor at the Idaho National Engineering and Environmental Laboratory, the High Flux Isotope Reactor and Advanced Neutron Source at Oak Ridge, and the High Flux Beam Reactor at Brookhaven. The DOE also chose RELAP5 for the independent safety analysis of the New Production Reactor proposed for Savannah River .

RELAP5-3D© has worldwide usage for nuclear safety analysis. Users participate in the International RELAP5 Users Group (IRUG) which provides a forum for code users to share their RELAP5 development and analysis experiences. Meeting participants also communicate new features and applications that have been developed for RELAP5-3D©. Code users include reactor vendors, nuclear industry suppliers, a naval nuclear propulsion laboratory, universities, and international organizations. NuScale is a participant in IRUG.

RELAP5-3D© has been chosen as a code development platform for small break LOCA analysis by Mitsubishi Heavy Industries for APWR (Reference 23). Furthermore, U.S. NRC has performed a detailed adequacy evaluation of RELAP5/MOD3 Version 3.2.1.2 for analysis of design-basis small break LOCA in the Westinghouse AP600 reactor (Reference 74). This usage of RELAP5-3D© over a long period of time has produced a large amount of user feedback. Submission of code error reports and the follow up code development has resulted in a robust code which can be used with a high level of confidence that significant code problems have been identified and corrected.

The more than 18 year history of code assessment and successful application of the RELAP5-3D© code, and codes based on the RELAP5-3D© platform, by the worldwide user community has successfully exercised the fundamental capabilities of RELAP5-3D© that are the critical characteristics required of NRELAP5 for NuScale's application.

The NRELAP5 code is developed following the requirements of the NuScale QAPD (Reference 4). The NuScale corporate Software Configuration Management Plan provides a framework for NRELAP5 configuration management and change control in conformance with the requirements outlined in the NuScale Software Program Plan. Review and approval of the NuScale corporate Software Configuration Management Plan is not within the scope of this report.

6.1 Quality Assurance Requirements

The NuScale QAPD complies with the requirements of 10 CFR 50 Appendix B, Quality Assurance Criteria for Nuclear Power Plants and Fuel Reprocessing Plants (Reference 10) and American Society of Mechanical Engineers (ASME) NQA-1-2008 and NQA-1a-2009 Addenda, "Quality Assurance Program Requirements for Nuclear Facility Applications," (Reference 12).

© Copyright 2016 by NuScale Power, LLC

6.2 NRELAP5 Hydrodynamic Model

The NRELAP5 hydrodynamic model is a transient, two-fluid model for flow of a two phase vapor/gas-liquid mixture that can contain non-condensable components in the vapor/gas phase as well as a soluble component (i.e., boron) in the liquid phase.

The two-fluid equations of motion that are used as the basis for the NRELAP5 hydrodynamic model are formulated in terms of volume and time-averaged parameters of the flow. Phenomena that depend upon transverse gradients, such as friction and heat transfer, are formulated in terms of the bulk properties using empirical transfer coefficient formulations. In situations where transverse gradients cannot be represented within the framework of empirical transfer coefficients, such as subcooled boiling, additional models specially developed for the particular situation are employed. The system model is solved numerically using a semi-implicit, finite-difference technique.

6.2.1 Field Equations

The NRELAP5 thermal-hydraulic model solves eight field equations for eight primary dependent variables. The primary dependent variables are pressure, phase-specific internal energies, vapor or gas volume fraction, phasic velocities, non-condensable quality, and boron density. For the one-dimensional equations, the independent variables are time and distance. Non-condensable quality is defined as the ratio of the non-condensable gas mass to the total vapor or gas phase mass.

The secondary dependent variables used in the equations are phasic densities, phasic temperatures, saturation temperature, and non-condensable mass fraction in the non-condensable gas phase for the i_{th} non-condensable species.

The basic field equations for the two-fluid, non-equilibrium model consist of two phasic continuity equations, two phasic momentum equations, and two phasic energy equations. The equations are time averaged and one-dimensional. The phasic continuity equations are shown in Equation 6-1 and Equation 6-2.

$$\frac{\partial}{\partial t}\left(\alpha_g \rho_g\right) + \frac{1}{A}\frac{\partial}{\partial x}\left(\alpha_g \rho_g \mathrm{v}_g A\right) = \Gamma_g \qquad \text{Equation 6-1}$$

$$\frac{\partial}{\partial t}\left(\alpha_f \rho_f\right) + \frac{1}{A}\frac{\partial}{\partial x}\left(\alpha_f \rho_f \mathrm{v}_f A\right) = \Gamma_f \qquad \text{Equation 6-2}$$

Continuity consideration yields the interfacial condition of Equation 6-3.

© Copyright 2016 by NuScale Power, LLC

$$\Gamma_f = -\Gamma_g \qquad \text{Equation 6-3}$$

The interfacial mass transfer model assumes that total mass transfer can be partitioned into mass transfer at the vapor/liquid interface in the bulk fluid (Γ_{ig}) and mass transfer at the vapor/liquid interface in the thermal boundary layer near the walls (Γ_w) as defined by Equation 6-4.

$$\Gamma_g = \Gamma_{ig} + \Gamma_w \qquad \text{Equation 6-4}$$

The phasic momentum equations are in the form of Equation 6-5 and Equation 6-6.

$$\begin{aligned}\alpha_g\rho_g A\frac{\partial \mathrm{v}_g}{\partial t} + \frac{1}{2}\alpha_g\rho_g A\frac{\partial \mathrm{v}_g^2}{\partial x} &= -\alpha_g A\frac{\partial P}{\partial x} + \alpha_g\rho_g B_x A - \left(\alpha_g\rho_g A\right)FWG\cdot \mathrm{v}_g \\ &+ \Gamma_g A\left(\mathrm{v}_{gI} - \mathrm{v}_g\right) - \left(\alpha_g\rho_g A\right)FIG\cdot\left(\mathrm{v}_g - \mathrm{v}_f\right) \\ &- C\alpha_g\alpha_f\rho_m A\left[\frac{\partial\left(\mathrm{v}_g - \mathrm{v}_f\right)}{\partial t} + \mathrm{v}_f\frac{\partial \mathrm{v}_g}{\partial x} - \mathrm{v}_g\frac{\partial \mathrm{v}_f}{\partial x}\right]\end{aligned} \qquad \text{Equation 6-5}$$

$$\begin{aligned}\alpha_f\rho_f A\frac{\partial \mathrm{v}_f}{\partial t} + \frac{1}{2}\alpha_f\rho_f A\frac{\partial \mathrm{v}_f^2}{\partial x} &= -\alpha_f A\frac{\partial P}{\partial x} + \alpha_f\rho_f B_x A - \left(\alpha_f\rho_f A\right)FWF\cdot \mathrm{v}_f \\ &- \Gamma_g A\left(\mathrm{v}_{fI} - \mathrm{v}_f\right) - \left(\alpha_f\rho_f A\right)FIF\cdot\left(\mathrm{v}_f - \mathrm{v}_g\right) \\ &- C\alpha_g\alpha_f\rho_m A\left[\frac{\partial\left(\mathrm{v}_f - \mathrm{v}_g\right)}{\partial t} + \mathrm{v}_g\frac{\partial \mathrm{v}_f}{\partial x} - v_f\frac{\partial \mathrm{v}_g}{\partial x}\right]\end{aligned} \qquad \text{Equation 6-6}$$

The force terms on the right sides of Equation 6-5 and Equation 6-6 are, respectively, the pressure gradient, the body force (i.e., gravity and pump head), wall friction, momentum transfer due to interface mass transfer, interface frictional drag, and force due to virtual mass. The terms FWG and FWF are part of the wall frictional drag, which are linear in velocity, and are products of the friction coefficient, the frictional reference area per unit volume, and the magnitude of the fluid bulk velocity. The coefficients FIG

© Copyright 2016 by NuScale Power, LLC

and FIF are part of the interface frictional drag; two different models (drift flux and drag coefficient) are used for the interface friction drag, depending on the flow regime.

Conservation of momentum at the interface requires that the force terms associated with interface mass and momentum exchange sum to zero as shown by Equation 6-7.

$$\Gamma_g A v_{gI}(\alpha_g \rho_g A) FIG \cdot (v_g - v_f) - C\alpha_g \alpha_f \rho_m A \left[\frac{\partial(v_g - v_f)}{\partial t}\right]$$

Equation 6-7

$$-\Gamma_g A v_{fI}(\alpha_f \rho_f A) FIF \cdot (v_f - v_g) - C\alpha_f \alpha_g \rho_m A \left[\frac{\partial(v_f - v_g)}{\partial t}\right] = 0$$

The phasic thermal energy equations are defined by the following two equations:

$$\frac{\partial}{\partial t}(\alpha_g \rho_g U_g) + \frac{1}{A}\frac{\partial}{\partial x}(\alpha_g \rho_g U_g v_g A) = -P\frac{\partial \alpha_g}{\partial t} - \frac{P}{A}\frac{\partial}{\partial x}(\alpha_g v_g A)$$

Equation 6-8

$$+Q_{wg} + Q_{ig} - \Gamma_{ig} h_g^* - \Gamma_w h_g^{`} + DISS_g$$

$$\frac{\partial}{\partial t}(\alpha_f \rho_f U_f) + \frac{1}{A}\frac{\partial}{\partial x}(\alpha_f \rho_f U_f v_f A) = -P\frac{\partial \alpha_f}{\partial t} - \frac{P}{A}\frac{\partial}{\partial x}(\alpha_f v_f A)$$

Equation 6-9

$$+Q_{wf} + Q_{if} - \Gamma_{ig} h_f^* - \Gamma_w h_f^{`} + DISS_f$$

In the phasic energy equations, Q_{wg} and Q_{wf} are the phasic wall heat transfer rates per unit volume. These phasic wall heat transfer rates satisfy Equation 6-10 where Q is the total wall heat transfer rate to the fluid per unit volume.

$$Q = Q_{wg} + Q_{wf}$$

Equation 6-10

The vapor generation (or condensation) consists of two parts, vapor generation that results from energy exchange in the bulk fluid (Γ_{ig}) and energy exchange in the thermal boundary layer near the wall (Γ_w) (Equation 6-4). Each of the vapor generation (or condensation) processes involves interface heat transfer effects. The interface heat

© Copyright 2016 by NuScale Power, LLC

transfer terms (Q_{ig} and $\mathrm{Q_{if}}$) appearing in Equation 6-8 and Equation 6-9 include heat transfer from the fluid states to the interface due to interface energy exchange in the bulk and in the thermal boundary layer near the wall. The vapor generation (or condensation) rates are established from energy balance considerations at the interface.

The phasic energy dissipation terms, $\mathrm{DISS_g}$ and $\mathrm{DISS_f}$, are the sums of wall friction, pump, and turbine effects. The dissipation effects due to interface mass transfer, interface friction, and virtual mass are neglected.

6.2.2 State Relations

The six-equation model uses five independent state variables with an additional equation for the non-condensable gas component. The independent state variables are chosen to be P, α_g, U_g, U_f, and X_n. All the remaining thermodynamic fluid variables (temperatures, densities, partial pressures, qualities, etc.) are expressed as functions of these five independent state variables. In addition to these variables, several state derivatives are needed for some of the linearizations used in the numerical scheme.

$$\left(\frac{\partial \rho_g}{\partial P}\right)_{U_g,X_n}, \quad \left(\frac{\partial \rho_g}{\partial U_g}\right)_{P,X_n}, \quad \left(\frac{\partial \rho_g}{\partial X_n}\right)_{P,U_g}, \quad \left(\frac{\partial \rho_f}{\partial P}\right)_{U_f}, \quad \left(\frac{\partial \rho_f}{\partial U_f}\right)_{P} \qquad \text{Equation 6-11}$$

The interphase mass and heat transfer models use an implicit (linearized) evaluation of the temperature potentials $T_I - T_f$ and $T_I - T_g$. The quantity T_I is the temperature that exists at the phase interface. The implicit (linearized) evaluation of the temperature potentials in the numerical scheme requires the derivatives of the phasic and interface temperatures defined by Equation 6-12.

$$\left(\frac{\partial T_g}{\partial P}\right)_{U_g,X_n}, \left(\frac{\partial T_g}{\partial U_g}\right)_{P,X_n}, \left(\frac{\partial T_g}{\partial X_n}\right)_{P,U_g}, \left(\frac{\partial T_f}{\partial P}\right)_{U_f}, \left(\frac{\partial T_f}{\partial U_f}\right)_{P}, \left(\frac{\partial T^s}{\partial P}\right)_{U_g,X_n}, \left(\frac{\partial T^s}{\partial U_g}\right)_{P,X_n}, \left(\frac{\partial T^s}{\partial X_n}\right)_{P,U_g} \qquad \text{Equation 6-12}$$

6.2.2.1 Water Property Tables

The set of basic properties for light water is used for all LOCA calculations. Implementation is activated by the user. These thermodynamic tables tabulate saturation properties as a function of temperature, saturation properties as a function of pressure, and single-phase properties as a function of pressure and temperature. The tables are based on the 1995 Steam Tables from the International Association for the Properties of Water and Steam (IAPWS) and are known as IAPWS-95. The properties and derivatives in the tables are saturation pressure, saturation temperature, specific volume (υ), specific internal energy, specific entropy, and three derivatives: the isobaric thermal expansion coefficient (β), the isothermal compressibility (κ), and the specific heat at constant pressure (C_p).

© Copyright 2016 by NuScale Power, LLC

6.2.2.2 Single-Component, Two-Phase Mixture

Liquid properties are obtained from the thermodynamic tables, given P and U_f. All the desired density and temperature derivatives can then be obtained from the derivatives of κ_f, β_f, and C_{pf}. In the case of the vapor being subcooled or the liquid being superheated, (i.e., metastable states) the calculation of υ, T, κ, β, and C_p incorporates a constant pressure extrapolation from the saturation state for the temperature and specific volume.

6.2.3 Flow Regime Maps

The one-dimensional nature of the field equations for the two-fluid model used in NRELAP5 precludes direct simulation of effects that depend upon transverse gradients of any physical parameter, such as velocity or energy. Consequently, such effects must be accounted for through algebraic terms added to the conservation equations.

The mapping for flow conditions to a specific flow regime is required to provide closure to the two-fluid equations. The selected flow regime determines the constitutive relationships that are applied for interphase friction, the coefficient of virtual mass, wall friction, wall heat transfer, and interphase heat and mass transfer. The flow regime maps are based on the work of Taitel and Dukler (References 14 and 15) and Ishii (References 16, 17, and 18). Taitel and Dukler have simplified flow regime classifications and developed semi-empirical relations to describe flow regime transitions. However, some of their transition criteria are complex, and further simplification has been carried out in order to efficiently apply these criteria in NRELAP5.

The flow regime maps for the volumes and junctions are identical but used differently as a result of the finite difference scheme and staggered mesh used in the numerical scheme. The volume map is based on volume quantities. It is used for interphase heat and mass transfer, wall friction, and wall heat transfer. Meanwhile, the junction map is based on junction quantities and is used to calculate the interfacial friction coefficient.

Three flow-regime maps in both volumes and junctions for two-phase flow are used in the NRELAP5 code: (a) a horizontal map for flow in pipes; (b) a vertical map for flow in pipes, annuli, and bundles; and (c) a high mixing map for flow through pumps.

Wall heat transfer depends on the volume flow regime maps in a less direct way. Generally, void fraction and mass flux are used to incorporate the effects of the flow regime. Since the wall heat transfer is calculated before the hydrodynamics, the flow information is taken from the previous time step.

6.2.3.1 Vertical Volume Flow Regime Maps

The vertical volume flow regime map is for upflow, downflow, and counter current flow in volumes whose inclination (vertical) angle ϕ is such that $60 < |\phi| \leq 90$ degrees. An interpolation region between vertical and horizontal flow regimes is used for volumes whose absolute value of the inclination (vertical) angle is between 30 and 60 degrees.

This map is modeled as nine regimes:

© Copyright 2016 by NuScale Power, LLC

- four regimes for pre-CHF heat transfer - bubbly, slug, annular-mist, and dispersed (droplet or mist)
- four regimes for post-CHF heat transfer - inverted annular, inverted slug, mist, and dispersed (droplet or mist)
- one regime for vertical stratification

A schematic of the vertical flow regime map as coded in NRELAP5 is shown in Figure 6-1. The schematic is three-dimensional to illustrate flow-regime transitions as functions of void fraction (α_g), average mixture velocity (v_m), and boiling.

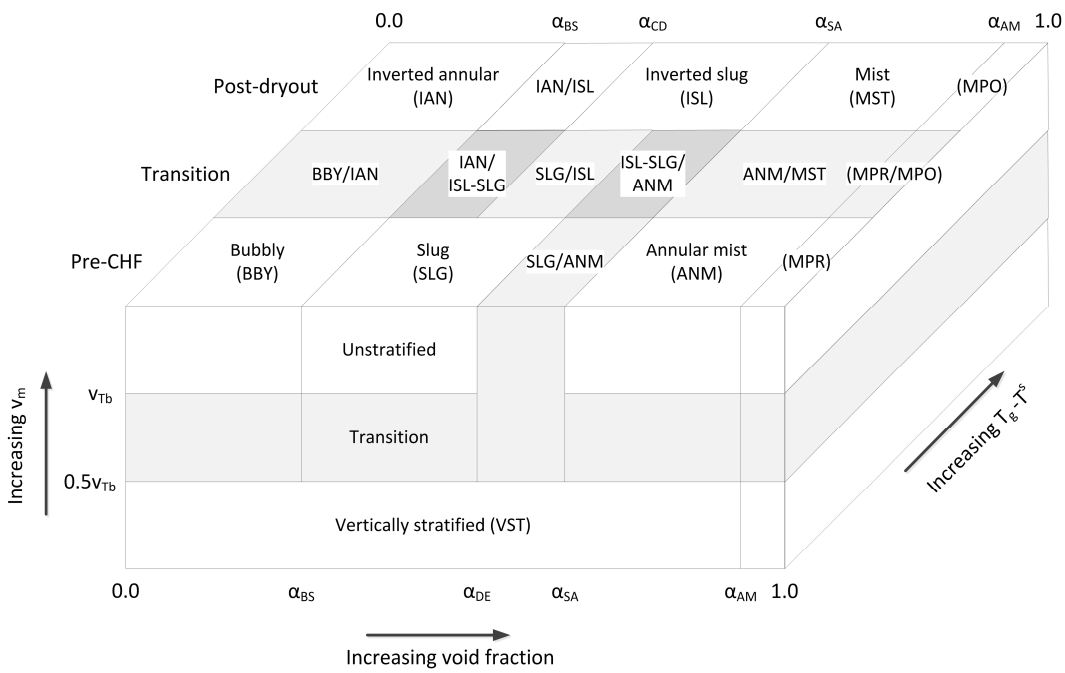

Figure 6-1. Schematic of vertical flow-regime map indicating transitions

6.2.3.2 Junction Flow Regime Maps

The junction map is based on both junction and volume quantities. It is used for the interphase drag and shear, as well as the coefficient of virtual mass. The flow regime maps used for junctions are the same as used for the volumes and are based on the work of Taitel and Dukler (Reference 14), Ishii (Reference 16), and Tandon, et. al. (Reference 19)

As with the volumes, three junction flow regime maps are used:

- horizontal map for flow in pipes
- vertical map for flow in pipes/bundles
- high mixing map for flow in pumps

© Copyright 2016 by NuScale Power, LLC

The vertical flow regime map is for junctions whose junction inclination (vertical) angle ϕ_j is such that $60 \leq |\phi_j| \leq 90$ degrees. The horizontal flow regime map is for junctions whose junction inclination (vertical) angle ϕ_j is such that $0 \leq |\phi_j| \leq 30$ degrees. An interpolation region between vertical and horizontal flow regimes is used for junctions whose junction inclination (vertical) angle ϕ_{j} is such that $30 < |\phi_j| < 60$ degrees. This interpolation region is used to smoothly change between vertical and horizontal flow regimes.

Junction quantities used in the map decisions are junction phasic velocities, donored (based on phasic velocities) phasic densities, and donored (based on superficial mixture velocity) surface tension.

The junction void fraction $(\alpha^*_{g,j})$ is calculated from either of the volume void fractions of the neighboring volumes, $\alpha_{g,k}$ or $\alpha_{g,L}$, using a donor direction based on the mixture superficial velocity (j_m).

6.2.4 Momentum Closure Relations

NRELAP5 uses two different models for the phasic interfacial friction force computation, the drift flux method and the drag coefficient method. The choice of which model to use depends upon the flow regime.

6.2.4.1 Drift Flux Model

The drift flux approach is used only in the bubbly and slug-flow regimes for vertical flow. The drift flux model specifies the distribution coefficient and the vapor/gas drift velocity. These two quantities must be converted into a constitutive relation for the interfacial frictional force per unit volume.

Such a relation can be found by assuming that the interfacial friction force per unit volume is given by Equation 6-13.

$$\mathrm{F_i} = C_i|\mathrm{v}_R|\mathrm{v}_R = \alpha_f \alpha_g (\rho_f - \rho_g) g \qquad \text{Equation 6-13}$$

where the interfacial frictional force per unit volume is balanced by the buoyancy force per unit volume where C_i is an unknown coefficient and v_R is the relative velocity between the phases. Within the context of the drift flux model, the relative velocity between the phases is not the difference between the phasic velocities but is a weighted difference between the phase velocities given by Equation 6-14.

$$\mathrm{v}_R = C_1 \mathrm{v}_g - C_0 \mathrm{v}_f \qquad \text{Equation 6-14}$$

© Copyright 2016 by NuScale Power, LLC

where C_0 is given by the drift flux correlations and C_1 is given by Equation 6-15.

$$C_1 = \frac{1 - \alpha_g C_0}{1 - \alpha_g} \qquad \text{Equation 6-15}$$

Substituting these relations into Equation 6-13 gives the interfacial friction force per unit volume in terms of the phasic velocities, given by Equation 6-16.

$$F_i = C_i \left| C_1 \mathrm{v}_g - C_0 \mathrm{v}_f \right| \left(C_1 \mathrm{v}_g - C_0 \mathrm{v}_f \right) \qquad \text{Equation 6-16}$$

Here the coefficient C_i is yet undetermined. The drift flux model also specifies that the relative velocity (v_R) can be written as the ratio of the vapor/gas drift velocity and the liquid volume fraction, and is given by Equation 6-17.

$$\mathrm{v}_R = \frac{\mathrm{v}_{gj}}{\alpha_f} \qquad \text{Equation 6-17}$$

where the vapor/gas drift velocity $\left(\mathrm{v}_{gj}\right)$ is given by the drift flux correlations. Substituting this value of the relative velocity into Equation 6-13 allows the coefficient C_i to be determined from Equation 6-18.

$$C_\mathrm{i} = \frac{\alpha_g \alpha_f^3 \left(\rho_f - \rho_g \right) g}{\mathrm{v}_{gj}^2} \qquad \text{Equation 6-18}$$

6.2.4.2 Drag Coefficient Model

The drag coefficient approach is used in all flow regimes other than vertical bubbly and slug-flow. The model uses correlations for drag coefficients and for the computation of the interfacial area density.

The constitutive relation for the frictional force on a body moving relative to a fluid is given by Equation 6-19.

© Copyright 2016 by NuScale Power, LLC

$$\mathrm{F} = \frac{1}{2}\rho \mathrm{v}^2 C_D A \qquad \text{Equation 6-19}$$

where,

F = drag force

ρ = fluid density,

v = velocity of body relative to the fluid,

C_D = drag coefficient, and

A = projected area of the body.

Expressing the frictional force for a group of bodies moving relative to a fluid (e.g., bubbles moving through liquid or droplets moving through vapor/gas) in terms of the frictional force for each body leads to the constitutive relation of Equation 6-20 for the interfacial frictional force per unit volume:

$$\mathrm{F_i} = \frac{1}{8}\rho_c \left|\mathrm{v}_g - \mathrm{v}_f\right|\left(\mathrm{v}_g - \mathrm{v}_f\right) C_D S_F a_{gf} = C_i \left|\mathrm{v}_g - \mathrm{v}_f\right|\left(\mathrm{v}_g - \mathrm{v}_f\right) \qquad \text{Equation 6-20}$$

where,

F_i = interfacial friction force per unit volume,

C_i = $\frac{1}{8}\rho_c C_D S_F a_{gf}$

ρ_c = density of continuous phase

a_{gf} = interfacial area per unit volume, and

S_F = shape factor.

The additional factor of 1/4 comes from the conversion of the projected area of spherical particles (i.e., πr^2) into the interfacial area (i.e., $4\pi r^2$) and the shape factor is included to account for non-spherical particles. The drag coefficient model for the global interfacial friction coefficient has been reduced to the specification of the continuous density, drag coefficient, interfacial area density, and shape factor for the flow regimes. Once these quantities have been computed, the interfacial friction force per unit volume (F_i) is

© Copyright 2016 by NuScale Power, LLC

computed from Equation 6-20 from which the global interfacial friction coefficient can be computed.

6.2.4.3 Wall Friction

The wall friction is determined based on the volume flow regime map. The wall friction force terms include only wall shear effects. Losses due to abrupt area change are calculated using mechanistic form-loss models. Other losses due to elbows or complicated flow passage geometry are modeled using energy-loss coefficients that must be input by the user.

The semi-implicit scheme, one-dimensional, finite difference equations for the sum momentum equation and the difference momentum equation contain the terms of Equation 6-21 that represent the phasic wall frictional pressure drop.

$$FWG_j^n \cdot \left(\mathrm{v}_g\right)_j^{n+1} \Delta x_j \, \Delta t \text{ and } FWF_j^n \cdot \left(\mathrm{v}_f\right)_j^{n+1} \Delta x_j \, \Delta t \qquad \text{Equation 6-21}$$

These terms represent the pressure loss due to wall shear from cell center to cell center of the cell volumes adjoining the particular junction that the momentum equation is considering. The wall drag or friction depends not only on the phase of the fluid, but also on the flow regime characteristics.

The wall friction model is based on a two-phase multiplier approach in which the two-phase multiplier is calculated from the heat transfer and fluid flow service (HTFS) modified Baroczy correlation. The individual phasic wall friction components are calculated by apportioning the two-phase friction between the phases using a technique derived from the Lockhart-Martinelli model (Reference 20). The model is based on the assumption that the frictional pressure drop may be calculated using a quasi-steady form of the momentum equation, as used by Chisholm. This wall friction partitioning model is used with the drag coefficient method of the interphase friction model.

The Lockhart-Martinelli model computes the overall two-phase friction pressure drop in terms of the liquid-alone and vapor/gas-alone wall friction pressure drop as shown in Equation 6-22.

$$\left(\frac{dP}{dx}\right)_{2\phi} = \phi_f^2 \left(\frac{dP}{dx}\right)_f = \phi_g^2 \left(\frac{dP}{dx}\right)_g \qquad \text{Equation 6-22}$$

Here ϕ_f and ϕ_g are the liquid-alone and vapor/gas-alone two-phase Darcy-Weisbach friction multipliers, respectively. The phasic wall friction pressure gradients are expressed by Equation 6-23 for the liquid and vapor/gas alone.

© Copyright 2016 by NuScale Power, LLC

$$\left(\frac{dP}{dx}\right)_f = \frac{\lambda_f' Re_f' M_f^2}{2D\rho_f A^2} \quad \text{and} \quad \left(\frac{dP}{dx}\right)_g = \frac{\lambda_g' Re_g' M_f^2}{2D\rho_g A^2}$$ Equation 6-23

Here the prime indicates the liquid and vapor/gas-alone Darcy-Weisbach friction factors, respectively, calculated at the respective Reynolds numbers given by Equation 6-24.

$$Re_f' = \frac{M_f D}{\mu_f A} \quad \text{and} \quad Re_g' = \frac{M_g D}{\mu_g A}$$ Equation 6-24

The liquid and vapor/gas mass flow rates, respectively, are defined by Equation 6-25.

$$M_f = \alpha_f \rho_f \mathrm{v}_f A \quad \text{and} \quad M_g = \alpha_g \rho_g \mathrm{v}_g A$$ Equation 6-25

The overall two-phase friction pressure gradient is calculated using two-phase friction multiplier correlations. The multipliers are interrelated using Equation 6-22 and Equation 6-23 and the Lockhart-Martinelli ratio defined by Equation 6-26.

$$\chi^2 = \frac{\left(\frac{dP}{dx}\right)_f}{\left(\frac{dP}{dx}\right)_g} = \frac{\phi_g^2}{\phi_f^2}$$ Equation 6-26

The HTFS correlation is used to calculate the two-phase friction multipliers. This correlation was chosen because it is correlated to empirical data over broad ranges of phasic volume fractions, phasic flow rates and phasic flow regimes. The correlation has also been shown to give good agreement with empirical data.

The HTFS correlation for the two-phase friction multiplier is expressed with Equation 6-27.

$$\phi_f^2 = 1 + \frac{1}{\chi} + \frac{1}{\chi^2} \quad \text{and} \quad \phi_g^2 = \chi^2 + C\chi + 1$$ Equation 6-27

C is the correlation coefficient and χ is the Lockhart-Martinelli ratio given by Equation 6-26. If the HTFS correlation is combined with the wall friction formulations by combining

© Copyright 2016 by NuScale Power, LLC

Equation 6-22 and Equation 6-23, Equation 6-25 and Equation 6-26, and Equation 6-27, then the combined two-friction pressure drop is expressed by Equation 6-28.

$$\left(\frac{dP}{dx}\right)_{2\phi} = \phi_g^2\left(\frac{dP}{dx}\right)_f = \phi_g^2\left(\frac{dP}{dx}\right)_f = \frac{1}{2D}\left\{\lambda_f'\rho_f\left(\alpha_f \mathrm{v}_f\right)^2 + C\left[\lambda_f'\rho_f\left(\alpha_f \mathrm{v}_f\right)^2\lambda_g'\rho_g\left(\alpha_g \mathrm{v}_g\right)^2\right]^{\frac{1}{2}} + \lambda_g'\rho_g\left(\alpha_g \mathrm{v}_g\right)^2\right\} \quad \text{Equation 6-28}$$

The phasic wall friction coefficients are defined by Equation 6-29 and Equation 6-30.

$$FWF\left(\alpha_f\rho_f \mathrm{v}_f\right)A = \tau_f p_f = \alpha_f\left(\frac{dP}{dx}\right)\Big|_{2\phi}\left(\frac{Z^2}{\alpha_g + \alpha_f Z^2}\right)A \quad \text{Equation 6-29}$$

$$FWG\left(\alpha_G\rho_G \mathrm{v}_G\right)A = \tau_g p_g = \alpha_g\left(\frac{dP}{dx}\right)\Big|_{2\phi}\left(\frac{1}{\alpha_g + \alpha_f Z^2}\right)A \quad \text{Equation 6-30}$$

Here Z is defined by Equation 6-31.

$$Z^2 = \frac{\lambda_f Re_f \rho_f \mathrm{v}_f^2 \frac{\alpha_{fw}}{\alpha_f}}{\lambda_g Re_g \rho_g \mathrm{v}_g^2 \frac{\alpha_{gw}}{\alpha_g}} \quad \text{Equation 6-31}$$

Taking the sum of these two equations gives the overall quasi-static, two-phase wall friction pressure gradient as shown by Equation 6-32.

$$FWF\left(\alpha_f\rho_f \mathrm{v}_f\right)A + FWG\left(\alpha_G\rho_G \mathrm{v}_G\right)A = \left(\frac{dP}{dx}\right)\Big|_{2\phi}A \quad \text{Equation 6-32}$$

The phasic friction factors used in the wall friction model are computed from correlations for laminar and turbulent flows with interpolation in the transition regime. The friction factor

© Copyright 2016 by NuScale Power, LLC

model is simply an interpolation scheme linking the laminar, laminar-turbulent transition, and turbulent flow regimes. The laminar friction factor is calculated by Equation 6-33.

$$\lambda_L = \frac{64}{Re\phi_S} \; for \; 0 \leq Re \leq 2{,}200 \qquad \text{Equation 6-33}$$

Here ϕ_S is a user-input shape factor for non-circular flow channels (ϕ_S is 1.0 for circular channels).

The friction factor in the transition region between laminar and turbulent flows is computed by reciprocal interpolation with Equation 6-34.

$$\lambda_{L,T} = \left(3.75 - \frac{8{,}250}{Re}\right)\left(\lambda_{T,300} - \lambda_{L,2200}\right) + \lambda_{L,2200}$$

$$for \;\; 2{,}200 < Re < 3{,}000 \qquad \text{Equation 6-34}$$

Here $\lambda_{L,2200}$ is the laminar factor at a Reynolds number of 2,200, $\lambda_{T,3000}$ is the turbulent friction factor at a Reynolds number of 3,000, and the interpolation factor is defined to lie between zero and one.

The turbulent friction factor is given by the Zigrang-Sylvester approximation (Reference 22) to the Colebrook-White correlation (Reference 23) with Equation 6-35, where ε is the surface roughness.

$$\frac{1}{\sqrt{\lambda_T}} = -2\log_{10}\left\{\frac{\varepsilon}{3.7D} + \frac{2.51}{Re}\left[1.14 - 2\log_{10}\left(\frac{\varepsilon}{D} + \frac{21.25}{Re^{0.9}}\right)\right]\right\}$$

$$for \;\; Re \geq 3{,}000 \qquad \text{Equation 6-35}$$

6.2.5 Heat Transfer

The liquid and vapor/gas energy solutions include the wall heat flux to liquid or vapor/gas. During boiling, the saturation temperature based on the total pressure is the reference temperature, and during condensation the saturation temperature based on the partial pressure is the reference temperature. The general expression for the total wall heat flux is defined by Equation 6-36:

© Copyright 2016 by NuScale Power, LLC

$$q''_{total} = h_{Wgg}\left(T_W - T_g\right) + h_{wgspt}\left(T_W - T_{spt}\right) + h_{wgspp}\left(T_W - T_{spp}\right) + h_{wff}\left(T_W - T_f\right) + h_{wfspt}\left(T_W - T_{spt}\right)$$ Equation 6-36

where,

h_{wgg} = heat transfer coefficient to vapor/gas, with the vapor/gas temperature as the reference temperature (W/m^2 K),

h_{wgspt} = heat transfer coefficient to vapor/gas, with the saturation temperature based on the total pressure as the reference temperature (W/m^2 K),

h_{wgspp} = heat transfer coefficient to vapor/gas, with the saturation temperature based on the vapor partial pressure as the reference temperature (W/m^2 K),

h_{wff} = heat transfer coefficient to liquid, with the liquid temperature as the reference temperature (W/m^2 K),

h_{wfspt} = heat transfer coefficient to liquid, with the saturation temperature based on the total pressure as the reference temperature (W/m^2 K),

T_W = wall surface temperature (K),

T_g = vapor/gas temperature (K),

T_f = liquid temperature (K),

T_{spt} = saturation temperature based on the total pressure (K), and

T_{spp} = saturation temperature based on the partial pressure of vapor in the bulk (K).

A boiling curve is used in NRELAP5 to govern the selection of the wall heat transfer correlations when the wall surface temperature is above the saturation temperature (superheated relative to the saturation temperature based on total pressure). When a hydraulic volume is voided and the adjacent surface temperature is subcooled, vapor condensation on the surface is predicted. If non-condensable gases are present, the phenomena are more complex because condensation is based on the partial pressure of vapors present in the region. When the wall temperature is less than the saturation temperature based on total pressure, but greater than the saturation temperature based on vapor partial pressure, a convection condition exists. Figure 6-2 illustrates these three regions of the curve.

© Copyright 2016 by NuScale Power, LLC

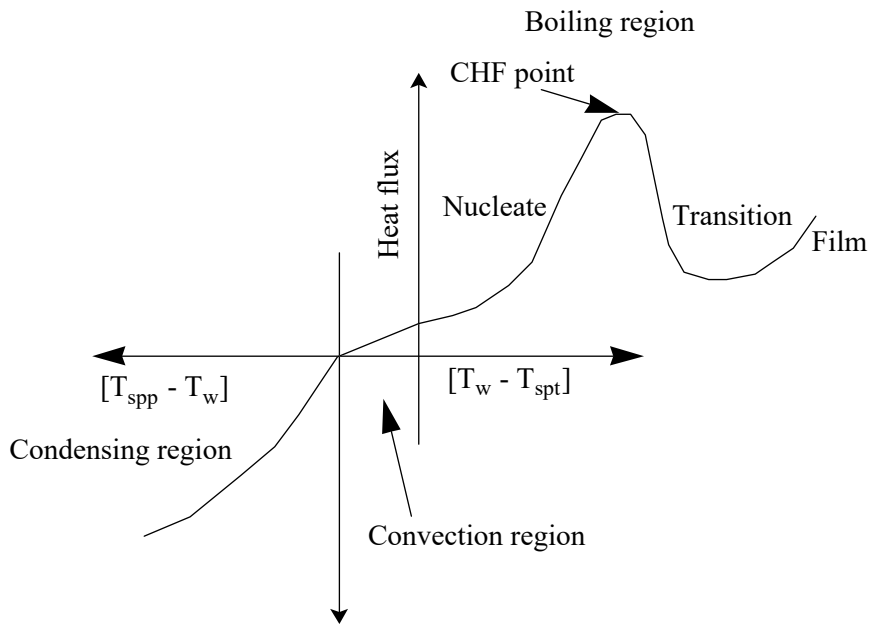

Figure 6-2. NRELAP5 boiling and condensing curves

The boiling curve uses the Chen boiling correlation (Reference 24) up to the CHF point.

NRELAP5 will issue a message and stop running if CHFR reduces below one for heat conductors that are in the core. Post-CHF heat transfer is allowed to occur on surfaces outside the core. For instance, post-CHF heat transfer can occur on the outside of the RPV where boiling occurs in the pool of liquid that accumulates in the CNV. Post-CHF heat transfer could also occur on the SG tube surfaces, depending on local conditions.

6.3 Heat Structure Models

Heat structures provided in NRELAP5 permit calculation of the heat transfer across solid boundaries of hydrodynamic volumes. Modeling capabilities of heat structures are general and include fuel pins or plates with nuclear or electrical heating, heat transfer across SG tubes, and heat transfer from pipe and vessel walls. Temperatures and heat transfer rates are computed from the one-dimensional form of the transient heat conduction equation.

Heat structures are represented using rectangular, cylindrical, or spherical geometry. Surface multipliers are used to convert the unit surface of the one-dimensional calculation to the actual surface of the heat structure. Temperature-dependent and space-dependent thermal conductivities and volumetric heat capacities are provided in tabular or functional form either from built-in or user-supplied data.

Finite differences are used to advance the heat conduction solutions. Each mesh interval may contain different mesh spacing, a different material, or both. The spatial dependence

© Copyright 2016 by NuScale Power, LLC

of the internal heat source, if any, may vary over each mesh interval. The time-dependence of the heat source can be obtained from reactor kinetics, one of several tables of power versus time, or a control system variable. Boundary conditions include symmetry or insulated conditions; a heat transfer correlation package; and tables of surface temperature versus time, heat flux versus time, heat transfer coefficient versus time, and heat transfer coefficient versus surface temperature.

The heat transfer correlation package can be used for heat structure surfaces connected to hydrodynamic volumes. The heat transfer correlation package contains correlations for convective, nucleate boiling, transition boiling, and film boiling heat transfer from the wall to the fluid, and it contains reverse heat transfer from the fluid to the wall including correlations for condensation (see Section 6.2.5 and Section 6.8). The heat conduction model also includes a gap conduction model and a radiation enclosure model.

The integral form of the heat conduction equation is defined by Equation 6-37.

$$\iiint_V \rho C_p(T,\bar{x})\frac{\partial T}{\partial t}(\bar{x},t)dV = \iint_s k(t,\bar{x})\bar{\nabla}T(t,\bar{x})\cdot d\bar{s} + \iiint_V S(\bar{x},t)dV \qquad \text{Equation 6-37}$$

where,

$k(t,\bar{x})$ = thermal conductivity,

s = surface,

S = internal volumetric heat source,

t = time,

T = temperature,

V = volume,

x = space coordinates, and

ρC_P = volumetric heat capacity.

The boundary conditions applied to the exterior surface have the form of Equation 6-38.

$$A(T)T(t) + B(T)\frac{\partial T(t)}{\partial n} = D(T,t) \qquad \text{Equation 6-38}$$

The n denotes the unit normal vector away from the boundary surface. Thus, if the desired boundary condition is that the heat transferred out of the surface equals a heat transfer

© Copyright 2016 by NuScale Power, LLC

coefficient (h) times the difference between the surface temperature (T) and the sink temperature (T_{sk}) as shown by Equation 6-39.

$$-k\frac{\partial T(t)}{\partial n} = h(T - T_{sk}) \qquad \text{Equation 6-39}$$

then the correspondence between the above expression and Equation 6-38 yields $A = h, B = k, and\ D = hT_{sk}$.

One-dimensional heat conduction in rectangular, cylindrical, and spherical geometry can be used to represent the heat structures in any of the components in NRELAP5. The equations governing one-dimensional heat conduction are defined by Equation 6-40, Equation 6-41, and Equation 6-42.

$$\rho C_P \frac{\partial T}{\partial t} = \frac{\partial}{\partial x}\left(k\frac{\partial T}{\partial x}\right) + S \text{ for rectangular geometry} \qquad \text{Equation 6-40}$$

$$\rho C_P \frac{\partial T}{\partial t} = \frac{1}{r}\left[\frac{\partial}{\partial r}\left(rk\frac{\partial T}{\partial r}\right)\right] + S \text{ for cylindrical geometry} \qquad \text{Equation 6-41}$$

$$\rho C_P \frac{\partial T}{\partial t} = \frac{1}{r^2}\left[\frac{\partial}{\partial r}\left(r^2k\frac{\partial T}{\partial r}\right)\right] + S \text{ for spherical geometry} \qquad \text{Equation 6-42}$$

Heat may flow across the external heat structure boundaries to either the environment or to the working fluid. For heat structure surfaces connected to hydrodynamic volumes containing the working fluid, a heat transfer package is provided containing correlations for heat transfer from wall-to-liquid and reverse heat transfer from liquid-to-wall. Any number of heat structures may be connected to each hydrodynamic volume, or heat transfer coefficient versus surface temperature can be used to simulate the boundary conditions.

The heat conduction equation can be solved by various numerical techniques. NRELAP5 uses the Crank-Nicolson method (Reference 26) for solving this equation.

6.4 Point Reactor Kinetics Model

NRELAP5 allows the user to model the power generated in the reactor core as specified from a table or as determined by point-reactor kinetics with reactivity feedback. This power is modeled as an internal heat source in user-defined heat structures and can be

© Copyright 2016 by NuScale Power, LLC

partitioned by inputting weighting factors to distribute the energy to the various portions of the core as the user desires.

The power is computed using the space-independent or point kinetics approximation, which assumes that power can be separated into space and time functions. The point reactor kinetics model computes both the immediate (prompt and delayed neutrons) fission power and the power from decay of fission products. The immediate (prompt and delayed neutrons) power is that released at the time of fission and includes power from kinetic energy of the fission products and neutron moderation. Decay power is generated as the fission products undergo radioactive decay. The LOCA methodology uses the ANS 1973 decay heat standard (see Section 6.10).

The point kinetics equations are (see Glasstone and Sesonske, Reference 27) defined by

$$\frac{dn(t)}{dt} = \frac{[\rho(t) - \beta]}{\Lambda} n(t) + \sum_{i=1}^{N_d} \lambda_i C_i(t) + S \qquad \text{Equation 6-43}$$

$$\frac{dC_i(t)}{dt} = \frac{\beta f_i}{\Lambda} n(t) - \lambda_i C_i(t) \quad i = 1, 2, \ldots, N_d \qquad \text{Equation 6-44}$$

$$\varphi(t) = n(t)v \qquad \text{Equation 6-45}$$

$$\Psi(t) = V \Sigma_f \varphi(t) \qquad \text{Equation 6-46}$$

$$P_f(t) = Q_f \Psi(t) \qquad \text{Equation 6-47}$$

where,

t = time (s),

n = neutron density (neutrons/m^3),

φ = neutron flux (neutrons/m^2·s),

v = neutron velocity (m/s),

C_i = delayed neutron precursor concentration in group i (nuclei/m^3),

© Copyright 2016 by NuScale Power, LLC

β = effective delayed neutron fraction = $\sum_{i=1}^{N_d} \beta_i$,

Λ = prompt neutron generation time (s)

ρ = reactivity (only the time-dependence has been indicated; however, the reactivity is dependent on other variables),

f_i = fraction of delayed neutrons of group i = β_i/β,

β_i = effective delayed neutron precursor yield of group i,

λ_i = decay constant of group i (1/s),

S = source rate density (neutrons/m^3·s),

ψ = fission rate (fissions/s),

Σ_f = macroscopic fission cross-section (1/m),

P_f = immediate (prompt and delayed neutron) fission power (MeV/s),

Q_f = immediate (prompt and delayed neutron) fission energy per fission (MeV/fission),

V = volume (m^3), and

N_d = number of delayed neutron precursor groups.

After some modifications and variable substitutions, these equations are solved by the modified Runge-Kutta method.

Reactivity feedback can be input into NRELAP5 in one of two models: a separable model and a tabular model. The separable model is so defined that it assumes that each effect is independent of the other effects. This model also assumes nonlinear feedback effects from moderator density and fuel temperature changes and linear feedback from moderator temperature changes.

6.5 Trips and Control System Models

The control system provides the capability to evaluate simultaneous algebraic and ordinary differential equations. The capability is primarily intended to simulate control systems typically used in hydrodynamic systems, but it can also model other phenomena described by algebraic and ordinary differential equations. Another use is to define auxiliary output quantities, such as differential pressures, so they can be printed in major and minor edits and be plotted.

The control system consists of several types of control components. Each component defines a control variable as a specific function of time-advanced quantities. The time-advanced quantities include hydrodynamic volume, junction, pump, valve, heat structure, reactor kinetics, trip quantities, and the control variables themselves (including the control variable being defined). This permits control variables to be developed from components that perform simple, basic operations.

© Copyright 2016 by NuScale Power, LLC

The trip system consists of the evaluation of logical statements. Each trip statement is a simple logical statement that has a true or false result and an associated variable. Two types of trip statements are provided (variable and logical trips).

6.6 Special Solution Techniques

Certain models in NRELAP5 have been developed to simulate special processes. Special process models are used in NRELAP5 to model those processes, which are sufficiently complex that they must be modeled by empirical models. The following sections summarize those models.

6.6.1 Choked Flow

6.6.1.1 Moody Critical Flow Model

Because the Moody model (Reference 28) is required by 10 CFR 50 Appendix K when the break flow is calculated to be two-phase, a critical flow model that complies with the 10 CFR 50 Appendix K requirements was incorporated in NRELAP5. Two options are available in NRELAP5 for use of the Moody model. {{

}}2(a),(c)

Moody developed his critical flow model from theory to predict the maximum flow rate of a single component, two-phase mixture. The model assumes that the liquid phase is incompressible and that the flow is isentropic so that the stagnation enthalpy is constant throughout the system. The flow is maximized with respect to local slip ratio and static pressure for known stagnation conditions. The specific volume (υ) and specific enthalpy (h) of water can be calculated from two state variables, entropy (s) and pressure (*P*), i.e., $h = h(s_0, P)$ and $\upsilon = \upsilon(s_0, P)$, where the subscript *0* denotes break entrance conditions. Because entropy is constant, h and υ are functions of *P*, the stagnation pressure. From the continuity and energy equations for homogeneous flow entering and leaving an ideal nozzle the mass flux, *G*, satisfies:

© Copyright 2016 by NuScale Power, LLC

$$G = [2(h_0 - h)/v^2]^{1/2}$$ Equation 6-48

The maximum flow rate occurs at the throat, where

$$\frac{dG}{dP}|_t = 0$$ Equation 6-49

Moody showed that the maximum flow occurs when the slip ratio K = $(v_g/v_f)^{1/3}$. With this value of the slip ratio, Moody derived a complex equation for the critical flow rate that was used to create Moody lookup tables for the flow rate as a function of stagnation pressure and stagnation enthalpy. The range of the tables that are used in NRELAP5 covers local static pressure from {{ }}$^{2(a),(c)}$ with local quality from 0.0 to 1.0 and local stagnation pressures and enthalpies covering the range of saturation states. {{

}}$^{2(a),(c)}$

6.6.1.2 Henry-Fauske Critical Flow Model

The principle assumption used in the Henry-Fauske model is that, for most applications, the amount of thermal non-equilibrium at the throat is more important in determining the critical flow rate than the amount of mechanical non-equilibrium. Thus, it is assumed that the phase velocities are equal. Henry and Fauske then argued that for normal nozzle configurations, there is little time for mass transfer to take place, and it is reasonable to assume that the amount of mass transferred during the expansion is negligible and also that the amount of heat transferred between the phases during the expansion is insignificant, so that the liquid temperature is essentially constant. Interfacial viscous terms were neglected. Based on these assumptions Henry and Fauske derived an equation for the mass flux at the throat. The mass flow rate exhibits a maximum with respect to the throat pressure at critical flow, which yields a complex relationship for the critical mass flux that includes dependency on the throat pressure.

The Henry-Fauske model requires only knowledge of the upstream stagnation conditions and, unlike earlier critical flow models, it accounts for the non-equilibrium nature of the flow. Henry and Fauske noted that the critical flow rates are in reasonable agreement with the homogeneous equilibrium model for stagnation qualities greater than 0.10, and that for qualities less than this value, the homogeneous equilibrium model underestimates the data. Therefore, they required that the model input use only stagnation conditions, and yet at the same time account for the non-equilibrium nature of the flow. To address this issue

© Copyright 2016 by NuScale Power, LLC

Henry and Fauske correlated the effect of thermal non-equilibrium on the mass transfer rate at the throat as:

$$\frac{dX}{dP}|_t = N\frac{dX_{eq}}{dP}|_t \qquad \text{Equation 6-50}$$

where N is a thermal non-equilibrium factor defined in terms of the equilibrium quality at the throat ($X_{eq,t}$).

$$N = \frac{X_{eq,t}}{0.14} \qquad \text{Equation 6-51}$$

The final remaining unknown is the value of the pressure at the throat. To determine the throat pressure, the two-phase momentum equation was integrated between the stagnation and the throat locations to give an equation for the critical pressure ratio, i.e., the ratio of the throat pressure to the upstream stagnation pressure when the flow is choked. The use of this equation for the throat pressure in the equation for the critical mass flux results in a transcendental equation for the critical mass flux. The solution of the transcendental equation implicitly involves the critical flow rate and hence its solution yields predictions of the critical pressure ratio and the critical flow rate as functions of the upstream stagnation pressure and quality. The critical pressure ratio determines the transition to non-choked flow. If the mass flux predicted by the critical flow model is less than that resulting from the normal solution of the momentum equations, then the junction is choked. Assessment of the Henry-Fauske model shows excellent agreement against the Marviken 22 and 24 tests (Section 7.2.11).

6.6.1.3 Choked Flow for Orifices, Nozzles and Valves

To provide the user with the ability to better characterize the orifice, nozzle or valve behavior, the form of the Henry-Fauske model was retained in RELAP5-3D© and carried over into NRELAP5. The constant in the thermal non-equilibrium factor is included as an adjustable parameter.

$$N = MIN(1, \frac{X_{eq,t}}{C_{ne}}) \qquad \text{Equation 6-52}$$

where the thermal non-equilibrium constant, C_{ne}, is user input with a default value of 0.14. A user input discharge coefficient, default value of 1.0, can also be applied to the critical mass flux. The ability to input these parameters allows the user to adjust the critical flow model to account for the different amount of thermal non-equilibrium at the throat.

© Copyright 2016 by NuScale Power, LLC

While the model development was based on a converging nozzle, the authors of the model extended the results to orifices and short tubes by comparison to experimental data for these geometries. The Henry-Fauske model can be applied to cases where the upstream condition is subcooled liquid or single-phase vapor. While the Henry-Fauske model can handle non-condensable gas, the total amount of non-condensable gas in the NPM is negligible so this capability is not addressed in the following discussion.

During the development of the RELAP5 codes, modifications were made to the original model to ensure continuity at phase transitions to better characterize nozzles and orifices. Specifically,

- the phase transition modifications provide a smooth transition of the critical flow at the subcooled liquid to two-phase mixture interface.
- two adjustable coefficients, a discharge coefficient and a thermal non-equilibrium constant are provided in order to better characterize nozzles and orifices. The discharge coefficient is a multiplier on the flow area. The non–equilibrium constant is an assumed throat equilibrium quality that was assigned an average value of 0.14 by Henry and Fauske, but can be specified by the code user.

With these modifications, the Henry-Fauske model is applicable to two-phase and single-phase superheated and subcooled critical flow. The two adjustable coefficients allow the code user to more closely match test data from the valve vendor and calibration data from orifices and nozzles used in experimental facilities.

6.6.2 Abrupt Area Change

The general reactor system contains piping networks with many sudden area changes and orifices. To apply the NRELAP5 hydrodynamic model to such systems, analytical models for these components are included in the code. The basic hydrodynamic model is formulated for slowly varying (continuous) flow area variations; therefore, special models are not required for this case.

The abrupt area change model, is based on the Borda-Carnot formulation (Reference 30) for a sudden (i.e., sharp, blunt) enlargement and standard pipe flow relations, including the vena-contracta effect for a sudden (i.e., sharp, blunt) contraction or sharp-edge orifice or both. This is referred to as the full abrupt area change model. It does not include the case where an enlargement, contraction, or orifice is rounded or beveled.

Quasi-steady continuity and momentum balances are employed at points of an abrupt area change. The numerical implementation of these balances is such that hydrodynamic losses are independent of upstream and downstream nodalization. In effect, the quasi-steady balances are employed as jump conditions that couple fluid components having abrupt changes in cross-sectional area. This coupling process is achieved without change to the basic numerical time-advancement schemes.

The basic assumption used for the transient calculation of two-phase flow in flow passages with points of abrupt area change is that the transient flow process can be approximated as a quasi-steady flow process that is instantaneously satisfied by the upstream and

© Copyright 2016 by NuScale Power, LLC

downstream conditions (that is, transient inertia, mass, and energy storage are neglected at abrupt area changes). However, the upstream and downstream flows are treated as fully transient flows.

The volume of fluid and associated mass, energy, and inertia at points of abrupt area change is generally small compared with the volume of upstream and downstream fluid components. The transient mass, energy, and inertia effects are approximated by lumping them into upstream and downstream flow volumes. Finally, the quasi-steady approach is consistent with modeling of other important phenomena in transient codes (that is, heat transfer, pumps, and valves).

Activation of the full abrupt area change model in NRELAP5 results in the code internally calculating the form and interfacial losses across a junction. Utilization of the partial area change model allows the user to specify the form loss while allowing the code to internally calculate the interfacial loss. Activation of the smooth area change model allows the user to specify the form loss with no internal calculation of the interfacial losses.

More detailed discussion concerning this model can be found in the NRELAP5 theory manual (Reference 9).

6.6.3 Counter Current Flow Limitation

A general CCFL model is implemented in a form proposed by Bankoff (Reference 31), which has the structure

$$H_g^{1/2} + mH_f^{1/2} = c \qquad \text{Equation 6-53}$$

where,

H_g = dimensionless vapor/gas flux,

H_f = dimensionless liquid flux,

c = vapor/gas intercept (value of $H_g^{1/2}$ when $H_f = 0$, i.e., complete flooding), and

m = “slope”, that is the vapor or gas intercept divided by the liquid intercept (the value of $H_f^{1/2}$ when $H_g = 0$).

The dimensionless fluxes have the form as defined by Equation 6-54 and Equation 6-55.

© Copyright 2016 by NuScale Power, LLC

$$H_g = j_g \left[\frac{\rho_g}{gw(\rho_f - \rho_g)}\right]^{1/2}$$ Equation 6-54

$$H_f = j_f \left[\frac{\rho_f}{gw(\rho_f - \rho_g)}\right]^{1/2}$$ Equation 6-55

In these equations j_g is the vapor/gas superficial velocity $(\alpha_g v_g)$, j_f is the liquid superficial velocity $(\alpha_f v_f)$, $\rho_g$is the vapor/gas density, ρ_f is the liquid density, α_g is the vapor/gas volume fraction, α_f is the liquid volume fraction, g is the gravitational acceleration. In Equation 6-54 and Equation 6-55, w is the length scale and is given by Equation 6-56.

$$w = D_j^{1-\beta} L^{\beta}$$ Equation 6-56

Where β is a user-input constant, D_j is the junction hydraulic diameter and L is the Laplace capillary length constant given by Equation 6-57.

$$L = \left[\frac{\sigma}{g(\rho_f - \rho_g)}\right]^{1/2}$$ Equation 6-57

Bankoff recommends a formula for computing the value of β:

$$\beta = \tanh\left(\frac{A_h}{A_t} \cdot \frac{2\pi}{t_p} \cdot D_j\right)$$ Equation 6-58

where A_h is the total area of the holes through the plate, A_t is the total area of the plate, including the holes, and t_p is the thickness of the plate.

The Bankoff correlation specifies that the vapor/gas intercept (c) is of the form:

© Copyright 2016 by NuScale Power, LLC

$$c = (1.07 + 0.00433 \cdot L^B) \qquad \text{Equation 6-59}$$

when the dimensionless Bond number, L^B, is less than 200 and $c = 2$ for all L^B greater than or equal to 200.

The bond number is:

$$L^B = n\pi D \left[\frac{g(\rho_f - \rho_g)}{\sigma}\right]^{1/2} = \frac{n\pi D_j}{L} \qquad \text{Equation 6-60}$$

where n is the number of holes in the plate at the CCFL junction, D_j is the hydraulic diameter, and L is the Laplace capillary length constant, previously defined. More detailed discussion concerning this model can be found in the NRELAP5 theory manual (Reference 9).

Assessment of the CCFL model demonstrates excellent agreement against Bankoff perforated plate test data (Section 7.2.10). A sensitivity study of the effects of the CCFL model is presented in Section 9.6.3 for its application at the NPM pressurizer baffle plate.

6.7 Helical Coil Steam Generator Component

A new hydrodynamic component and heat transfer package have been added to NRELAP5 to model flow and heat transfer inside a helical coil SG. These are developed based on helical coil geometry-specific heat transfer and wall friction correlations. The need for improved models is based on inadequate agreement with pressure drop and heat transfer performance with the baseline RELAP5-3D© code results against prototypic helical coil SG testing performed at SIET. Improvements and adequacy of the implemented models in NRELAP5 are demonstrated through prototypic assessments of the NuScale helical coil SG using SIET test data (see Sections 7.4.1 and 7.4.2). These tests assessed heat transfer and pressure drop on both the secondary side (within tubes) and primary side (external to tubes) of the helical coil SG.

A wide range of pressure drop and heat transfer correlations were investigated for analyzing the inside of the helical coils. A down selection was performed of these investigated models for implementation into the NRELAP5 code based on the applicability of the models to the NPM helical coil SG.

© Copyright 2016 by NuScale Power, LLC

6.7.1 Helical Coil Tube Friction

6.7.1.1 Helical Coil Single-Phase Tube Wall Friction

The {{ }}2(a),(c) provided the best global coverage and as such have been implemented into NRELAP5. {{

}}2(a),(c)

6.7.1.2 Helical Coil Two-Phase Tube Wall Friction

The two-phase inner wall friction for a helical coil is computed in a similar fashion to the Lockhart-Martinelli model implemented in the RELAP5 code series. A modification is made to the two-phase friction multiplier for the helical coil component as presented in its final form by Equation 6-62.

© Copyright 2016 by NuScale Power, LLC

{{

}}2(a),(c)

{{

}}2(a),(c)

6.7.2 Helical Coil Tube Heat Transfer

A new heat transfer package has been added to NRELAP5 and differs from that of the standard RELAP5 pipe geometry in {{

}}2(a),(c) A new geometry type represents the {{

}}2(a),(c)

{{

}}2(a),(c)

© Copyright 2016 by NuScale Power, LLC

6.7.2.1 Helical Coil Single-Phase Heat Transfer

The laminar heat transfer correlation {{

}}2(a),(c)

6.7.2.2 Helical Coil Two-Phase Subcooled and Saturated Flow Boiling Heat Transfer

The saturated flow boiling heat transfer correlation is used for {{

}}2(a),(c)

© Copyright 2016 by NuScale Power, LLC

{{

}}2(a),(c)

6.8 Wall Condensation

{{

}}2(a),(c)

© Copyright 2016 by NuScale Power, LLC

{{

}}2(a),(c)

© Copyright 2016 by NuScale Power, LLC

{{

}}2(a),(c)

Table 6-1. Dimensionless vapor velocity transition criteria for condensation

{{

}}2(a),(c)

Table 6-2. Regime Nusselt relations for condensation

{{

}}2(a),(c)

© Copyright 2016 by NuScale Power, LLC

6.9 Interfacial Drag in Large Diameter Pipes

RELAP5-3D© contains the Kataoka-Ishii (Reference 40) formulation of the drift-flux model for use in the bubbly flow case in intermediate $(0.018 < D \leq 0.08\ m)$ and large pipes $(D > 0.08\ m)$. This same dimensional formulation is maintained within NRELAP5.

RELAP5-3D© originally implemented the modified Rouhani distribution coefficient (Reference 42) as shown by Equation 6-87.

$$C_\infty = 1 + 0.2\sqrt{\frac{\rho_f\sqrt{gD_h}}{|G| + 0.001}} \qquad \text{Equation 6-87}$$

{{

}}2(a),(c)

6.10 Fission Decay Heat and Actinide Models

The ANS 1973 fission decay heat standard (Reference 46) is presented in terms of the Shure curve (Reference 47) and tabular data. The NRELAP5 implementation of the ANS 1973 standard applies the Shure curve, which is a fit to differential equations for one isotope and 11 groups. Assuming infinite operating time, the fission product decay power is calculated with Equation 6-89. Table 6-3 provides the 11-group constants derived from the Shure curve as implemented into NRELAP5. Figure 6-3 provides the comparison of the ANS 1973 standard to the as implemented curve.

$$\mathrm{P} = \mathrm{P_o}\gamma\sum_{n=1}^{11} A_n \exp(-a_n t_s) \qquad \text{Equation 6-89}$$

where,

P = fission decay power,

P_0 = infinite operating time fission power prior to shutdown,

© Copyright 2016 by NuScale Power, LLC

γ = fission product yield factor,

A_n, a_n = fit coefficients, and

t_s = time after shutdown.

Table 6-3. ANS 1973 11-group fission decay constants

{{

}}2(a),(c)

© Copyright 2016 by NuScale Power, LLC

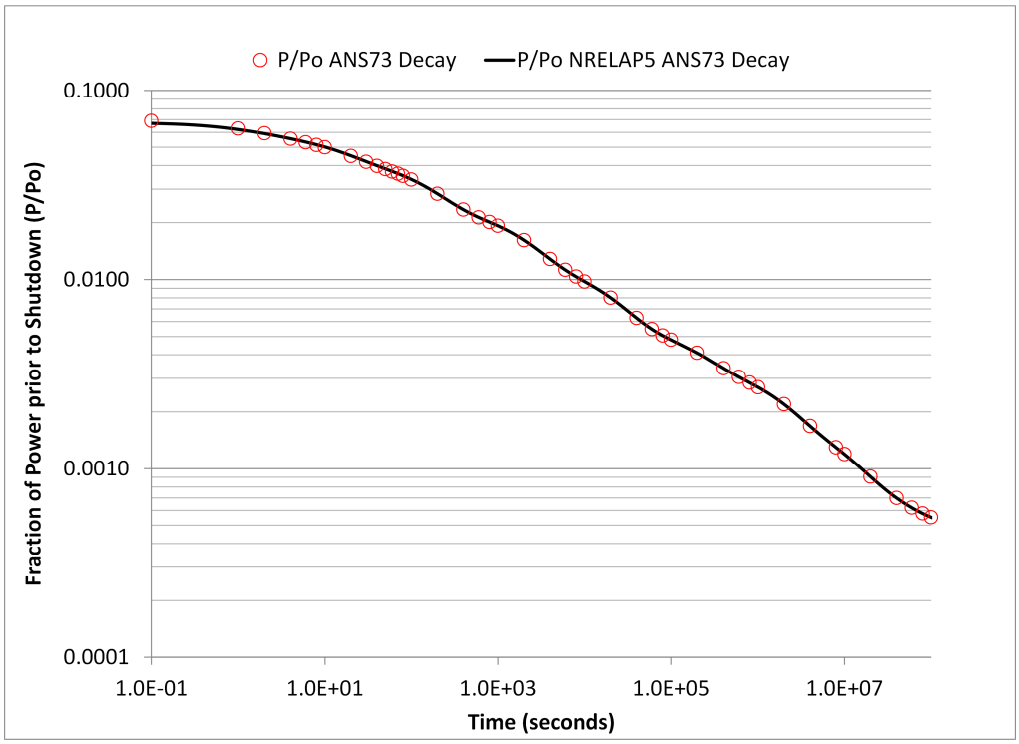

Figure 6-3. NRELAP5 ANS 1973 implemented fission decay heat curve

The actinide model describes the production of ^{239}U, ^{239}Np, and ^{239}Pu from neutron capture by ^{238}U based on the decay equations of Equation 6-90.

$$\frac{d\gamma_{U(t)}}{dt} = F_U \Psi(t) - \lambda_U \gamma_U$$

$$\frac{d\gamma_N(t)}{dt} = \lambda_U \gamma_U - \lambda_N \gamma_N \qquad \text{Equation 6-90}$$

$$P_\alpha(t) = \eta_U \lambda_U \gamma_U(t) + \eta_N \lambda_N \gamma_N(t)$$

The quantity F_U is user-specified and is the number of atoms of ^{239}U produced by neutron capture in ^{238}U per fission from all isotopes. The λ and η values can be user-specified, or default values equal to those stated in the 1979 ANS standard (Table 6-4), the 1994 Standard, or the 2005 Standard can be used.

The first equation describes the rate of change of atoms of ^{239}U. The first term on the right represents the production of ^{239}U; the last term is the loss of ^{239}U due to beta decay.

© Copyright 2016 by NuScale Power, LLC

The second equation describes the rate of change of ^{239}Np. The production of ^{239}Np is from the beta decay of ^{239}U, and ^{239}Pu is formed from the decay of ^{239}Np. $\Psi(t)$ is the solution from the NRELAP5 fission source. The implemented model yields the result quoted in the 1979 Standard (Reference 48), the 1994 Standard (Reference 49), and the 2005 Standard (Reference 50) as demonstrated by Figure 6-4.

Table 6-4. ANS-79 actinide model constants.

Isotope	λ (s^{-1})	η (MeV)
^{239}U	1.772	0.00299
^{239}Np	0.5774	0.00825

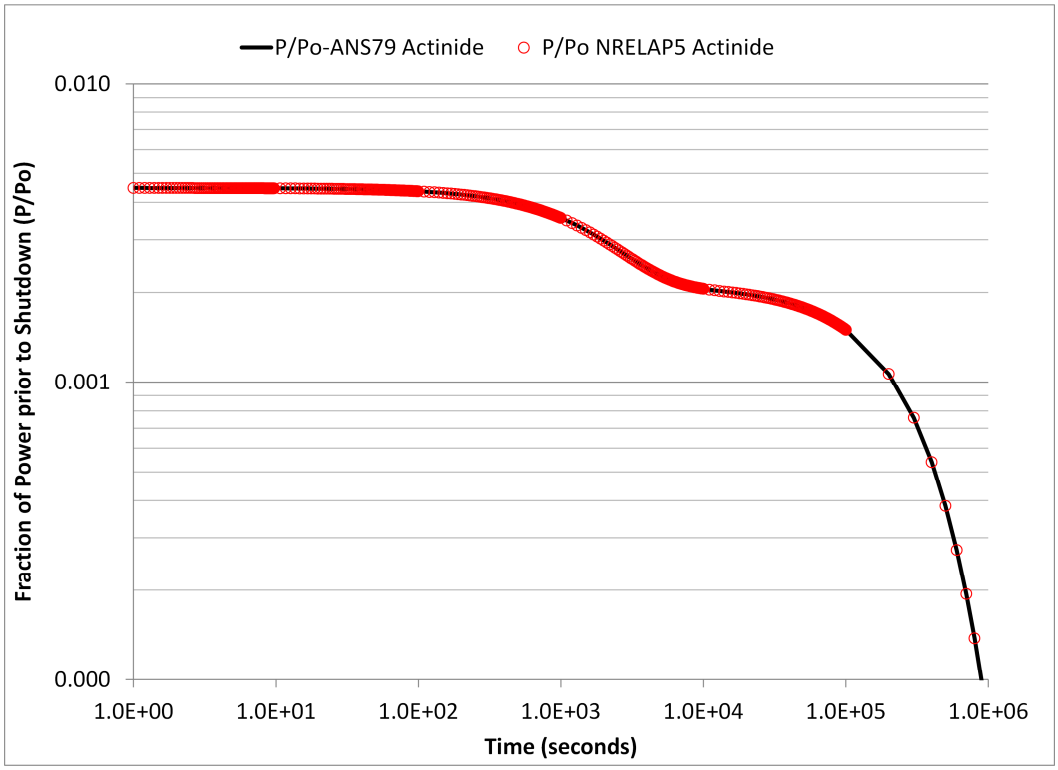

Figure 6-4. NRELAP5 ANS-79 implemented actinide heat curve

6.11 Critical Heat Flux Models

The CHF is calculated using a combination of the {{

}}2(a),(c)

© Copyright 2016 by NuScale Power, LLC

{{

}}2(a),(c)

6.11.1 {{ }}2(a),(c)

{{

}}2(a),(c)

© Copyright 2016 by NuScale Power, LLC

{{

}}2(a),(c)

Figure 6-5. {{ }}2(a),(c)

{{

}}2(a),(c)

© Copyright 2016 by NuScale Power, LLC

{{

}}2(a),(c)

6.11.2 Implementation of Critical Heat Flux correlations

{{ }}2(a),(c) are implemented in NRELAP5 as follows:

- {{

}}2(a),(c)

6.11.3 {{ }}2(a),(c)

{{

}}2(a),(c)

© Copyright 2016 by NuScale Power, LLC

{{

}}2(a),(c)

© Copyright 2016 by NuScale Power, LLC

{{

}}2(a),(c)

Table 6-5. Coefficient of revised pressure correction term in Equation 6-102

{{

}}2(a),(c)

© Copyright 2016 by NuScale Power, LLC

{{

}}2(a),(c)

Figure 6-6. {{
}}2(a),(c)

{{

}}2(a),(c)

© Copyright 2016 by NuScale Power, LLC

Table 6-6. {{ }}2(a),(c) critical heat flux correlation application range

{{

}}2(a),(c)

{{

}}2(a),(c)

6.11.4 {{ }}2(a),(c)

{{

}}2(a),(c)

© Copyright 2016 by NuScale Power, LLC

{{

}}2(a),(c)

© Copyright 2016 by NuScale Power, LLC

7.0 NRELAP5 Assessments

The following section provides a summary of the SET and IET assessments that have been completed for NRELAP5. The results of these assessments are considered in Section 8.0 to justify the adequacy on NRELAP5 for modeling of high-ranked phenomena in the NuScale LOCA PIRT.

To assess the adequacy of NRELAP5, code simulations are compared to measured experimental data. Acceptance criterion from Table 1-2 are applied in rating NRELAP5 performance in terms of “excellent”, “reasonable” or “minimal” agreement. These ratings take into consideration the ability to predict overall data trends as well as the magnitude of the data itself.

7.1 Assessment Methodology

Various experimental tests, inclusive of SETs, IETs, and analytic problems have been used to assess the performance of NRELAP5 using the process identified in Element 2 of RG 1.203. The database employed to assess the adequacy of the NRELAP5 code was chosen to be consistent with the requirements to adequately model the high-ranked phenomena derived in the NuScale LOCA PIRT.

The high-ranked phenomena selected in Section 4 are mapped onto an assessment matrix of experiments, and are listed in Table 7-1. The analytic problems (fundamental tests) used to assess NRELAP5 are not shown in Table 7-1.

© Copyright 2016 by NuScale Power, LLC

Table 7-1. NRELAP5 loss-of-coolant accident assessment matrix

{{

}}2(a),(c)

Summarized within this section for each assessment are the following:

- a brief description and purpose of the experimental facility,
- a summary of the phenomenon addressed,
- the experiment procedure,
- important NRELAP5 modeling techniques, and
- performance of NRELAP5 against the data.

Assessment cases are divided into two categories:

© Copyright 2016 by NuScale Power, LLC

- Legacy Assessments – these are assessments performed against data collected from historical test programs not encompassed within the NuScale test programs
- NuScale Test Assessments – these are assessments performed against data collected as part of the NuScale testing program

The following sections document the various assessments completed with NRELAP5.

7.2 Legacy Test Data

This section describes those test programs which have produced data that were not performed under the NuScale QAPD (Reference 4). With the exception of Marviken JIT-11 data, these tests are qualified for use by applying non-mandatory guidance provided by NQA-1 2008/2009 Addendum (Reference 10). Use of Marviken JIT-11 data is based on published literature data.

7.2.1 Ferrell-McGee

The Ferrell-McGee tests were performed in vertical pipes over a wide range of single-phase and two-phase flow conditions with uniform, contraction, and expansion flow areas. The data assessed includes single- and two-phase pressure drop and void fraction under different pressures, flow rates, and inlet quality.

7.2.1.1 Facility Description

The report for the Ferrell-McGee experiments (Reference 58) describes the test facility. Figure 7-1 shows the schematic of the test section. The test apparatus consists of a heated section that controls the degree of sub-cooling of the liquid entering into an adiabatic test section, where pressure drops and void fractions were measured. The lower test section is 40.5 in. (1.0287 m) in height and the upper test section is 49.5 in. (1.2573 m) for a total of 90.0 in. (2.286 m). The two test sections were connected by mating flanges. The tests were organized into seven test groups. Each test group had a different combination of pipe diameters for the lower and upper sections. The tests of Group 1 and Group 4 used pipes of uniform diameter of 0.46 in. (0.0117 m) and 0.34 in. (0.00864 m) and are designed to assess two-phase frictional pressure drop. Tests of Groups 2, 5 and 6 are tests with abrupt area expansion with area ratios of 0.608, 0.332 and 0.546, respectively. The tests of Groups 3 and 7 are tests with abrupt contraction with area ratios of 0.546 and 0.608, respectively. In this section the area ratios are defined as small area or large area. Tests with abrupt area expansion and contractions are designed to assess frictional and form losses. Multiple sets of tests were run with different combinations of pressure, flow, and inlet quality.

© Copyright 2016 by NuScale Power, LLC

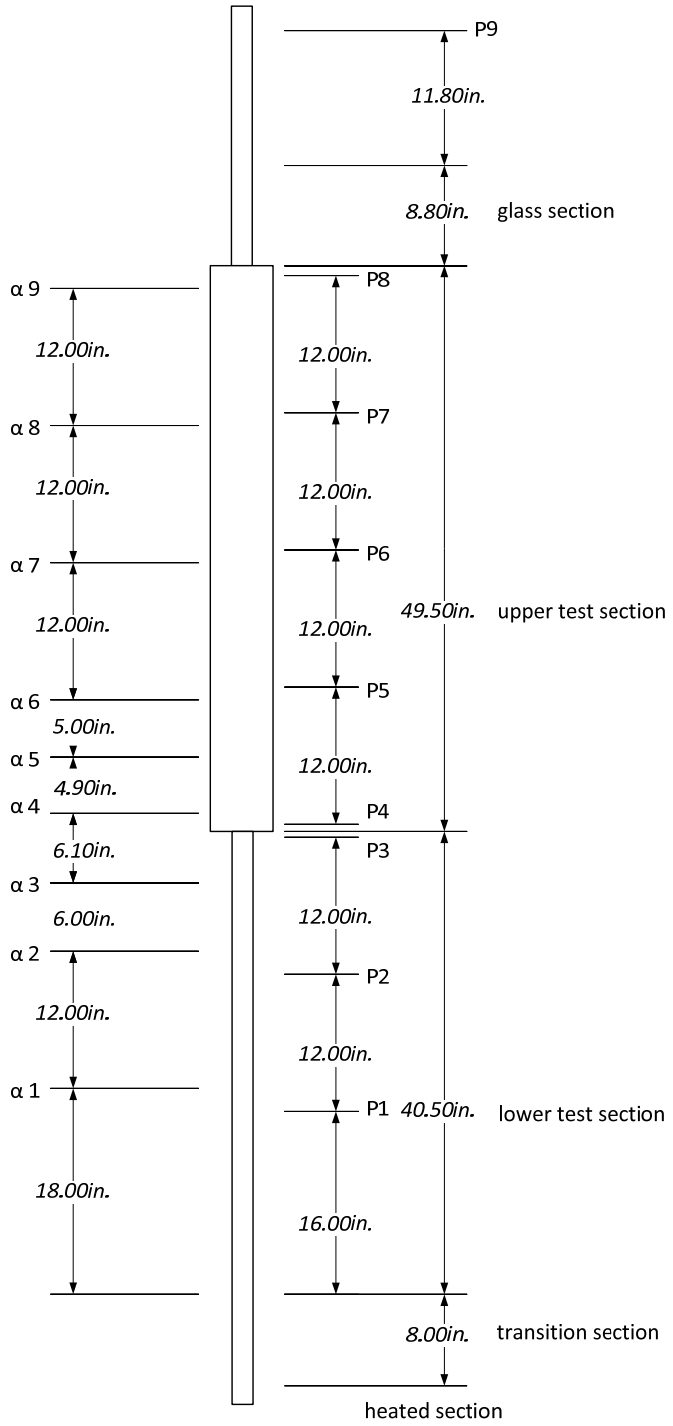

Figure 7-1. Schematic of the Ferrell-McGee test section

© Copyright 2016 by NuScale Power, LLC

7.2.1.2 Phenomena Addressed

The phenomenon addressed with the Ferrell-McGee assessment cases is the ability of NRELAP5 to predict {{

}}2(a),(c)

7.2.1.3 Experimental Procedure

The part of the stainless steel flow loop of particular interest is the vertical adiabatic test section in which an upward flowing steam-water mixture entered at a controlled pressure, mass flow rate, and quality. Pressure drops and steam volume fractions (α) were measured along the channel at the locations shown in Figure 7-1.

The two-phase mixture exited from the test section into a 0.460-in. inside diameter glass section through which the mixture could be photographed. The vapor-liquid mixture was partially separated in a surge tank and sub-cooled in a bank of six parallel concentric-tube heat exchangers.

The sub-cooled liquid passed through a pump, a manual flow control valve, a volumetric flowmeter, and a preheater which controlled the quality of two-phase flow entering the heated section. In the heated section, a 0.462-in. inside diameter by 0.083-in. wall tube heated by an alternating current flowing in the tube wall, the water was brought to the desired quality before injection into the adiabatic test section.

System pressure was maintained by a hydraulic accumulator. Loop fluid, cooling water, heated channel wall, and manometer line temperatures were also recorded.

The summary of ranges of recorded data for the 201 runs is provided in Table 7-2. The initial boundary conditions covered a range of three different mass flow rates of 460, 920 and 1,150 lbm/hr (209, 417, and 522 kg/hr), a range of three different pressures of 60, 120 and 240 psi (0.414, 0.827, and 1.65 MPa) and void fractions from 0.0 to 1.0.

Table 7-2. Summary of Ferrell-McGee experimental test data range

Parameter	Range Min	Range Max	Units
Pressure	60 (0.414)	240 (1.65)	psia (MPa)
Inlet flow rate	460 (209)	1,150 (522)	lbm/hr (kg/hr)
Inlet void fraction range[1]	-0.110	1.038	n/a
Expansion area ratio	0.332	0.608	n/a
Contraction area ratio	0.546	0.608	n/a

[1]Negative void fractions refer to sub-cooling estimates which are calculated.

Although the measured data includes void distributions at nine different locations, shown in Figure 7-1, only the void at measurement locations 1, 2 and 3 were considered. These locations have the void measurements near the center of NRELAP5 nodes. The rest of the void fraction measurement taps were not taken into account because placing all void

© Copyright 2016 by NuScale Power, LLC

measurement locations near the center of nodes would result in small nodes with a length-to-diameter (L/D) ratio less than 1.0.

The total pressure drop measurement uncertainty was estimated to be ±0.45 psi (0.0031 MPa). The average void fraction measurement uncertainty was estimated to be ±3 percent.

It is noted that test cases 1A6, 1A7, 1A11, 4A5, 4A9, 5A5, 5A10 and 6A9 with void fractions at Void Tap 1 larger than 0.97 were excluded from comparative results. The NRELAP5 total pressure drop predictions for these test cases showed a high deviation from the measurement, which subsequent analysis revealed to result from uncertainty of the inlet void fraction measurement.

7.2.1.4 Special Analysis Techniques

For test groups 2, 3, 5, 6 and 7, at the position of expansion and contraction {{

}}2(a),(c)

7.2.1.5 Assessment Results

Figure 7-2 shows the predicted versus measured pressure drop for uniform, expansion, and contraction tests. NRELAP5 predicted the experimental data with reasonable-to-excellent agreement. These results validate the ability of NRELAP5 to predict {{

}}2(a),(c)

© Copyright 2016 by NuScale Power, LLC

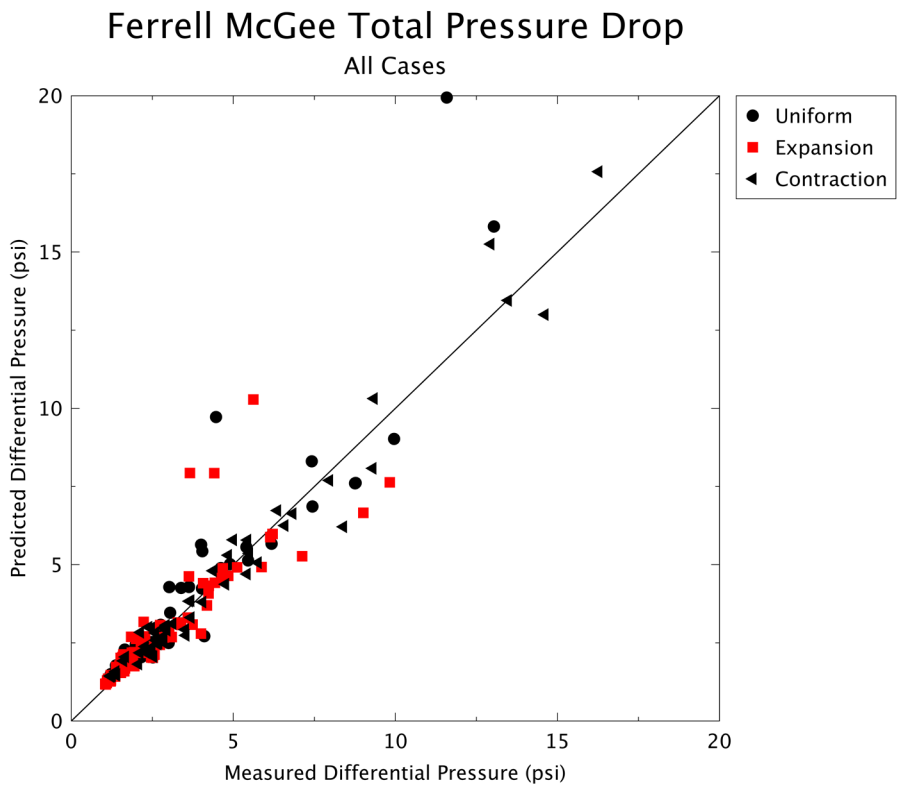

Figure 7-2. Predicted versus measured pressure drop for selected contraction tests

7.2.2 GE Level Swell (1 ft)

During various phases of a blowdown event in the NPM, such as a LOCA, the fluid within the RCS will experience flashing, vapor generation, level swell, and conditions representative of rapid depressurization. Reference 59 produced a suitable experimental database extending across a large range of pressures and fluid conditions that is used to assess the ability of NRELAP5 to predict {{ }}[2(a),(c)] The assessment of NRELAP5 against the 1 ft. diameter GE level swell test is summarized in this section, while the assessment of NRELAP5 against the 4 ft. GE level swell test is provided in Section 7.2.3.

7.2.2.1 Facility Description

The experimental facility is fully described in Reference 58 and summarized in this section. The experiment facility shown in Figure 7-3 consists of a pressure vessel made of carbon steel with a volume of 10 ft^3 (0.283 m^3), a diameter of approximately 12 in. (0.305 m) and a 14-ft (4.2672 m) length. The small vessel experiments (1 ft.) include a blowdown line with orifice plates that are interchanged to control the blowdown flow rate and

© Copyright 2016 by NuScale Power, LLC

depressurization rate. The effluent from the vessel blowdown is discharged into a suppression tank.

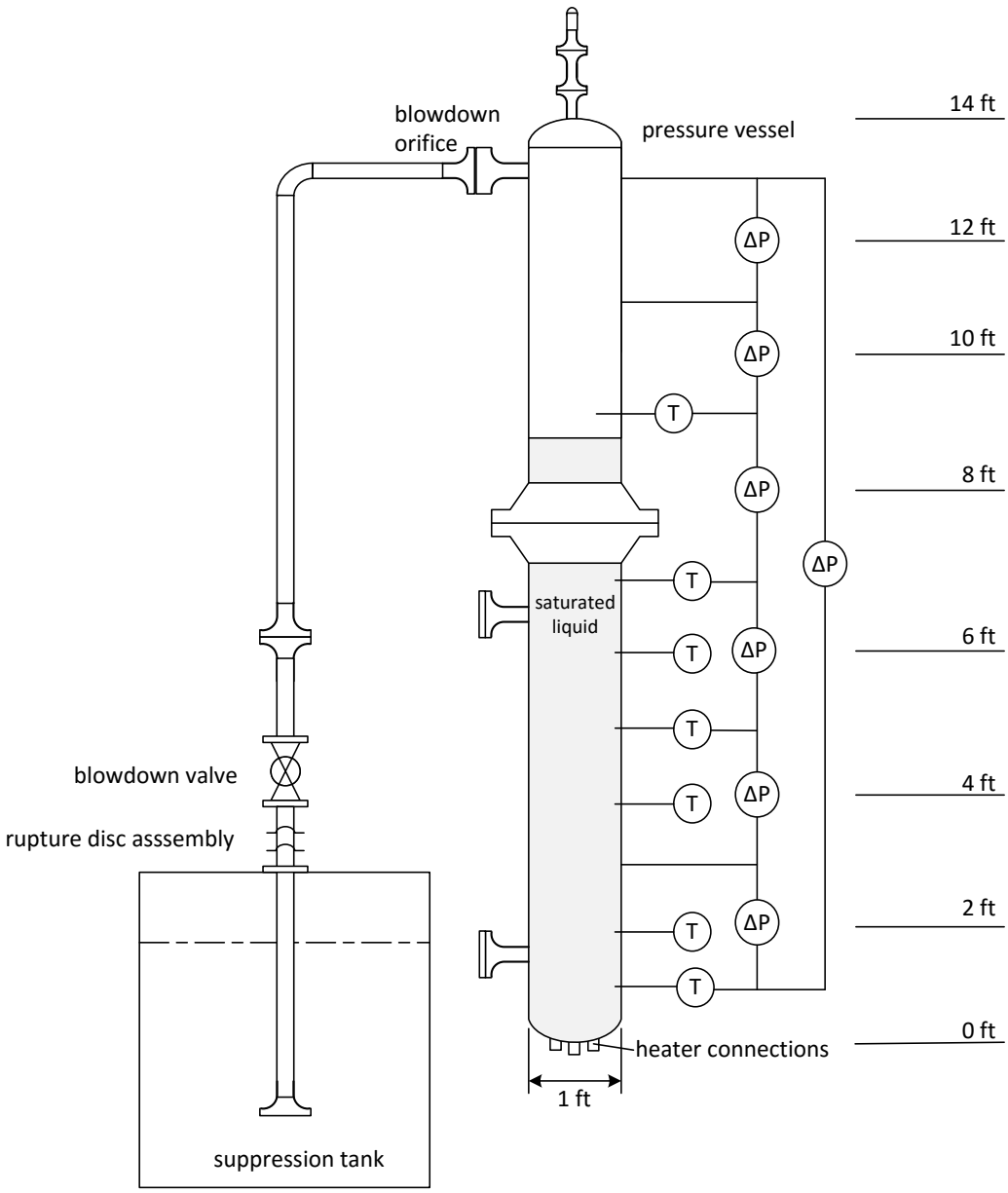

Figure 7-3. Schematic of the GE 1 ft. blowdown vessel

Three basic types of measurements were obtained during each experiment: static pressures, differential pressures, and temperatures.

Figure 7-3 shows the location of the instrumentation. There are six measurement sections between the adjacent differential pressure taps, numbered sequentially. The two-phase density (or mixture density) in each measurement section during blowdown experiments

© Copyright 2016 by NuScale Power, LLC

is derived from the axial differential pressure measurements. The fluid mass inventory is obtained from the density and known volume of the measurement section.

The average void fraction in each measurement section is determined from the measured mixture density and thermodynamic properties of the liquid and vapor phases at the system pressure as shown in Equation 7-1 (Reference 59).

$$\bar{\alpha}_i = (\bar{\rho}_i - \rho_f)/(\rho_g - \rho_f) \qquad \text{Equation 7-1}$$

Where $\bar{\alpha}_i$ is the average void fraction in the i-th measurement section, $\bar{\rho}_i$ is the average mixture density in the i-th measurement section, and ρ_f, ρ_g are the liquid and vapor densities as a function of the measurement sectionpressure.

7.2.2.2 Phenomena Addressed

The phenomena addressed with the GE level swell (1 ft. diameter) test include {{

}}2(a),(c)

Specifically, the GE level swell test assesses the ability of NRELAP5 to predict key in-vessel thermal-hydraulic phenomena associated with a rapid depressurization event.

7.2.2.3 Experimental Procedure

The experiment consisted of filling the vessel with demineralized water and boiling the inventory at atmospheric pressure to remove any dissolved gas. The top vent was then closed and the fluid was heated to the specified initial conditions, which was typically saturated conditions at the desired pressure. The initial water level was dependent upon the experiment of interest as listed in Table 7-3. Once conditions were reached a blowdown was initiated from a discharge valve located at the top of the vessel and measurements were recorded.

Table 7-3 summarizes the experiment conditions for the GE 1 ft. level swell test selected for the assessment. The parameters listed are used as boundary conditions in the NRELAP5 inputs or for comparisons to the NRELAP5 predictions. The blowdown experiment is initiated at a pressure of 1,011 psia (6.97 MPa) with saturated fluid conditions. The blowdown and fluid response is measured for approximately 300 seconds. Void fractions ranging from 0.0 to 1.0 are present during the test.

Table 7-3. Summary of GE 1 ft. vessel level swell experiments

Test Number	Orifice Size inches (mm)	Restriction Plate Configuration	Initial Pressure psia (MPa)	Initial Liquid Level ft (m)
1004-3	3/8 (9.525)	No plate	1,011 (6.971)	10.4 (3.17)

© Copyright 2016 by NuScale Power, LLC

7.2.2.4 Special Analysis Techniques

Based on sensitivity studies it was determined that applying the {{ }}2(a),(c) improved the depressurization comparisons from reasonable-to-excellent agreement. The discussion here, however, provides a summary with default discharge coefficient input of {{ }}2(a),(c)

7.2.2.5 Assessment Results

Figure 7-4 through Figure 7-8 present the vessel pressure and axial void fraction comparisons between NRELAP5 using the {{ }}2(a),(c) choking model and the measured data for experiment 1004-3. The initial 100 seconds of the simulations are to confirm a steady state condition. The blowdown event is initiated at 100 seconds and is therefore the initial time for all figures.

Figure 7-4 presents the calculated vessel pressure versus the measured data. The comparisons are in reasonable-to-excellent agreement. The predicted depressurization rate is slightly higher compared to the data.

Figure 7-5 through Figure 7-8 present the calculated axial void fraction versus the measured data for several points in time during the transient. The comparisons are presented for 10, 40, 100, and 160 seconds into the transient. The results show reasonable-to-excellent agreement. The trend of increased void fraction along the height of the vessel is predicted rather well. Deviations are observed at the lower elevations.

The results of mixture level in the vessel, not presented here, also show reasonable-to-excellent agreement between the calculated NRELAP5 results and the experimental data. The results validate the ability of NRELAP5 to predict key in-vessel thermal-hydraulic phenomena associated with a rapid depressurization event.

© Copyright 2016 by NuScale Power, LLC

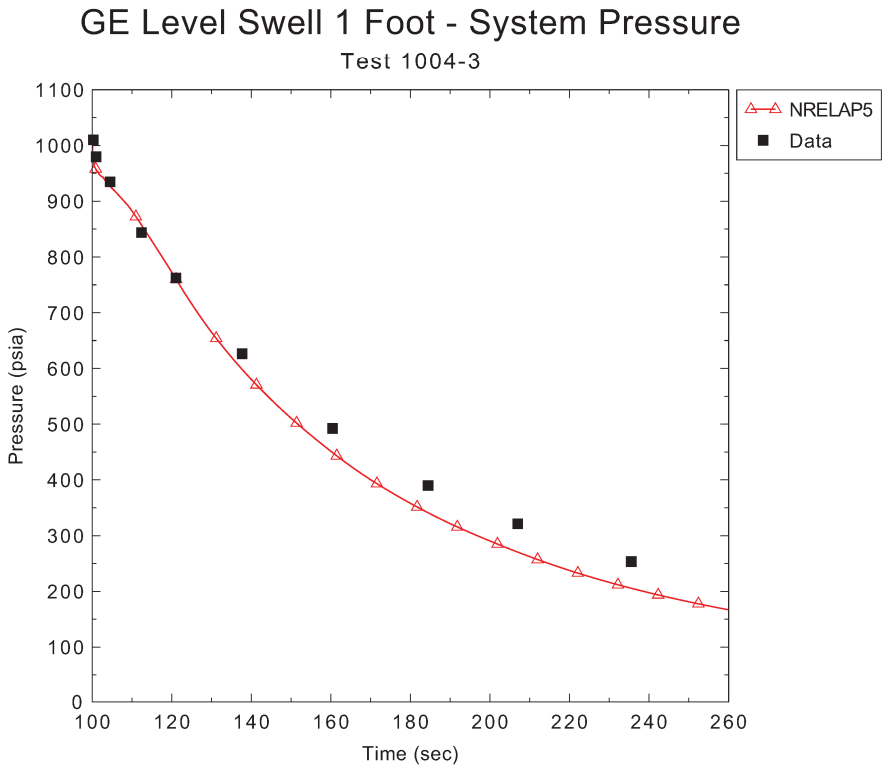

Figure 7-4. GE level swell 1 ft. vessel pressure versus time

© Copyright 2016 by NuScale Power, LLC

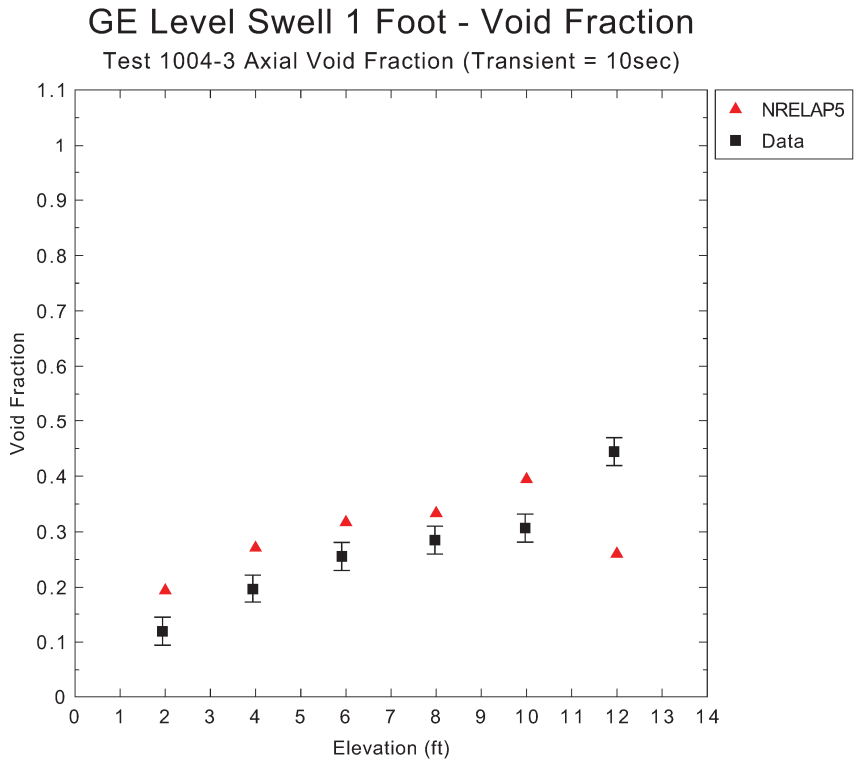

Figure 7-5. GE level swell 1 ft. vessel void fraction versus elevation at 10 seconds

© Copyright 2016 by NuScale Power, LLC

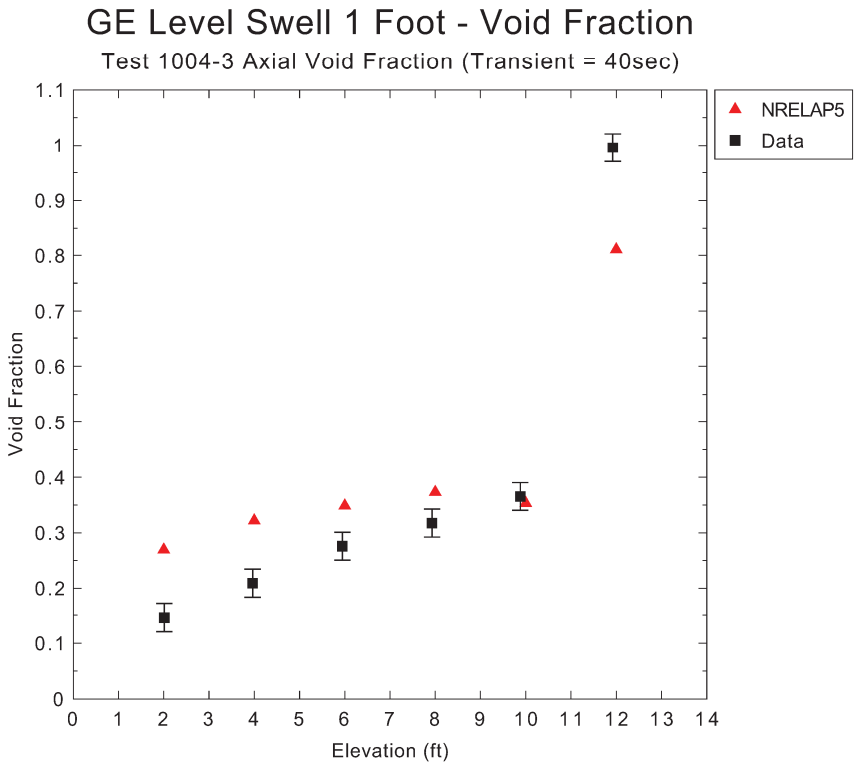

Figure 7-6. GE level swell 1 ft. vessel void fraction versus elevation at 40 seconds

© Copyright 2016 by NuScale Power, LLC

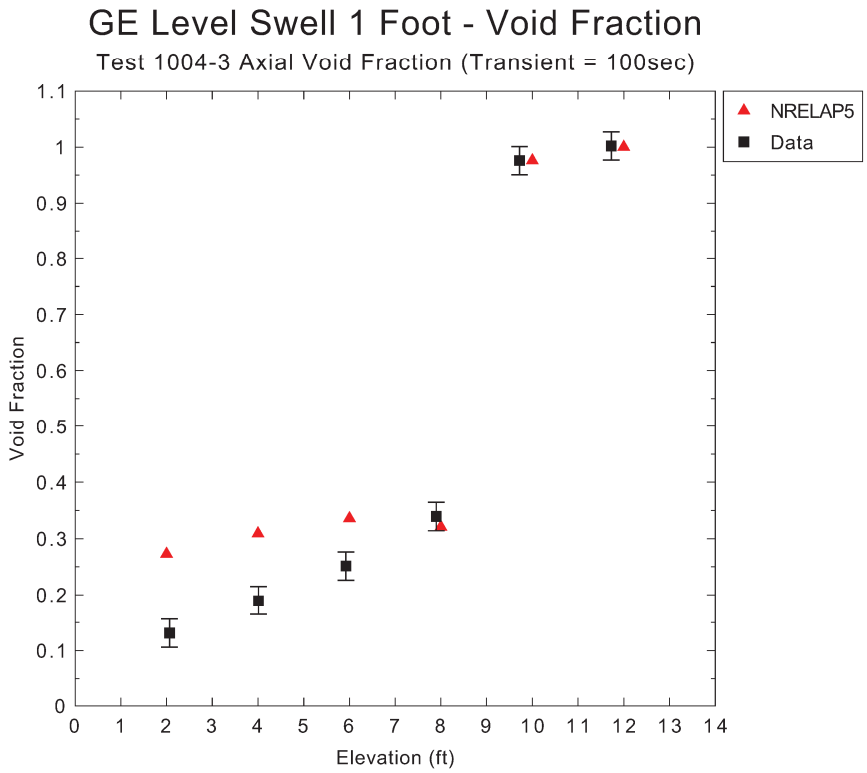

Figure 7-7. GE level swell 1 ft. vessel void fraction versus elevation at 100 seconds

© Copyright 2016 by NuScale Power, LLC

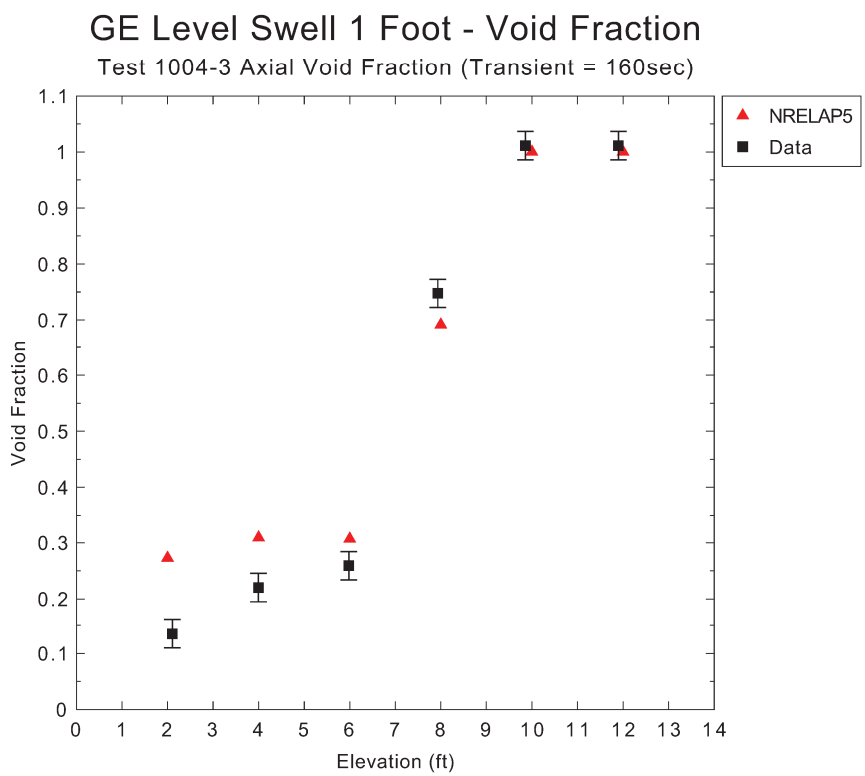

Figure 7-8. GE level swell 1 ft. vessel void fraction versus elevation at 160 seconds

7.2.3 GE Level Swell (4 ft)

7.2.3.1 Facility Description

The 4 ft. GE Level Swell test facility is fully described in Reference 59 and summarized in this section. The experimental facility shown in Figure 7-9 consists of a pressure vessel made of carbon steel with a volume of 160 ft^3 (4.5306 m^3), 47 in. (1.1938 m) in diameter and 14 ft (4.2672 m) in length. The test facility included a 10 in. (0.254 m) diameter vertical blowdown dip tube to simulate top break locations and a horizontal blowdown line to simulate bottom break locations. The effluent from the vessel blowdown is discharged to a suppression tank.

© Copyright 2016 by NuScale Power, LLC

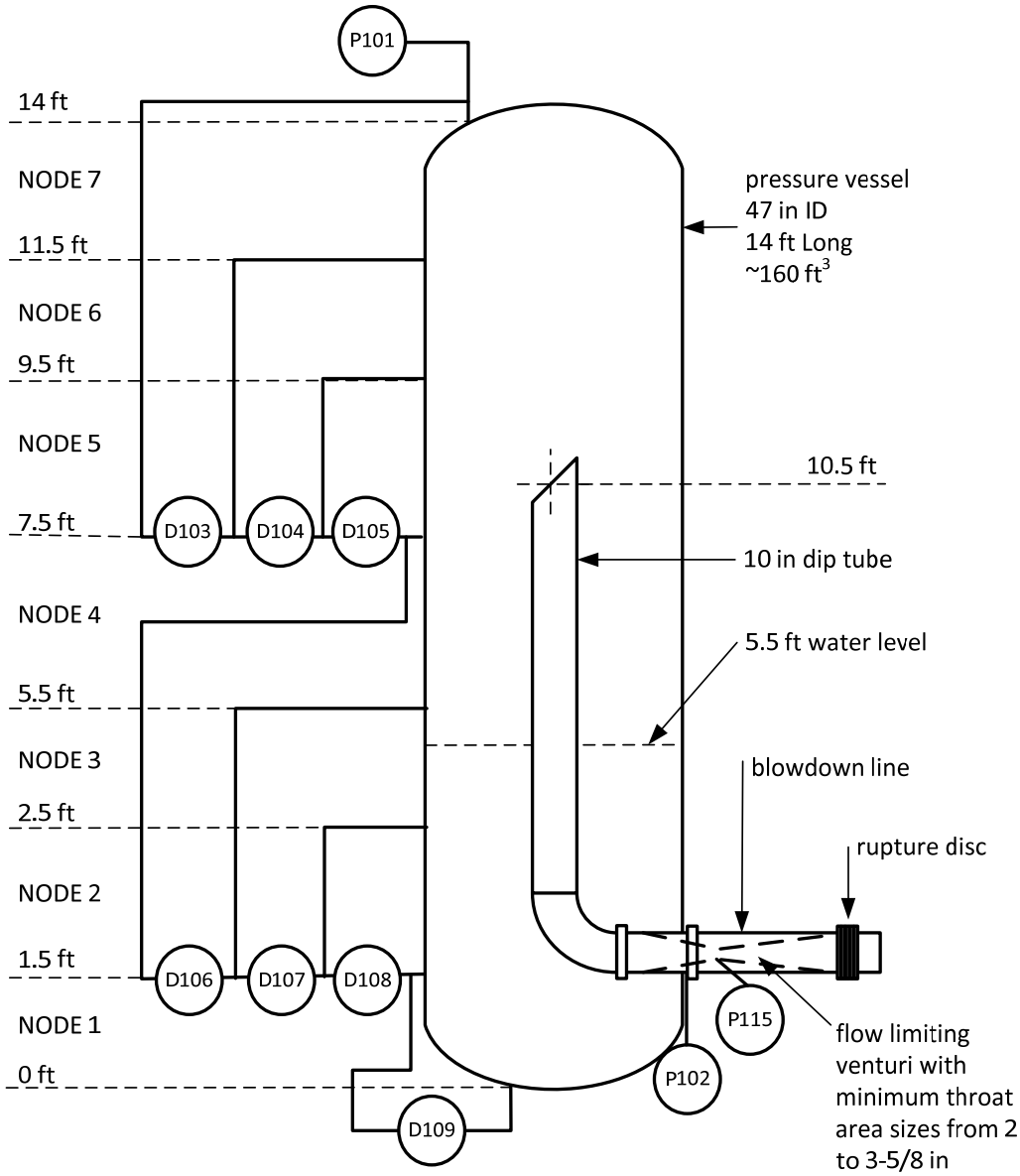

Figure 7-9. Schematic of the GE 4 ft. blowdown vessel

Three basic types of measurements were obtained during each experiment: pressures, differential pressures, and temperatures.

As shown in Figure 7-9 the pressure drop is measured at seven sections between the adjacent differential pressure taps, numbered sequentially. Similar to the 1 ft. GE level swell test, the mixture density and void fraction in each measurement section were calculated from the measured pressure drop (see Section 7.2.2.1).

© Copyright 2016 by NuScale Power, LLC

7.2.3.2 Phenomena Addressed

The phenomena addressed with the 4 ft. GE level swell are same as in the 1 ft. GE level test (see Section 7.2.2.2)

7.2.3.3 Experimental Procedure

The experiment procedure consisted of filling the vessel with demineralized water and boiling the inventory at atmospheric pressure to remove any dissolved gas. The top vent was then closed and the fluid was heated to the starting conditions, which was typically saturated conditions at 1,060 psia (7.308 MPa) for the large blowdown vessel experiments. The initial water level was dependent upon the experiment of interest. Top and bottom break blowdown events were conducted utilizing rupture discs.

A test 5801-15 with top break and initial liquid level of 5.5 ft (1.676 m) is selected for the assessment.

7.2.3.4 Special Analysis Techniques

The {{ }}$^{2(a),(c)}$ improves the depressurization for the sensitivity modeling the discharge and choking into an atmospheric blowdown tank. The discussion here, however, provides a summary with {{ }}$^{2(a),(c)}$

7.2.3.5 Assessment Results

The results of the GE level swell (4 ft. vessel) from NRELAP5, using the {{ }}$^{2(a),(c)}$ choking model and the measured data are compared. Key parameters are plotted together with the test data in Figure 7-10 through Figure 7-13. The results show reasonable-to-excellent agreement based on the comparison of the pressure and void fractions in the vessel. These results validate the ability of NRELAP5 to predict key in-vessel thermal-hydraulic phenomena associated with a rapid depressurization event.

© Copyright 2016 by NuScale Power, LLC

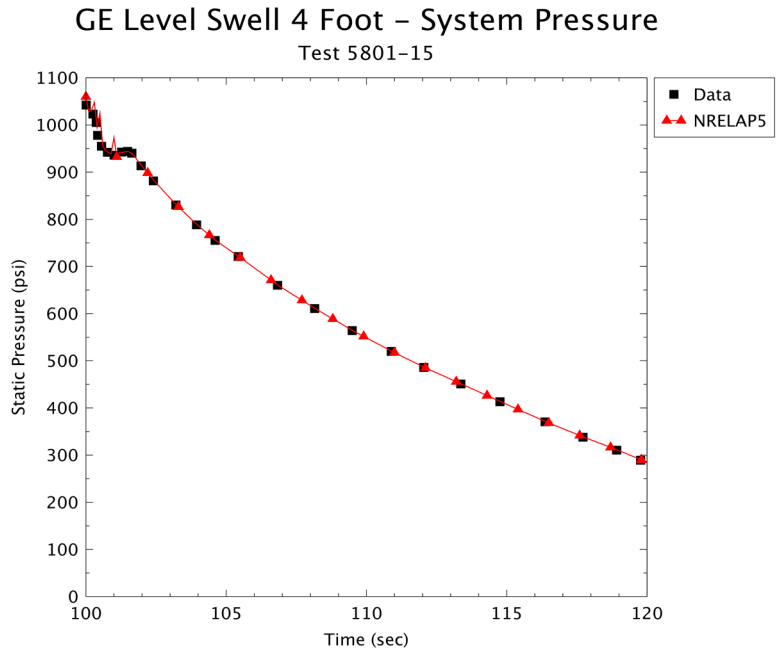

Figure 7-10. GE level swell 4-ft vessel pressure versus time

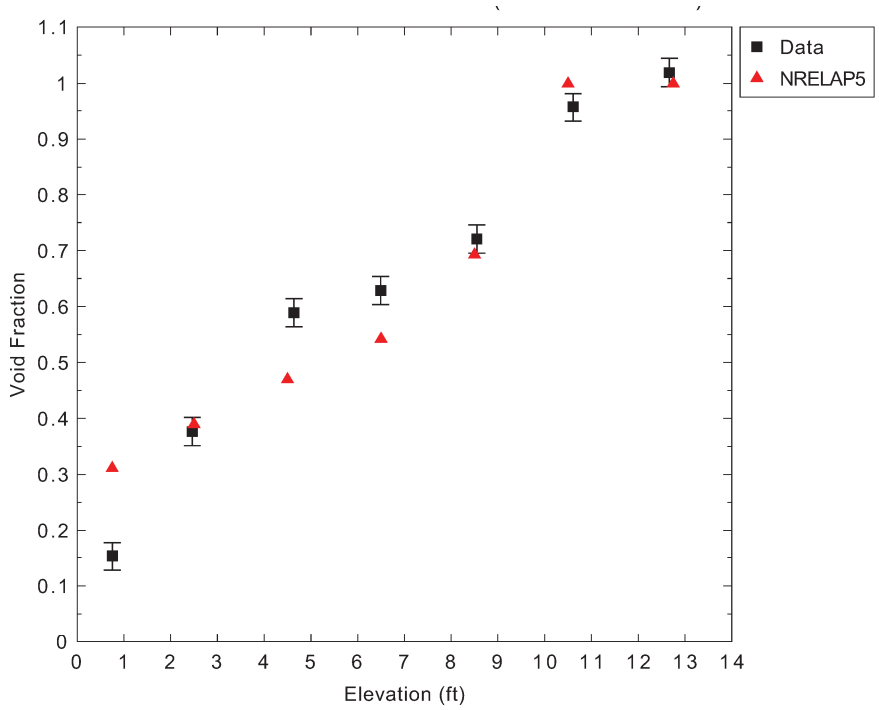

Figure 7-11. GE level swell 4-ft vessel void fraction versus elevation at 5 seconds

© Copyright 2016 by NuScale Power, LLC

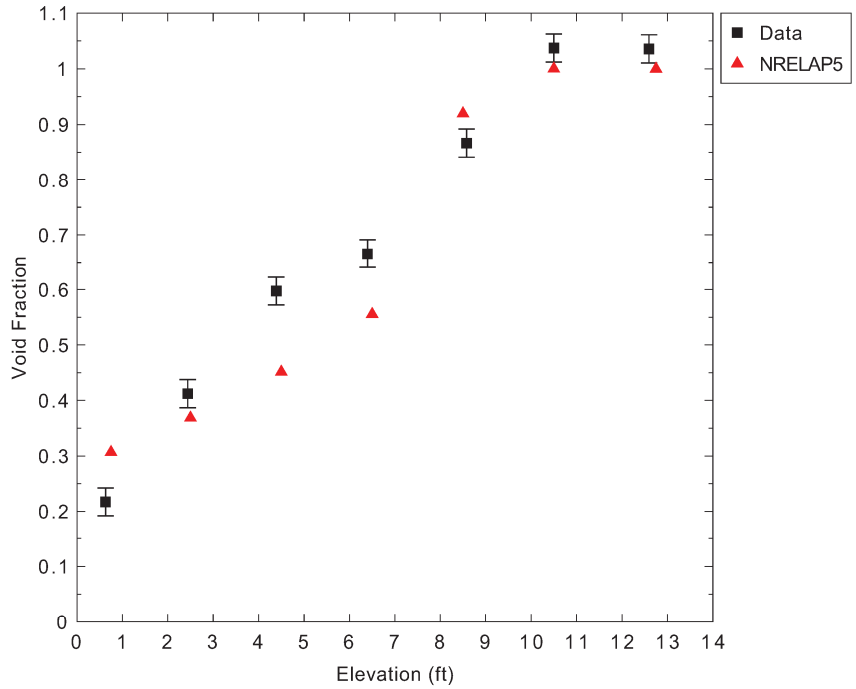

Figure 7-12. GE level swell 4-ft vessel void fraction versus elevation at 10 seconds

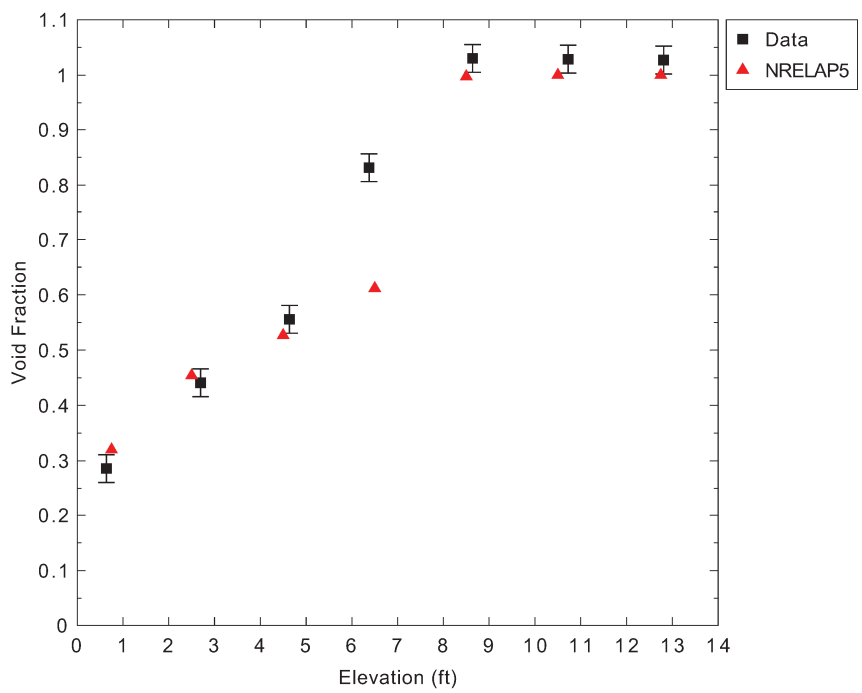

Figure 7-13. GE level swell 4-ft vessel void fraction versus elevation at 20 seconds

© Copyright 2016 by NuScale Power, LLC

7.2.4 KAIST

In the NuScale design, the DHRS is a passive safety-related system that relies on film condensation and natural circulation to remove heat from the RCS through the SG and reject heat to the reactor pool through the DHRS condenser. Reference 60 produced a suitable high pressure steam condensation experimental database which is used to assess the condensation model in NRELAP5.

The KAIST test data varied the pressure and non-condensable gas fraction of the steam entering the test section (mockup of a condenser tube). {{

}}2(a),(c),ECI

7.2.4.1 Facility Description

A schematic of the KAIST test facility is shown in Figure 7-14. Figure 7-15 shows the schematic of the test section. The maximum design pressure and temperature of the test facility were 7.5 MPa (1.088 psia) and 300 degrees C (752 degrees F), respectively.

The major components of the test facility include: SG which supplied steam (maximum power 200 kWe), test section tube, cooling pool (cools the test section), steam line (transports steam from SG to the test section inlet), condensate drain line, LP (or condensate collection tank), and air supply system. The test section was immersed in the cooling pool and was cooled by boiling and single-phase convective heat transfer on the outside surface of the test section.

The test section was a vertical tube with an inside diameter of 4.62 cm (1.82 in.) and an effective heat transfer length of 1.8 m (71 in.). The thickness of the tube wall was 2.3 mm (0.09 in.). To reduce the entrance effect, the top 0.5 m (20 in.) length of the test section was insulated. The test section was submerged in a cooling pool of width 1.2 m × 1.2 m (47 in. x 47 in.) and 2.5 m (98 in.) height. A steam line with an inside diameter 2.34 cm (0.92 in.) was connected from the top of the SG to the top of the test section. The condensate from the test section was drained to the LP (or condensate collection tank) by gravity and then pumped back to the SG.

© Copyright 2016 by NuScale Power, LLC

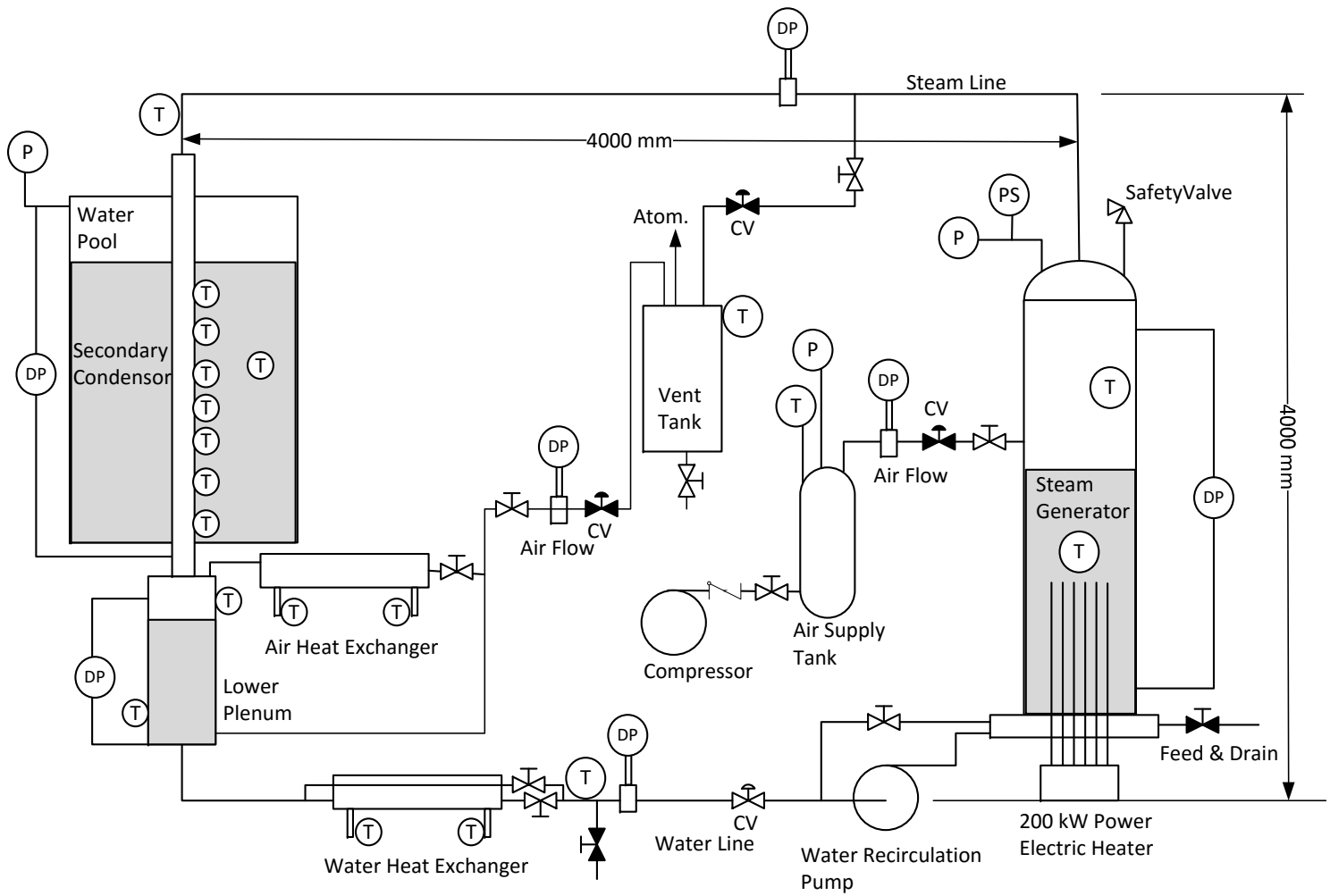

Figure 7-14. Schematic of KAIST test facility

© Copyright 2016 by NuScale Power, LLC

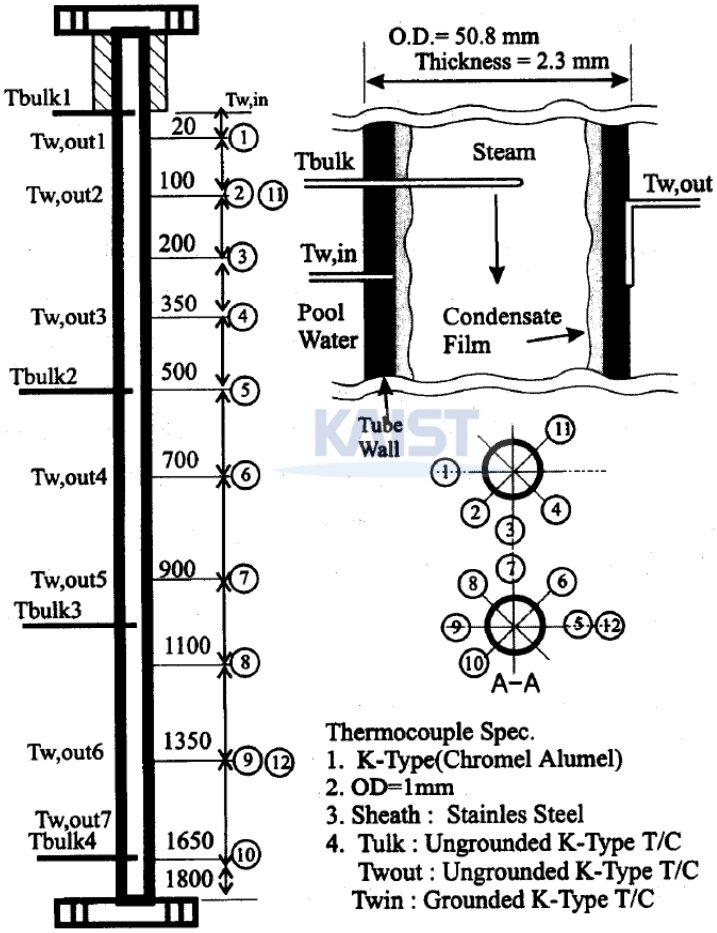

Figure 7-15. Schematic of the KAIST test section

7.2.4.2 Phenomena Addressed

The phenomena addressed with the KAIST assessment include {{

}}2(a),(c)

7.2.4.3 Experimental Procedure

The experiments were started by purging all non-condensable gas (i.e., air) from the test loop. This was done by supplying steam to the test loop and venting it to the atmosphere through the vent valve located below the test section. After all non-condensable gas was purged, the vent valve was closed and the test section was allowed to fill with the condensate by keeping the condensate drain valve closed. After the test section was completely filled, the SG pressure was increased to the test pressure. As soon as the test pressure was reached, the condensate drain valve was opened and the condensate

© Copyright 2016 by NuScale Power, LLC

recirculation pump was started. A constant water level in the LP was maintained by control of the recirculation pump flow rate. Data acquisition was started after the process had reached a steady state. Parameter ranges for the KAIST tests are summarized in Table 7-4.

Table 7-4. Range of KAIST test data

Parameter	Value
Pressure (MPa)	0.794 to 7.457 (115 to 1082 psia)
Reduced pressure (P_r)	0.036 to 0.34 (using critical pressure of 220.64 bar (3,200 psia)
Inlet steam mass flow (kg/s)	0.01 to 0.1 (0.022 to 0.22 lb/s)
Inlet air concentration (percent)	0.0 to 30.0
Prandtl number (Pr_f)	0.84 to 2.63
Liquid Reynolds number (Re_{LT})	2,300 to 3,2000
Inlet gas Reynolds number (Re_{GS})	16,400 to 15,0000

7.2.4.4 Special Analysis Techniques

Based on sensitivity studies, {{

}}2(a),(c)

7.2.4.5 Assessment Results

The results show reasonable-to-excellent agreement between the NRELAP5 calculations and the KAIST measured experimental data, on the comparison of condensed liquid flows, heat transfer coefficients, and inner wall temperatures. This is a result of implementation of the {{ }}2(a),(c) in NRELAP5 (see Section 6.8), which is intended to improve the predicted high pressure condensation response.

Figure 7-16 presents the measured versus calculated heat transfer coefficient for the KAIST steam condensation experiments. The majority of the predictions lie within the experimental uncertainty (28 percent for heat transfer coefficient).

© Copyright 2016 by NuScale Power, LLC

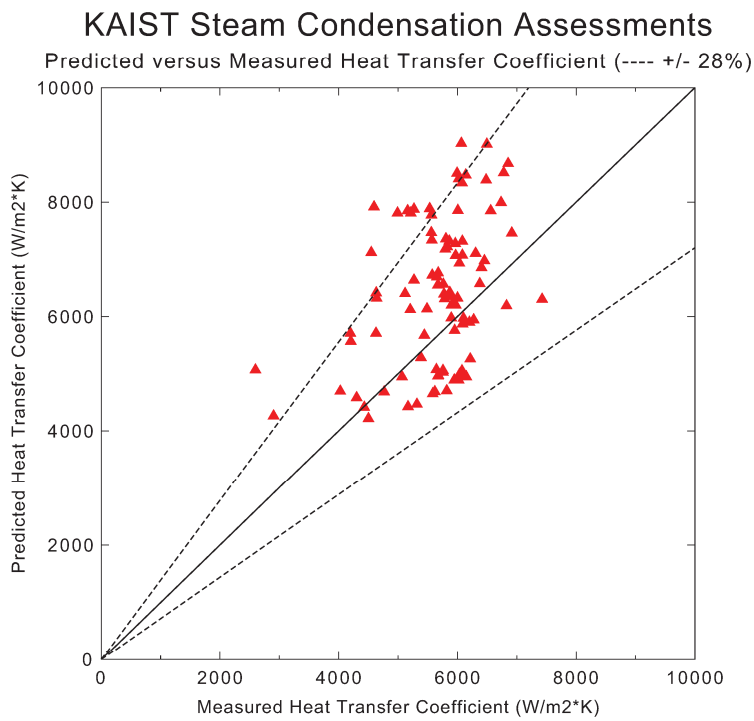

Figure 7-16. Measured versus predicted heat transfer coefficient

Figure 7-17 through Figure 7-19 present heat transfer coefficient, temperature and mass flow rate versus test section elevation. The majority of the predicted values (all but one) lie within the uncertainty range of the data.

Overall, the results show that NRELAP5 calculations are in excellent agreement with the KAIST measured experimental data. These results validate NRELAP5 for prediction of key thermal-hydraulic phenomena associated {{ }}2(a),(c)

© Copyright 2016 by NuScale Power, LLC

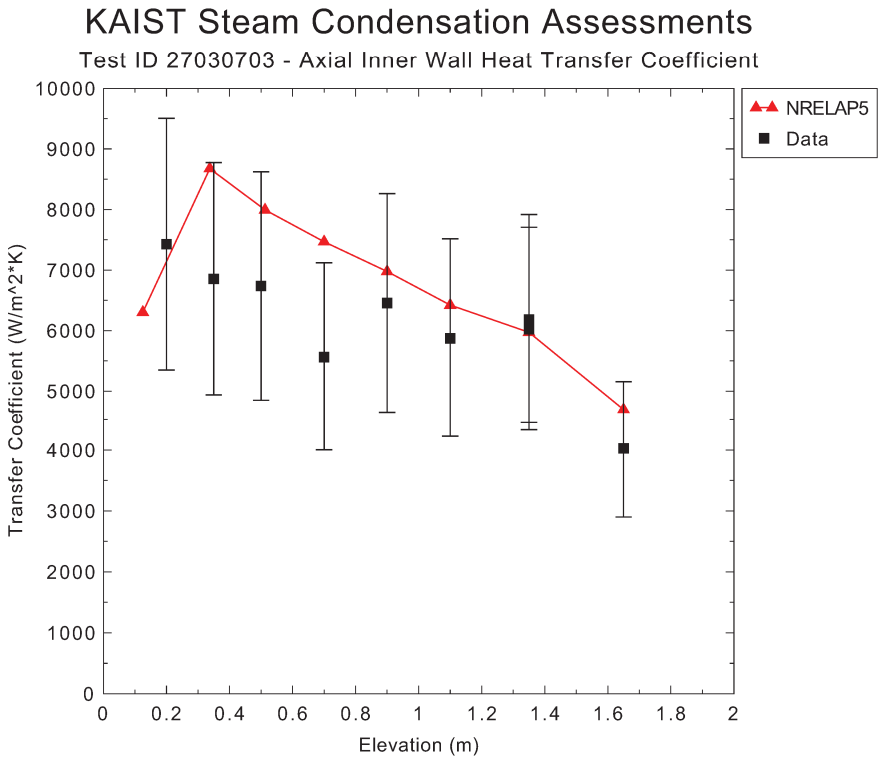

Figure 7-17. KAIST and NRELAP5 axial heat transfer coefficient

© Copyright 2016 by NuScale Power, LLC

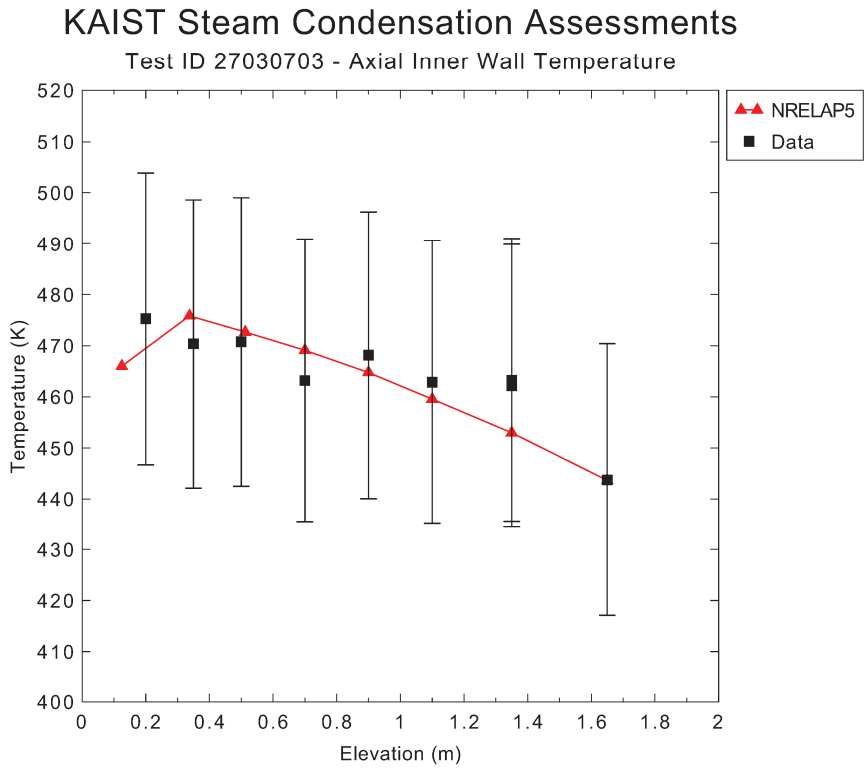

Figure 7-18. KAIST and NRELAP5 axial inner wall temperature

© Copyright 2016 by NuScale Power, LLC

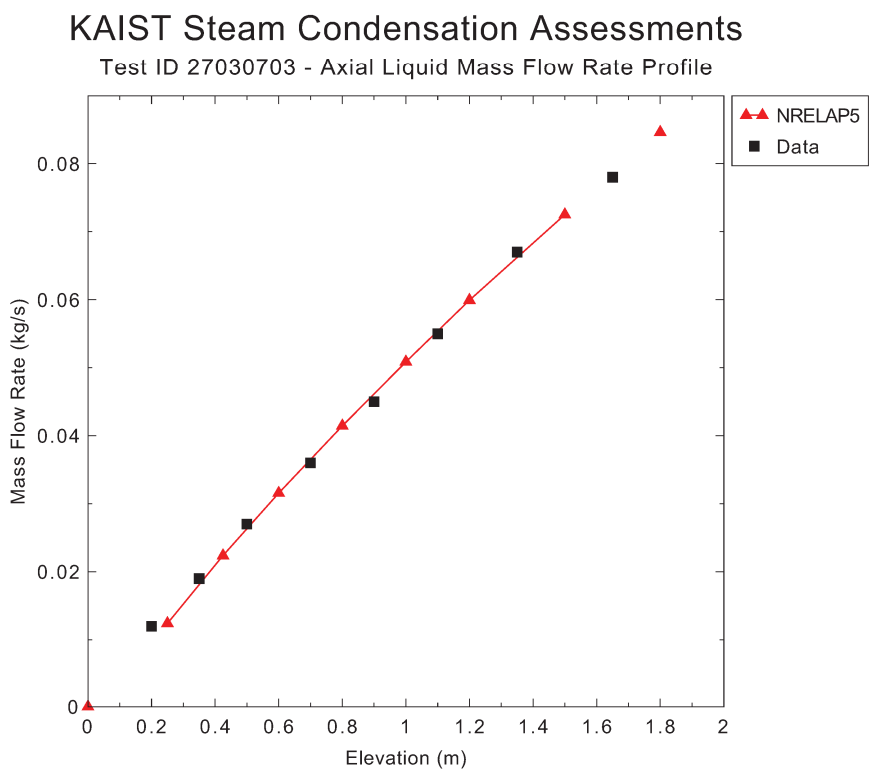

Figure 7-19. KAIST and NRELAP5 axial liquid mass flow rate

7.2.5 FRIGG

The FRIGG loop tests for the Marviken boiling heavy water reactor project were executed in four phases by ASEA-ATOM during the years 1967-1970 (Reference 61). These experiments included measurements of axial and radial void distribution, single-phase and two-phase pressure drop, natural circulation mass velocity, stability limits as well as detailed dynamic characteristics, and burnout in natural and forced circulation.

The axial and radial void distribution data as a function of mass flow, inlet sub-cooling, system pressure, and thermal power provide an excellent data set for evaluating the NRELAP5 interphase drag and heat transfer models under two-phase flow conditions. The FRIGG phase 4 (FRIGG-4) tests applied both a non-uniform radial and axial thermal power profile on the heated rod bundle best simulating the power profiles associated with a typical operating reactor core. As such the FRIGG-4 tests are used to assess NRELAP5 performance.

7.2.5.1 Facility Description

The FRIGG-4 test facility consisted of a vertical circular test section containing 36 electrically heated rods, a riser, a steam separator, a downcomer, a condenser, a pump, and connecting pipes. The power supply for the FRIGG loop was capable of providing a

© Copyright 2016 by NuScale Power, LLC

maximum of 8 MW of direct current power to the heated rods in the test section. A schematic of the test loop is shown in Figure 7-20. Figure 7-21 shows the locations of the void and pressure sensors used in the test section. Reference 61 provides detailed information on the characteristics of the facility.

The rod bundle simulated a full-scale boiling heavy water reactor fuel element. Each rod had a 4.365 m (172 in.) heated length and a 13.8 mm (0.543 in.) outside diameter. The bundle also included a 20 mm (0.787 in) outside diameter unheated center rod that supported the prototype reactor core grid spacers. The heated rods were arranged in equal intervals in three rings, the inner ring having six rods, the middle ring twelve rods, and the outer ring eighteen rods. The rod bundles were contained within a 159.5 mm (6.28 in.) ID shroud.

The heated rod bundle had axial and radial thermal power peaking factors typical of an equilibrium reactor core. The FRIGG-4 tests have no thermal power variation in the azimuthal (circumferential) direction. The average heat flux for each test was determined by dividing the total thermal power by the total heated surface. The local heat flux at any given radial or axial zone can be determined by multiplying the measured average heat flux by the radial and axial coordinate scale factors.

© Copyright 2016 by NuScale Power, LLC

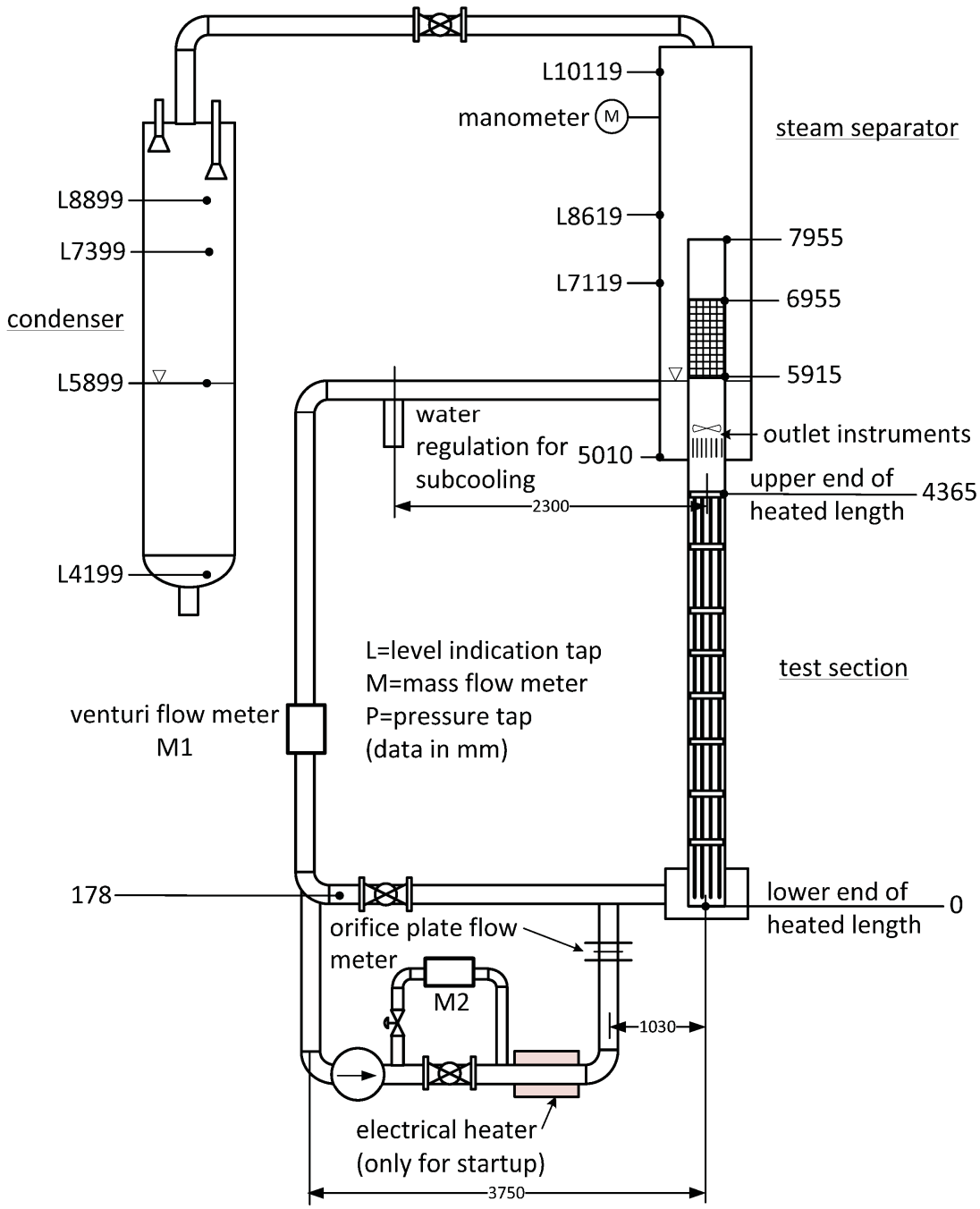

Figure 7-20. FRIGG-4 experimental loop

© Copyright 2016 by NuScale Power, LLC

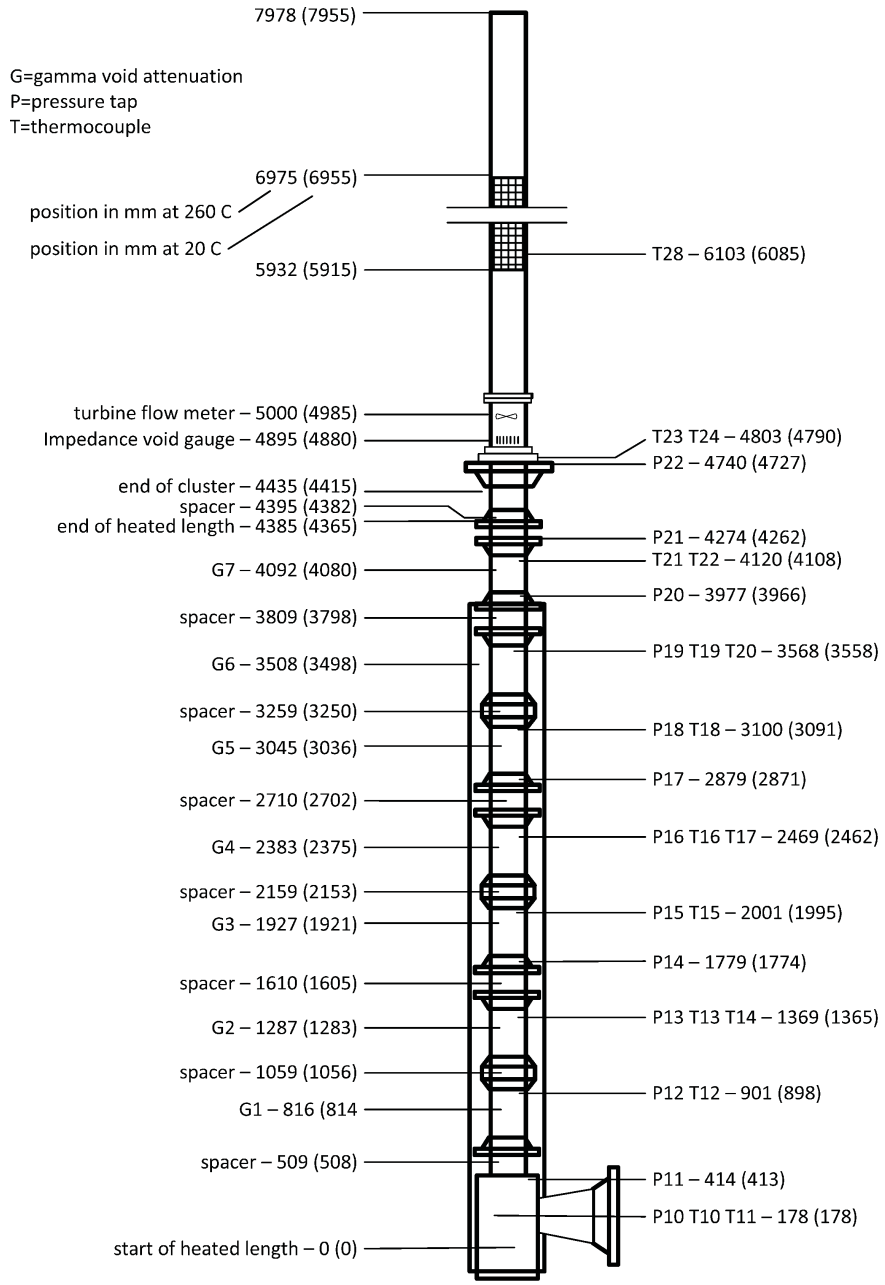

Figure 7-21. FRIGG-4 36 rod test section

© Copyright 2016 by NuScale Power, LLC

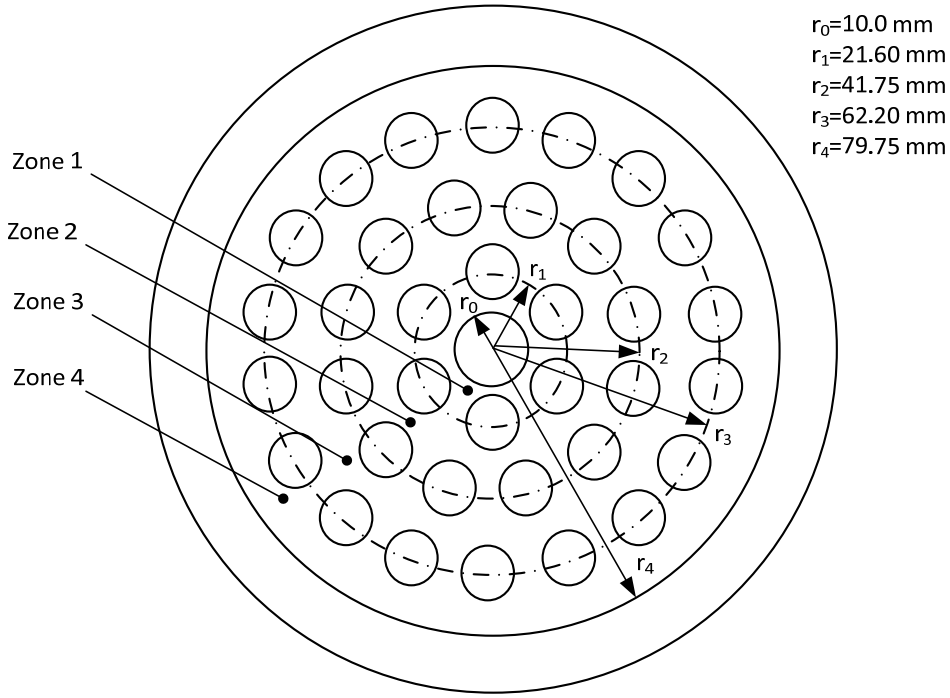

Figure 7-22. FRIGG-4 zones for evaluation of radial void distribution

7.2.5.2 Phenomena Addressed

The phenomena addressed with the FRIGG-4 assessment include {{ }}2(a),(c)

Specifically, the FRIGG-4 tests assess the ability of NRELAP5 to predict the void distribution data in a rod bundle geometry as a function of mass flow, inlet sub-cooling, system pressure, and thermal power for evaluating interphase drag and heat transfer models under two-phase flow conditions in the core.

7.2.5.3 Experimental Procedure

Test points were obtained by specifying the core electric power, inlet flow rate, inlet sub-cooling, and system pressure. Measurements of axial void fractions were collected for each radial zone of the rod bundle.

7.2.5.4 Special Analysis Techniques

There were no special analysis techniques utilized.

© Copyright 2016 by NuScale Power, LLC

7.2.5.5 Assessment Results

One-dimensional NRELAP5 model of the test section was used to analyze this test. Figure 7-23 to Figure 7-26 below show the area-weighted average void fractions in axial zones G1 through G7 for tests 613123, 613130, 613010 and 613118. NRELAP5 predicted the experimental void fraction data with reasonable agreement justifying use of {{

}}2(a),(c)

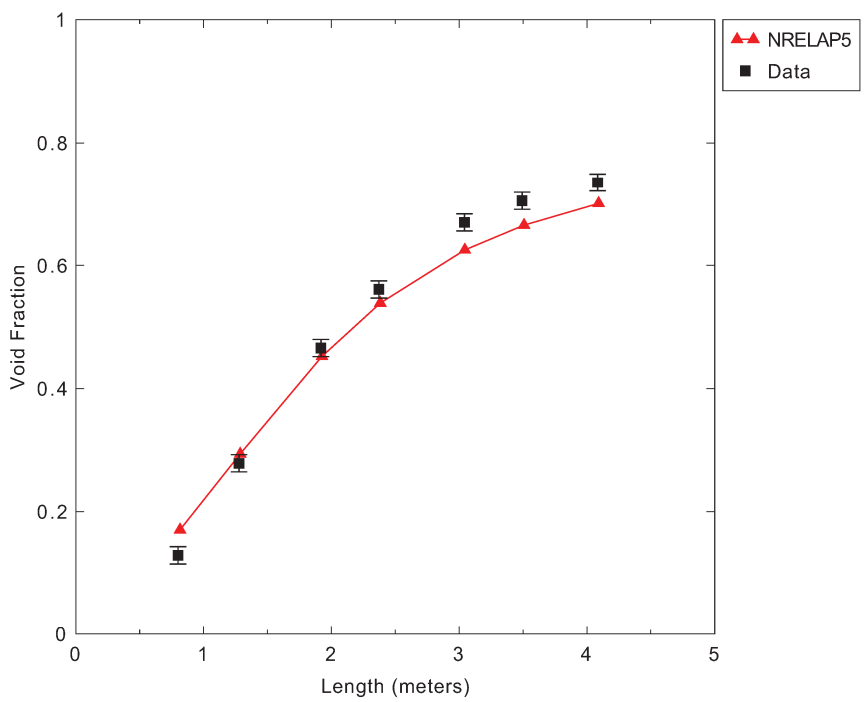

Figure 7-23. FRIGG mean void data of NRELAP5 versus Test 613123 data

© Copyright 2016 by NuScale Power, LLC

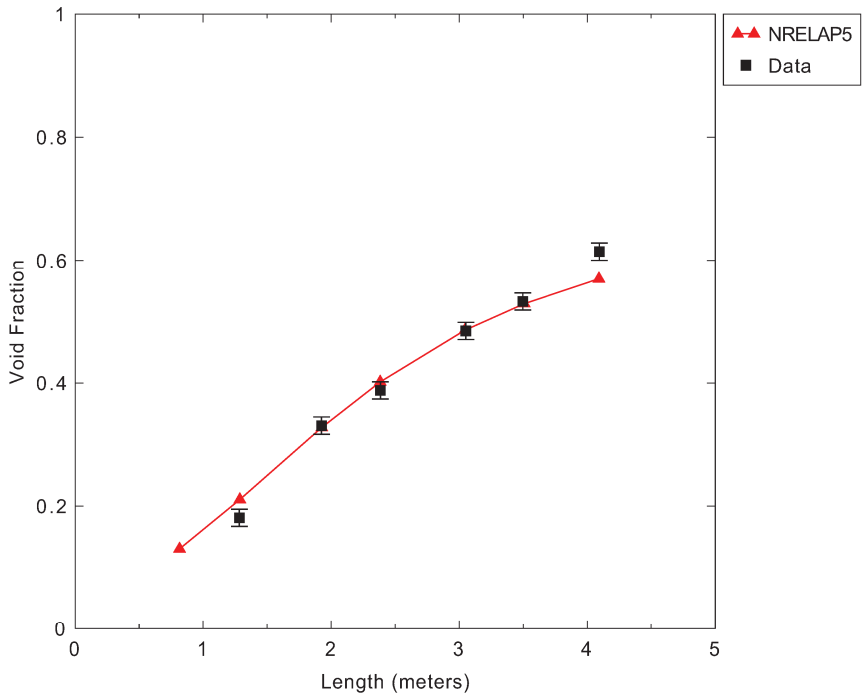

Figure 7-24. FRIGG mean void data of NRELAP5 versus Test 613130 data

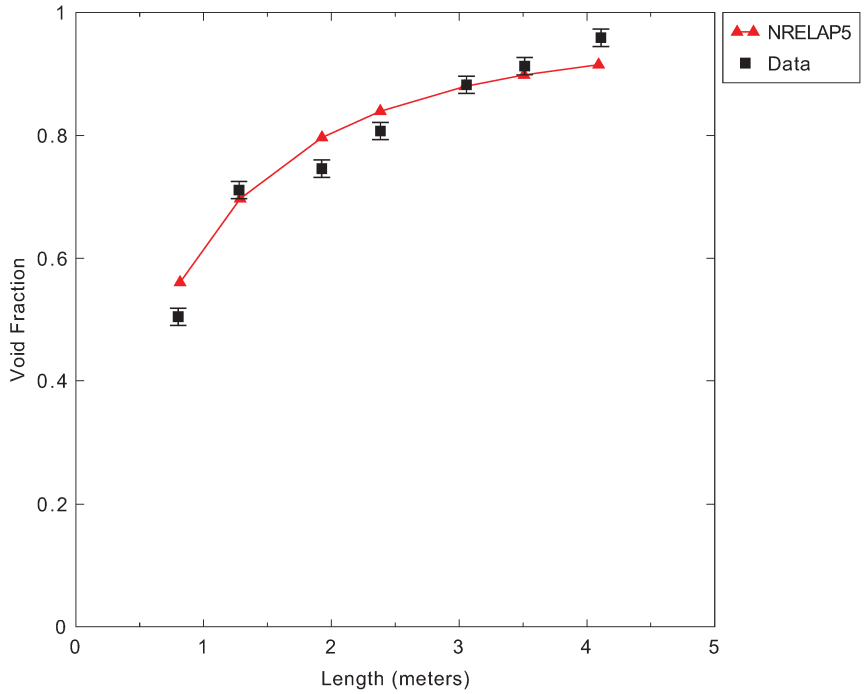

Figure 7-25. FRIGG mean void data of NRELAP5 versus Test 613010 data

© Copyright 2016 by NuScale Power, LLC

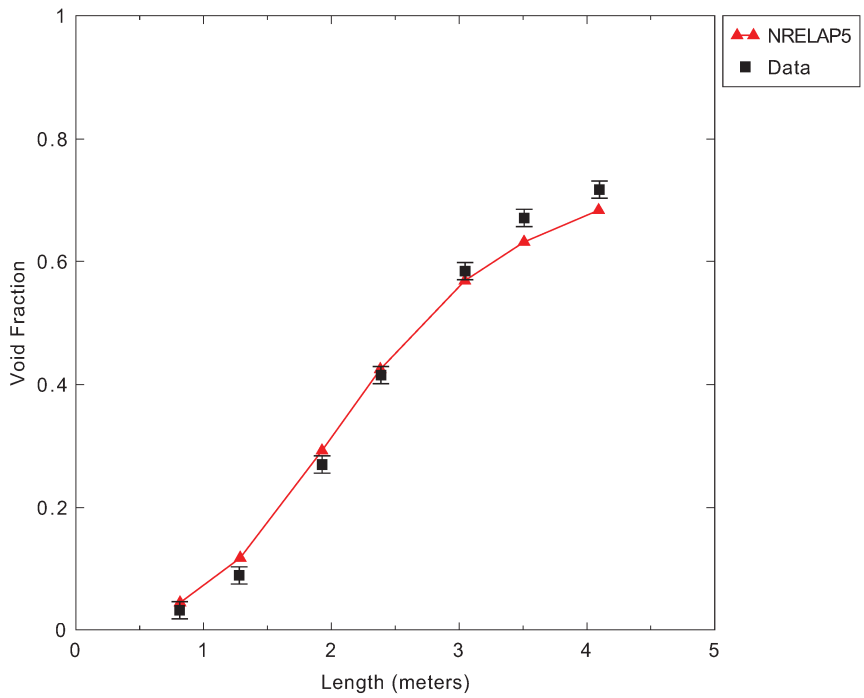

Figure 7-26. FRIGG mean void data of NRELAP5 versus Test 613118 data

7.2.6 FLECHT-SEASET

The FLECHT-SEASET tests (References 62 and 63) consisted of forced and gravity reflood experiments using electrical heater rods to simulate fuel bundles similar to the Westinghouse 17 x 17 design. The test program was originally designed to study large-break LOCA events. Following the Three Mile Island accident, it was re-oriented to obtain data relevant to small break LOCA events.

Because the NuScale core remains covered with coolant for all design basis LOCA events, reflood phenomena does not occur. However, the test campaign included bundle boil-off tests which are relevant for the NuScale design because the NPM uses boiling in the core to remove heat following a number of accident scenarios that result in actuation of the ECCS. Following ECCS initiation and pressure equalization in the NPM, the RPV and CNV are essentially a pool boiler system with coolant boiled off in the RPV being replaced by an inflow of coolant from the CNV.

7.2.6.1 Facility Description

The facility loop with test section is shown in Figure 7-27. The heater rods were manufactured with a prototypical PWR axial cosine power shape.

© Copyright 2016 by NuScale Power, LLC

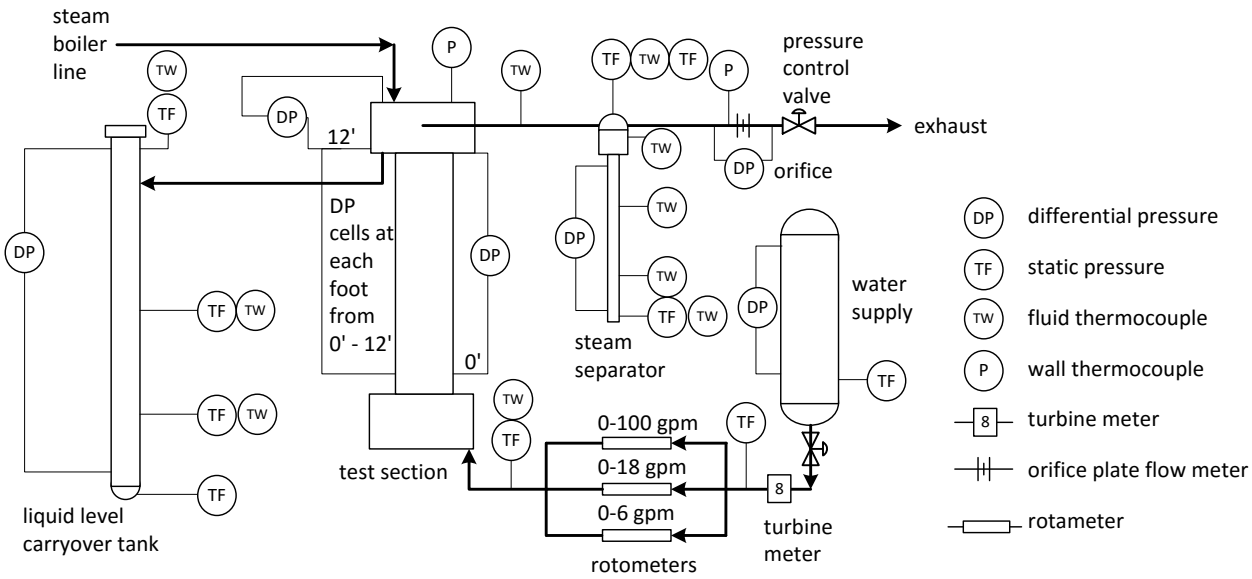

Figure 7-27. FLECHT-SEASET experimental facility

7.2.6.2 Experimental Procedure

The FLECHT-SEASET boil-off tests were conducted by filling the 12 ft. tall vessel with approximately 10 ft. of (slightly sub-cooled) water. The power to the heater rods was turned on, and the water was allowed to boil. The test was terminated and reflood initiated when a rod thermocouple registered a temperature greater than or equal to 2,000 degrees F. Three separate boil-off tests are used to assess NRELAP5. These tests were conducted with initial system pressures of 20, 40, and 60 psia.

7.2.6.3 Phenomena Addressed

The phenomenon addressed with the FLECHT-SEASET assessment include {{ }}2(a),(c)

Specifically, the FLECHT-SEASET boil off tests assess the ability of NRELAP5 to predict the axial void profile, mixture level (interfacial drag), and cladding temperature response during boil-off of a PWR core.

7.2.6.4 Special Analysis Techniques

Based on sensitivity studies using one-dimensional components, it is concluded that {{

}}2(a),(c)

© Copyright 2016 by NuScale Power, LLC

7.2.6.5 Assessment Results

The results for Test 35557 performed at 60 psia are shown in Figure 7-28 through Figure 7-35. The predictions for the void fraction at different elevation are shown in Figure 7-28 through Figure 7-31. The comparisons for the collapsed water levels for all sections are provided in Figure 7-32 through Figure 7-35. While the model and data show reasonable agreement, NRELAP5 over-predicts void fractions as a function of time in most of the core region (Figure 7-28 through Figure 7-31) resulting in a conservative earlier prediction of core uncovery when compared to test data. Similar comparisons were obtained for the test runs at 20 psia and 40 psia.

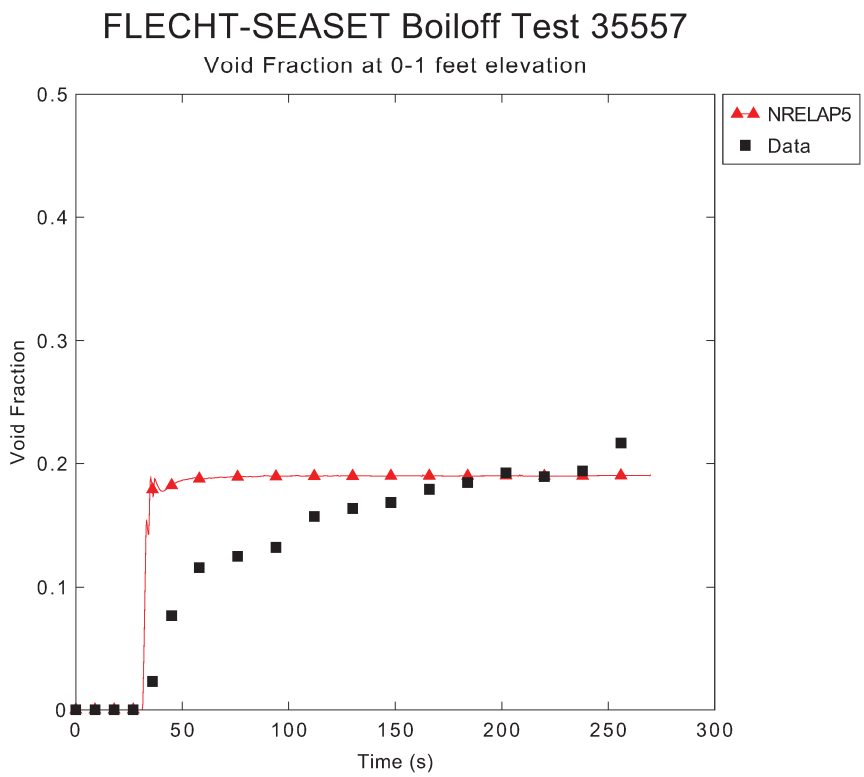

Figure 7-28. FLECHT-SEASET level 1 void fraction versus time – Test 35557

© Copyright 2016 by NuScale Power, LLC

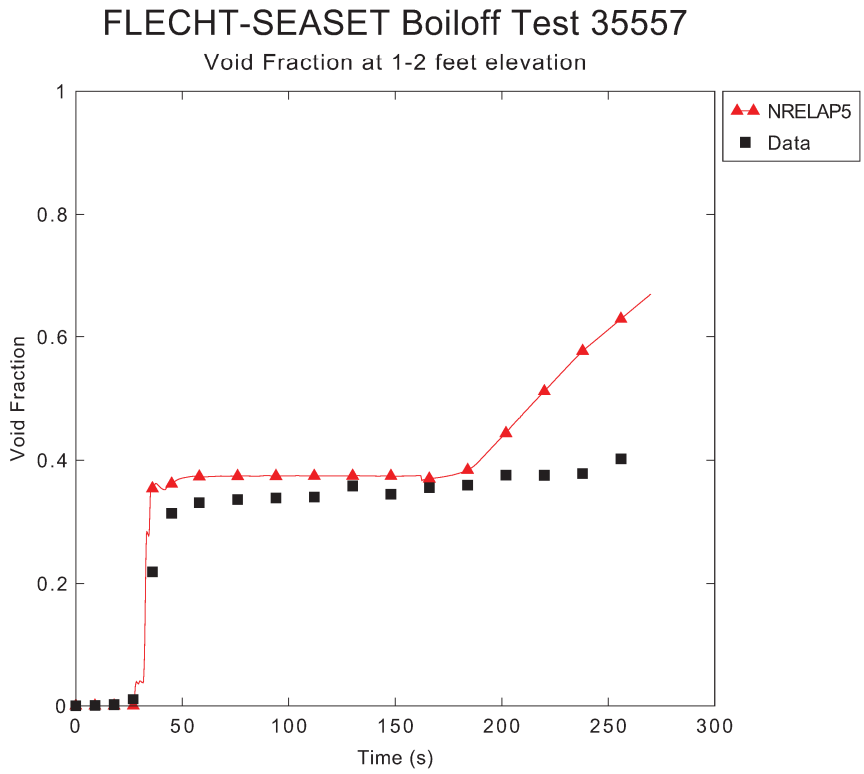

Figure 7-29. FLECHT-SEASET level 2 void fraction versus time – Test 35557

© Copyright 2016 by NuScale Power, LLC

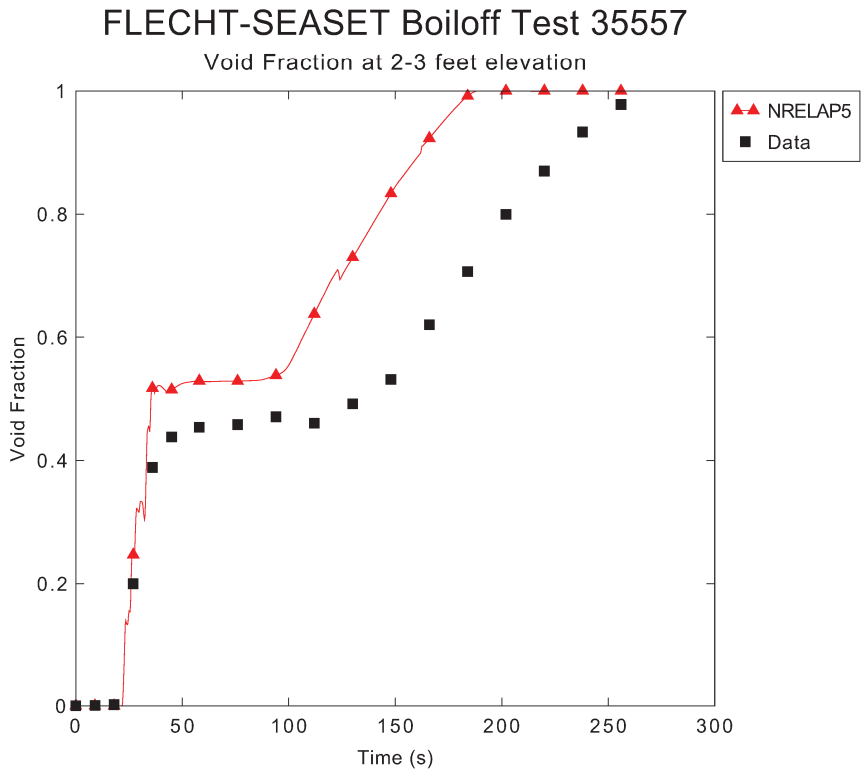

Figure 7-30. FLECHT-SEASET level 3 void fraction versus time – Test 35557

© Copyright 2016 by NuScale Power, LLC

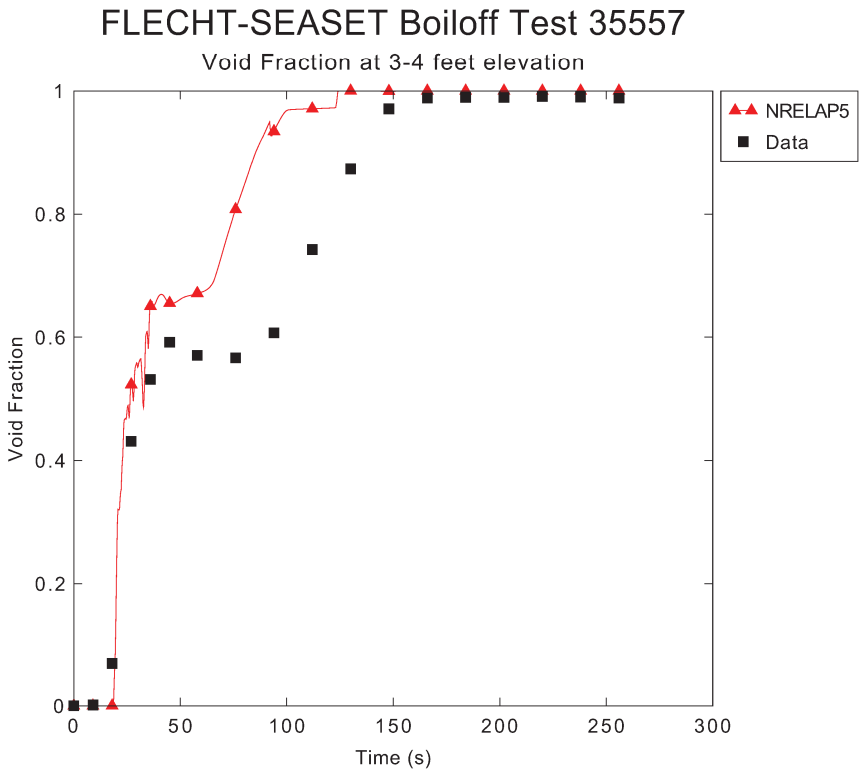

Figure 7-31. FLECHT-SEASET level 4 void fraction versus time – Test 35557

© Copyright 2016 by NuScale Power, LLC

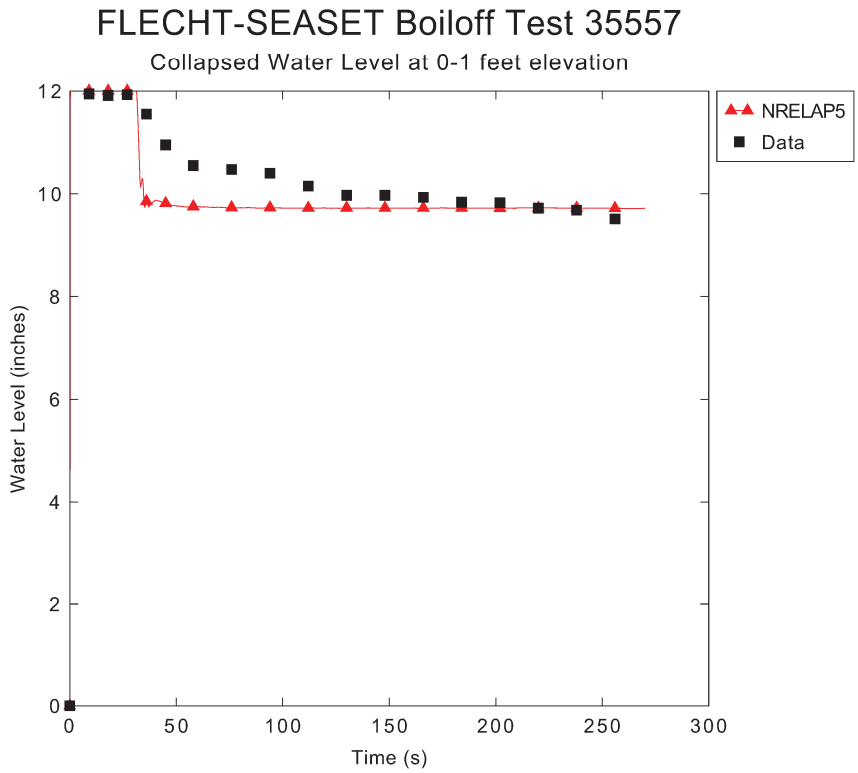

Figure 7-32. FLECHT-SEASET level 1 collapsed water level versus time – Test 35557

© Copyright 2016 by NuScale Power, LLC

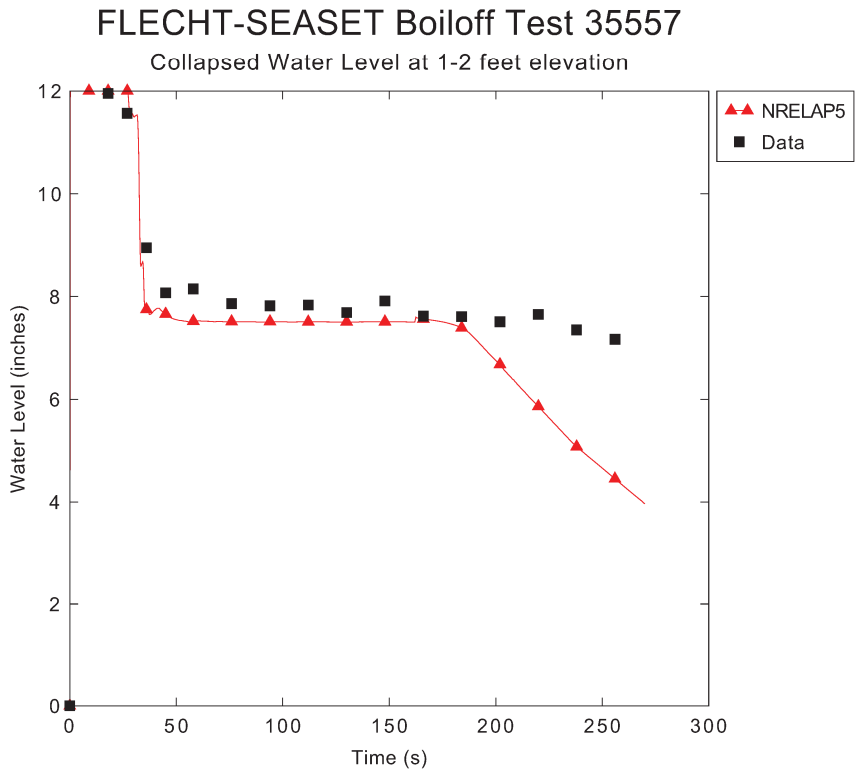

Figure 7-33. FLECHT-SEASET level 2 collapsed water level versus time – Test 35557

© Copyright 2016 by NuScale Power, LLC

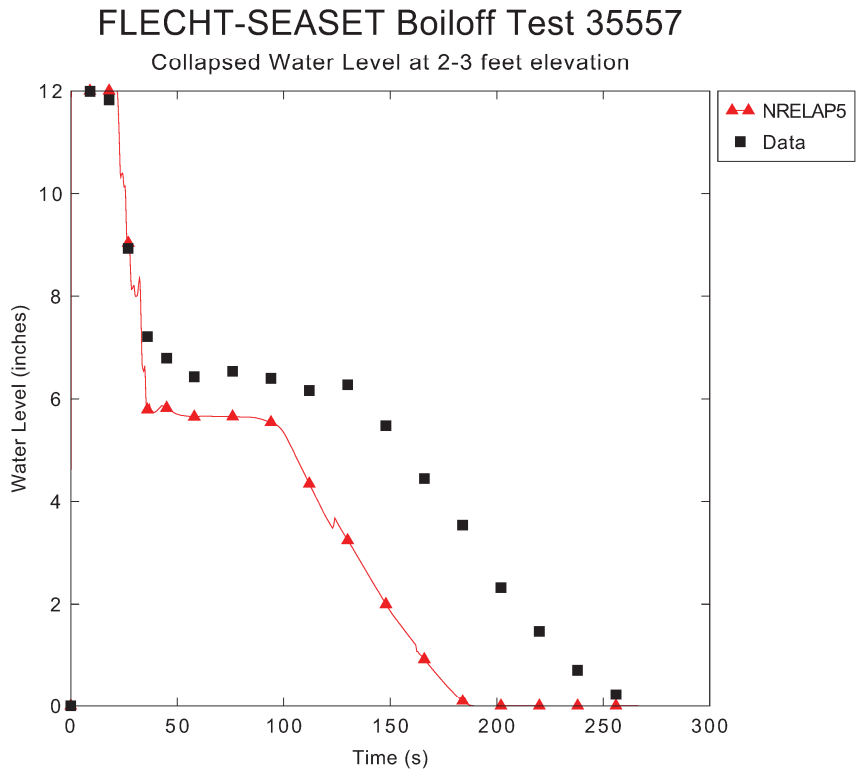

Figure 7-34. FLECHT-SEASET level 3 collapsed water level versus time – Test 35557

© Copyright 2016 by NuScale Power, LLC

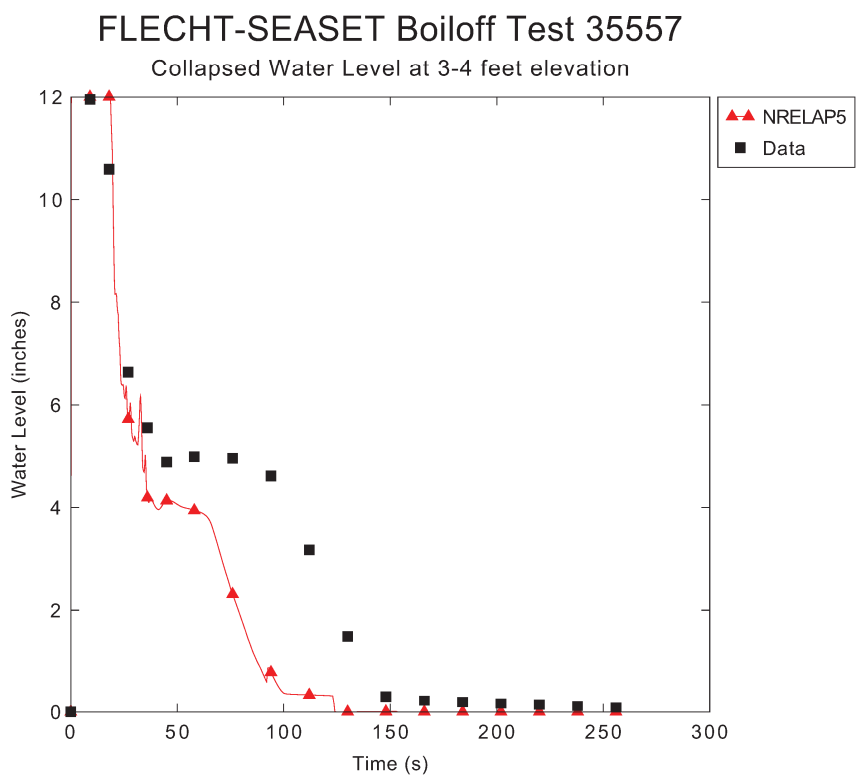

Figure 7-35. FLECHT-SEASET level 4 collapsed water level versus time – Test 35557

7.2.7 SemiScale (S-NC-02 and S-NC-10)

The Semiscale test loop modeled a typical PWR. The goal of the Semiscale S-NC-2 and S-NC-10 tests was to obtain experimental data on the natural circulation single-phase and two-phase flow conditions at various system inventories for differing system powers. Three powers were investigated: 30 kW, 60 kW, and 100 kW. At each power level the mass inventory was reduced from at or near 100 percent conditions. With the reduction of primary inventory two-phase flow developed resulting in an enhancement of the total system flow rate. Further reduction in system inventory resulted in a degradation of the total system flow rate.

7.2.7.1 Facility Description

The Semiscale Mod-2A test facility is a full-height 1/1,705 power-to-volume scaled model of a typical four-loop PWR. Only one loop was used for the S-NC-2 and S-NC-10 tests discussed here. The single-loop configuration is shown in Figure 7-36. The reactor coolant pump was removed and replaced by an orifice to model the loss of a seized pump.

© Copyright 2016 by NuScale Power, LLC

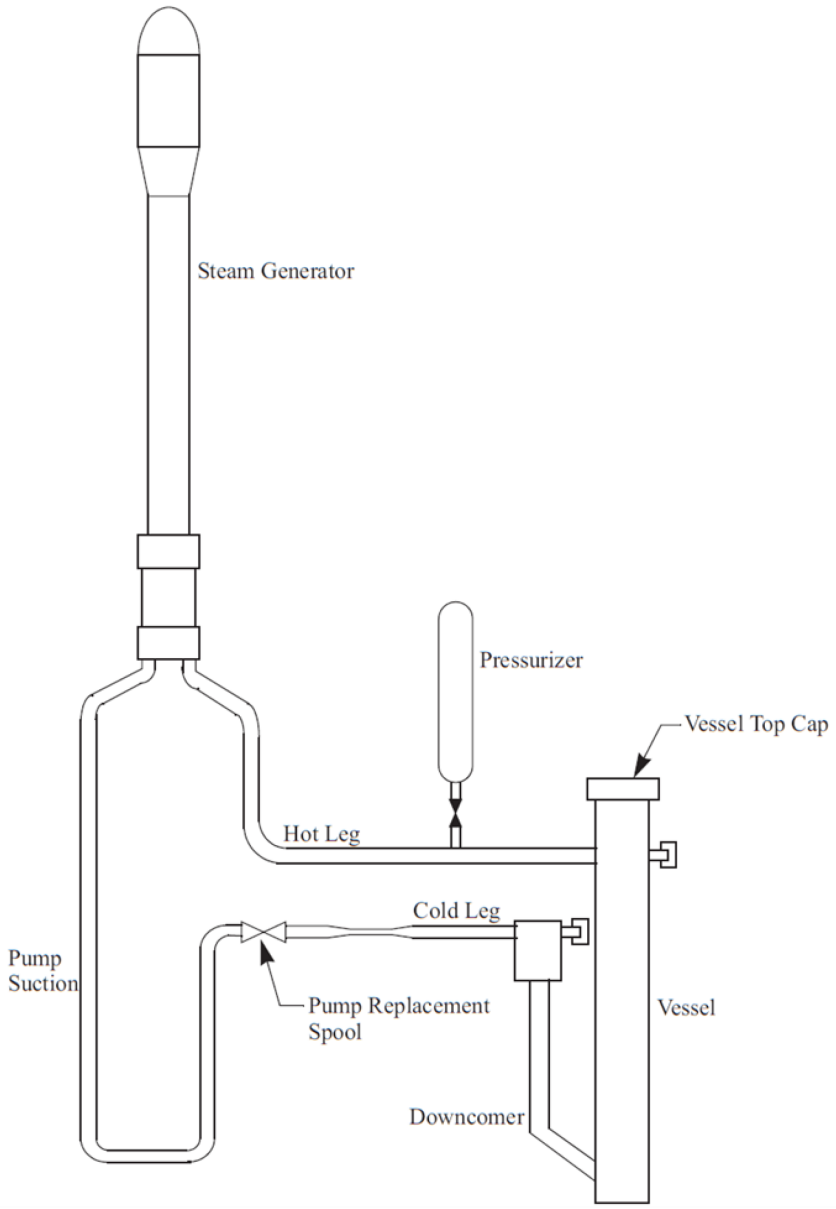

Figure 7-36. Semiscale Mod-2A single (intact) loop test facility configuration

7.2.7.2 Phenomenon Addressed

The phenomenon addressed with the Semiscale assessment includes {{
}}2(a),(c)

Specifically, the Semiscale natural circulation tests assess the ability of NRELAP5 to predict natural circulation during single- and two-phase flow conditions at various system inventories and system powers in a complex geometry.

© Copyright 2016 by NuScale Power, LLC

7.2.7.3 Experimental Procedure

Prior to initiation of the tests, the primary system was filled with demineralized water and vented to ensure it was liquid-full. The primary system was heated using core power as a heat source and the SG secondary system as a heat sink. Single-phase natural circulation flow driven by density gradients in the loop was used to thermally condition the system to obtain a specified set of initial conditions.

For those steady-state tests in which the primary system was to be drained, the pressurizer was used only to establish initial conditions. The pressurizer was disconnected from the coolant loop prior to draining the primary system.

Primary system mass inventory was controlled by draining fluid from the vessel LP in discrete steps. This fluid was condensed and measured using a static pressure transducer.

The SG secondary levels were controlled by a feed-and-bleed process combined with secondary system draining. The secondary-system pressure was maintained such that saturation conditions prevailed through the use of a steam control valve.

The steady-state natural circulation tests used constant core powers from 30kW to 100kW, representing 1.5 percent to 5.0 percent of the 2,000 kW full Semiscale core power.

During the steady-state experiments, the independent variables were controlled in discrete, step-wise manners, allowing steady conditions to be established between the times when changes in the independent variables were made.

External heaters were used to offset heat losses from the primary coolant system that would affect loop natural circulation behavior. The heaters were located on the hot leg, pump suction, cold leg and vessel downcomer sections of the experiment system. The external heater powers were adjusted to follow previously-determined system heat loss versus system temperature relations. The effectiveness of the external heaters was verified by ensuring constant temperatures (indicative of no heat losses) across these sections.

Three test cases (30kW, 60kW, and 100kW) of S-NC-2 and S-NC-10 were evaluated.

7.2.7.4 Special Analysis Techniques

During the NRELAP5 assessment of the Semiscale test cases, it was noted that the {{

}}2(a),(c)

7.2.7.5 Assessment Results

The NRELAP5 models for S-NC-02 at 30 kW and 60 kW, and S-NC-10 at 100 kW were run at various system mass inventories. Once steady conditions are obtained for each

© Copyright 2016 by NuScale Power, LLC

inventory reduction, the last 200 seconds of the interval are averaged to obtain key FOMs for comparison to data.

The NRELAP5 predictions of loop mass flow rate as a function system inventory are compared to the experimental data in Figure 7-37 to Figure 7-39. In general, NRELAP5 provides reasonably to excellent agreement when predicting the trends, the peak two-phase flow rate, and the enhanced flow rate region (region to the right of the peak). Minor discrepancies are noted to exist in the degraded loop flow region (75 percent – 80 percent inventory levels). These results validate the ability of NRELAP5 to predict natural circulation during single- and two-phase flow conditions at various system inventories and system powers in a complex geometry.

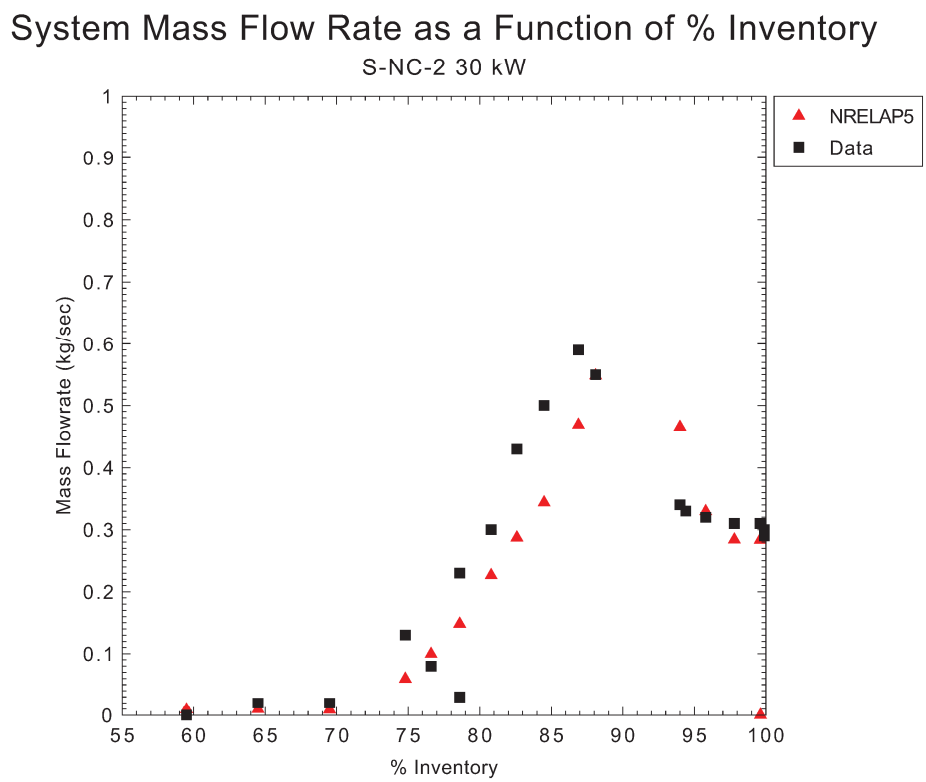

Figure 7-37. S-NC-2 30 kW average mass flow rate versus percent inventory

© Copyright 2016 by NuScale Power, LLC

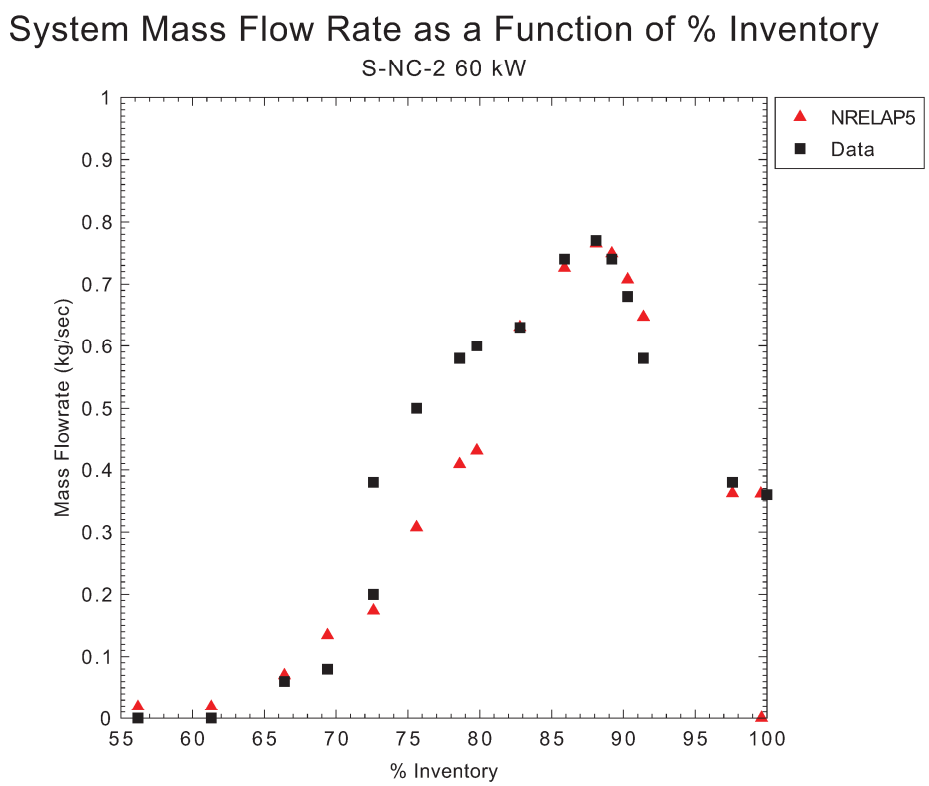

Figure 7-38. S-NC-2 60 kW average mass flow rate versus percent inventory

© Copyright 2016 by NuScale Power, LLC

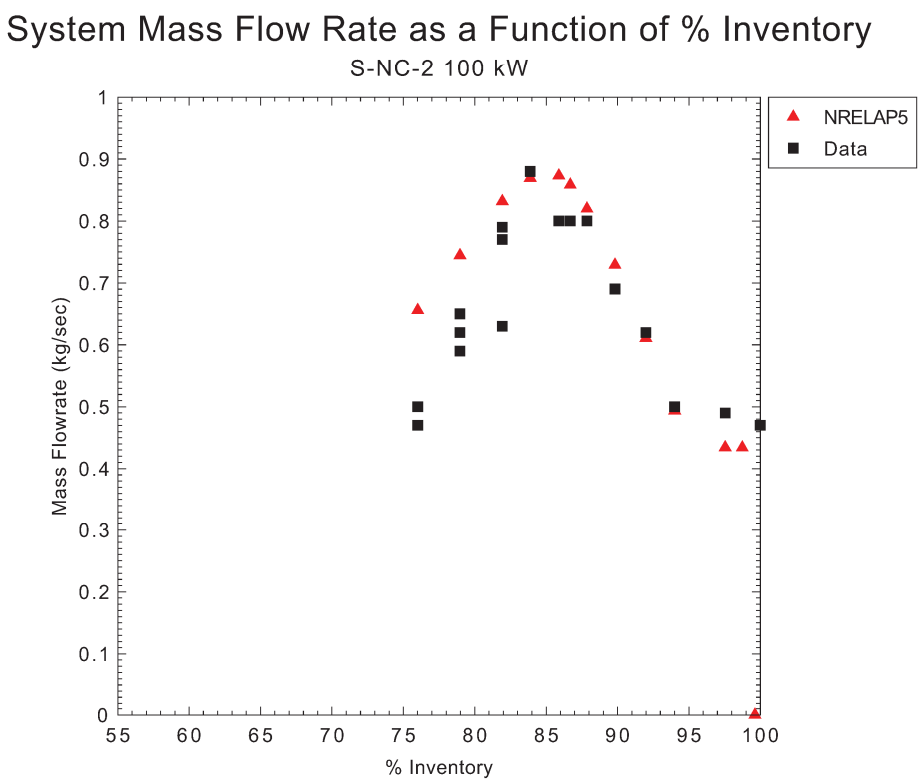

Figure 7-39. S-NC-10 100 kW average mass flow rate versus percent inventory

7.2.8 Wilson Bubble Rise

The NPM hot leg riser is a large-diameter pipe. During various phases of a LOCA, a nearly stagnant two-phase mixture will be present in the riser. The Wilson bubble rise experimental data are useful to validate NRELAP5 for prediction of void fraction distribution in the hot leg riser.

7.2.8.1 Facility Description

The test facility shown in Figure 7-40 includes a steam inlet and exit nozzle as well as an 18-in. (0.457 m) diameter channel inserted vertically within a 36-in. (0.914 m) diameter vessel. A simplified portion of the test section has been modeled with selected boundary conditions. The boundary conditions consist of the inlet steam mass flow rate and exit pressure. Steam enters the test section from the bottom and exits at the top.

© Copyright 2016 by NuScale Power, LLC

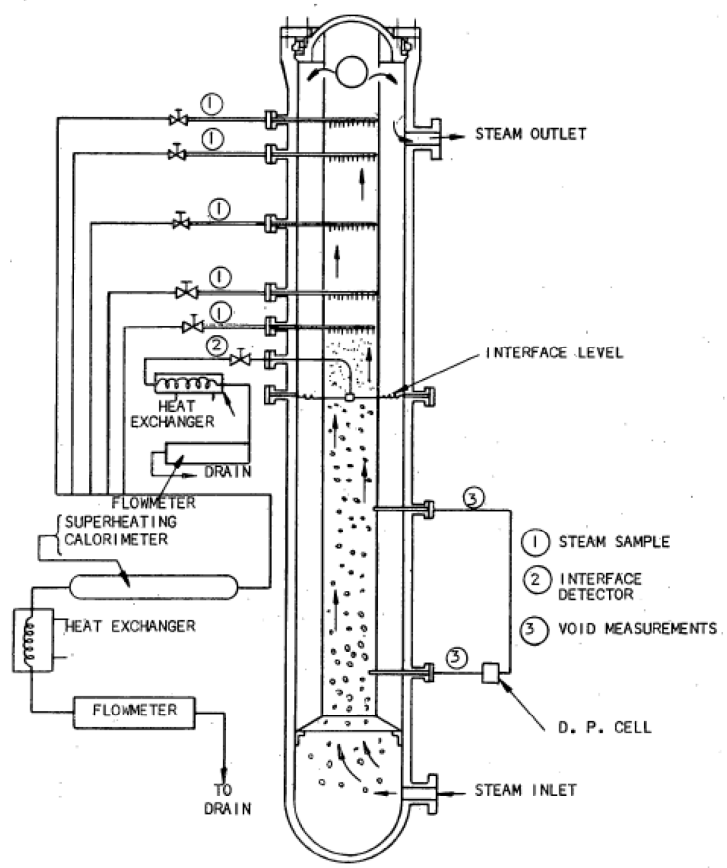

Figure 7-40. Schematic of Wilson bubble rise test facility

7.2.8.2 Experimental Procedure

The Wilson bubble rise experiments were executed by the vessel being slowly heated and brought to equilibrium at the desired test pressure. The water level and steam flow rates were adjusted to the desired values. After the system reached equilibrium, the necessary instrument readings were taken. These readings were the vessel pressure, steam flow, and the three radial void fraction readings (outer radial region, median region and central region of channel). After the readings were taken, the next steam flow was set and the process was repeated. The steam flow was varied from 5,000 to 60,000 lb/hr (2,268 to 27,216 kg/hr) and the pressures ranged from 600 to 2,000 psi (4.14 to 13.8 MPa).

7.2.8.3 Phenomena Addressed

The phenomenon addressed with the Wilson bubble rise assessment case are {{ }}$^{2(a),(c)}$

Specifically, the Wilson bubble rise tests assess the ability of NRELAP5 to predict axial void distribution (dependent on interfacial drag) within a large diameter vertical channel.

© Copyright 2016 by NuScale Power, LLC

7.2.8.4 Special Analysis Techniques

Based on sensitivity studies, {{

}}2(a),(c)

7.2.8.5 Assessment Results

The results in Figure 7-41 through Figure 7-43 show the comparison of predicted and measured void fraction at different pressures. Figure 7-44 shows the data for all cases plotted on predicted versus measured graph. A reasonable agreement is observed between the calculated NRELAP5 results and the Wilson bubble rise measured experimental data. In general NRELAP5 conservatively predicted higher void fraction (or lower mass inventory).

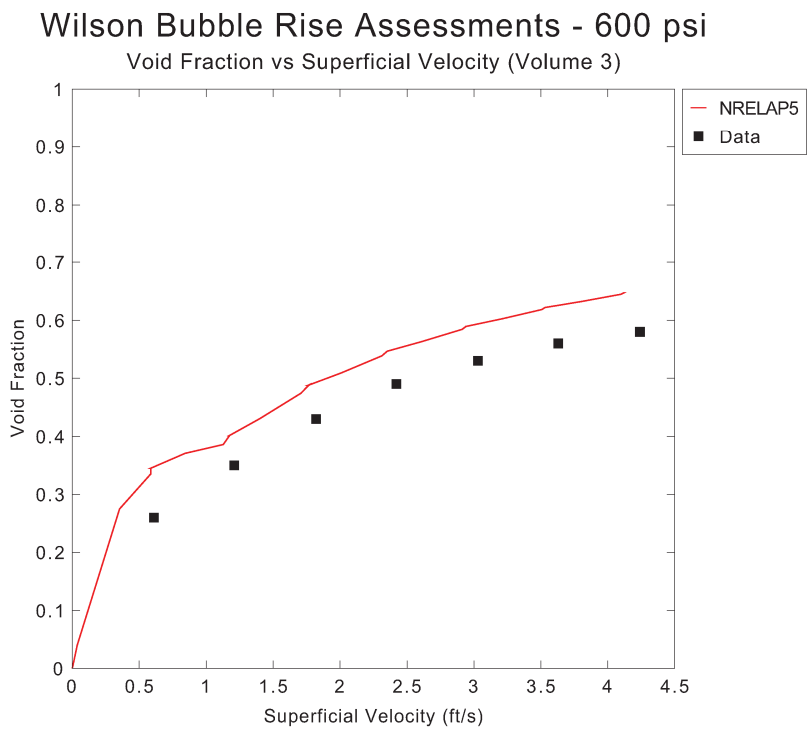

Figure 7-41. NRELAP5 and Wilson void fraction versus superficial velocity at 600 psig (4.14 MPa)

© Copyright 2016 by NuScale Power, LLC

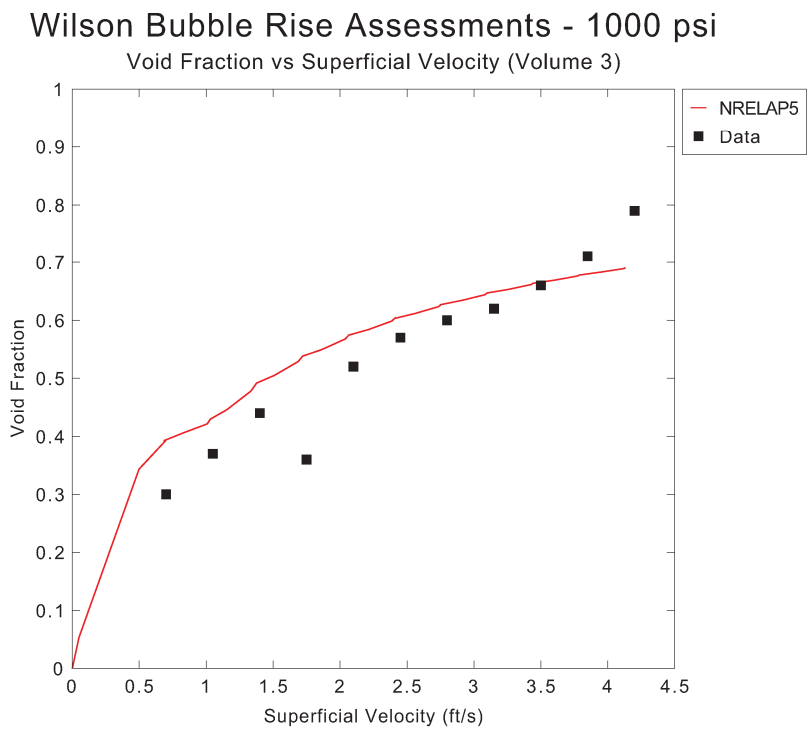

Figure 7-42. NRELAP5 and Wilson void fraction versus superficial velocity 1,000 psig (6.89 MPa)

© Copyright 2016 by NuScale Power, LLC

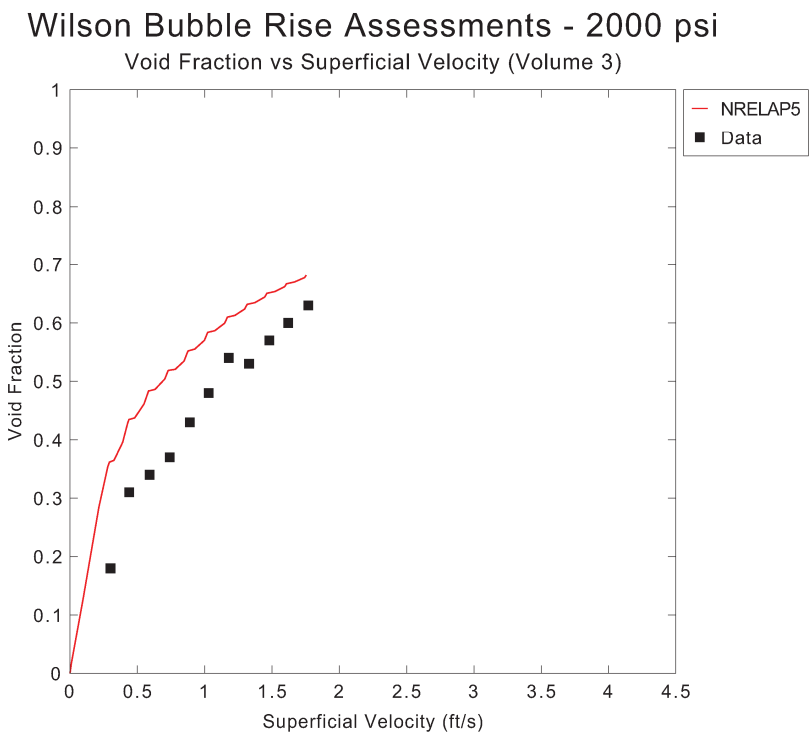

Figure 7-43. NRELAP5 and Wilson void fraction versus superficial velocity 2,000 psig (13.8 MPa)

© Copyright 2016 by NuScale Power, LLC

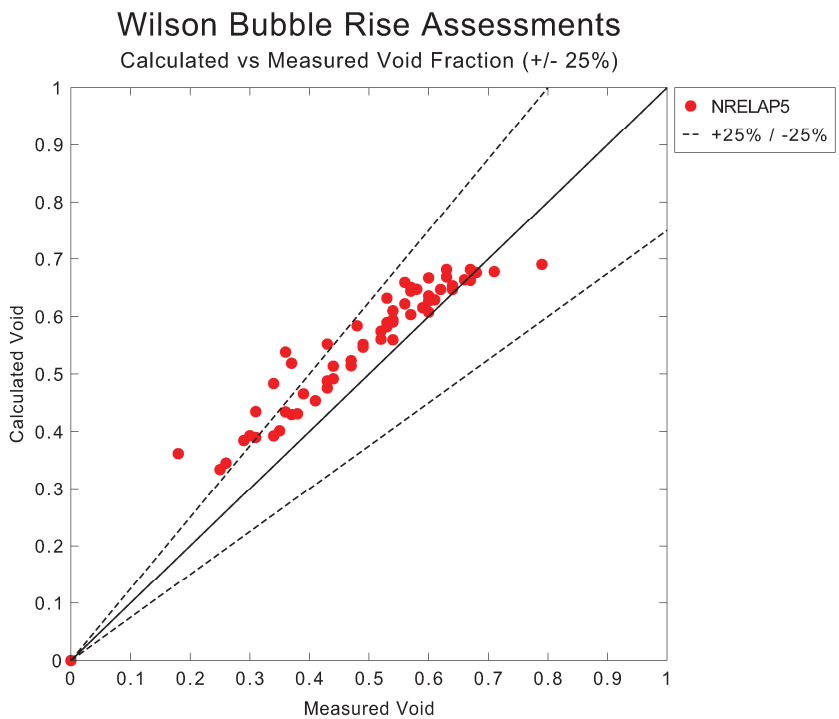

Figure 7-44. Predicted versus measured area averaged void fraction (all cases)

7.2.9 Marviken Jet Impingement Test (JIT) 11

The Marviken JIT-11 (Reference 66) was chosen to assess the single-phase choked flow model in NRELAP5.

7.2.9.1 Facility Description

A schematic of the experimental setup is shown in Figure 7-45. The facility consisted of a pressure vessel of fluid at specified conditions, discharge pipe, ball valve, and discharge nozzle. The facility was constructed with focus on measuring loads due to discharged fluid impingement on a flat plate and full-scale critical flow data. The facility was constructed with a stand-pipe such that only single-phase steam was discharged through the break nozzle.

© Copyright 2016 by NuScale Power, LLC

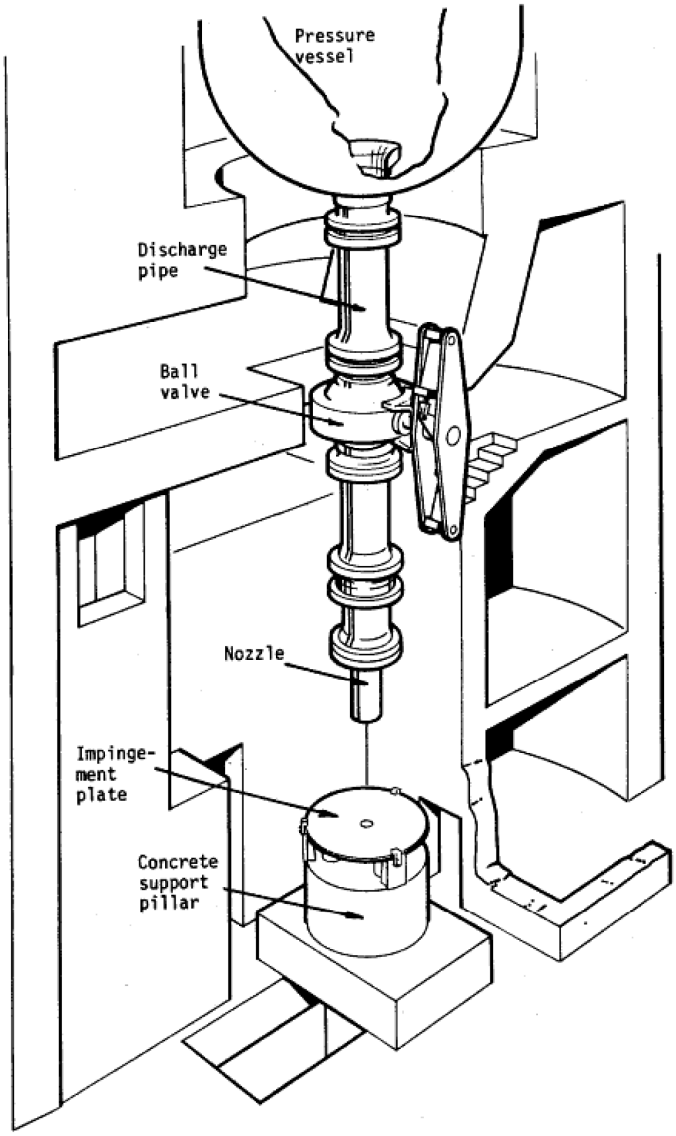

Figure 7-45. Marviken jet impingement test facility

7.2.9.2 Experimental Procedure

Each test consisted of first obtaining desired initial conditions in the pressure vessel followed by bursting the rupture disk in the discharge pipe. For JIT-11 a stand-pipe was installed in the pressure vessel such that only steam from the upper plenum of the vessel was discharged. The test was conducted at 5 MPa (725 psia) and nearly-saturated liquid in the vessel. The nozzle diameter for was 299.0 mm (0.098 ft) with a nozzle length of 1.18 mm (7.4×10^{-3} in.).

© Copyright 2016 by NuScale Power, LLC

7.2.9.3 Phenomenon Addressed

The Marviken JIT-11 addresses the ability of NRELAP5 to predict single-phase (vapor) choked flow (mass and energy release).

7.2.9.4 Special Analysis Techniques

{{

}}2(a),(c)

7.2.9.5 Assessment Results

Figure 7-46 and Figure 7-47 compare the experimental data and the NRELAP5 simulated mass flow rate and density for various values of the discharge coefficient. Excellent agreement is shown with the experimental data for {{

}}2(a),(c)

{{

}}2(a),(b),(c)

Figure 7-46. Marviken jet impingement test 11 flowrate

© Copyright 2016 by NuScale Power, LLC

{{

}}2(a),(b),(c)

Figure 7-47. Marviken jet impingement test 11 density

7.2.10 Bankoff Perforated Plate

Bankoff, et al. (References 67, 68, and 69) conducted air/water and steam/water counter current flow tests in a small scale test apparatus that established counter current flow through a number of different perforated plates. The Bankoff correlation assessment uses the CCFL implementation as described in Section 6.6.3.

7.2.10.1 Facility Description

Reference 69 describes the Bankoff CCFL test apparatus. Additional information on the test apparatus and additional tests are reported in References 67 and 68. A horizontal perforated plate is located in a vertical test assembly. Steam or air can be introduced below the plate and water can be injected above the plate. A water overflow line is located above the plate to limit the height of the “bubbly pool” of water above the plate. The perforated plate could be moved so that the height of the ”bubbly pool” could be varied. There is a drain at the bottom of the test section to prevent water level from building up below the plate. A beam scale is placed at the drain to measure the flow of water that penetrates through the plate. Air or steam that was not condensed on the injected water exited at the top of the test apparatus. The test simulated for this assessment used a 15-hole plate with a ”bubbly pool” height of 267 mm (10.5 in.). The

© Copyright 2016 by NuScale Power, LLC

test was conducted at atmospheric pressure. A schematic of the test facility is shown in Figure 7-48.

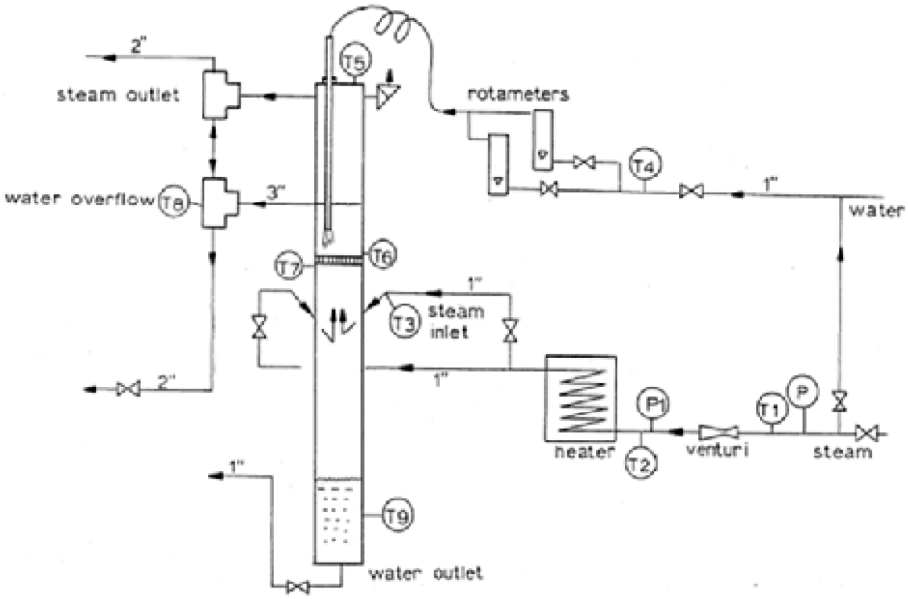

Figure 7-48. Schematic of Bankoff counter current flow apparatus (from Reference 68)

7.2.10.2 Phenomenon Addressed

The phenomenon addressed with the Bankoff assessment case is CCFL at pressurizer baffle plate and upper core plate (UCP) (or top nozzle).

7.2.10.3 Experimental Procedure

The test was conducted by establishing a water inlet flow rate and then increasing the air flow rate in a stepwise manner. The rate of water flow through the perforated plate was measured by weighing the flow out of the bottom of the test section. The test was concluded when the air flow was sufficient to prevent water downflow through the perforated plate.

7.2.10.4 Assessment Results

Figure 7-49 compares predicted vapor superficial velocity versus predicted liquid superficial velocity. The comparison shows that the predictions are in excellent agreement with the experimental data.

© Copyright 2016 by NuScale Power, LLC

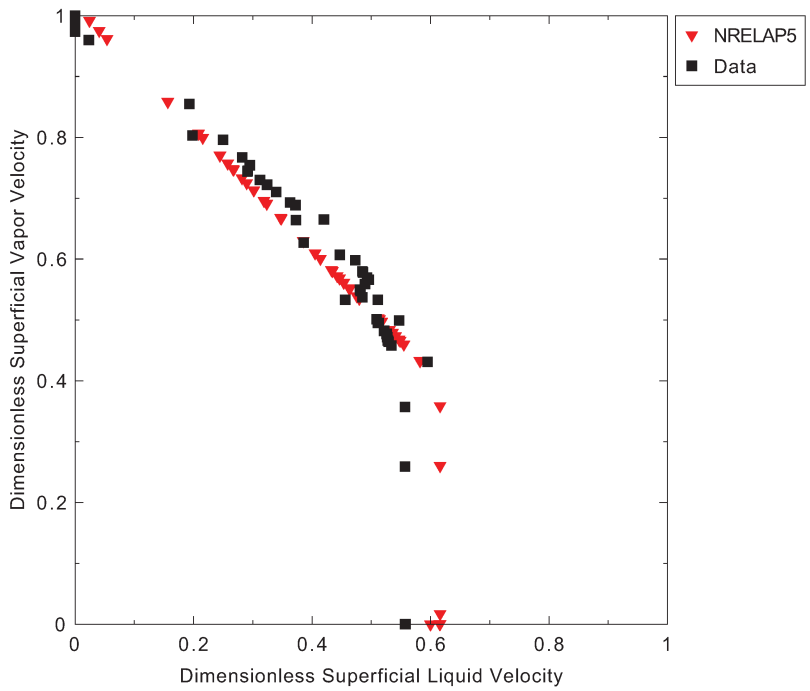

Figure 7-49. Superficial vapor velocity versus superficial liquid velocity

7.2.11 Marviken Critical Flow Test 22 and 24

The Marviken critical flow tests (CFTs) (Reference 70 and 71) were conducted to characterize the conditions of blowdown given {{

}}2(a),(b),(c)

7.2.11.1 Facility Description

{{

}}2(a),(b),(c)

© Copyright 2016 by NuScale Power, LLC

{{

}}2(a),(b),(c)

Figure 7-50. Schematic of the Marviken pressure vessel

© Copyright 2016 by NuScale Power, LLC

{{

}}2(a),(b),(c)

Figure 7-51. Discharge pipe dimensions and instrument locations

© Copyright 2016 by NuScale Power, LLC

7.2.11.2 Experimental Procedure

{{

}}2(a),(b),(c)

7.2.11.3 Phenomenon Addressed

The phenomenon addressed with the Marviken assessment is two-phase and single-phase choked flow.

7.2.11.4 Special Analysis Techniques

{{

}}2(a),(b),(c)

7.2.11.5 Assessment Results

7.2.11.5.1 Comparison to Marviken Critical Flow Test-22

{{

}}2(a),(b),(c)

© Copyright 2016 by NuScale Power, LLC

{{

}}2(a),(b),(c)

© Copyright 2016 by NuScale Power, LLC

{{

}}2(a),(c)

Figure 7-52. Measured versus calculated mass flow rate for Marviken critical flow test 22

© Copyright 2016 by NuScale Power, LLC

{{

}}2(a),(c)

Figure 7-53. Marviken critical flow test 22 comparison to calculated mixture density

© Copyright 2016 by NuScale Power, LLC

7.2.11.5.2 Comparison to Marviken Critical Flow Test-24

{{

}}2(a),(b),(c)

© Copyright 2016 by NuScale Power, LLC

{{

}}2(a),(c)

Figure 7-54. Measured versus calculated mass flow rate for Marviken critical flow test 24

© Copyright 2016 by NuScale Power, LLC

{{

}}2(a),(c)

Figure 7-55. Marviken critical flow test 24 mixture density and calculated mixture density

Analysis shows that NRELAP5 has the capability to perform critical flow calculations with reasonable-to-excellent agreement to test data.

7.3 NuScale Stern Critical Heat Flux Tests

The CHF correlations described in Section 6.11 were assessed against steady state CHF experiments performed by NuScale in the Stern facility, and this assessment is presented in this section.

The Stern tests were performed on a preliminary prototypical bundle geometrically comparable to the NuFuel HTP2™ design, but with {{ }}2(a),(b),(c),ECI The Stern preliminary prototypical bundle tests provide data over wide parameter ranges, which encompass the NPM operating parameter values and can be used to assess the capability of NRELAP5 to predict the onset of the CHF. Key FOMs to assess agreement include the critical power and the critical power ratio as a function of mass flux, pressure, and inlet sub-cooling.

© Copyright 2016 by NuScale Power, LLC

7.3.1 Facility Description

The Stern CHF tests made use of a 5x5 fuel bundle comprised of {{ }}2(a),(b),(c),ECI heated length fuel simulators arranged in three configurations including:

- {{ }}2(a),(b),(c) (U-1 series)
- {{ }}2(a),(b),(c) (U-2 series)
- {{ }}2(a),(b),(c) (C-1 series).

A prototypical fuel diameter {{

}}2(a),(b),(c),ECI

{{

}}2(a),(b),(c),ECI

{{

}}2(a),(b),(c),ECI

Figure 7-56. U1 & C1 (left) versus U2 (right) radial layout

An axial layout of the test section with key instrument locations is shown in Figure 7-57. The test section includes a pressure housing, a channel box (flow channel), fuel simulators, spacer grids, and instrumentation. Four spacers are installed within the heated section of the assembly at prototypical locations with a spacer pitch of {{ }}2(a),(b),(c),ECI The resistance temperature detectors are used to measure the average inlet and outlet temperatures of the coolant. In addition to the

© Copyright 2016 by NuScale Power, LLC

absolute pressure measurements at the inlet and outlet of the test section, there are nine differential pressure transducers installed within the heated section to measure the pressure drop across various axial sections.

{{

}}2(a),(b),(c),ECI

Figure 7-57. Stern test section axial layout

7.3.2 Experimental Procedure

At the Stern test facility, the steady state CHF tests were performed in the following manner:

© Copyright 2016 by NuScale Power, LLC

- loop conditions were established with the heated assembly at a power below the critical power,
- loop conditions were maintained steady as much as possible while the power was {{ }}2(a),(b),(c) until the critical power was reached,
- the data acquisition program continuously scans the assembly signals and critical power is considered to occur when the {{

}}2(a),(b),(c),ECI

- when the occurrence of critical power is confirmed the loop conditions were held steady and the steady-state data was recorded, and
- once the test point was recorded the power was reduced, as necessary, and loop conditions changed for the next test.

7.3.3 Phenomenon Addressed

The Stern CHF benchmark assesses the ability of NRELAP5 to predict CHF and {{ }}2(a),(c)

7.3.4 Parameter Ranges Assessed

The Stern steady state CHF tests were conducted across a systematic range of mass flows, inlet pressures, and inlet sub-cooling. A total of {{ }}2(a),(b),(c),ECI steady state CHF data were collected for pressures ranging from {{

}}2(a),(b),(c),ECI as described in Table 7-5. A series of repeat tests was also performed to determine the repeatability of the test data. A total of {{ }}2(a),(b),(c),ECI repeat test points are identified. Only the {{ }}2(a),(b),(c),ECI high flow data points with mass fluxes greater than {{ }}2(a),(b),(c),ECI are excluded from the assessment presented in this document.

© Copyright 2016 by NuScale Power, LLC

Table 7-5. Range of Stern steady state critical heat flux data

{{

}}2(a),(b),(c),ECI

7.3.5 Special Analysis Techniques

The NRELAP5 model consists of a {{

}}2(a),(c)

7.3.6 Assessment Results

{{

}}2(a),(c)

© Copyright 2016 by NuScale Power, LLC

{{

}}2(a),(c)

{{

}}2(a),(b),(c),ECI

Figure 7-58. Predicted versus measured Stern power

7.4 NuScale SIET Steam Generator Tests

This section addresses assessments performed against experiments conducted under the NuScale testing program at SIET laboratories, in Piacenza, Italy. Two test programs were conducted as described below.

© Copyright 2016 by NuScale Power, LLC

7.4.1 SIET Tests

The SIET experimental program is a two test activity with helical coil SG tubes characterized on an electrically heated test section (TF-1), and on a fluid heated test section (TF-2). The electrically heated test provides detailed in-tube information for the secondary side, while the fluid heated test allows investigation of the general behavior of the tube bundle heated by the primary side fluid. This section deals with the detailed description of the electrically heated test (TF-1) and NRELAP5 assessment results.

The electrically heated test section incorporates three full scale coils of the helical coil SG, providing information focused on the SG secondary side. Direct heating of the test section is provided by passing current through the tubes using three different axial heating zones (subcooled, saturated and superheat).

{{ }}$^{2(a),(b),(c),ECI}$ coils of the electrically heated test section represent the {{ }}$^{2(a),(b),(c),ECI}$ coils of the NuScale SG, in terms of diameter, length and angle of inclination, and they allow investigation into the effects of tube curvature on thermal-hydraulic parameters. The {{ }}$^{2(a),(b),(c),ECI}$ coil reproduces the {{ }}$^{2(a),(b),(c),ECI}$ coil of the NuScale SG, in terms of diameter and length, {{ }}$^{2(a),(b),(c),ECI}$

7.4.1.1 Facility Description

The main components and loops of the SIET TF-1 facility in the NuScale helical coil SG test configuration are described here. A pump system drives water from a water storage tank to the pre-heating zone where it is brought to the specified operating conditions and sent to a feedwater header. The header feeds the three coils of the test section that can be activated by valves: singularly or two in parallel. Superheated steam exits the test section toward a header connected to the separation and discharge system. A schematic of the test loop is provided in Figure 7-59.

© Copyright 2016 by NuScale Power, LLC

{{

}}2(a),(b),(c),ECI

Figure 7-59. SIET electrically-heated test instrumentation diagram

© Copyright 2016 by NuScale Power, LLC

7.4.1.2 Phenomena Addressed

The SIET TF-1 assessment cases addresses {{
}}2(a),(c)

7.4.1.3 Experimental Procedure

For adiabatic tests the inlet flowrate is specified along with the outlet pressure for each test point. For diabatic tests the inlet temperature, flowrate, and tube/zone heat flux (by setting the current) are specified along with the outlet pressure. This section only covers diabatic tests.

{{

}}2(a),(b),(c)

7.4.1.4 Special Analysis Techniques

The helical coil component used includes the helical coil friction model and heat transfer packages inside the coil (see Section 6.7).

7.4.1.5 Assessment Results

In general, NRELAP5 predicted the experimental data with reasonable-to-excellent agreement. The following specific conclusions were drawn from the assessment

- Calculated axial fluid and wall temperatures are within reasonable-to-excellent agreement of data.
- Calculated single- and two-phase pressure drops along the coil are in reasonable-to-excellent agreement with the test data.

Results from two Coil 2 tests are presented first to illustrate variation between predicted and measured wall temperature along the length of the coil. Subsequently, pressure drop for tests on Coil 1 through 3, and fluid temperature and wall temperature for tests on Coil1 are presented.

© Copyright 2016 by NuScale Power, LLC

Wall temperature profile for the three heating zones (subcooled, saturated, and superheat) of coil 2 are depicted in Figure 7-60 and Figure 7-61 for diabatic tests TD0015 and TD0003, respectively. From inspection of the wall temperatures, {{

}}2(a),(b),(c),ECI

{{

}}2(a),(b),(c),ECI

Figure 7-60. Time averaged wall temperature profile for coil 2 test TD0015

© Copyright 2016 by NuScale Power, LLC

{{

}}2(a),(b),(c),ECI

Figure 7-61. Time averaged wall temperature profile for coil 2 test TD0003

Pressure drops for the five sections along the length of Coil 1 (i.e., axial pressure drop) are given in Figure 7-62. The error bands on these figures represent the uncertainty in measurement of pressure drops. Calculated pressure drops over the first {{ }} 2(a),(b),(c),ECI are predicted with excellent agreement and within the experimental error, as shown by Figure 7-62. Similar results are shown for pressure drops in Coil 2 and Coil 3 in Figure 7-63 and Figure 7-64. In general, NRELAP5 does a reasonable-to-excellent job of predicting the axial pressure drops taking into account that the standard deviation of the experimental data (not shown on plots) is larger than the reported measurement uncertainty (shown on plot).

© Copyright 2016 by NuScale Power, LLC

{{

}}2(a),(b),(c),ECI

Figure 7-62. SIET electrically-heated test differential pressure for all coil 1 diabatic tests

© Copyright 2016 by NuScale Power, LLC

{{

}}2(a),(b),(c),ECI

Figure 7-63. SIET electrically-heated test differential pressure for all coil 2 diabatic tests

© Copyright 2016 by NuScale Power, LLC

{{

}}2(a),(b),(c),ECI

Figure 7-64. SIET electrically-heated test differential pressure for all coil 3 diabatic tests

Fluid temperatures for {{ }}2(a),(b),(c),ECI of coil 1 are depicted in Figure 7-65. The error bands on these figures represent the uncertainty in measurement of fluid temperature. The calculated values are in reasonable-to-excellent agreement with experimental data.

© Copyright 2016 by NuScale Power, LLC

{{

}}2(a),(b),(c),ECI

Figure 7-65. SIET electrically-heated test fluid temperatures for all coil 1 diabatic tests

Corresponding wall temperatures at several axial locations of coil 1 are depicted in Figure 7-66. The error bands on these figures represent the uncertainty in measurement of wall temperature. Wall temperature results are similar to the corresponding fluid temperature results {{

}}2(a),(b),(c),ECI

© Copyright 2016 by NuScale Power, LLC

{{

}}2(a),(b),(c),ECI

Figure 7-66. SIET electrically-heated test wall temperature for all coil 1 diabatic tests

7.4.2 SIET Fluid-Heated Test

The SIET fluid-heated tests were performed in support of the NuScale design development, with particular emphasis on providing experimental data for validation of NRELAP5 for prediction of helical coil SG primary and secondary heat transfer and pressure drop.

7.4.2.1 Facility Description

The SIET TF-2 facility consists of a 252 helical coil tube bundle installed inside a pressure vessel. The tube bundle consists of 5 tube banks, simulating the {{

}}2(a),(b),(c),ECI All five tube bundles are placed in an annulus, formed by two cylindrical barrels, installed axially within the pressure vessel. The helical coils are wrapped around the inner barrel and kept in position by four supports,

© Copyright 2016 by NuScale Power, LLC

{{

}}2(a),(b),(c),ECI

Each tube bank is fed by a feed-water vertical header, inside the vessel, that distributes water to each helical tube. Steam from each the exit of each tube bank is collected in a steam vertical header and driven outside the vessel top nozzle by pipes.

The primary-side of the test section consists of an inlet riser barrel, connection bellows, internal barrel, pressure vessel dome, free volume (i.e., unoccupied by the tubes) between the internal and external barrels (i.e., annulus), and free volume of the pressure vessel around the inlet riser and connection bellows. Water on the primary side is circulated by pumps and pre-heated by an electric heater before entering the pressure vessel. The pressure on the primary side is maintained using the electrically heated pressurizer.

Primary water, entering the pressure vessel from the bottom nozzle, rises through a vertical channel and enters the central cylindrical part of the test section, representing the riser. After reaching the vessel dome, water turns down into the test section annulus to cross the helical coil tube bundle. Exiting at the bottom, water is driven again to the circulation pumps.

Instruments are installed for the measurement of primary side mass flow rate, inlet and exit temperatures, pressures and differential pressures. Instruments are installed to measure the secondary side feed water flow rate, feed water temperature, pressures and differential pressure along the tubes, and exit steam temperatures and flow rates.

7.4.2.2 Phenomenon Addressed

Adiabatic tests were performed to characterize the primary side pressure losses in the facility. These tests were run without heat input to the primary flow and there was no secondary flow to the coils.

Diabatic tests measured pressure drop and heat transfer on both the primary and secondary, and the thermal crisis (dryout) location on the secondary side during heated operation of the coils. These tests characterize the thermal performance of the coils for a range of primary and secondary side inlet flows and temperatures.

7.4.2.3 Experimental Procedure

Target boundary conditions are obtained for the diabatic tests. The duration of the data recording for each test was a minimum 300 seconds for the pre-steady state and 150 seconds for the steady state.

© Copyright 2016 by NuScale Power, LLC

7.4.2.4 Special Analysis Techniques

This benchmark assesses {{

}}2(a),(c)

7.4.2.5 Assessment Results

In general, NRELAP5 predicted the experimental data with reasonable-to-excellent agreement with few exceptions, as identified below. The following specific conclusions were drawn from the assessment:

- {{

}}2(a),(b),(c),ECI

7.4.2.5.1 Assessment of Adiabatic Experiment Data

Adiabatic experimental data from TF-2 testing is used to assess the modeling of primary side friction and form losses. The primary side pressure drop was measured at {{ }}2(a),(b),(c),ECI Figure 7-67 shows the comparison of predicted and measured primary side pressure drop at all axial elevations for all adiabatic tests. The error bands represent the uncertainty in measurement of pressure drops. Excellent agreement between NRELAP5 predictions and measured test data exists with primary side pressure drop predicted within the measurement uncertainty. Similar results are obtained for other primary side pressure drop measurement elevations.

© Copyright 2016 by NuScale Power, LLC

{{

}}2(a),(b),(c),ECI

Figure 7-67. SIET fluid-heated test adiabatic primary differential pressure

7.4.2.5.2 Primary Side Pressure Drop and Fluid Temperatures of Diabatic Experiments

{{

}}2(a),(b),(c),ECI

© Copyright 2016 by NuScale Power, LLC

{{

}}2(a),(b),(c),ECI

Figure 7-68. SIET fluid-heated test diabatic test primary differential pressure

© Copyright 2016 by NuScale Power, LLC

{{

}}2(a),(b),(c),ECI

Figure 7-69. SIET fluid-heated test diabatic test primary temperature

7.4.2.5.3 Steam Generator Tube Wall Temperature of Diabatic Experiments

{{

}}2(a),(b),(c),ECI

© Copyright 2016 by NuScale Power, LLC

{{

}}2(a),(b),(c),ECI

Figure 7-70. Comparison of wall temperatures in TD0001 (Case 1)

© Copyright 2016 by NuScale Power, LLC

{{

}}2(a),(b),(c),ECI

Figure 7-71. Comparison of wall temperatures in TD0007 (Case 1)

© Copyright 2016 by NuScale Power, LLC

{{

}}2(a),(b),(c),ECI

Figure 7-72. Comparison of wall temperatures in TD0002 (Case 1)

7.4.2.5.4 Secondary Side Fluid Temperature of Diabatic Experiments

Figure 7-73 and Figure 7-74 show the comparison of predicted and measured secondary side fluid temperatures at all elevations in Row 3 for selected tests. Most secondary side fluid temperatures are predicted reasonably well by NRELAP5, as shown in Figure 7-73. {{

}}2(a),(b),(c),ECI

© Copyright 2016 by NuScale Power, LLC

{{

}}2(a),(b),(c),ECI

Figure 7-73. Comparison of secondary side fluid temperatures Row 3 (Case 1)

© Copyright 2016 by NuScale Power, LLC

{{

}}2(a),(b),(c),ECI

Figure 7-74. Comparison of secondary side fluid temperatures in TD0002 (Case 1)

7.5 NuScale NIST-1 Test Assessment Cases

A scaled facility of the NPM was constructed at Oregon State University, referred to as the NIST-1 facility, to assist in validation of the NRELAP5 system thermal-hydraulic code. The facility is designed to perform various tests, including LOCA tests. The NIST-1 facility consists of the major components in the NPM. These components include: an RPV, helical coil SG system with DHRS, CNV, and cooling pool vessel (CPV) representing the reactor pool. The NIST-1 ECCS connects the RPV to the CNV and consists of two RVVs and two RRVs, each on separate lines. Breaks can be simulated for the RCS lines that connect the RPV to the CNV to simulate piping breaks within the CNV. This system consists of a RCS discharge line, a RCS injection line, and a pressurizer spray supply line. The CVCS is not functional in the NIST-1 facility and is used only for simulation of CVCS line break LOCAs.

© Copyright 2016 by NuScale Power, LLC

Instrumentation is included in the facility to capture the response of the system under steady-state and transient situations. The instrumentation includes pressure, differential pressure, water level, mass flow rate, heat flux, and temperature measurements.

7.5.1 Test Facility Description

Due to the unique nature of the NPM design the number of IET facilities suitable for code assessment is limited. What is now the NIST-1 facility was originally conceived at OSU in 2000 as a proof-of-concept testing platform for development of Small Modular Reactor (SMR) technology. During this period it was referred to as the multi-application small light water reactor facility (Reference 72).

Although the NuScale design was based on the Multi-Application Small Light Water Reactor (MASLWR), the concept has evolved considerably since the inception of NuScale in 2008. At the time that NuScale was formed, the facility was renamed the NIST facility. The NIST facility is a scaled, non-nuclear reactor that uses electric heater rods to represent the heat produced from fission. It is designed to produce experimental data in support of verification and validation of thermal-hydraulic codes.

In 2014 and 2015, the original NIST facility was modified by NuScale to facilitate accurate simulation and to bring the facility in-line with the current NuScale plant design configuration. Following the upgrade, the NIST facility was renamed NIST-1 facility. A scaling analysis was employed for design of the NIST test facility to ensure that the facility design is capable of capturing important plant phenomena with minimal distortions. Further discussion on the NIST-1 facility scaling and distortions is available in Sections 8.3.2 and 8.3.4.

Updates to the NIST facility included in NIST-1 are:

- {{

}}2(a),(b),(c),ECI

The updated NIST-1 facility provides a well-scaled representation of the current NuScale reactor design that minimizes distortions and provides the measurements necessary for safety code and reactor design validation. A schematic of the NIST-1 facility is shown in Figure 7-75.

© Copyright 2016 by NuScale Power, LLC

{{

}}2(a),(c),ECI

Figure 7-75. Schematic of NuScale integral test facility and NRELAP5 nodalization

© Copyright 2016 by NuScale Power, LLC

The NIST-1 facility models the NPM at {{ }}2(a),(b),(c),ECI scale. There are three vessels in the NIST-1 facility: the RPV, CNV, and CPV as shown in Figure 7-75. Unlike the plant, the RPV and CNV are not concentric and the CNV is not immersed in the CPV. Rather the RPV and CNV are connected by piping that contains valves that perform the functions of the RRVs, RVVs and breaks as shown in Figure 7-75. This approach enables flow measurements to be made in this piping during testing. The CNV is connected to the CPV through a HTP that is scaled to allow energy transfer to the pool in the same proportion as in the NPM.

Natural circulation flow in the primary circuit is driven by heat input in the core region and heat removal to the SG tubes. Fluid heated in the core region flows upward through the hot leg riser, and then downward around the outside of the SG tubes, the cold leg and the downcomer. The flow then returns to the core through the LP. The core is comprised of a {{ }}2(a),(b),(c),ECI electric heater rod bundle with a maximum power of {{ }}2(a),(b),(c),ECI kW, a power level scaled to simulate decay heat. System pressure is controlled by the pressurizer component which contains heater rods to bring the pressurizer fluid up to saturation temperature.

7.5.1.1 Reactor Pressure Vessel

Major internal components in the RPV are the core, hot leg riser, pressurizer, and SG bundle. The pressurizer is at the top, separated from the lower part of the RPV by a perforated pressurizer baffle plate. The upper plenum occupies the region below the pressurizer baffle plate and above the hot leg riser that extends down to the top of the core. The upper annulus between the hot leg riser and the RPV shell contains the helical coil SG tubes. The lower part of the annulus immediately below the SG tubes is the cold leg. The lower annulus at the core elevation is the downcomer, which is separated from the core by the core shell. The LP occupies the bottom of the RPV and hydraulically connects the downcomer and the core.

The RPV shells and flanges are covered by {{

}}2(a),(b),(c),ECI

© Copyright 2016 by NuScale Power, LLC

7.5.1.1.1 Reactor Core

The RPV houses the core, which is modeled by a {{

}}2(a),(b),(c),ECI

7.5.1.1.2 Hot Leg Riser

After leaving the core, the flow enters the chimney of the hot leg riser. The hot leg riser extends from above the core shroud to the upper plenum, creating a riser and downcomer configuration to enable natural circulation. The hot leg riser consists of a lower shell, a conical transition, a middle shell containing the flowmeter for the primary circuit, and an upper shell. Flow exits the riser into the upper plenum, which is the space between the hot leg riser outlet and the bottom of the pressurizer baffle plate.

7.5.1.1.3 Upper Plenum

After leaving the top of the hot leg riser, the flow enters the upper plenum and is directed radially outward to flow down in the annulus between the riser and the RPV shell. The pressurizer baffle plate separates the upper plenum from the pressurizer. Hydraulic communication between the pressurizer and the RPV occurs via holes located in the pressurizer baffle plate.

7.5.1.1.4 Pressurizer

The pressurizer is located above the upper plenum and is in thermal-hydraulic communication with the upper plenum via the pressurizer baffle plate holes. The pressurizer maintains primary system pressure during normal steady-state and transient conditions through the use of three heater elements. Each element has {{ }}2(a),(b),(c),ECI of power and is modulated by the facility control system to maintain system pressure.

7.5.1.1.5 Cold Leg Downcomer

After leaving the upper plenum, the flow continues downward through the SG section and into the cold leg downcomer region. The cold leg downcomer is the annular space bounded by the RPV shell ID and the hot leg riser outer diameter. When fluid reaches the hot leg riser conical transition shell, the flow area is reduced. Flow exits the cold leg downcomer into the LP before it recirculates back into the core.

© Copyright 2016 by NuScale Power, LLC

7.5.1.1.6 Steam Generators

The SG is a helical-coil, once-through heat exchanger consisting of {{ }}2(a),(b),(c),ECI that wrap counter to each other in the annular space between the hot leg riser and the RPV shell inner surface. In the NIST-1 facility, the primary coolant is circulated on the outside of the SG tubes, similar to the NPM. Feedwater supplied from the feedwater storage tank is pumped through the SG coils by a regenerative turbine pump. Pressure in the secondary side is regulated by a pneumatically operated variable position valve located in the steam line portion of the flow loop.

7.5.1.1.7 Lower Plenum

The LP is the region bounded between the tubesheet and the lower core flow plate. The LP provides the connection between the downcomer and the core, thus completing the RPV flow loop.

7.5.1.2 Containment

The CNV, representing the cavity volume between the RPV outer surface and the containment inside surface, is conjoined to the CPV and thermally separated by a scaled HTP. For the NPM, the RPV is located inside containment. However, with the NIST-1 facility, to maintain both volume and surface area scaling similitude, as well as allow proper instrumentation, the RPV is thermal hydraulically separated from the CNV. The CNV models the scaled condensation heat transfer surface between the CNV and CPV. Fluid in the CPV, which is at ambient pressures, models the scaled volume in which an NPM CNV is submerged.

7.5.1.3 Cooling Pool Vessel

The CPV has a set of four ports allowing for the installation of one of three decay heat removal heat exchangers. The baseline configuration is with a {{

}}2(a),(b),(c)

7.5.1.4 Emergency Core Cooling System and Chemical and Volume Control System Lines

Eight lines connect the RPV to the CNV. Five of these lines belong to the facility ECCS, whereas the other three are part of the CVCS. As part of the ECCS, there are two independent reactor vent lines near the top of the pressurizer section and two reactor recirculation lines in the lower downcomer of the RPV. The fifth ECCS line is an SET line that also models reactor recirculation. For the CVCS, two lines penetrate the vessel near the bottom of the SG. One of these lines penetrates both the vessel wall and the hot leg riser, simulating the make-up line into the hot leg. The other CVCS line connects to the

© Copyright 2016 by NuScale Power, LLC

cold leg and penetrates only the RPV wall. This line represents the facility CVCS discharge break line. A third CVCS line between the RPV and CNV is located at the top of the pressurizer and functions as an analogy for the pressurizer spray supply line. Each line has a pneumatic isolation valve that is actuated through the test facility control system. Any lines that are not installed use a blank flange for isolation.

7.5.1.5 Facility Instrumentation and Control

Instrumentation is used throughout the NIST-1 facility to measure the thermal-hydraulic behavior during steady-state and transient operations. The following information is recorded by the DACS:

- {{

}}2(a),(b),(c),ECI

The data generated and collected by the facility DACS is used to validate applicability of the NRELAP5 thermal-hydraulic code for LOCA analysis.

7.5.1.6 Integral Effects LOCA Test Procedure

Prior to startup, a valve and switch lineup is performed to place the facility in the desired configuration for the upcoming test. The break line modeling the break location specified for the test is connected between the RPV and its associated CNV penetration. To prevent an accidental actuation of an incorrect break valve a blind flange is installed in all other break lines. Orifices with the specified diameters are installed in the RVV and RRV lines to model the number of valves that are to open when ECCS actuates.

Because the NIST-1 facility has a nominal operating pressure of {{ }}2(a),(b),(c),ECI that is less than the NPM pressure of 1,850 psia (12.76 MPa), the test in the NIST-1 facility simulates the NPM transient in progress. Specifically, the RPV and CNV

© Copyright 2016 by NuScale Power, LLC

fluid masses in NIST-1 are scaled such that they are {{ }}2(a),(b),(c),ECI that of the RPV and CNV fluid masses in the NPM at a corresponding pressure of {{ }}2(a),(b),(c),ECI Thus the initial RCS mass inventory and pressure are preserved on a scaled basis and fluid property similitude is maintained throughout the transient.

As part of the NIST-1 LOCA tests, {{

}}2(a),(b),(c),ECI

7.5.2 Facility NRELAP5 Model

The NRELAP5 model of the NIST-1 facility is constructed to {{

}}2(a),(c) These model features are shown in the NRELAP5 nodalization shown in Figure 7-75.

7.5.3 Facility Test Matrix

This NIST-1 facility is used to perform design certification IETs and SETs for the purpose of validating NuScale computer codes, model development and assessment, correlation development, verifying compliance with design requirements, demonstrating design features and capabilities, and addressing regulatory concerns.

This section briefly describes the test matrix for the NIST-1 facility. Descriptions of tests used for NRELAP5 code validation are provided in Table 7-6. These are the NIST-1 tests that are the essential subset of tests required to validate NRELAP5 for NPM LOCA calculations.

© Copyright 2016 by NuScale Power, LLC

Table 7-6. Facility high priority tests for NRELAP5 code validation

{{

}}2(a),(b),(c),ECI

Tests NIST-1 HP-06, HP-07 and HP-09 are the IETs that are used for validating the NRELAP5 EM for LOCA applications. Test HP-09 is included because spurious opening of an RVV results in the bounding RPV depressurization rate.

7.5.4 Separate Effect High Pressure Condensation Tests

The NIST-1 facility HP-02 test was used to assess the capability of NRELAP5 to predict condensation rates at high pressure test conditions by comparing experimental data and NRELAP5 predictions.

© Copyright 2016 by NuScale Power, LLC

7.5.4.1 Facility Description

The HP-02 test is an SET performed at the NIST-1 facility. The test involves injecting steam at known conditions into the CNV and measuring the CNV pressure, level, and temperature response. Only the CNV, CPV, and interconnecting HTP are important to this test. During testing, the RPV was pressurized and heated using core heat to supply superheated steam from the SG to the CNV at the desired mass flow rate.

The feedwater flowrate was measured with individual Coriolis flowmeters to each of the three SG inlet tube banks. Also, one Coriolis meter measured the total SG feedwater inlet flow and one vortex flowmeter measured the total steam flow at the SG exit. The Coriolis flowmeter measuring the combined inlet flow was used as a mass flow boundary condition in the NRELAP5 model as it provided the most stable flow measurement with the lowest measurement uncertainty.

7.5.4.2 Phenomenon Addressed

The pertinent phenomena validated with the NIST-1 facility HP-02 assessment are {{

}}2(a),(b),(c),ECI

7.5.4.3 Experimental Procedure

Initial steam conditions in the CNV were obtained by first operating the NIST-1 facility in its normal mode, heating the RPV with core heaters with heat rejection through the SG to the environment. The SG feedwater flowrate, core power, and steam exit pressure were established to obtain the desired conditions for steam. Once the desired conditions were established, steam was diverted from the stack (rejected to the environment) to the CNV.

Five tests were run to evaluate steady-state condensation at varying CNV pressures. For each test, superheated steam was discharged into the CNV until the CNV target pressure was reached, after which the inlet steam flow was ramped down in an effort to achieve steady state conditions at the target pressure.

Steady steam inlet conditions were maintained through the injection period. After steam was injected into the CNV, condensation occurred on the HTP. Condensation energy was then thermally conducted through the HTP and convected into the CPV.

© Copyright 2016 by NuScale Power, LLC

7.5.4.4 Parameter Ranges Assessed

Test conditions were selected to obtain condensation data at various CNV pressures. Five tests were conducted at steady CNV pressure varying from {{

}}2(a),(b),(c),ECI

7.5.4.5 Assessment Results

The HP-02 test facility data was compared to NRELAP5 predictions designed to simulate the test conditions and test procedures in effect during the experiment. HP-02 test data trends were well predicted by NRELAP5 with reasonable-to-excellent agreement for condensation rates at pressures ranging {{
}}2(a),(b),(c),ECI NRELAP5 has demonstrated its capability to predict CNV level, CNV pressure, CNV temperature, and CPV temperature with reasonable-to-excellent agreement.

The following subsections provide a brief summary of the results for three HP-02 runs analyzed.

7.5.4.5.1 Run 1 Results

Both the CNV pressure and level responses for Run 1 depicted in Figure 7-76 and Figure 7-77 are in excellent agreement with the data. The NRELAP5-simulated pressure peak occurs at the same time as the data; reaching a maximum of {{

}}2(a),(b),(c)

The CNV and CPV fluid temperatures predicted by NRELAP5 are in excellent agreement with the data. Figure 7-78 and Figure 7-79 show that the predictions closely following the data trend and magnitude during the earlier transient as well as the steady-state period.

© Copyright 2016 by NuScale Power, LLC

{{

}}2(a),(b),(c),ECI

Figure 7-76. HP-02 Run 1 containment vessel pressure response

© Copyright 2016 by NuScale Power, LLC

{{

}}2(a),(b),(c),ECI

Figure 7-77. HP-02 Run 1 containment vessel collapsed level response

© Copyright 2016 by NuScale Power, LLC

{{

}}2(a),(b),(c),ECI

Figure 7-78. HP-02 Run 1 upper containment vessel fluid temperature response (in vapor space)

© Copyright 2016 by NuScale Power, LLC

{{

}}2(a),(b),(c),ECI

Figure 7-79. HP-02 Run 1 upper cooling pool vessel temperature response

7.5.4.5.2 Run 2 Results

During run 2 a maximum pressure of {{ }}2(a),(b),(c),ECI was reached. NRELAP5 is in excellent agreement with the experimental data for CNV pressure, as shown in Figure 7-80. NRELAP5 predicts the general trends for level, with reasonable-to-excellent agreement to data (Figure 7-81), but slightly over-predicts collapsed level.

The NRELAP5 containment vessel and CPV temperatures shown in Figure 7-82 and Figure 7-83 are in excellent agreement with the data, closely following the trend and lying almost entirely within the instrument uncertainty.

© Copyright 2016 by NuScale Power, LLC

{{

}}2(a),(b),(c),ECI

Figure 7-80. HP-02 Run 2 containment vessel pressure response

© Copyright 2016 by NuScale Power, LLC

{{

}}2(a),(b),(c),ECI

Figure 7-81. HP-02 Run 2 containment vessel collapsed level response

© Copyright 2016 by NuScale Power, LLC

{{

}}2(a),(b),(c),ECI

Figure 7-82. HP-02 Run 2 upper containment vessel fluid temperature response (in vapor space)

© Copyright 2016 by NuScale Power, LLC

{{

}}2(a),(b),(c),ECI

Figure 7-83. HP-02 Run 2 upper cooling pool temperature response

7.5.4.5.3 Run 3 Results

{{

}}2(a),(b),(c),ECI

© Copyright 2016 by NuScale Power, LLC

{{

}}2(a),(b),(c),ECI

{{

}}2(a),(b),(c),ECI

Figure 7-84. HP-02 Run 3 containment vessel pressure response

© Copyright 2016 by NuScale Power, LLC

{{

}}2(a),(b),(c),ECI

Figure 7-85. HP-02 Run 3 containment vessel collapsed level response

© Copyright 2016 by NuScale Power, LLC

{{

}}2(a),(b),(c),ECI

Figure 7-86. HP-02 Run 3 upper containment vessel fluid temperature response (in vapor space)

© Copyright 2016 by NuScale Power, LLC

{{

}}2(a),(b),(c),ECI

Figure 7-87. HP-02 Run 3 upper cooling pool temperature response

Based on this assessment, NRELAP5 has demonstrated its capability to predict CNV level, CNV pressure, CNV temperature, and CPV temperature with reasonable-to-excellent agreement for high pressure condensation conditions.

7.5.5 Natural Circulation Test at Power

The NIST-1 test HP-05 was used to assess the capability of NRELAP5 to predict natural circulation flow at various core powers and test conditions by comparing experimental data and NRELAP5 predictions.

7.5.5.1 Facility Description

The HP-05 test configuration uses the RPV and SG to drive steady-state natural circulation within the RPV at various core heater rod power levels. Core heater rods supply energy to heat the working fluid which, due to buoyancy forces, travels up the riser entering the upper plenum. The fluid then turns 180 degrees and passes over the integrated helical coil SG, exchanging energy to the secondary side. The primary working fluid exits the SG

© Copyright 2016 by NuScale Power, LLC

traveling downward through the downcomer, entering the LP where another 180 degree turn (upward) is made into the entrance of the electrically heated core.

Various instruments measure differential pressures, flow, temperatures, pressures, and heater power to assess the loop flowrate and pressure losses.

7.5.5.2 Phenomenon Addressed

The pertinent phenomena addressed with the HP-05 assessment case are {{

}}2(a),(c)

7.5.5.3 Experimental Procedure

The HP-05 experiment consists of inducing a core power ramp at a constant RPV pressure of approximately {{ }}2(a),(b),(c),ECI and a secondary-side pressure of approximately {{ }}2(a),(b),(c),ECI Differential pressures around the primary loop were measured to characterize the pressure drops due to form and friction losses. The mass flow rate in the riser and fluid temperatures around the loop are measured. To facilitate comparing to code predictions the core power and temperature rise across the core are used to calculate a theoretical flowrate based on an energy balance.

Test HP-05 initiates from a power of {{ }}2(a),(b),(c),ECI, at a pressure of {{ }}2(a),(b),(c),ECI , and the steady-state natural circulation flow condition. Once steady-state conditions are achieved, {{

}}2(a),(b),(c),ECI

7.5.5.4 Special Analysis Techniques

{{

}}2(a),(c) The global response was then confirmed by comparing the experimental loop flow rate to that predicted by NRELAP5.

© Copyright 2016 by NuScale Power, LLC

7.5.5.5 Parameter Ranges Assessed

{{

}}2(a),(b),(c)

7.5.5.6 Assessment Results

{{
}}2(a),(b),(c) The NRELAP5 mass flow signal is taken from the same location. The NRELAP5 prediction is closely aligned with the data and shows excellent agreement, with the exception of the behavior demonstrated at the lowest core power level, where reasonable agreement is obtained. At the lower power level, facility constraints on the secondary side made it difficult to obtain steady state conditions.

{{

}}2(a),(c)

The NRELAP5 calculated loop mass flow rate follows the trends presented by the data, with reasonable-to-excellent agreement determined by the uncertainty bands as shown in Figure 7-88.

© Copyright 2016 by NuScale Power, LLC

{{

}}2(a),(b),(c),ECI

Figure 7-88. HP-05 NIST-1 averaged mass flowrate and NRELAP5 results

The core inlet temperature was measured in the LP upstream of where the fluid enters the core. The NRELAP5 signal is taken from the same region. Comparisons to the measure data are provided in Figure 7-89. The NRELAP5 core inlet temperatures are in excellent agreement with the data.

© Copyright 2016 by NuScale Power, LLC

{{

}}2(a),(b),(c),ECI

Figure 7-89. HP-05 NIST-1 averaged core inlet temperature and NRELAP5 results

Core outlet temperature was measured in the riser near the core exit. The NRELAP5 signal is located in the same region. Each time the core power is lowered the hot leg temperature first falls and then recovers. In the data, the temperature usually over-shoots the previous steady state value prior to settling down at the next steady state value. Except for these power transients, the data and NRELAP5 predictions are in excellent agreement as demonstrated in Figure 7-90.

© Copyright 2016 by NuScale Power, LLC

{{

}}2(a),(b),(c),ECI

Figure 7-90. HP-05 NIST-1 averaged core outlet temperature and NRELAP5 results

Based on this assessment, NRELAP5 has demonstrated its capability to predict primary flow rate, core inlet temperature, and core outlet temperature with reasonable-to-excellent agreement for natural circulation flow conditions.

7.5.6 Chemical and Volume Control System Loss-of-Coolant Accident Integral Effects Tests

The HP-06 test was used to assess the capability of NRELAP5 to predict the integral response of the NIST-1 facility for a single-ended discharge line break inside containment. The discharge line and valve connect the downcomer side of the RPV to the CNV.

© Copyright 2016 by NuScale Power, LLC

The HP-06b test was similar to the HP-06 test, with the exception of the core power. This test was performed to assess the impact of core power on the progression of the LOCA. {{

}}2(a),(b),(c),ECI

7.5.6.1 Facility Description

The entire NIST-1 facility except for the DHRS was used for this IET, including:

- the SG was active to remove heat from the primary side and drive natural circulation in conjunction with the electrically heated core during the steady state
- {{

  }}2(a),(b),(c)
- the CPV was filled to accept rejected heat from the HTP

In addition, {{

}}2(a),(b),(c)

7.5.6.2 Phenomenon Addressed

The HP-06 and HP-06b tests are IETs modeling a single-ended discharge line break inside containment. The purpose of these IETs was to assess the integral response of the scaled NIST-1 facility. The pertinent phenomena addressed by these tests are:

- {{

}}2(a),(b),(c),ECI

© Copyright 2016 by NuScale Power, LLC

7.5.6.3 Experimental Procedure

The IET test procedure is described in Section 7.5.1.6. When the CNV pressure reached the specified CNV break initiation pressure, the CVCS break valve was opened, initiating the transient.

Within the NIST-1 facility, the ECCS actuation occurs when the compensated level in the RPV downcomer reads lower than a specified value. Once this occurs, open signals are sent to the RRVs and the RVVs. The opening of the ECCS valves causes a large amount of mass and energy transfer to occur between the RPV and the CNV over a short period of time. The CNV pressurization and heat-up occurs rapidly, followed by a long depressurization and cooldown profile. Test data was recorded for an extended period of time, well into the long-term cooling phase.

7.5.6.4 Special Analysis Techniques

The RCS discharge line orifice has a length of approximately {{ }}$^{2(a),(b),(c),ECI}$ and an ID of approximately {{ }}$^{2(a),(b),(c),ECI}$ Thus, the orifice has an L/D ratio roughly equal to {{ }}$^{2(a),(b),(c),ECI}$ Analysis indicates that a NRELAP5 discharge coefficient near {{ }}$^{2(a),(b),(c),ECI}$ produces reasonable agreement with the break flow test data.

The {{

}}$^{2(a),(c)}$

7.5.6.5 Assessment Results (HP-06)

The NRELAP5 transient model is designed to simulate initial test conditions and includes logic that follows facility controls and test procedures. The NRELAP5-calculated RCS discharge line break mass flow rate is shown in Figure 7-91 with a peak flowrate of approximately {{ }}$^{2(a),(b),(c),ECI}$ lbm/s. For this experiment, the break mass flow rate was not measured. The calculated break flow rate is reasonable because the differential pressure across the RCS discharge line orifice (Figure 7-92), the RPV level response (Figure 7-95), the CNV level response (Figure 7-96), the RPV pressure response (Figure 7-99), and the CNV pressure response (Figure 7-97) are all in excellent agreement.

The NIST-1 v-cone flowmeter (measuring primary loop flowrate) is designed for positive single-phase liquid conditions. During the HP-06 test, two-phase conditions occur at the location of the v-cone meter. The time period shown in Figure 7-93 captures the RPV primary-flow coast-down period after break initiation with reasonable-to-excellent accuracy. Calculated values for RPV mass flow rate were set to {{ }}$^{2(a),(b),(c),ECI}$ after {{ }}$^{2(a),(b),(c),ECI}$ seconds post-test initiation to avoid presenting instrument-based data when two-phase conditions are present. From Figure 7-93, it can be seen that NRELAP5 captures the loop flow stagnation within {{ }}$^{2(a),(b),(c),ECI}$

© Copyright 2016 by NuScale Power, LLC

The pressurizer level is compared in Figure 7-94. The comparisons show reasonable-to-excellent agreement. NRELAP5 predicts complete draining of the pressurizer at about {{ }}2(a),(b),(c),ECI

NRELAP5 provides reasonable-to-excellent agreement for level response in the RPV and CNV as shown in Figure 7-95 and Figure 7-96. The CNV peak pressure and pressure response are also predicted with excellent agreement to data as shown in Figure 7-97 and Figure 7-98. The timing of ECCS actuation is predicted with reasonable-to-excellent agreement to the test data. Primary pressure response is predicted with reasonable-to-excellent agreement (Figure 7-99).

{{

}}2(a),(b),(c),ECI

Figure 7-91. NIST-1 HP-06 NRELAP5 chemical and volume control system discharge line break mass flow rate

© Copyright 2016 by NuScale Power, LLC

{{

}}2(a),(b),(c),ECI

Figure 7-92. NIST-1 HP-06 break orifice differential pressure

© Copyright 2016 by NuScale Power, LLC

{{

}}2(a),(b),(c),ECI

Figure 7-93. NIST-1 HP-06 primary mass flow rate

© Copyright 2016 by NuScale Power, LLC

{{

}}2(a),(b),(c),ECI

Figure 7-94. NIST-1 HP-06 pressurizer level comparison

© Copyright 2016 by NuScale Power, LLC

{{

}}2(a),(b),(c),ECI

Figure 7-95. NIST-1 HP-06 reactor pressure vessel level comparison

© Copyright 2016 by NuScale Power, LLC

{{

}}2(a),(b),(c),ECI

Figure 7-96. NIST-1 HP-06 containment vessel level comparison

© Copyright 2016 by NuScale Power, LLC

{{

}}2(a),(b)(c),ECI

Figure 7-97. NIST-1 HP-06 containment vessel pressure comparison

© Copyright 2016 by NuScale Power, LLC

{{

}}2(a),(b),(c),ECI

Figure 7-98. NIST-1 HP-06 containment vessel pressure comparison

© Copyright 2016 by NuScale Power, LLC

{{

}}2(a),(b),(c),ECI

Figure 7-99. NIST-1 HP-06 primary pressure comparison

7.5.6.6 Assessment Results (HP-06b)

{{

}}2(a),(b),(c),ECI

Other HP-06b initial and boundary conditions were similar to the HP-06 test {{

}}2(a),(b),(c),ECI

© Copyright 2016 by NuScale Power, LLC

{{

}}2(a),(b),(c),ECI

Figure 7-100. Comparison of core power in HP-06 and HP-06b tests with the NuScale Power Module decay power after reactor trip (scaled)

Figure 7-101 and Figure 7-102 show the comparisons of predicted and measured RPV and CNV pressures, respectively. Similar comparisons for the RPV and CNV levels are shown in Figure 7-103 and Figure 7-104, respectively. Overall, NRELAP5 predicted the HP-06b data with reasonable-to-excellent agreement.

Figure 7-105 and Figure 7-106 show the comparisons of measured RPV and CNV pressures in HP-06 and HP-06b tests, respectively. Similar comparisons for the measured RPV and CNV levels are shown in Figure 7-107 and Figure 7-108, respectively. {{

}}2(a),(b),(c),ECI

© Copyright 2016 by NuScale Power, LLC

{{

}}2(a),(b),(c),ECI

Figure 7-101. NIST-1 HP-06b primary pressure comparison

© Copyright 2016 by NuScale Power, LLC

{{

}}2(a),(b),(c),ECI

Figure 7-102. NIST-1 HP-06b containment vessel pressure comparison

© Copyright 2016 by NuScale Power, LLC

{{

}}2(a),(b),(c),ECI

Figure 7-103. NIST-1 HP-06b reactor pressure vessel level comparison

© Copyright 2016 by NuScale Power, LLC

{{

}}2(a),(b),(c),ECI

Figure 7-104. NIST-1 HP-06b containment vessel level comparison

© Copyright 2016 by NuScale Power, LLC

{{

}}2(a),(b),(c),ECI

Figure 7-105. Comparison of NIST-1 HP-06 and HP-06b reactor pressure vessel pressure

© Copyright 2016 by NuScale Power, LLC

{{

}}2(a),(b),(c),ECI

Figure 7-106. Comparison of NIST-1 HP-06 and HP-06b containment vessel pressure

© Copyright 2016 by NuScale Power, LLC

{{

}}2(a),(b),(c),ECI

Figure 7-107. Comparison of NIST-1 HP-06 and HP-06b reactor pressure vessel level

© Copyright 2016 by NuScale Power, LLC

{{

}}2(a),(b),(c),ECI

Figure 7-108. Comparison of NIST-1 HP-06 and HP-06b containment vessel level

7.5.7 Pressurizer Spray Supply Line Loss-of-Coolant Accident Integral Effects Test

The HP-07 test was used to assess the capability of NRELAP5 to predict the integral response of the NIST-1 facility modeling a single-ended pressurizer spray supply line break inside containment.

7.5.7.1 Facility Description

The entire NIST-1 facility, except for the DHRS, was used for this IET.

- The SG was active to remove heat from the primary side and drive natural circulation in conjunction with the electrically heated core during steady state.
- {{

  }}2(a),(b),(c)
- The CPV was filled to accept rejected heat from the HTP.

© Copyright 2016 by NuScale Power, LLC

7.5.7.2 Phenomenon Addressed

The phenomena addressed in the test facility HP-07 test are same as in the HP-06 test (see Section 7.5.6.2).

7.5.7.3 Experimental Procedure

The LOCA test procedure is discussed in Section 7.5.1.6. When the CNV pressure reached the specified CNV break initiation pressure, the pressurizer spray supply line break valve was opened, initiating the transient.

Within the NIST-1 facility, the ECCS actuation occurs when the compensated level in the RPV downcomer reaches a pre-specified value. Once this occurs, open signals are sent to the RRVs and the RVVs. The opening of the ECCS valves causes a large amount of mass and energy transfer to occur between the RPV and the CNV over a short period of time. Containment vessel pressurization and heat-up occurs rapidly, followed by a long depressurization and cooldown profile. Test data was recorded for an extended period of time, well into the long-term cooling phase.

7.5.7.4 Special Analysis Techniques

The pressurizer spray supply line orifice has a length of approximately {{ }}$^{2(a),(b),(c),ECI}$. Thus, the orifice has an L/D ratio roughly equal to {{ }}$^{2(a),(b),(c),ECI}$. Analysis indicates that a NRELAP5 discharge coefficient near {{ }}$^{2(a),(b),(c),ECI}$ produces the best overall agreement with the break flow test data.

The {{ }}$^{2(a),(c)}$

7.5.7.5 Assessment Results

Figure 7-109 shows the comparison of core power in the HP-07 test to the scaled NPM total power after reactor trip (i.e., fission product decay, actinide decay, and fission power). The HP-07 power is approximately representative {{ }}$^{2(a),(b),(c),ECI}$ of the NPM power.

© Copyright 2016 by NuScale Power, LLC

{{

}}2(a),(b),(c),ECI

Figure 7-109. Comparison of core power in HP-07 with the NuScale Power Module power (fission and decay) after reactor trip (scaled)

The break flowrate predicted by NRELAP5 (Figure 7-110) provided results with excellent agreement to data with the use of the {{ }}2(a),(c) choking model and a discharge coefficient of {{ }}2(a),(b),(c)ECI

© Copyright 2016 by NuScale Power, LLC

{{

}}2(a),(b),(c),ECI

Figure 7-110. NIST-1 HP-07 pressurizer spray supply line break discharge mass flow rate

{{

}}2(a),(b),(c),ECI

© Copyright 2016 by NuScale Power, LLC

{{

}}2(a),(b),(c),ECI

Figure 7-111. NIST-1 HP-07 primary mass flow rate

© Copyright 2016 by NuScale Power, LLC

{{

}}2(a),(b),(c),ECI

Figure 7-112. NIST-1 HP-07 reactor pressure vessel level response comparison with data

© Copyright 2016 by NuScale Power, LLC

{{

}}2(a),(b),(c),ECI

Figure 7-113. NIST-1 HP-07 containment vessel level response

© Copyright 2016 by NuScale Power, LLC

{{

}}2(a),(b),(c),ECI

Figure 7-114. NIST-1 HP-07 containment vessel pressure comparison

© Copyright 2016 by NuScale Power, LLC

{{

}}2(a),(b),(c),ECI

Figure 7-115. NIST-1 HP-07 primary pressure comparison

7.5.8 Spurious Reactor Vent Valve Opening Test

The HP-09 test was used to assess the capability of NRELAP5 to predict the integral response of the NIST-1 facility to inadvertent depressurization of the RPV initiated by RVV spurious opening without DHRS. Furthermore, this test also provided bounding depressurization rate for a LOCA initiated by break from pressurizer gas space.

7.5.8.1 Facility Description

The entirety of the NIST-1 facility except for the DHRS was used for this IET.

- The SG was active to remove heat from the primary side and drive natural circulation in conjunction with the electrically heated core during the steady state.
- {{

  }}2(a),(b),(c)
- {{

  }}2(a),(b),(c)

© Copyright 2016 by NuScale Power, LLC

- The CPV was filled to accept rejected heat from the HTP.

7.5.8.2 Phenomenon Addressed

The phenomena addressed in the NIST-1 HP-09 test are same as in the HP-06 and HP-07 IETs (see Section 7.5.6.2).

7.5.8.3 Experimental Procedure

The experimental procedure is consistent with the LOCA test procedure discussed in Section 7.5.1.6.

7.5.8.4 Special Analysis Techniques

The {{ }}$^{2(a),(c)}$ at the valve orifice. Furthermore, the modified PV term was activated at the valve orifice. The Bankoff CCFL model was applied at pressurizer baffle plate.

Analysis indicates that a NRELAP5 discharge coefficient near {{ }}$^{2(a),(b),(c),ECI}$ produces the best overall agreement with the valve flow test data.

7.5.8.5 Assessment Results

Figure 7-116 shows the comparison of core power in the HP-09 test to the scaled NPM total power after reactor trip (i.e., fission product decay, actinide decay, and fission power). The HP-09 core power is {{ }}$^{2(a),(b),(c),ECI}$ of the power in NPM.

© Copyright 2016 by NuScale Power, LLC

{{

}}2(a),(b),(c),ECI

Figure 7-116. Comparison of HP-09 core power with the scaled NuScale Power Module fission and decay power

Figure 7-117 through Figure 7-124 compare NIST-1 HP09 test data with the NRELAP5 transient response. The calculated RVV mass flow rate is shown in Figure 7-117 with a peak flowrate of approximately {{ }}2(a),(b),(c),ECI lbm/s. The mass flow rate is over-predicted during the first {{ }}2(a),(b),(c),ECI seconds of the transient. Thereafter, the calculated flow shows excellent agreement with the measured flow rate.

© Copyright 2016 by NuScale Power, LLC

{{

}}2(a),(b),(c),ECI

Figure 7-117. NIST-1 HP-09 valve mass flow rate

The calculated pressurizer pressure is compared to data in Figure 7-118. The calculated pressure shows excellent agreement with the data, including the time of ECCS initiation. An examination of the first {{ }}2(a),(b),(c),ECI seconds of the RPV pressure (Figure 7-119) shows that the NRELAP5 predicted pressure is higher than the measured pressure.

Figure 7-120 compares the NRELAP5-predicted and NIST-1-measured CNV pressure response. Figure 7-121 shows the short-term response. The peak pressure from data and model are {{ }}2(a),(b),(c),ECI psia and {{ }}2(a),(b),(c),ECI psia, respectively. The comparison shows reasonable-to-excellent agreement with the measured data. As with the RPV pressure response, after about {{ }}2(a),(b),(c),ECI seconds, the CNV pressure is under-predicted. The trends of the data are well represented in the calculation.

© Copyright 2016 by NuScale Power, LLC

{{

}}2(a),(b),(c),ECI

Figure 7-118. NIST-1 HP-09 pressurizer pressure comparison

{{

}}2(a),(b),(c),ECI

Figure 7-119. NIST-1 HP-09 pressurizer pressure comparison

© Copyright 2016 by NuScale Power, LLC

{{

}}2(a),(b),(c),ECI

Figure 7-120. NIST-1 HP-09 containment vessel pressure comparison

© Copyright 2016 by NuScale Power, LLC

{{

}}2(a),(b),(c),ECI

Figure 7-121. NIST-1 HP-09 containment vessel pressure comparison

The pressurizer and RPV levels are compared in Figure 7-122 and Figure 7-123, respectively. The comparisons show reasonable-to-excellent agreement. Note that the code-to-data comparison presented in Figure 7-122 shows that NIST-1 pressurizer draining fully occurs between {{ }}2(a),(b),(c),ECI seconds, i.e., when the data (LDP-1401_calc) reaches a value of approximately {{ }}2(a),(b),(c),ECI inches, the low range of the measurement. When the data is extrapolated out past {{ }}2(a),(b),(c),ECI, it appears full draining of the pressurizer occurs at about {{ }}2(a),(b),(c),ECI seconds. NRELAP5 predicts pressurizer draining to fully occur at about {{ }}2(a),(b),(c),ECI seconds.

NRELAP5 predicts {{ }}2(a),(b),(c),ECI As shown in Figure 7-123 the RPV level prediction is in reasonable-to-excellent agreement with the test data.

A closer look at the RPV level comparison over the first {{ }}2(a),(b),(c),ECI seconds (Figure 7-124) shows excellent agreement.

© Copyright 2016 by NuScale Power, LLC

{{

}}2(a),(b),(c),ECI

Figure 7-122. NIST-1 HP-09 pressurizer level comparison

{{

}}2(a),(b),(c),ECI

Figure 7-123. NIST-1 HP-09 reactor pressure vessel level comparison

© Copyright 2016 by NuScale Power, LLC

{{

}}2(a),(b),(c),ECI

Figure 7-124. NIST-1 HP-09 reactor pressure vessel level comparison

© Copyright 2016 by NuScale Power, LLC

8.0 Assessment of Evaluation Model Adequacy

The adequacy of the NRELAP5 code (Reference 9) for analysis of design-basis LOCAs in the NPM is demonstrated by closure model and correlation reviews, and assessments against relevant experimental data. Establishing the adequacy of the NRELAP5 code as a component of the NuScale LOCA methodology is an essential part of the EMDAP (RG 1.203).

8.1 Adequacy Demonstration Overview

The adequacy demonstration process used here is similar to that used for the AP-600 (Reference 74). As the NuScale PIRT is a primary input to the adequacy evaluation, the findings of the PIRT summarized in Section 4 are used to guide the adequacy of the evaluation process. The adequacy of the NuScale LOCA EM is demonstrated through the following steps:

1. Section 8.2 documents the bottom-up assessment of the NRELAP5 models and correlations to determine their adequacy to predict the high (H) ranked phenomena. The code models used to represent each high (H) ranked phenomena are identified, with emphasis on the phenomena with low-knowledge level. These assessments address the fidelity of the models and correlations to the appropriate fundamental or SET data. Fidelity of the assessments is evaluated using the criteria of excellent, reasonable, minimal and insufficient from RG 1.203. These criteria are defined in Table 1-2. The comparisons to data can identify modeling deficiencies which could impose limitations on the application of the NRELAP5 based LOCA EM.
2. Section 8.3 covers the top-down assessment of the EM including a review of EM governing equations and numerics to determine their applicability to NPM LOCA analysis, and evaluation of the integral code performance based on the assessments of the EM against relevant IETs.
3. Section 8.4 summarizes the adequacy findings. The report shows how each PIRT high (H) ranked phenomenon is covered by the LOCA methodology models and correlations. Models which are marginally adequate, or ranges where PIRT phenomena are not covered, are identified. The manner of addressing code limitations is described.

8.2 Evaluation of Models and Correlations (Bottom-Up Assessment)

The adequacy of the models and correlations in NRELAP5 for modeling the high (H) ranked phenomena is examined by considering their pedigree, applicability, and fidelity to appropriate fundamental or SET data (established by assessment of the EM against legacy and NuScale-specific SET data), and scalability to the NuScale LOCA scenario.

The following steps are used to perform the evaluations.

© Copyright 2016 by NuScale Power, LLC

{{

}}2(a),(c)

© Copyright 2016 by NuScale Power, LLC

1. {{

}}2(a),(c)

The result of these assessments for each model or correlation is used to identify whether there are any shortcomings in the parametric space and provide information needed for the development effort where additional models, assumptions, or conservatisms may be required.

The first three steps described above are addressed in Section 8.2.1. Step 4 is discussed in Sections 8.2.2 through 8.2.22.

8.2.1 Important Models and Correlations

Table 8-1 identifies the dominant code models and correlations for the PIRT, defined as high-ranked phenomena in Section 4. Key parameters that are influenced by the dominant models and correlations are listed, along with phenomenological and separate effects cases that are used to assess the model or correlation capabilities. This information is used to establish adequacy of the dominant code models or correlations for NPM LOCA applications.

© Copyright 2016 by NuScale Power, LLC

Table 8-1. Dominant NRELAP5 models and correlations

{{

}}2(a),(c)

© Copyright 2016 by NuScale Power, LLC

{{

}}2(a),(c)

Table 8-2 is a summary of the estimated range of key parameters over which each dominant model or correlation should be applicable for the NPM steady-state and design basis LOCA. Parameter ranges obtained are intended to identify the minimum range that needs to be covered; the applicability of models and correlations are not restricted to these

© Copyright 2016 by NuScale Power, LLC

ranges. Several sources are used to obtain the values of the ranges. This includes design values, proposed technical specification limits, and limiting initial and boundary conditions. The ranges for some parameters are obtained from NRELAP5 LOCA break spectrum calculations described in Section 9.0. An explanation of how each limiting range was determined is provided in the Comments column of Table 8-2.

© Copyright 2016 by NuScale Power, LLC

Table 8-2. NuScale Power Module range of process parameters

{{

}}2(a),(c),ECI

© Copyright 2016 by NuScale Power, LLC

{{

}}2(a),(c),ECI

Table 8-3 lists the range of geometric parameters that could influence high-ranked phenomena for the NPM LOCA. Values given for each parameter are intended to identify the minimum range geometric parameters that need to be covered by the LOCA EM; applicability of the NuScale LOCA EM is not restricted to these values. These values have been obtained from a compilation of geometric information and plant parameters determined from design drawings.

© Copyright 2016 by NuScale Power, LLC

Table 8-3. Range of NuScale Power Module geometric parameters

{{

}}2(a),(c),ECI

© Copyright 2016 by NuScale Power, LLC

{{

}}2(a),(c),ECI

© Copyright 2016 by NuScale Power, LLC

Each of the NRELAP5 dominant models or correlations listed in Table 8-1 has been evaluated with respect to the extent that the model or correlation, as assessed for the NPM LOCA application, covers all or a portion of the NPM range given in Table 8-2. Where the range provided in the model or correlation development does not cover the full range of the NPM LOCA application, the range is extended by extrapolation of assessments against experimental data, or justification is provided based on legacy RELAP5-3D© assessments and applications. The range covered by models and correlations is discussed for the key parameters that define the response for high-ranked phenomena.

8.2.1.1 Applicability Evaluation

To determine adequacy of the models and correlations to simulate the high-ranked phenomena, the results of assessments against phenomenological and SETs are discussed. The assessment results are drawn from the NRELAP5 assessments discussed in Section 7.0 where descriptions of the test facilities, instrumentation, and test procedures are provided.

8.2.1.2 Overview

A graded approach is used to address the items described in Section 8.2, Step 4. More emphasis is given to high-ranked phenomena with a low-knowledge level. Less emphasis is placed on phenomena that are well understood with a high-knowledge level. This includes industry standard and handbook models.

Each of the following four areas is evaluated to the extent that they are relevant for each high-ranked phenomenon.

{{

}}2(a),(c)

© Copyright 2016 by NuScale Power, LLC

8.2.1.2.1 High-Ranked, Low-Knowledge Level Phenomena

The PIRT identified some phenomena within specified components as high-importance phenomena that have a low-knowledge level. These high-importance and low-knowledge phenomena are given the greatest focus in the development of the LOCA EM. They include:

{{

}}2(a),(c)

8.2.2 {{ }}2(a),(c)

8.2.2.1 Background

{{

}}2(a),(c)

© Copyright 2016 by NuScale Power, LLC

{{

}}2(a),(c)

© Copyright 2016 by NuScale Power, LLC

{{

}}2(a),(c)

8.2.2.2 Technical Evaluation

{{

}}2(a),(c)

© Copyright 2016 by NuScale Power, LLC

Table 8-4. Marviken range of parameters compared to the NuScale Power Module

{{

}}2(a),(c),ECI

{{

}}2(a),(c)

© Copyright 2016 by NuScale Power, LLC

{{

}}2(a),(c)

© Copyright 2016 by NuScale Power, LLC

{{

}}2(a),(c)

8.2.3 {{ }}2(a),(c)

8.2.3.1 Background

{{

}}2(a),(c)

© Copyright 2016 by NuScale Power, LLC

{{

}}2(a),(c)

8.2.3.2 Technical Evaluation

{{

}}2(a),(c)

© Copyright 2016 by NuScale Power, LLC

Table 8-5. Ferrell-McGee range of parameters compared to the NuScale Power Module

{{

}}2(a),(c),ECI

{{

}}2(a),(c)

© Copyright 2016 by NuScale Power, LLC

8.2.4 {{ }}2(a),(c)

8.2.4.1 Background

{{

}}2(a),(c)

8.2.4.2 Technical Evaluation

{{

}}2(a),(c)

© Copyright 2016 by NuScale Power, LLC

{{

}}2(a),(c)

© Copyright 2016 by NuScale Power, LLC

Table 8-6. Dimensions of NuScale Power Module, NIST-1 and Bankoff pressurizer plate

{{

}}2(a),(c),ECI

{{

}}2(a),(c)

© Copyright 2016 by NuScale Power, LLC

{{

}}2(a),(c)

8.2.5 {{ }}2(a),(c)

8.2.5.1 Background

{{

}}2(a),(c)

© Copyright 2016 by NuScale Power, LLC

{{

}}2(a),(c)

8.2.5.2 Technical Evaluation

{{

}}2(a),(c)

8.2.6 {{ }}2(a),(c)

8.2.6.1 Background

{{

}}2(a),(c)

© Copyright 2016 by NuScale Power, LLC

{{

}}2(a),(c)

© Copyright 2016 by NuScale Power, LLC

{{

}}2(a),(c)

8.2.6.2 Technical Evaluation

{{

}}2(a),(c)

© Copyright 2016 by NuScale Power, LLC

{{

}}2(a),(c)

Table 8-7. Range of riser interphase friction - separate effects tests and NuScale Power Module

{{

}}2(a),(c),ECI

© Copyright 2016 by NuScale Power, LLC

{{

}}2(a),(c),ECI

{{

}}2(a),(c)

© Copyright 2016 by NuScale Power, LLC

8.2.7 {{ }}2(a),(c)

8.2.7.1 Background

{{

}}2(a),(c)

8.2.7.2 Technical Evaluation

{{

}}2(a),(c)

© Copyright 2016 by NuScale Power, LLC

{{

}}2(a),(c)

8.2.8 {{ }}2(a),(c)

8.2.8.1 Background

{{

}}2(a),(c)

8.2.8.2 Technical Evaluation

{{

}}2(a),(c)

© Copyright 2016 by NuScale Power, LLC

{{

}}2(a),(c)

© Copyright 2016 by NuScale Power, LLC

{{

}}2(a),(c)

© Copyright 2016 by NuScale Power, LLC

{{

}}2(a),(c)

8.2.9 {{ }}2(a),(c)

8.2.9.1 Background

{{

}}2(a),(c)

8.2.9.2 Technical Evaluation

{{

}}2(a),(c)

© Copyright 2016 by NuScale Power, LLC

{{

}}2(a),(c)

8.2.10 Flashing

8.2.10.1 Background

Flashing is the fundamental thermodynamic process of vaporization that occurs when a saturated liquid undergoes a reduction in pressure below its boiling point, resulting in a phase change from liquid to vapor. In the pressurizer, the liquid inventory that is normally at saturated conditions will flash as the RCS depressurizes in response to a LOCA and the actuation of the ECCS. As the RPV continues to depressurize, flashing will also occur in the hot leg riser, core, LP, and downcomer. Flashing will cause level swell which can affect the quality at the break and at the ECCS valves.

The interphase heat and mass transfer models in NRELAP5 are the dominant models that determine the flashing rate. The vapor generation (or condensation) consists of two parts, vapor generation which results from energy exchange in the bulk fluid (flashing) and energy exchange in the thermal boundary layer near the wall (boiling). Flashing is addressed in this section and boiling in Section 8.2.19.

Each of the vapor generation processes involves interfacial heat transfer effects. The interfacial heat transfer area and heat transfer coefficient models used in NRELAP5 are summarized in Table 2.5-1 of Reference 9. The models that govern the flashing phenomenon are those for the superheated liquid fluid state. For bubbly flow bulk interfacial heat transfer between the vapor and liquid phases is handled using the maximum of a correlation derived from the Plesset-Zwick (Reference 90) equation for the growth rate of a bubble and the modified Lee-Ryley (Reference 91) correlation. For droplets in flow regimes such as annular mist and dispersed, NRELAP5 uses a heat transfer coefficient $k_f/D\ f(\Delta T_{sf})$ where k_f is the liquid thermal conductivity, D is hydraulic diameter, and ΔT_{sf} is the difference between the saturation and the liquid temperatures; $f(\Delta T_{sf})$ is a flow-type dependent function. A {{

}}2(a),(c) heat transfer coefficient is used for films. In all cases, a large heat transfer coefficient is calculated so that the difference between the superheated liquid temperature and the saturation temperature at any time is small. Hence for the NPM, while the pressure is decreasing, the liquid temperature remains very close to the saturation temperature due to the relatively slow depressurization resulting from the small break sizes. The time constant for the vapor generation process is much smaller than the time constant for the

© Copyright 2016 by NuScale Power, LLC

depressurization. A non-equilibrium superheated liquid state can exist for a time period on the order of milliseconds while the depressurization process is taking place over a period of minutes. Hence, high accuracy in the vapor generation rate due to flashing is not required because any model with a small time constant will generate the amount of vapor necessary to keep the phases in thermal equilibrium.

Implementation of these correlations is described in Reference 9 (Section 2.5.1.1). The pedigree of the model is established by application and validation of RELAP5-3D©. In Table 2.2-2 of Reference 87, it is noted that the flashing model is validated against the Edward pipe and Marviken CFT-22 and CFT-24 tests. Validation of NRELAP5 for the suite of assessment cases confirms that this pedigree is maintained in the NRELAP5 code.

8.2.10.2 Technical Evaluation

Important parameters associated with flashing phenomenon are pressure, void fraction/interfacial area, and phasic temperatures that interact to determine the vapor generation rate. The flashing model in NRELAP5 covers the entire range of the water properties tables, which encompasses the NPM LOCA application.

The GE level swell (1-ft and 4-ft) tests are the primary assessment cases used to validate the applicability of NRELAP5 to predict the flashing phenomenon. In Section 8.2.6, it is shown that the NRELAP5 predictions of the GE level swell assessments show reasonable-to-excellent agreement with the test data, thus demonstrating that NRELAP5 is applicable for predicting flashing phenomenon that occurs in NPM LOCA events. Furthermore, flashing is an inherent phenomenon in the NIST-1 LOCA IETs. Therefore, NRELAP5 analysis against the NIST-1 IET data provides additional assessment of the flashing model.

Because the heat transfer coefficient resulting from the Plesset-Zwick correlation depends only on fluid properties and all of the heat transfer coefficients are very large, there are no scaling restrictions for the vapor generation model in NRELAP5 which could impose limitations on the application of the NRELAP5 model to the configuration and conditions of the NPM hot leg riser in the LOCA transient domain.

8.2.11 {{ }}2(a),(c)

8.2.11.1 Background

{{

}}2(a),(c)

© Copyright 2016 by NuScale Power, LLC

{{

}}2(a),(c)

8.2.11.2 Technical Evaluation

{{

}}2(a),(c)

© Copyright 2016 by NuScale Power, LLC

{{

}}2(a),(c)

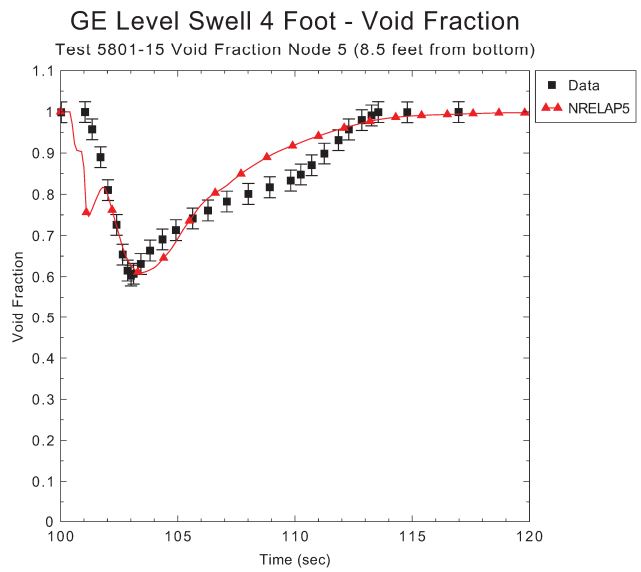

Figure 8-1. Transient void fraction in node 5 for the GE 4-ft level swell test

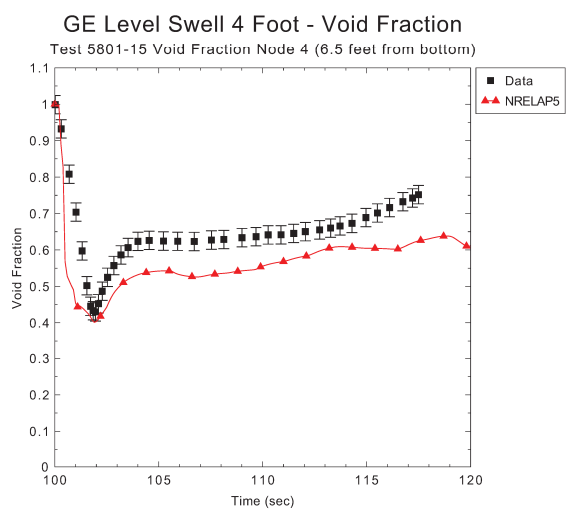

Figure 8-2. Transient void fraction in node 4 for the GE 4-ft level swell test

© Copyright 2016 by NuScale Power, LLC

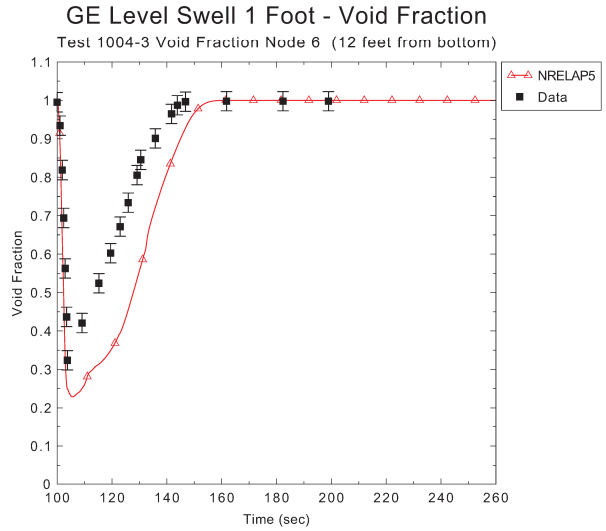

Figure 8-3. Transient void fraction in node 6 for the GE 1-ft level swell test

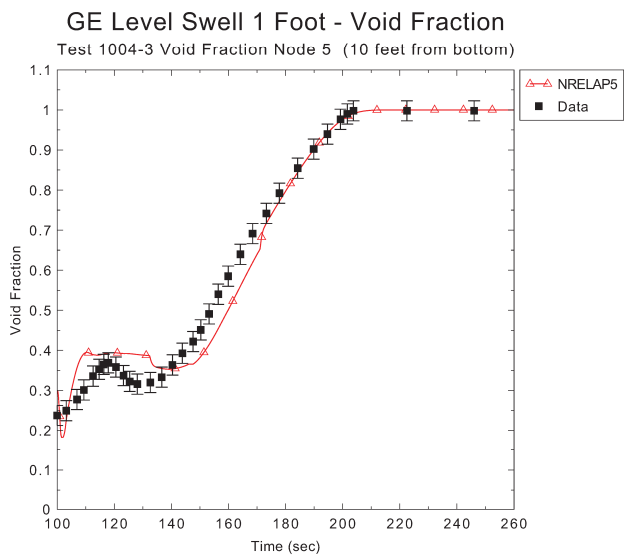

Figure 8-4. Transient void fraction in node 5 for the GE 1-ft level swell test

{{

}}2(a),(c)

© Copyright 2016 by NuScale Power, LLC

{{

}}2(a),(c)

8.2.12 {{ }}2(a),(c)

8.2.12.1 Background

{{

}}2(a),(c)

8.2.12.2 Technical Evaluation

{{

}}2(a),(c)

© Copyright 2016 by NuScale Power, LLC

{{

}}2(a),(c)

8.2.13 {{ }}2(a),(c)

8.2.13.1 Background

{{

}}2(a),(c)

© Copyright 2016 by NuScale Power, LLC

{{

}}2(a),(c)

8.2.13.2 Technical Evaluation

{{

}}2(a),(c)

8.2.14 {{ }}2(a),(c)

8.2.14.1 Background

{{

}}2(a),(c)

© Copyright 2016 by NuScale Power, LLC

{{

}}2(a),(c)

8.2.14.2 Technical Evaluation

{{

}}2(a),(c) {{

}}2(a),(c),ECI {{

}}2(a),(c) {{

}}2(a),(c),ECI {{

}}2(a),(c)

© Copyright 2016 by NuScale Power, LLC

{{

}}2(a),(c)

© Copyright 2016 by NuScale Power, LLC

{{

}}2(a),(c),ECI

Figure 8-5. Hot leg riser flow for NIST-1 chemical and volume control system discharge line break integral effects test HP-06

{{

}}2(a),(c),ECI

Figure 8-6. Hot leg riser flow for NIST-1 pressurizer spray supply line break integral effects test HP-07

© Copyright 2016 by NuScale Power, LLC

8.2.15 {{ }}2(a),(c)

8.2.15.1 Background

{{

}}2(a),(c)

8.2.15.2 Technical Evaluation

{{

}}2(a),(c)

8.2.16 {{ }}2(a),(c)

8.2.16.1 Background

{{

}}2(a),(c)

© Copyright 2016 by NuScale Power, LLC

8.2.16.2 Technical Evaluation

{{

}}2(a),(c)

8.2.17 {{ }}2(a),(c)

8.2.17.1 Background

{{

}}2(a),(c)

© Copyright 2016 by NuScale Power, LLC

{{

}}2(a),(c)

8.2.17.2 Technical Evaluation

Table 8-1 lists the flow, void fraction, pressure, heat rate, and core geometry as key parameters for the NRELAP5 interfacial drag model, the dominant NRELAP5 model that affects phase slip and flow regimes. Table 8-2 identifies the range of parameters encountered by NPM steady-state and design basis accidents and transients. This is the source of the ranges used for the NPM {{

}}2(a),(c) SETs used to validate the NRELAP5 interphase drag model for the core geometry are FRIGG tests 613130, 613010, 613118 and 613123, and FLECHT-SEASET boil off tests 35557, 35658 and 35759

The FRIGG tests are steady-state runs with set inlet and boundary conditions to a 36-rod electrically-heated bundle. The void fraction profile along the heated channel was measured and compared to NRELAP5 predictions (see Section 7.2.5).

The FLECHT-SEASET tests (see Section 7.2.6) are boil off transient tests in which a 161-rod bundle was initially filled with saturated water and then boiled to the point at which heater rod temperature reached 2,000 degrees F (1,093 degrees C), and the test was terminated by cutting the rod power and flooding the bundle.

Table 8-8 shows the ranges of the key variables for the NRELAP5 {{

}}2(a),(c)

Table 8-8. Ranges of key parameters for core interphase friction - separate effects tests and plant

{{

}}2(a),(c),ECI

© Copyright 2016 by NuScale Power, LLC

{{

}}2(a),(c),ECI

{{

}}2(a),(c)

© Copyright 2016 by NuScale Power, LLC

{{

}}2(a),(c)

8.2.18 {{ }}2(a),(c)

8.2.18.1 Background

{{

}}2(a),(c)

8.2.18.2 Technical Evaluation

{{

}}2(a),(c)

© Copyright 2016 by NuScale Power, LLC

Table 8-9. Range of key parameters for core flow – separate effects tests and plant

{{

}}2(a),(c),ECI

{{

}}2(a),(c)

© Copyright 2016 by NuScale Power, LLC

{{

}}2(a),(c)

8.2.19 {{ }}2(a),(c)

8.2.19.1 Background

{{

}}2(a),(c)

© Copyright 2016 by NuScale Power, LLC

{{

}}2(a),(c)

8.2.19.2 Technical Evaluation

{{

}}2(a),(c)

Table 8-10. Range of key parameters for core boiling - separate effects tests and plant

{{

}}2(a),(c)

© Copyright 2016 by NuScale Power, LLC

{{

}}2(a),(c)

{{

}}2(a),(c)

© Copyright 2016 by NuScale Power, LLC

8.2.20 {{ }}2(a),(c)

8.2.20.1 Background

{{

}}2(a),(c).

8.2.20.2 Technical Evaluation

{{

}}2(a),(c)

© Copyright 2016 by NuScale Power, LLC

{{

}}2(a),(c)

8.2.21 {{ }}2(a),(c)

8.2.21.1 Background

{{

}}2(a),(c)

© Copyright 2016 by NuScale Power, LLC

{{

}}2(a),(c)

8.2.21.2 Technical Evaluation

{{

}}2(a),(c)

© Copyright 2016 by NuScale Power, LLC

Table 8-11. Range of key parameters for subcooling boiling and separate effects tests and plant

{{

}}2(a),(c)

{{

}}2(a),(c)

8.2.22 {{ }}2(a),(c)

8.2.22.1 Background

{{

}}2(a),(c)

© Copyright 2016 by NuScale Power, LLC

{{

}}2(a),(c)

8.2.22.2 Technical Evaluation

{{

}}2(a),(c)

8.3 Evaluation of Integral Performance (Top-Down Assessment)

There are three primary areas addressed by the top-down assessment.

- {{

}}2(a),(c)

To ensure maximum fidelity of the assessments, the NRELAP5 NIST-1 and NPM input models were developed using consistent nodalization and option selection. Code assessments are also performed against SETs to establish code capabilities for predicting local behavior within unique NPM components. Assessments against SETs are addressed in Section 8.2.1.

© Copyright 2016 by NuScale Power, LLC

8.3.1 Review of Code Governing Equations and Numerics

The NRELAP5 Theory Manual (Reference 9) describes the NRELAP5 code architecture, field equations, and solution techniques, which are essentially unchanged compared to the RELAP5-3D© code. The descriptions of code modifications/features made to address unique aspects of the NuScale application are included in the NRELAP5 Theory Manual and summarized in Section 6.0. This review is based primarily on the information in Reference 9.

The field equations solved by NRELAP5 are discussed in Section 2.1 of Reference 9 and summarized in Section 6.2. Applicability of the field equations to represent the processes and phenomena that can occur in the NPM is evaluated, along with an assessment of the ability of the NRELAP5 numerical solution to approximate the set of governing field equations. This evaluation addresses the mathematical models implemented in NRELAP5 for the NuScale LOCA analysis, and considers the applicability of the assumptions and processes involved in developing the NRELAP5 system of governing equations, and closure relations.

The numeric solution evaluation considers convergence, conservation of physical properties, and stability of code calculations performed to solve the set of governing equations for an NRELAP5 NPM model. The objective of this evaluation is to summarize information regarding the domain of applicability of the numerical techniques and user options that may impact the accuracy, stability, and convergence of NRELAP5 calculations. User guidelines for model development and execution were developed based on “lessons learned” during the code reviews and assessments. The guidelines include requirements for assuring convergence of solutions, accounting for uncertainty in results and monitoring code function to ensure that the basic conservation equations are being solved correctly.

8.3.1.1 Conservation of Mass, Momentum and Energy

NRELAP5 LOCA applications do not use the three-dimensional modeling capability of RELAP5-3D©. The one-dimensional equations and numerics have been used in versions of the RELAP5 codes for many years so their pedigree has been well established by code assessments and applications. The semi-implicit solution technique used by NuScale has been in the RELAP5 codes as the primary solution technique for the governing conservation equations since the initial development of the code. The solution technique continues to be used in NRELAP5 as discussed in Section 2.1.3 of the NRELAP5 code manual (Reference 9).

The basic governing equations for mass, momentum, and energy conservation use area-averaging for vapor and liquid fields. Mass, momentum, and energy conservation equations are written for each field, resulting in what is referred to as a six-equation model. The governing equations are discussed in Sections 6.2.1 through 6.2.4. The basic governing equations in NRELAP5 are generally accepted as reasonable representations of the applicable physical laws that govern the steady-state and transient behavior of thermal-hydraulic systems.

© Copyright 2016 by NuScale Power, LLC

Energy transfer into and out of the phases from the boundaries is governed by correlations discussed in Sections 6.2.5. Heat conduction within structures is modeled by the one-dimensional heat conduction equation discussed in Section 6.3.

Models are also included for trips and control systems as discussed in Section 6.5. This feature is used to model the safety-related system actuations, control power, set boundary conditions, determine ranges (minimum and maximum values) of selected variables including the FOMs, and other functions within the NRELAP5 models.

NuScale performed acceptance testing and procurement requirements as part of the commercial grade dedication of RELAP5-3D© to serve as the development platform for NRELAP5. The testing and inspection verified that RELAP5-3D© has the necessary critical characteristics to be used as the code development platform for NRELAP5. The critical characteristics include the suitability of the basic governing equations described above for the NuScale application.

8.3.1.2 Numerical Solution Techniques

The entire fluid domain of interest is divided into control volumes connected via junctions where the flow velocities are defined. The heat transfer into or out of control volumes are defined through heat structures where the heat conduction equation is solved considering the relevant heat transfer regime in the communicated control volume.

The difference equations implement mass and energy conservation by equating accumulation to the rate of mass or energy in through the cell boundaries, minus the rate of mass or energy out through the cell boundaries, plus source and sink terms. This approach necessitates defining mass and energy volume average properties and requiring knowledge of velocities at the volume boundaries. The velocities at the cell edges are defined through the use of momentum control volumes centered on the mass and energy cell boundaries. This approach results in a numerical scheme having a staggered spatial mesh with the momentum control volumes extending from the mass and energy cell centers to the neighboring mass and energy cell centers. The scalar properties of the flow (pressure, specific internal energies, and void fraction) are defined at mass and energy cell centers, while the vector quantities (velocities) are defined on the mass and energy cell boundaries.

The governing equations for the system model are solved numerically using a semi-implicit finite-difference technique. A nearly-implicit finite-difference technique which allows violation of the material Courant limit, is also available. However, the LOCA EM and the supporting assessment calculations use only the semi-implicit numerical scheme. The semi-implicit numerical solution scheme is based on replacing the system of differential equations with a system of finite difference equations partially implicit in time.

When generating a solution of finite difference equations, there is a possibility that the solution may not be converged. This could be the result of an ill-posed problem, inappropriate time step size selection, inadequate spatial nodalization, or an instability. Sensitivity studies have proven useful to ensure convergence and stability of the NRELAP5 solutions.

© Copyright 2016 by NuScale Power, LLC

Adherence to the modeling requirements of RELAP5 assist in ensuring that the governing equations are well posed. Requirements for nodalization and time step sensitivity studies comply with 10 CFR 50 Appendix K requirements and ensure converged solutions. Solutions are examined to identify unstable or unphysical behavior.

8.3.2 NuScale Facility Scaling

The NIST-1 facility is designed to simulate the integral system behavior of a single NPM immersed in a single bay within the reactor pool. The scaling analysis was performed to determine the geometric dimensions and operating conditions for the NIST-1 facility. The purpose of the scaling analysis was to design an IET facility that can be used to obtain quality data for thermal-hydraulic system safety analysis code validation. The hierarchical two-tiered scaling (H2TS) (Reference 99) method was used to perform the RCS natural circulation scaling and the scaling of LOCA and ECCS. The scaling analysis generated the sets of dimensionless groups that needed to be preserved to accurately simulate the high-ranked phenomena identified in the NuScale LOCA PIRT. The figures of merit were the peak CNV pressure and the collapsed liquid level above the top of the core. The scaling analysis also documented the scaling distortions between the NIST-1 facility and the NPM design, and evaluated the effects of these distortions.

Detailed documentation of the NIST-1 scaling analysis is available in the NIST-1 Facility Scaling Report. Section 8.3.2.1 summarizes the scaling objectives and methodology. The approaches for RCS scaling natural circulation scaling and the scaling of LOCA and ECCS are briefly presented in Sections 8.3.2.2 and 8.3.2.3, respectively.

8.3.2.1 Scaling Objectives and Methodology

The general objective of the scaling analysis was to obtain the physical dimensions and operating conditions of a reduced-scale test facility capable of simulating the important flow and heat transfer behavior of a NPM under the LOCA conditions. To develop a properly scaled test facility, the following specific objectives were met for each operational mode of interest.

- The thermal-hydraulic processes that should be modeled were identified.
- The similarity criteria that should be preserved between the test facility and the full-scale prototype were obtained.
- The priorities for preserving the similarity criteria were established.
- Specifications for the test facility design were established.
- Biases due to scaling distortions were quantified.
- The critical attributes of the test facility that must be preserved to meet testing requirements were identified.

Different similarity criteria were obtained for the different modes of system operation. These criteria depend on the geometry of the components, the scaling level required to

© Copyright 2016 by NuScale Power, LLC

address the transport phenomena of interest, and the initial and boundary conditions for each particular mode of operation.

To ensure that the scaling objectives were met in an organized and clearly traceable manner, a general design framework (GDF) was established. The model for this framework includes features drawn from the NRC severe accident scaling methodology presented in NUREG/CR-5809 (Reference 99). A flow diagram for the GDF is presented in Figure 8-7.

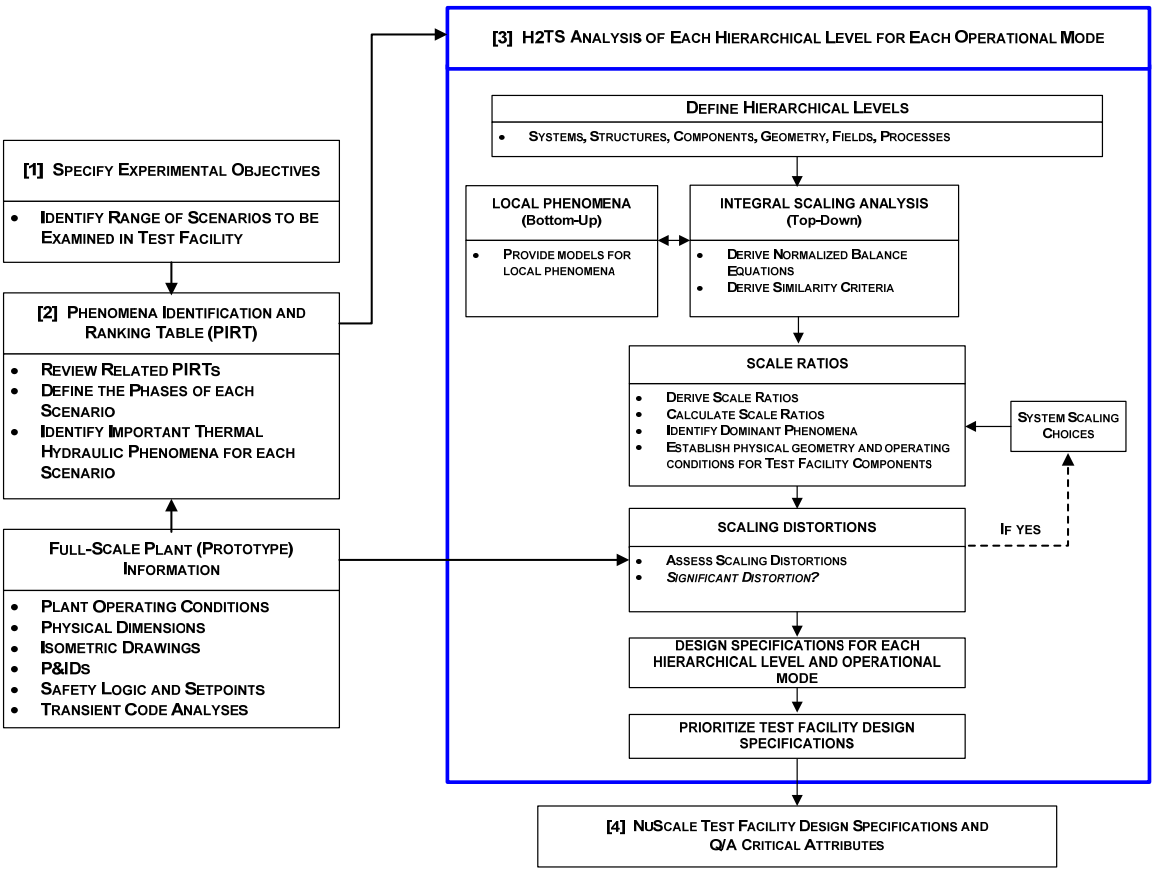

Figure 8-7. General design framework for the NuScale Integral System Test facility

Experimental Objectives

The first task outlined by the GDF was to specify the experimental objectives. The experimental objectives define the types of tests that will be performed to address specific design or certification needs. These objectives determined the general modes of operation that should be simulated in the test facility.

The objective of the NuScale LOCA test program was to obtain qualified data to benchmark the computer codes and models that will be used to evaluate the safety of the NPM. This includes: 1) measurements of transient and steady-state, single-phase natural

© Copyright 2016 by NuScale Power, LLC

circulation flow in the integrated RPV, and 2) characterization of the thermal-hydraulic phenomena in the RPV, containment, and CPV during the three periods of the LOCA.

Loss-of-Coolant Accident Phenomena Identification and Ranking Table

The second task outlined by the GDF was the development of a PIRT. The PIRT presented in Section 4 was used as the basis. The nature of scaling forbids exact similitude of all of the parameters of a reduced-scale test facility with those of a full-scale prototype. As a result, the design and operation of the test facility was based on simulating the thermal-hydraulic processes most important to the system operational modes that will be explored. The PIRT identified the different phases of a LOCA and most important thermal-hydraulic phenomena within those phases that should be simulated in the test facility. All of the highly ranked integral system phenomena identified in the NuScale LOCA PIRT are observed in the NIST facility to some degree. Although majority of the high-ranked PIRT phenomena are fully covered in NIST-1, the NIST facility is not the primary source of validation data for some phenomena. For example, the NIST facility does not model the details of the core fuel rods or core sub-channels; therefore, CHF data has been obtained in a separate full-scale test facility (see Section 7.3). Similarly, detailed information regarding the helical coil SG thermal-hydraulic performance is obtained from SIET TF-1 and TF-2 experiments (see Section 7.4).

Description of the H2TS Method

The third step in the GDF was to perform a scaling analysis for each of the hierarchical levels (e.g., systems and subsystems) and their modes of operation defined in the previous section. The H2TS method has been successfully used to develop the similarity criteria necessary to scale the APEX-600 and APEX-1000 systems for LOCA transients. The H2TS method was developed by the NRC and is fully described in Appendix D of NUREG/CR 5809 (Reference 99).

Figure 8-8 presents the four basic elements of the H2TS analysis method. The first element consists of subdividing the plant into a hierarchy of systems. Each system is subdivided into interacting subsystems which are further subdivided into interacting modules which are further subdivided into interacting constituents (materials) which are further subdivided into interacting phases (liquid, vapor or solid). Each phase can be characterized by one or more geometrical configurations and each geometrical configuration can be described by three field equations (mass, energy and momentum conservation equations). Each field equation can incorporate several processes. Figure 8-9 presents the breakdown of the NuScale system into hierarchical levels and high level processes to be scaled. It represents a roadmap used to structure the scaling analyses. The RCS and the ECCS were the focus of the scaling study.

© Copyright 2016 by NuScale Power, LLC

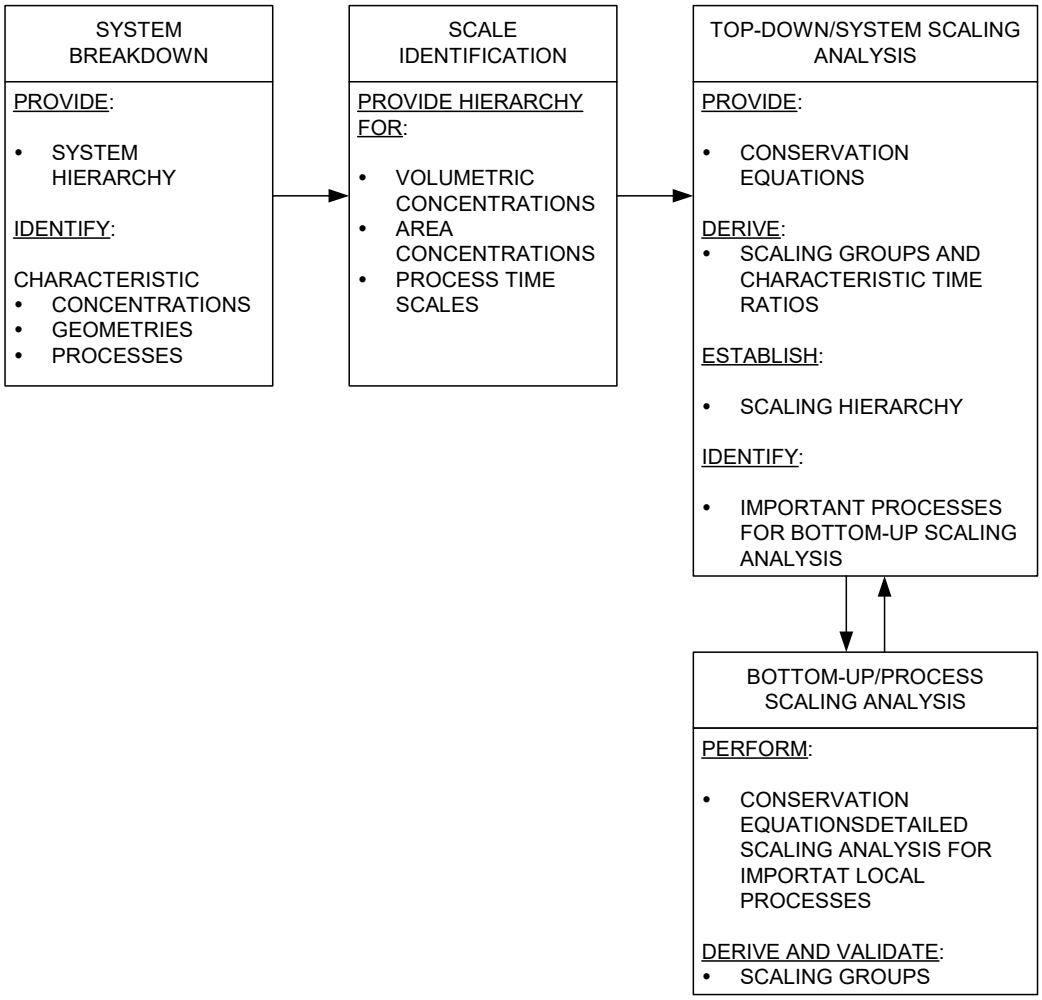

Figure 8-8. Flow diagram for the hierarchical, two-tiered scaling analysis (NUREG/CR-5809)

© Copyright 2016 by NuScale Power, LLC

{{

}}2(a),(c)

Figure 8-9. NuScale system breakdown into hierarchical levels and primary operational modes to be scaled

After identifying and subdividing the system of interest, the next step was to identify the scaling level at which the similarity criteria should be developed. This was determined by examining the phenomena being considered. For example, if the phenomenon being considered involves mass, momentum or energy transport between materials such as water and solid particles, then the scaling analysis would be performed at the constituent level. If the phenomenon of interest involves mass, momentum, or energy transport between vapor and liquid, then the scaling analysis would be performed at the phase level. Therefore, identifying the scaling level depends on the phenomenon being addressed.

© Copyright 2016 by NuScale Power, LLC

Thermal-hydraulic phenomena involving integral RCS interactions, such as primary system depressurization or loop natural circulation, would be examined at the “system” level. Thermal-hydraulic phenomena, such as SG heat transfer, would be examined at the “subsystem” level. Specific interactions between the steam-liquid mixture and the stainless steel structure would be examined at the “constituent” level.

The H2TS method required performing a “top-down” (system) scaling analysis. The top-down scaling analysis examines the synergistic effects on the system caused by complex interactions between the constituents deemed important by the PIRT. Its purpose is to use the conservation equations at a given scaling level to obtain characteristic time ratios and similarity criteria. It also identifies the important processes to be addressed in the bottom-up scaling analysis.

The H2TS method also required performing a “bottom-up” (process) scaling analysis. This analysis provides similarity criteria for specific processes such as flow pattern transitions and flow dependent heat transfer. The focus of the bottom-up scaling analysis is to develop similarity criteria to scale individual processes of importance to system behavior as identified by the PIRT.

Test Facility Specifications and Scaling Ratios

The fourth step of the GDF was to document all of the test facility design and operation specifications. All of the essential geometric features and operating parameters that must be carefully measured and documented to ensure accurate code simulations of the important thermal-hydraulic phenomena were identified and designated as critical attributes.

The NIST-1 facility was developed by modifying the existing MASLWR test facility at Oregon State University. This was accomplished by establishing a fixed set of scale factors for component lengths, flow areas, and volumes. These scale factors were obtained through an iterative process that included a practical assessment of component costs, ease of operation, material availability, and instrumentation accuracy for the scale selected. Having fixed the length, volume, and flow area scale factors for the test facility, and assuming fluid property similitude, the scaling ratios obtained using the governing equations for loop natural circulation were used to define the scale factors for the adjustable parameters. That is, the core power, component heat transfer areas, SG heat removal rate, and loop resistance were adjusted to preserve the requirement of isochronicity. Table 8-12 lists the required temporal and geometric scale factors for the NIST-1 facility under the requirement of isochronicity and fluid property similitude.

© Copyright 2016 by NuScale Power, LLC

Table 8-12. Scaling factors for NIST-1 facility

{{

}}2(a),(c)

The initial conditions in the NIST-1 facility have been scaled to simulate single-phase natural circulation flow in a single NPM operating at 50 percent of full power with all heat rejection through one SG. The test facility operates near prototypic pressures and temperatures and operates with the same working fluid: water. Therefore, fluid property similitude is invoked. This means that the fluid property ratios are near to unity in all of the scale ratios, thereby simplifying the analysis.

8.3.2.2 Reactor Coolant System Natural Circulation Scaling

Figure 8-10 provides a flow diagram that describes the scaling analysis process for the RCS natural circulation operational mode. First, a top-down scaling analysis was performed. This included an analysis at the system level (integrated loop behavior) for normal operating conditions. {{

}}2(a),(c) Further details are available in the NIST-1 facility scaling report.

© Copyright 2016 by NuScale Power, LLC

{{

}}2(a),(c)

Figure 8-10. Scaling analysis flow diagram for single-phase primary loop natural circulation

8.3.2.3 Loss-of-Coolant Accident and Emergency Core Cooling System Scaling

The scaling analysis approach for LOCA and actuation of the ECCS includes the following four related scaling analyses:

- RCS depressurization
- containment vessel pressurization
- long-term recirculation cooling
- Reactor Building pool heat-up

During ECCS operation, the RPV transports energy and mass to the containment. All of the mass and energy leaving the RPV is captured by the CNV. The CNV transports energy to the reactor pool.

The objectives of the LOCA/ECCS scaling analyses were to scale the

- RCS depressurization and containment pressurization behavior during the blowdown and venting phases of the LOCA.

© Copyright 2016 by NuScale Power, LLC

- RCS, containment cooling, and the reactor pool heat-up during the long-term recirculation cooling phase of the LOCA.

Reactor Coolant System Depressurization Scaling

Figure 8-11 shows top-down and bottom-up scaling analyses performed for RCS depressurization scaling. This included an analysis at the system level (integrated loop behavior) for RCS initial conditions at 50 percent power. {{

}}2(a),(c)

{{

}}2(a),(c)

Figure 8-11. Scaling analysis flow diagram for reactor coolant system depressurization

Containment Pressurization Scaling

Top-down and bottom-up scaling analyses performed for the scaling of containment pressurization are shown in Figure 8-12. {{

}}2(a),(c)

© Copyright 2016 by NuScale Power, LLC

{{

}}2(a),(c)

{{

}}2(a),(c)

Figure 8-12. Scaling analysis flow diagram for containment pressurization

Long-Term-Cooling Phase Scaling

Long-term recirculation occurs after the CNV and RPV pressures have become nearly equalized and the flow through the RRVs is from containment to RPV. As shown in Figure 8-13, top-down and bottom-up scaling analyses were performed for long-term phase scaling. {{

}}2(a),(c)

© Copyright 2016 by NuScale Power, LLC

{{

}}2(a),(c)

{{

}}2(a),(c)

Figure 8-13. Scaling analysis flow diagram for long-term recirculation cooling mode

Reactor Pool Heatup Scaling

Heat transferred from the CNV exterior surface creates a heated plume of fluid that rises to the top of the pool. The heated plume mixes with the liquid at the top of the pool to create a thermally stratified layer. The thermally stratified layer consists of two regions; a well-mixed layer with uniform temperature at the surface of the pool and a partially mixed thermocline that extends downward and serves as a transition layer to the colder liquid in the pool. The thermal stratification layer grows over time. During the heat up of the pool, heat and mass are lost from the pool to the air at the pool interface due to evaporation. Heat is also transferred to the Reactor Building pool steel liner and concrete structures.

Top-down and bottom-up scaling analyses performed for reactor pool heatup scaling are shown in Figure 8-14. {{ }}2(a),(c)

© Copyright 2016 by NuScale Power, LLC

{{

}}2(a),(c)

{{

}}2(a),(c)

Figure 8-14. Scaling analysis flow diagram for Reactor Building pool heat-up

© Copyright 2016 by NuScale Power, LLC

8.3.2.4 NuScale Facility Scaling Summary

The scaling analysis showed that the NIST-1 facility is well scaled for single-phase natural circulation during operating conditions.

The distortions during the RCS depressurization, CNV pressurization, long-term recirculation cooling, and Reactor Building pool heat-up periods of the LOCA were analyzed in the scaling analyses for CVCS discharge line break LOCA. The scaling analysis indicated that none of the distortions have an impact on peak CNV pressure and represent only a minor impact to the RPV collapsed liquid level above the top of the core. These distortions are further discussed as follows:

- {{

}}2(a),(c)

© Copyright 2016 by NuScale Power, LLC

- {{

}}2(a),(c)

In addition to the distortions identified in the scaling analysis the IET data may get affected by the differences in initial conditions, boundary conditions, and operating procedures, as well as distortions due to changes to the NPM design.

The differences in initial/boundary conditions include the differences in initial CPV temperature, decay heat, break configuration, etc. The differences in operating procedure include the differences in SG secondary-side operation, pressurizer heat operation, etc. {{

}}2(a),(c)

The scaling distortions as well as the differences identified above are evaluated to determine their impact in Section 8.3.4. It is shown that NRELAP5 is capable of accounting for these distortions/differences, thereby establishing the scalability of NRELAP5 to model the phenomena in NPM.

8.3.3 Assessment of NuScale Facility Integral Effects Test Data

The NIST-1 IET data that supports the validation of NRELAP5 for NPM LOCA analysis includes following tests.

- {{

}}2(a),(c)

© Copyright 2016 by NuScale Power, LLC

- {{

}}2(a),(c)

As shown in Sections 7.5.5 to 7.5.8, in general, NRELAP5 predicted the NIST-1 IET data with excellent agreement. This shows that NRELAP5 is capable of predicting the phenomena and process occurring in the NIST-1 facility including system interactions. Further, evaluations of these assessments for each high-ranked PIRT phenomenon are summarized in Table 8-14.

8.3.4 Evaluation of NuScale Facility Distortions and NRELAP5 Scalability

The NuScale NRELAP5 LOCA EM was updated to simulate NIST-1 IETs HP-05, HP-06, HP-07, and HP-09. {{

}}2(a),(c)

The results show that the differences and distortions between the NPM design and the NIST-1 facility can be accounted for using NRELAP5, and NRELAP5 is scalable to model phenomena and process in the NPM during LOCA events.

8.3.4.1 NuScale Facility Powered Natural Circulation Test (HP-05)

The NPM relies on natural circulation flow as the primary mechanism to remove energy produced in the core and to deposit that energy in the SG tubes. The core power provides the driving force, with resistance to the flow caused by form and friction losses along the primary coolant path. The NIST-1 test facility is a scaled model of the NPM that uses the same natural circulation mechanism to move energy from the core heater rods to the model SG tubes. Scaling factors for the NIST-1 facility are as shown in Table 8-12.

Test NIST-1 HP-05 was conducted to characterize the natural circulation flow rate and pressure drop in the NIST-1 test facility at various core power levels. As shown in Section

© Copyright 2016 by NuScale Power, LLC

7.5.5 NRELAP5 predicted the HP-05 test data for the primary loop flow rate, core inlet temperature, and core outlet temperature with reasonable-to-excellent agreement (see Figure 7-88 to Figure 7-90). These results demonstrate the applicability of NRELAP5 to predict the natural circulation flow in the NIST-1 facility over a range of power levels.

{{

}}2(a),(c)

Figure 8-15 shows that the scaled NPM feedwater flow compares well with the test data. The oscillations in the NPM feedwater flow are damped over the course of each power step and the flow approaches the experimental flow rate near the end of each step. Figure 8-16 shows comparison of scaled NPM natural circulation flow to the test data. The excellent agreement between the scaled NPM predicted mass flow rate and the NIST-1 test data demonstrates that NRELAP5 is applicable for predicting the magnitude of the NPM natural circulation flow over a range of power levels.

© Copyright 2016 by NuScale Power, LLC

{{

}}2(a),(c),ECI

Figure 8-15. Comparison of HP-05 feedwater flow to test data

© Copyright 2016 by NuScale Power, LLC

{{

}}2(a),(c),ECI

Figure 8-16. Comparison of HP-05 reactor pressure vessel flow to test data

The predicted core exit subcooling is compared to test data in Figure 8-17. {{

}}2(a),(c),

Bands at ±5 degrees F (±2.8 degrees C) of the target subcooling are shown on the figure. While there is considerable variation in the subcooling, the NPM prediction is comparable to the test data in this regard. The oscillations in subcooling are to some extent driven by the oscillations in feedwater flow shown in Figure 8-15. This is further evidenced by the oscillations in core inlet temperature shown in Figure 8-18. It is apparent that the oscillations are initiated when the feedwater flow is ramped from one level to the next and that they are damped out when the feedwater flow demand is held constant. This trend is shown in both the predictions and in the test data. The predicted temperatures are in excellent agreement with the test data, thus demonstrating that NRELAP5 is applicable for predicting temperature response in NPM during changes in natural circulation flow.

© Copyright 2016 by NuScale Power, LLC

{{

}}2(a),(c),ECI

Figure 8-17. Comparison of HP-05 core exit subcooling to test data

{{

}}2(a),(c)ECI

Figure 8-18. Comparison of HP-05 core inlet temperature to test data

© Copyright 2016 by NuScale Power, LLC

8.3.4.2 NuScale Facility Loss-of-Coolant Accident and Spurious Reactor Vent Valve Opening Integral Effects Tests (HP-06, HP-07, and HP-09)

This section summarizes the comparisons of the scaled NPM NRELAP5 predictions to the NIST-1 LOCA and spurious RVV opening IETs. Two NPM NRELAP5 predictions are presented to show the calculated phenomena prior {{

}}2(a),(c) The predictions for the NuScale facility NRELAP5 model are shown for comparison.

The primary (or RCS) and CNV pressure comparisons to the test data are shown in Figure 8-19 and Figure 8-20, respectively, for the HP-06 IET. The primary and CNV liquid level comparisons to the test data are shown in Figure 8-21 and Figure 8-22, respectively, for the HP-06 IET. Similar results were obtained for the comparison against the HP-07 and HP-09 IETs.

The figures show that the NRELAP5 predictions for the NPM are very close to the experimental data {{

}}2(a),(c)

{{

}}2(a),(c)

© Copyright 2016 by NuScale Power, LLC

{{

}}2(a),(c)

In summary, the evaluations show that the differences and distortions between the NIST-1 facility and the NPM design can be accounted for using NRELAP5. The comparison of the NPM NRELAP5 predictions against the NIST-1 IET data for the LOCAs and a spurious RVV opening shows reasonable-to-excellent agreement once the 10 CFR 50 Appendix K assumptions are removed, initial and boundary conditions as well as operating procedures are consistent, and the scaling distortions are accommodated. The remaining differences

© Copyright 2016 by NuScale Power, LLC

between the NRELAP5 NPM calculation and the experimental data are likely justified by the minor distortion due to the thermal inertia in the CNV shell heat structure which was not specifically examined.

{{

}}2(a),(c)ECI

Figure 8-19. Comparison of HP-06 primary pressure to test data

© Copyright 2016 by NuScale Power, LLC

{{

}}2(a),(c)ECI

Figure 8-20. Comparison of HP-06 containment vessel pressure to test data

© Copyright 2016 by NuScale Power, LLC

{{

}}2(a),(c)ECI

Figure 8-21. Comparison to HP-06 primary liquid level to test data

© Copyright 2016 by NuScale Power, LLC

{{

}}2(a),(c)ECI

Figure 8-22. Comparison of HP-06 containment vessel liquid level to test data

8.4 Summary of Adequacy Findings

8.4.1 Findings from Bottom-Up Evaluation

The bottom-up evaluation focused on determining the pedigree, applicability, fidelity to SET data, and scalability of the NRELAP5 closure relations and correlations that model the high-ranked phenomena as determined by the PIRT panel.

The pedigree of the identified closure relations and correlations was first established based on their historical development and subsequent assessment in the literature. Assessment cases were then identified to demonstrate the capability of NRELAP5 to predict the experimental data responses with reasonable-to-excellent agreement. Applicability of NRELAP5 to model the subject phenomena is established by demonstrating that the assessment cases cover the range of parameters that approximates the NPM range. The scalability evaluation was limited to whether the specific model or correlation is applicable for the NPM configuration over the range of conditions encountered in LOCA events.

Results of the bottom up evaluation are summarized in Table 8-13.

© Copyright 2016 by NuScale Power, LLC

Table 8-13. Summary of bottom-up evaluation of NRELAP5 models and correlations

{{

}}2(a),(c)

© Copyright 2016 by NuScale Power, LLC

{{

}}2(a),(c)

© Copyright 2016 by NuScale Power, LLC

{{

}}2(a),(c)

© Copyright 2016 by NuScale Power, LLC

{{

}}2(a),(c)

© Copyright 2016 by NuScale Power, LLC

{{

}}2(a),(c)

© Copyright 2016 by NuScale Power, LLC

{{

}}2(a),(c)

© Copyright 2016 by NuScale Power, LLC

8.4.2 Findings from Top-Down Evaluation

Results of the adequacy evaluation based on the NIST-1 IETs are summarized in Table 8-14 below. All high-ranked phenomena are included in the table. Where the NIST-1 IETs do not provide information, or provide limited information, regarding NRELAP5 applicability to model the phenomenon an explanation is provided. Areas not covered, or partly covered, by the IETs are addressed by SETs or other means, e.g., sensitivity studies, bounding assumptions, component test data.

© Copyright 2016 by NuScale Power, LLC

Table 8-14. Applicability summary for high-ranked phenomena

{{

}}2(a),(c)

© Copyright 2016 by NuScale Power, LLC

{{

}}2(a),(c)

© Copyright 2016 by NuScale Power, LLC

{{

}}2(a),(c)

© Copyright 2016 by NuScale Power, LLC

{{

}}2(a),(c)

8.4.3 Summary of Biases and Uncertainties

The NRELAP5 based LOCA EM was evaluated for applicability to analyzing LOCA events in the NPM. The applicability evaluation confirmed that the models and correlations in the NuScale LOCA EM are acceptable for simulating the important, i.e., high ranked, phenomena that determine the NPM response. Results of the LOCA EM applicability evaluation based on the bottom-up approach are summarized in Table 8-13. The overall evaluation of NRELAP5 applicability based on the top down approach is summarized in Table 8-14. The summaries in these tables show that the code is applicable for predicting LOCA response for the high-ranked phenomena that govern LOCA response in the NPM. A key element of the applicability confirmation is provided by SET and IET assessments that demonstrate reasonable-to-excellent agreement between NRELAP5 predictions and relevant experimental data.

© Copyright 2016 by NuScale Power, LLC

9.0 Loss-of-Coolant Accident Calculations

The primary purpose of the break spectrum calculations and sensitivity studies presented in this section is to support the development of the LOCA EM and to demonstrate its application for the evaluation of the NPM ECCS performance during postulated LOCAs. The specific objectives of this section are to:

- describe the progression of typical LOCA scenarios in the NPM with regard to the key phenomena and processes during different phases of the LOCA identified by the PIRT (Section 4.0),
- present the results of the LOCA break spectrum calculations and other sensitivity calculations required by 10 CFR 50 Appendix K, and
- present the results of additional sensitivity calculations that address the uncertainties in modeling of key phenomena affecting the LOCA progression.

The initial/boundary conditions and inputs for key LOCA EM parameters used for this analysis are summarized in Appendix A.

9.1 Loss-of-Coolant Accident Progression in the NuScale Power Module

The LOCA progression for both a liquid and steam space break is presented in this section. A detailed discussion is provided for a 100 percent break of the RCS injection line and the high point vent line. As described in Section 4.2, the NPM LOCA has two distinct phases

1. A LOCA blowdown phase (Phase 1a) begins with a postulated break in the RCS pressure boundary initiating a blowdown into the CNV and ends with opening the ECCS valves.
2. Phase 1b begins with the opening of ECCS valves resulting in pressure equalization between the RPV and CNV and the return of discharged fluid from the CNV to the RPV.

The long-term cooling phase begins when the pressure and level between the RPV and CNV stabilizes, and a stable natural recirculation flow pattern is established {{ }}$^{2(a),(c)}$

The LOCA calculations are extended to {{ }}$^{2(a),(c)}$ after the stable natural circulation flow is established. The LOCA scenarios described in the following sections assume full-break area, no loss of AC or DC power, no single failure, and do not credit either DHRS train. These conditions were chosen to represent a typical application of the conservative 10 CFR 50 Appendix K LOCA EM.

9.1.1 Liquid Space Break

The RCS injection line connects the CVCS system to the RPV riser section, and crosses the CNV (approximately {{ }}$^{2(a),(c)}$ above TAF). A 100 percent break on the RCS injection line inside the CNV at time zero causes immediate choking at the break location as shown in Table 9-1. The mass and energy release into the CNV through the break

© Copyright 2016 by NuScale Power, LLC

results in rapid pressurization of the CNV and depressurization of the RPV. The MPS generates the reactor trip signal based on {{ }}$^{2(a),(c)}$. This signal is followed by CNV isolation with {{ }}$^{2(a),(c)}$ The reactor trip signal includes a {{ }}$^{2(a),(c)}$ delay to account for {{ }}$^{2(a),(c)}$in the NPM core. The control rods drop to insert large negative reactivity and the drop is completed at approximately {{ }}$^{2(a),(c)}$ seconds. The containment isolation signal isolates {{ }}$^{2(a),(c)}$ If the DHRS was credited it would be activated at this time.

Phase 1a of the NPM LOCA includes the mass and energy release from the break location into the CNV and is terminated by the opening of the ECCS valves. For the 100 percent injection line break scenario, the ECCS valves are actuated on {{

}}$^{2(a),(c)}$. Figure 9-1 compares the break flow with the net ECCS valve flow during the transient. The RPV and CNV pressure responses shown in Figure 9-3 are a result of the behavior of each component of the energy balance shown in Figure 9-2. As shown, the energy release to the CNV through the break and ECCS valve flow is significantly larger than the energy release to the RPV by core heat transfer. Heat transfer from the CNV wall to the reactor pool causes a continuous depressurization of both RPV and CNV after the initial pressurization of the CNV. As shown in Figure 9-3, the peak containment pressure occurs at the time of the ECCS valve opening.

© Copyright 2016 by NuScale Power, LLC

Table 9-1. Event table for 100 percent reactor coolant system injection line break

{{

}}2(a),(c)

© Copyright 2016 by NuScale Power, LLC

{{

}}2(a),(c)

Figure 9-1. Break and emergency core cooling system valve flows to the containment vessel for injection line break

{{

}}2(a),(c)

Figure 9-2. Integrated energy for injection line break

© Copyright 2016 by NuScale Power, LLC

{{

}}2(a),(c)

Figure 9-3. Reactor pressure vessel and containment vessel pressure for injection line break

As the RCS loses inventory, first through the injection line break and later through the ECCS valves, the collapsed level continuously drops, as shown in Figure 9-4. After approximately {{ }}2(a),(c) seconds, the pressurizer is completely emptied (pressurizer level plotted on right side Y-axis of Figure 9-4) and the ECCS valves open when the collapsed liquid level is approximately {{ }}2(a),(c) above TAF. The collapsed liquid level drops another {{ }}2(a),(c) after the ECCS activation. Due to {{ }}2(a),(c), a portion of the RPV liquid inventory is temporarily {{ }}2(a),(c) at approximately {{ }}2(a),(c) seconds. As this inventory returns to the riser the RPV collapsed level increases. After the RPV and CNV pressure equilibrates, the pressurizer completely drains and an equilibrium fluid level is achieved at approximately {{ }}2(a),(c) above the TAF.

© Copyright 2016 by NuScale Power, LLC

{{

}}2(a),(c)

Figure 9-4. Comparison of collapsed liquid levels in reactor pressure vessel, containment vessel, and pressurizer

{{

}}2(a),(c)

The minimum core MCHFR occurs at steady state. {{

}}2(a),(c)

Because the core remains covered and CHF is not observed, the peak cladding and fuel centerline temperatures remain cool (see Figure 9-7). The maximum cladding temperature {{ }}2(a),(c) and maximum fuel centerline temperature {{ }}2(a),(c) occur at {{ }}2(a),(c). Therefore, the 10 CFR 50.46 requirement of maximum allowed cladding temperature of 2200 degrees F is not challenged.

© Copyright 2016 by NuScale Power, LLC

Phase 1b of the LOCA begins with the opening of the ECCS valves which produces the {{ }}2(a),(c) Stable natural circulation flow is established during this phase when the steam flowing into the CNV is condensed inside the CNV and condensate flow enters the RPV through the RRVs. The depressurization of both RPV and CNV continues as the heat transfer from the CNV wall to reactor pool is larger than the core decay power as shown in Figure 9-2.

{{

}}2(a),(c)

Figure 9-5. Core flow for injection line break

© Copyright 2016 by NuScale Power, LLC

{{

}}2(a),(c)

Figure 9-6. Core minimum critical heat flux ratio during injection line break

{{

}}2(a),(c)

Figure 9-7. Peak cladding and fuel centerline temperature during injection line break

© Copyright 2016 by NuScale Power, LLC

9.1.2 Steam Space Break

The largest steam space break occurs on the RCS high point vent line. The sequence of events is described in Table 9-2. Similar to the RCS injection line break discussed in the previous section, the 100 percent break on the high point vent line causes the immediate generation of the reactor trip signal based on the {{ }}2(a),(c) followed by a {{ }}2(a),(c) and a {{ }}2(a),(c) The control rods are fully inserted within {{ }}2(a),(c) seconds of break initiation. Containment and secondary isolation occurs {{ }}2(a),(c) after the {{ }}2(a),(c) If DHRS were credited, it would be activated at this time.

{{

}}2(a),(c)

© Copyright 2016 by NuScale Power, LLC

Table 9-2. Event table for {{ }}2(a),(c)

{{

}}2(a),(c)

On break initiation, the flow immediately chokes and remains choked for {{ }}2(a),(c) seconds. The discharge of high-enthalpy steam from the RPV causes rapid depressurization of the RPV and pressurization of the CNV as shown in Figure 9-8. This immediately causes a reactor trip as shown in Table 9-2. {{

}}2(a),(c)

The collapsed level above the TAF decreases after the LOCA initiation as shown in Figure 9-10. Similar to the injection line break, {{

}}2(a),(c) The sensitivity results are discussed in Section 9.6.3.

© Copyright 2016 by NuScale Power, LLC

As the RCS inventory is lost through the break, collapsed level continues to decrease. As condensate accumulates inside the CNV, {{

}}2(a),(c), which is similar to that of the injection line break discussed in Section 9.1.1.

The core MCHFR is not a concern as demonstrated in Figure 9-11. The minimum MCHFR in the transient is at steady state and the MCHFR margin increases with time due to power and flow mismatch. {{

}}2(a),(c)

{{

}}2(a),(c)

Figure 9-8. Comparison of pressure for injection line and high point vent line breaks

© Copyright 2016 by NuScale Power, LLC

{{

}}2(a),(c)

Figure 9-9. Break and emergency core cooling system valve flow during high point vent line break

{{

}}2(a),(c)

Figure 9-10. Collapsed liquid levels during high point vent line break

© Copyright 2016 by NuScale Power, LLC

{{

}}2(a),(c)

Figure 9-11. Minimum critical heat flux ratio during high point vent line break

9.2 Break Size

In Section 9.1, the LOCA progression is described for two unique break locations (RCS injection line and high point vent line). The purpose of this section is to discuss the effect of break area on the LOCA FOMs. The spectrum of break areas for different break locations is summarized in Table 5-7. The justification of the selected matrix is discussed in Section 5.4.2. The maximum break area for the pressurizer spray supply line break is determined by the {{ }}2(a),(c) on the connecting piping. The minimum area for the liquid and steam space breaks is determined by examining a wide range of break areas such that limiting values for the NPM LOCA FOMs are obtained within the analyzed range. {{

}}2(a),(c)

The timing of events is directly affected by the break area through the choking flow rate at the break location. The break flow rate is proportional to the area for similar upstream conditions. The smaller break size results in slower depressurization and lower mass/energy loss. Therefore, transient times for smaller breaks are longer than the larger break sizes. For instance, events for the 10 percent break size take {{ }}2(a),(c) times as long as during the maximum break size. The area ratios between break area and maximum break area described in Table 5-7 are used to scale the time in order to present the results of different break areas on the same time scale.

© Copyright 2016 by NuScale Power, LLC

The CNV pressure (maximum of all CNV control volumes) as a function of scaled time with different break areas are presented for the RCS injection line, RCS discharge line, and high point vent line breaks in Figure 9-12, Figure 9-13, and Figure 9-14, respectively. Figure 9-15 shows peak CNV pressure as a function of break size for different break locations.

For the liquid space breaks (injection and discharge line breaks), the occurrence of peak CNV pressure coincides with the ECCS activation and the peak CNV pressures are very similar for break sizes down to {{ }}2(a),(c) of the full-size break (Figure 9-12, Figure 9-13, Figure 9-15). Furthermore, with discharge line break, the scaled time of the peak CNV pressure is very similar for break sizes down to {{ }}2(a),(c) percent of the full-size (Figure 9-13). The smaller liquid space break sizes are shown to produce smaller peak pressure values (Figure 9-15). As shown in Figure 9-12 and Figure 9-13, the magnitude of CNV pressure rise at the time of ECCS activation are very similar for all the liquid space break sizes. The peak CNV pressure values differ for smaller break sizes due to lower CNV pressurization rates as result of lower break energy release.

In contrast to the liquid space break, the high point vent line break with different break areas produces different peak CNV pressures (Figure 9-14 and Figure 9-15). {{

}}2(a),(c)

{{

}}2(a),(c)

Figure 9-12. Peak containment vessel pressure and collapsed level above top of active fuel for different reactor coolant system injection line break sizes

© Copyright 2016 by NuScale Power, LLC

{{

}}2(a),(c)

Figure 9-13. Peak containment vessel pressure and collapsed level above top of active fuel for different reactor coolant system discharge line break sizes

{{

}}2(a),(c)

Figure 9-14. Peak containment vessel pressure and collapsed level above top of active fuel for different high point vent line break sizes

Figure 9-12 to Figure 9-14 also show the collapsed liquid level above TAF in the RPV riser section as a function of scaled time for different break sizes and three break locations; RCS injection line, RCS discharge line, and high point vent line breaks. Figure 9-15 shows the minimum collapsed liquid level above TAF in the RPV riser section for different break locations as function of break size.

© Copyright 2016 by NuScale Power, LLC

The final equilibrium levels established at the end of the transient are independent of break size and locations. The equilibrium collapsed liquid level is directly related to the geometry of the RPV and CNV as well as the value of the equilibrium pressure between two vessels. For the high point vent line break cases, the minimum level is always the equilibrium level {{

}}2(a),(c)

The core MCHFR as a function break size is plotted in Figure 9-16 for both RCS injection and high point vent line breaks. As discussed earlier in Section 9.1 for the full-size liquid and steam space breaks, the CHFR margin rapidly increases following the event initiation and {{

}}2(a),(c) However, the potential for fuel heat-up is not of concern as no CHFR limit violation is observed in any of the break spectrum cases.

{{

}}2(a),(c)

Figure 9-15. Peak containment vessel pressure and minimum collapsed liquid level as a function of break location and size

© Copyright 2016 by NuScale Power, LLC

{{

}}2(a),(c)

Figure 9-16. Minimum critical heat flux ratio for injection line (left) and high point vent line (right) breaks

9.3 Decay Heat Removal System Availability

In the previous sections, no credit is taken for the DHRS operation. The DHRS adds an additional heat sink capacity during the NPM LOCA that impacts primarily the smaller break sizes as shown in Figure 9-17 and Figure 9-18 for RCS injection line breaks. {{

}}2(a),(c) However, when the DHRS operation is taken into account, all break sizes behave similarly and minimum collapsed liquid levels are the same as the final equilibrium level for most all of the break sizes. Similar to the impact on the minimum collapsed levels, the MCHFR is defined by the hot assembly steady state value. As discussed previously, the NuScale LOCA EM does not take credit for the DHRS operation to introduce additional and significant conservatism in satisfying the LOCA FOMs. Consideration is given to the DHRS operation here only to confirm that more adverse conditions are not created when crediting the DHRS.

© Copyright 2016 by NuScale Power, LLC

{{

}}2(a),(c)

Figure 9-17. Reactor coolant system injection line pressure without decay heat removal system (left) and with decay heat removal system (right)

{{

}}2(a),(c)

Figure 9-18. Collapsed liquid level for reactor coolant system injection line break without decay heat removal system (left) and with decay heat removal system (right)

© Copyright 2016 by NuScale Power, LLC

9.4 Power Availability

The discussion presented previously assumes that both AC and DC power are available during the NPM LOCA. Loss of power is considered by assuming either loss of only AC power or loss of both AC and DC power. Figure 9-19 demonstrates that the loss of both AC and DC power has significant impact on the steam space breaks down to {{ }}2(a),(c) percent break size, but has minimal impact on liquid space breaks. The loss of all power causes an immediate reactor trip and de-energizes the ECCS valves. {{

}}2(a),(c)

{{

}}2(a),(c)

Figure 9-19. Effect of power availability on peak containment vessel pressure for injection line (left) and high point vent (right) line breaks

9.5 Single Failure

In all of the previous discussion, no single failure is assumed. As discussed in Section 5.4.3, the following single failures are considered in this section:

- failure of a single RVV to open,
- failure of a single RRV to open, and
- failure of one ECCS division (i.e., one RVV and one RRV)

Figure 9-20 demonstrates that the single failures listed above have negligible impact on the peak containment pressure. In fact, the opening failure of a single RVV produces

© Copyright 2016 by NuScale Power, LLC

slightly smaller peak pressures inside the containment. The peak containment pressure of approximately {{ }}2(a),(c) psia is not affected by the single failure assumptions for the liquid space break. Therefore, the simulations with no single failure produce similar or conservative peak containment pressures for different break sizes. Similar conclusions can also be reached for the minimum collapsed levels in the RCS as demonstrated in Figure 9-21 where failure of a single RRV produces slightly better minimum collapsed levels above the TAF. In conclusion, a single failure based on fail to open of an RVV and RRV does not produce non-conservative results on peak CNV pressure and minimum collapsed level. Similar to the previous discussion, no CHF violation is calculated with the single failures considered as part of the NPM LOCA break spectrum.

{{

}}2(a),(c)

Figure 9-20. The effect of single failure on peak containment vessel pressure for reactor coolant system injection line (left) and high point vent (right) line breaks

© Copyright 2016 by NuScale Power, LLC

{{

}}2(a),(c)

Figure 9-21. The effect of single failure on minimum collapsed level for reactor coolant system injection line (left) and high point vent line (right) breaks

9.6 Sensitivity Studies

Several sensitivity studies are performed to establish the basis for the NuScale LOCA EM. The sensitivity calculations are performed to address the effects of the modeling parameters such as nodalization, time-step size selection, CCFL behavior at the pressurizer baffle plate, ECCS valve parameters (such as IAB release pressure, differential threshold, size/capacity, as well as valve stroke time. An additional sensitivity study is performed on core power distribution addressing the effects of core axial power shape and radial peaking assigned to the hot assembly. The sensitivity calculations are also performed to determine the impact of initial and boundary conditions for axial power shapes and initial reactor cooling pool temperature. Justifications for other initial and boundary conditions selected for the conservative LOCA analysis are provided in Section 5.3.

9.6.1 Model Nodalization

Performing a nodalization sensitivity study is important to determine its impact on the key LOCA FOMs such as peak containment pressure and collapsed liquid level above TAF in the RPV riser. As described in Section 5.1, the NRELAP5 model uses one-dimensional components. In order to address the impact of nodalization on the NPM LOCA behavior, three nodalization schemes that conform to general NRELAP5 modeling guidelines are selected as shown in Table 9-3.

© Copyright 2016 by NuScale Power, LLC

Table 9-3. Number of volumes in reactor pressure vessel and containment vessel nodalization

{{

}}2(a),(c)

The full range of break sizes for both RCS injection line and high point vent line breaks with three nodalization schemes are investigated. Both break locations are considered without DHRS operation, loss of power, and no single failure.

Figure 9-22 shows the RPV and CNV pressures and collapsed liquid level above TAF in RPV riser for the RCS injection break with 100 percent break area without DHRS, no loss of power, and no single failure. With three different nodalization schemes, two key LOCA FOMs are shown to be similar including timing of event during the transient, {{

}}2(a),(c)

The results shown in Figure 9-24 for the 100 percent high point vent line break cases show the similarities. {{

}}2(a),(c) three different nodalization schemes provide similar LOCA response in RPV and CNV pressures and collapsed levels for the high point vent line break scenario.

© Copyright 2016 by NuScale Power, LLC

{{

}}2(a),(c)

Figure 9-22. Reactor pressure vessel and containment vessel pressure (left) and collapsed level above top of active fuel (right) for reactor coolant system injection line break

{{

}}2(a),(c)

Figure 9-23. Reactor pressure vessel and containment vessel pressure (left) and collapsed level above top of active fuel (right) for 10 percent reactor coolant system injection line break

© Copyright 2016 by NuScale Power, LLC

{{

}}2(a),(c)

Figure 9-24. Reactor pressure vessel and containment vessel pressure (left) and collapsed level above top of active fuel (right) for high point vent line break

The hot assembly mass flux and core-wide MCHFR during RCS injection line break are shown in Figure 9-25 for the three nodalization schemes. The MCHFR occurs at the beginning of the transient and is not affected by the number of hydrodynamic volumes in the NPM core, {{ }}2(a),(c) Furthermore, the identical MCHFRs are calculated for the {{ }}2(a),(c) correlation. When the hot channel assembly flow goes {{ }}2(a),(c) correlation that includes the {{ }}2(a),(c) is used. {{ }}2(a),(c) Therefore, the core nodalization has no material impact on predicting the CHF margin during a postulated NPM LOCA.

© Copyright 2016 by NuScale Power, LLC

{{

}}2(a),(c)

Figure 9-25. Hot channel core flow (left) and core critical heat flux ratio (right) during 100 percent reactor coolant system injection line break

9.6.2 Time-Step Size Selection

The NRELAP5 NuScale LOCA EM uses a semi-implicit numerical scheme with implicit coupling of the hydrodynamic and heat conduction solutions. The time-step size is restricted by the courant time-step size and the accumulation of the mass-error during the time integration. In general, the NPM LOCA simulations have a courant time-step size at approximately {{ }}2(a),(c) In order to address the effect of time-step size selection on the key NPM LOCA FOMs, various fractions of the problem courant time-step size are examined as shown in Figure 9-26 through Figure 9-29 for full size injection line and high point vent line breaks. For multipliers above approximately {{ }}2(a),(c) the max time-step size allowed for the calculations is mainly determined by the mass-error management. The figures show that the containment and RPV pressures, minimum collapsed level above the TAF in the RPV riser, hot channel mass flux, and hot channel MCHFR are all independent of the time-step sizes selected for the simulation.

© Copyright 2016 by NuScale Power, LLC

{{

}}2(a),(c)

Figure 9-26. Time-step size sensitivity on reactor and containment vessel pressures and reactor pressure vessel collapsed liquid level for 100 percent reactor coolant system injection line break.

{{

}}2(a),(c)

Figure 9-27. Time-step size sensitivity on hot assembly flow and minimum critical heat flux ratio for 100 percent reactor coolant system injection line break

© Copyright 2016 by NuScale Power, LLC

{{

}}2(a),(c)

Figure 9-28. Time-step size sensitivity on reactor and containment vessel pressures and reactor pressure vessel collapsed liquid level for high point vent line break

{{

}}2(a),(c)

Figure 9-29. Time-step size sensitivity on hot assembly flow and minimum critical heat flux ratio for high point vent break

9.6.3 Counter Current Flow Limitation Behavior on Pressurizer Baffle Plate

{{
}}2(a),(c) A few of the break spectrum cases activated the CCFL flag at the pressurizer baffle plate, which did not allow liquid to readily drain from the pressurizer to the downcomer in the presence of upward steam flow. These break cases were limited to the larger pressurizer spray and vent line breaks. A study was performed {{ }}2(a),(c)

© Copyright 2016 by NuScale Power, LLC

{{

}}2(a),(c)

{{

}}2(a),(c)

Figure 9-30. Effect of counter current flow limitation line slope on levels for high point vent line break

9.6.4 Emergency Core Cooling System Valve Parameters

Operation of the ECCS valves varies based on the valve characteristics. The NPM ECCS valve specification provides minimum and maximum valve sizes and a range of differential pressures at which the IAB arming valve closes (locks) and opens (releases). A study was performed with liquid and steam breaks to evaluate separate and combined effects of the range of these valve characteristics on the LOCA FOMs.

Figure 9-31 shows the effect of IAB release pressure on peak CNV pressure and minimum collapsed liquid level as function of break size. Since the large break size results in relatively rapid RCS depressurization, {{

}}2(a),(c)

© Copyright 2016 by NuScale Power, LLC

{{

}}2(a),(c)

Figure 9-32 and Figure 9-33 show the effect of RRV and RVV sizes on peak CNV pressure and minimum collapsed liquid level as function of break size. Overall the impact ECCS valve size on peak CNV pressure and collapsed liquid level is {{ }}2(a),(c). Figure 9-32 shows only {{ }}2(a),(c) in minimum collapsed liquid level with {{ }}2(a),(c).

Conclusions of this study show that the {{

}}2(a),(c)

{{

}}2(a),(c)

Figure 9-31. Effect of inadvertent actuation block release pressure on peak containment vessel pressure and minimum collapsed liquid level above top of active fuel as a function of break size for reactor coolant system injection line break

© Copyright 2016 by NuScale Power, LLC

{{

}}2(a),(c)

Figure 9-32. Effect of reactor recirculation valve size on peak containment vessel pressure and minimum collapsed liquid level for reactor coolant system injection line break

{{

}}2(a),(c)

Figure 9-33. Effect of reactor vent valve size on peak containment vessel pressure and minimum collapsed liquid level for reactor coolant system injection line break

9.6.5 Initial Reactor Pool Temperature

The maximum initial reactor cooling pool temperature of {{ }}2(a),(c) is used in the LOCA break spectrum calculations as discussed in the previous sections. Sensitivity studies covering the range of initial pool temperatures are performed to investigate the

© Copyright 2016 by NuScale Power, LLC

impact on the NuScale LOCA EM FOMs. Reactor pool temperatures ranging from {{ }}2(a),(c) to {{ }}2(a),(c) are considered. The RCS injection line break with sizes down to {{ }}2(a),(c) of the full-break size break area are analyzed. The peak CNV pressure and the minimum collapsed liquid level above TAF as a function of break size are plotted for the pool temperatures of {{ }}2(a),(c) in Figure 9-34. The effect of the initial pool temperature on the peak CNV pressure is more pronounced at {{ }}2(a),(c). Figure 9-35 compares the various components of the RPV and CNV energy balance for 100 percent (left figure) and 10 percent (right figure) injection line breaks. {{

}}2(a),(c) For all the initial pool temperatures investigated in the sensitivity calculation, no CHF violation is observed; therefore, the minimum MCHFR is defined by the steady state value.

{{

}}2(a),(c)

Figure 9-34. Effect of initial reactor pool temperature on peak containment vessel pressure and minimum collapsed liquid level above top of active fuel for reactor coolant system injection line break

© Copyright 2016 by NuScale Power, LLC

{{

}}2(a),(c)

Figure 9-35. Containment vessel to pool energy transfer at different initial pool temperatures for 100 percent (left) and 10 percent (right) reactor coolant system injection line break

9.6.6 Core Power Distribution

The sensitivity study is performed based on full-range of break sizes for the RCS injection line break for the core power distribution considering:

- Generic axial power shapes to bound the axial peakings
- {{ }}2(a),(c) core channel

Generic axial power shapes as shown in Figure 9-36 are used to investigate the effect on the key LOCA behavior and FOMs. The axial power shapes are chosen to represents a typical {{ }}2(a),(c). The {{ }}2(a),(c) shown in Figure 9-36 is used for all the LOCA calculations performed in this report. The axial peaking is determined to bound the values observed in the NPM core design (Appendix A).

{{

}}2(a),(c)

© Copyright 2016 by NuScale Power, LLC

{{

}}2(a),(c)

Figure 9-36. Generic normalized axial power shapes

The RCS injection line break with full break area spectrum is analyzed without DHRS operation, power loss, and single failure. Figure 9-37 compares the RPV and CNV pressures and collapsed liquid level above TAF for different axial power shapes for RCS injection line break. Figure 9-38 shows the impact of axial power shapes on peak CNV pressure and minimum collapsed liquid level as function of different injection line break sizes. {{

}}2(a),(c)

Figure 9-39 shows the impact of axial power shapes on hot channel mass flux and core MCHFR {{

}}2(a),(c) However, in all of the cases analyzed, the minimum core MCHFR corresponds to the values determined before the initiation of the event.

© Copyright 2016 by NuScale Power, LLC

{{

}}2(a),(c)

Figure 9-37. Effect of axial power shape on reactor pressure vessel and containment pressures and collapsed liquid level above top of active fuel for reactor coolant system injection line break

{{

}}2(a),(c)

Figure 9-38. Effect of axial power shape on peak containment vessel pressure and minimum collapsed liquid level above top of active fuel for reactor coolant system injection line break

© Copyright 2016 by NuScale Power, LLC

{{

}}2(a),(c)

Figure 9-39. Effect of axial power shape on hot assembly flow and minimum critical heat flux ratio during reactor coolant system injection line break

9.7 Loss-of-Coolant Accident Calculation Summary

The following conclusions are reached based on the beak spectrum calculations and sensitivity studies:

1. The core MCHFR rapidly increases following the initiation of a LOCA due to power/flow mismatch – power decreases faster than flow due to differences in process time constants.
2. {{ }}2(a),(c) In conclusion, there is no fuel CHF and hence no fuel heat-up for a NPM LOCA.
3. The most sensitive LOCA analysis parameters were determined to be DHRS unavailability (conservatively assumed), {{ }}2(a),(c)
4. {{ }}2(a),(c)
5. For all the break cases and sizes, the {{ }}2(a),(c) collapsed RPV level above TAF converges to approximately {{ }}2(a),(c) This value is independent of the LOCA progression. This value is directly related to the {{ }}2(a),(c)

© Copyright 2016 by NuScale Power, LLC

{{ }}2(a),(c) and the initial mass/energy inventory.

6. Minimum RPV collapsed level during NPM LOCA transient is invariant of the break size down to {{ }}2(a),(c)
7. {{ }}2(a),(c)
8. {{ }}2(a),(c)
9. {{ }}2(a),(c)

© Copyright 2016 by NuScale Power, LLC

10.0 Conclusions

The NPM is unique when compared to any current operating power plant. It is based on an integral PWR design without coolant loops, coolant pumps, or pressurizer surge lines. The primary reactor system is driven by natural circulation with few connecting pipes and a simple safety-related system to mitigate the consequences of postulated accidents. In particular, the NPM design is not significantly challenged by LOCA events as primary system coolant is captured completely by the CNV, cooled, and returned to the RPV using a large reactor pool as the ultimate heat sink, which can provide cooling for many weeks.

The LOCA EM uses a conservative bounding approach to analyzing LOCA transients. It adheres to the relevant requirements of 10 CFR 50 Appendix K and follows the EMDAP described in RG 1.203. Multiple layers of conservatism are incorporated in the LOCA EM to ensure that a conservative analysis result is obtained. These conservatisms stem from application of the relevant modeling requirements of 10 CFR 50 Appendix K and through a series of conservative modeling features that have been incorporated.

The methodology uses the proprietary NRELAP5 computer code. RELAP5-3D© was procured and commercial grade dedication was performed as part of the procurement process by NuScale to establish the baseline NRELAP5 code for development. Subsequently, features were added and changes made to NRELAP5 to address the unique aspects of the NPM design and licensing methodology. The models and correlations used in the NRELAP5 code have been reviewed and, where appropriate, modified for use within the NuScale LOCA EM. Features added and changes made to address unique aspects of the NPM design and NuScale LOCA EM that applies to 10 CFR 50 Appendix K include the following:

- helical coil SG heat transfer and pressure drop models
- core CHF models
- wall condensation models
- critical flow models
- interfacial drag models for large diameter pipes

The NRELAP5 code includes all of the necessary models for characterization of the NPM hydrodynamics, heat transfer between structures and fluids, modeling of fuel, reactor kinetics models, and control systems. The geometry of certain NPM components dictates the use of specific correlations, {{ }}$^{2(a),(c)}$ The CHF correlations chosen to assess fuel conditions were selected based on full-scale fuel bundle performance tests over the range of conditions (flows, temperatures, and pressures) anticipated in the NPM during a LOCA event.

A number of conservatisms are built into the NuScale LOCA EM to ensure that conservative analysis results are obtained. Not only are applicable 10 CFR 50 Appendix K conservatisms present, but additional conservatisms above and beyond 10 CFR 50 Appendix K have been incorporated.

© Copyright 2016 by NuScale Power, LLC

Conservatisms that are in addition to the 10 CFR 50 Appendix K requirements include:

- Not crediting actuation of DHRS in the break spectrum assessment to conservatively reduce the heat removed from the RPV
- {{

}}2(a),(c)

A PIRT was developed that identified all of the important phenomena that could occur during a LOCA event. Phenomena and process ranking was performed in relation to specified FOMs, as described by RG 1.203. The PIRT also established a knowledge ranking for each of the phenomena identified. Using these FOMs, 21 phenomena were identified as important to correctly capture in the LOCA EM.

Extensive NRELAP5 code validation has been performed to ensure that the LOCA EM is applicable for all important phenomena and processes over the range of conditions encountered in the NPM LOCA. The validation suite includes many legacy SETs and IETs, as well as many SETs and IETs developed and run specifically for the NPM application. The SETs run for the NPM application were performed at the SIET facility on a model helical coil SG and at the Stern facility to obtain CHF data on a full-scale rod bundle test section. Integral effects tests were performed at the NIST-1 facility, a scaled representation of the complete NPM primary and secondary systems, as well as the CPV.

The EMDAP requires an applicability demonstration of the NRELAP5 code and tests. A unique aspect of the EMDAP applicability demonstration is the comparison of NRELAP5 simulations of LOCA events to NIST-1 test data and NRELAP5 simulation of the same LOCA event in the NPM. {{

}}2(a),(c) The reasonable-to-excellent agreement obtained by these comparisons establishes both the fidelity of the NIST-1 design to the NPM, and the applicability of NRELAP5 to accurately predict LOCA phenomena at both the NIST-1 and NPM scales. Limitations and modeling requirements were determined in this assessment process and are accounted for in the application of the LOCA methodology.

© Copyright 2016 by NuScale Power, LLC

This topical report provides an example application of the LOCA EM in order to aid the reader's understanding of the context of the application of the NuScale LOCA EM. These calculations are presented for break spectra that cover a range of break locations, break sizes, single failures, equipment unavailability, and initial and boundary conditions. The nodalization and time-step sensitivity required by 10 CFR 50 Appendix K and additional sensitivity calculations that address the uncertainties in modeling of key phenomena are performed. The analyses conducted demonstrate that the NPM retains sufficient water inventory in the primary system such that the core does not uncover or experience a CHF condition during a LOCA and that containment design pressure is not challenged. The PCT is shown to occur at the beginning of the LOCA event and cladding temperature decreases as the transient evolves. Because no fuel heatup occurs for any design-basis LOCAs, the following regulatory acceptance criteria from 10 CFR 50.46 are met:

- PCT remains below 2,200 degrees Fahrenheit (1,204 degrees Celsius).
- Maximum fuel oxidation is less than 0.17 times total cladding thickness.
- Maximum hydrogen generation is less than 0.01 times that generated if all cladding were to react.
- Coolable geometry is retained.

© Copyright 2016 by NuScale Power, LLC

11.0 References

1. U.S. Nuclear Regulatory Commission, “Transient and Accident Analysis Methods,” Regulatory Guide 1.203, Rev. 0, December 2005.
2. *U.S. Code of Federal Regulations*, “Domestic Licensing of Production and Utilization Facilities”, Part 50, Title 10, Appendix K, “ECCS Evaluation Models,” (10 CFR 50 Appendix K).
3. *U.S. Code of Federal Regulations*, “Domestic Licensing of Production and Utilization Facilities”, Part 50, Title 10, Section 50.46,”Acceptance Criteria for Emergency Core Cooling System for Light-Water Nuclear Power Reactors," (10 CFR 50.46).
4. NuScale Topical Report, “NuScale Topical Report: Quality Assurance Program Description for the NuScale Power Plant,” NP-TR-1010-859-NP-A, Rev. 3.
5. U.S. Nuclear Regulatory Commission, “Clarification of TMI Action Plan Requirements,” NUREG-0737, November 1980.
6. U.S. Nuclear Regulatory Commission, "Design-Specific Review Standard for NuScale SMR Design," Chapter 15, Section 15.6.5, Rev.0, June 2016.
7. U.S. Nuclear Regulatory Commission, “Design-Specific Review Standard for NuScale SMR Design, Section 4.4, Thermal and Hydraulic Design,” Rev. 0, June 2016.
8. RELAP5-3D© Code Manual Volume V: “User’s Guidelines,” INEEL-EXT-98-00834 Revision 4.1.
9. SwUM-0304-17023, Revision 4, NRELAP5 Version 1.3 Theory Manual.
10. *U.S. Code of Federal Regulations*, “Domestic Licensing of Production and Utilization Facilities,” Part 50, Title 10, Appendix B, “Quality Assurance Criteria for Nuclear Power Plants and Fuel Reprocessing Plants”, (10 CFR 50 Appendix B).
11. NuScale Technical Report, “Long Term Cooling Methodology”, TR-0916-51299, Rev. 0.
12. American Society of Mechanical Engineers, *Quality Assurance Program Requirements for Nuclear Facility Applications*, ASME NQA-1-2008, NQA-1a-2009 Addenda
13. Reserved.
14. Taitel, Y., and A.E. Dukler, “A Model of Predicting Flow Regime Transitions in Horizontal and Near Horizontal Gas-Liquid Flow,” *AIChE Journal*,(1976): 22:47-55.
15. Taitel, Y., D. Bornea, and A.E. Dukler, “Modeling Flow Pattern Transitions for Steady Upward Gas-Liquid Flow in Vertical Tubes,” *AIChE Journal*, (1980): 26:345-354.
16. Ishii, M., and G. De Jarlais, “Inverted Annular Flow Modeling,” Advanced Code Review Group Meeting, Idaho Falls, ID, July 27, 1982.
17. U.S. Nuclear Regulatory Commission, “Local Drag Laws in Dispersed Two-Phase Flow,” NUREG/CR-1230, December 1979.
18. U.S. Nuclear Regulatory Commission, “Study of Two-Fluid Model and Interfacial Area,” NUREG/CR-1873, December 1980.
19. Tandon, T.N., H.K. Varma, and C.P. Gupta, “A New Flow Regime Map for Condensation Inside Horizontal Tubes,” *Journal of Heat Transfer*, (1982)”: 104:763-768.
20. Lockhart, R.W., and R.C. Martinelli, “Proposed Correlation of Data for Isothermal Two-Phase, Two-Component Flow in Pipes,” *Chemical Engineering Progress*, (1949): 45:39-48.

© Copyright 2016 by NuScale Power, LLC

21. Small Break LOCA Methodology for US-APWR, MUAP-07013-NP, October 2010.
22. Zigrang, D.J., and N.D. Sylvester, “A Review of Explicit Friction Factor Equations,” *Transactions of the ASME, Journal of Energy Resources Technology*, (1985): 107:280-283.
23. Colebrook, C.F., “Turbulent Flow in Pipes with Particular Reference to the Transition Region Between Smooth and Rough Pipe Laws,” *Journal of Institute of Civil Engineers*, (1939): 11:133-156.
24. Chen, J.C., "A Correlation for Boiling Heat Transfer to Saturated Fluids in Convective Flow," *Process Design and Development*, (1966), 5:322-327.
25. Shah, M.M., "A General Correlation for Heat Transfer during Film Condensation Inside Pipes," *International Journal of Heat and Mass Transfer*, (1979): 22:547-556.
26. Crank, J., and P. Nicolson, “A Practical Method for Numerical Evaluation of Solutions of Partial Differential Equations of the Heat Conduction Type,” *Proceedings of the Cambridge Philosophical Society*, (1947): 43:50-67.
27. Glasstone, S., and A. Sesonske, *Nuclear Reactor Engineering*, Von Nostrand Reinhold, New York, NY, 1981.
28. Moody, F.J., “Maximum Flow Rate of a Single Component, Two-Phase Mixture,” *Transactions of the ASME, Journal of Heat Transfer*, vol. 87, No. 1, 1965, pp. 134-142.
29. {{

}}2(a),(c)

30. Crane Co. “Flow of Fluids Through Valves, Fittings and Pipe”, Crane Technical Paper No. 410, 1988.
31. Bankoff, S.G., R.S. Tankin, M.C. Yuen, and C.L. Hsieh, "Countercurrent Flow of Air Water and Steam/Water Through a Horizontal Perforated Plate", *International Journal of Heat and Mass Transfer*, (1981): Vol. 24, No. 8 pp 1381-1395.
32. Ito, H., "Friction factors for turbulent flow in curved pipes,” *Transactions of the ASME, Journal of Basic Engineering*, (1959): 81:123-124.
33. Sreenivasan K.R., and P.J. Strykowski, "Stabilization Effects in Flow Through Helically Coiled Pipes," Experiments in Fluids 1, 1983, pp. 31-36.
34. Seban, R.A., and E.F. McLaughlin, "Heat transfer in tube coils with laminar and turbulent flow," *International Journal of Heat and Mass Transfer*, (1963): 6:387-395.
35. Prasad, B.V.S.S.S, D.H. Das, and A.K. Prabhakar, “Pressure drop, heat transfer and performance of a helically coiled tubular exchanger,” *Heat Recovery Systems and CHP*, (1989), 9: 249-256.
36. Dittus, F.W., and L.M.K. Boelter, “Heat transfer in automobile radiators of the tubular type,” *International Communications in Heat and Mass Transfer*, (1985), Vol 12, Issue 1, pp. 3-22. Originally published in University of California Publications in Engineering, Vol. 2, No. 13, October 13, 1930, pp. 443-46.
37. Colburn, A.P., and O.A. Hougen, "Design of Cooler Condensers for Mixtures of Vapors with Noncondensing Gases," *Industrial and Engineering Chemistry*, (1934): 26:1178-1182.
38. Green, D.W. and Perry, R.H., Perry's Chemical Engineers' Handbook, 8th Edition, McGraw-Hill, New York, NY, 2008.

© Copyright 2016 by NuScale Power, LLC

39. {{
}}2(a),(c)

40. Kataoka, I., Ishii, M., "Drift Flux Model for Large Diameter Pipe and New Correlation for Pool Void Fraction", *International Journal of Heat and Mass Transfer*, (1987): Vol. 30, No. 9, pp. 1927-1939.

41. Churchill, S.W., and H.H.S. Chu, "Correlating Equations for Laminar and Turbulent Free Convection From a Vertical Plate," *International Journal of Heat and Mass Transfer*, (1975): 18:1323-1329.

42. Rouhani, S.Z., "Modified Correlations for Void and Pressure Drop," AB Atomenergi, Sweden, Internal Report AE-RTC 841, March 1969.

43. Reserved.

44. Draft American Nuclear Society, “Decay Energy Release Rate Following Shutdown of Uranium-Fueled Thermal Reactors,” Proposed Standard ANS 5.1, LaGrange Park, IL, October 1973.

45. Ishii, M., "One-Dimensional Drift-Flux Model and Constitutive Equations for Relative Motion between Phases in Various Two-Phase Flow Regimes", Report No. ANL-77-47, Argonne National Laboratory, October 1977.

46. American Nuclear Society, “Decay Energy Release Rate Following Shutdown of Uranium-Fueled Thermal Reactors,” Proposed Standard ANS 5.1, LaGrange Park, IL, October 1971 (revised October 1973).

47. Shure, K., “Fission-Product Decay Energy,” WAPD-BT-24, Westinghouse Atomic Division, Bettis, December 1961.

48. American National Standards Institute/American Nuclear Society, “Decay Heat Power in Light Water Reactors,” ANSI/ANS-5.1-1979, LaGrange Park, IL.

49. American National Standards Institute/American Nuclear Society, “Decay Heat Power in Light Water Reactors,” ANSI/ANS-5.1-1994, LaGrange Park, IL.

50. American National Standards Institute/American Nuclear Society, “Decay Heat Power in Light Water Reactors,” ANSI/ANS-5.1-2005, LaGrange Park, IL.

51. Healzer, J.M., J.E. Hench, E. Janssen, and S. Levy, “Design Basis for Critical Heat Flux Condition in Boiling Water Reactors,” APED-5186, GE Company Private Report, July 1966.

52. General Electric, “General Electric BWR Thermal Analysis Basis (GETAB): Data, Correlation and Design Application,” NEDO-10958-A, 1977.

53. Biasi, L., et.al., “Studies on Burnout Part 3- A New Correlation for Round Ducts and Uniform Heating and Its Comparison with World Data,” Energy Nucl., (1967), 14:530-7.

54. Electric Power Research Institute, “Parametric Study of CHF Data,” Vol. 2, Palo Alto, California. 1983.

55. {{
}}2(a),(c)

56. Zuber, N., “Hydrodynamic Aspects of Boiling Heat Transfer,” Ph.D. thesis, University of California at Los Angeles, 1959.

57. Groeneveld, D.C., et al., “Lookup Tables for Predicting CHF and Film-Boiling Heat Transfer: Past, Present and Future,” *Nuclear Technology*, (2005): 152:87-104.

© Copyright 2016 by NuScale Power, LLC

58. Ferrell, J.K., and J. W. McGee, “Two-Phase Flow Through Abrupt Expansions and Contractions, Final Report, “Study of Convection Boiling Inside Channels”, TID-23394 (Vol. 3), June 1966.
59. U.S. Nuclear Regulatory Commission, "BWR Refill-Reflood Program Task 4.8-Model Qualification Task Plan," NUREG/CR-1899, August 1981.
60. Kim, S.J., “Turbulent film condensation of high pressure steam in a vertical tube of Passive Secondary Condensation System," PhD thesis, Korea Advanced Institute of Science and Technology, 2000.
61. Nylund O., et.al, “Hydrodynamic and heat transfer measurements on a full-scale simulated 36-rod BHWR fuel element with non-uniform axial and radial heat flux distribution”, 1970.
62. U.S. Nuclear Regulatory Commission, “Analysis of the FLECHT SEAST Unblocked Bundle Steam Cooling and Boiloff Tests,” NUREG/CR-1533, January 1981.
63. U.S. Nuclear Regulatory Commission, “PWR FLECHT SEASET Unblocked Bundle, Forced and Gravity Reflood Task Data Report,” NUREG/CR-1532, Volume 2, Appendix C, September 1981.
64. U.S. Nuclear Regulatory Commission, “Results of the Semiscale MOD-2A Natural Circulation Experiments,” NUREG/CR-2335, September 1982.
65. Reserved.
66. Electric Power Research Institute, “Final Report, Two-Phase Jet Modeling and Data Comparison,” EPRI NP-4362, March 1986.
67. U.S. Nuclear Regulatory Commission, "Countercurrent Flow of Air/Water and Steam/Water Flow above a Perforated Plate," NUREG/CR-1808, November 1980.
68. U.S. Nuclear Regulatory Commission, "Countercurrent Steam/Water Flow Above a Perforated Plate-Vertical Injection of Water," NUREG/CR-2323, September 1981.
69. Bankoff, S.G., R.S. Tankin, M.C. Yuen, and C.L. Hsieh, "Countercurrent Flow of Air Water and Steam/Water Through a Horizontal Perforated Plate", *International Journal of Heat and Mass Transfer*, (1981): Vol. 24, No. 8 pp 1381-1395.
70. U.S. Nuclear Regulatory Commission, “The Marviken Full Scale Critical Flow Tests, Summary Report, Joint Reactor Safety Experiments in the Marviken Power Station Sweden,” NUREG/CR-2671, May 1982.
71. The Marviken Full Scale Critical Flow Tests, Results from Test 22, Joint Reactor Safety Experiments in the Marviken Power Station Sweden, MXC-222, September 1979.
72. Modro, S.M., et. al., “Multi-Application Small Light Water Reactor Final Report,” INEEL/EXT-04-01626, Idaho National Engineering and Environmental Laboratory, December 2003.
73. Idelchik, I.E., “Handbook of Hydraulic Resistance,” Hemisphere Publishing, New York, NY, 3rd Edition.
74. Fletcher, C.D., et al., “Adequacy Evaluation of RELAP5/MOD3, Version 3.2.1.2 for Simulating AP600 Small-Break Loss-of-Coolant Accidents,” INEL-96/0400, April 1997.
75. NuScale Power, LLC, “Topical Report: Subchannel Analysis Methodology,” TR-0915-17564-P, Rev. 0, October 2016.
76. The RELAP5-3D Code Development Team, "RELAP5-3D Code Manual, Volume III: Developmental Assessment", INEEL-EXT-98-00834, Revision 4.1, October 2013.

© Copyright 2016 by NuScale Power, LLC

77. Jeandey, C., et al., "Auto Vaporisation D'Ecoulements Eau/Vapeur, Departement des Reacteurs a Eau Service des Transferts Thermiques (Centre D'Etudes Nucleaires de Grenoble)," Report T.T. No. 163, July 1981.
78. U.S. Nuclear Regulatroy Commission, "Assessment of Two-Phase Critical Flow Models Performance in RELAP5 and TRACE against Marviken Critical Flow Tests," NUREG/IA-0401, February 2012.
79. Elias, E., and G. S. Lellouche, "Two-Phase Critical Flow," *International Journal of Multiphase Flow*, (1994): Vol. 20, No. 91-168.
80. US Nuclear Regulatory Commission, “TRACE V5.0 Theory Manual – Volume 1: Field Equations, Solution Methods, and Physical Models,” June 2008, Agencywide Document Access and Management System (ADAMS) Accession No. ML120060218.
81. RELAP5 MOD3.3 Code Manual, Volume IV: Models and Correlations, October 2010.
82. Reserved.
83. Lee, K.W., H.C. No, and C.H. Song, "Onset of Water Accumulation in the Upper Plenum with a Perforated Plate," *Nuclear Engineering and Design*, (2007): 237:1088-1095.
84. Wallis, G.B., *One-dimensional Two-Phase Flow*, McGraw-Hill, New York, NY, 1969.
85. Ilic, V., S. Banerjee, and S. Behling, ”Qualified Database for the Critical Flow of Water, Final Report”, EPRI-NP-4556, May 1986.
86. Zuber, N., and J. A. Findlay, “Average Volumetric Concentrations in Two-Phase Flow Systems”, *Transactions of the ASME, Journal of Heat Transfer*, (1965): 87:453-568.
87. The RELAP5-3D Code Development Team, "RELAP5-3D Code Manual, Volume III: Developmental Assessment", INEEL-EXT-98-00834, Revision 4.1, October 2013.
88. McAdams, W.H., *Heat Transmission*, 3rd Edition, McGraw-Hill, New York, NY, 1954.
89. Minkowycz, W.J., and E. M., Sparrow, “Local Nonsimilar Solutions for Natural Convection on a Vertical Cylinder,” *Journal of Heat Transfer*, (1974): 96(2), 178-183.
90. Plesset, M.S., and S. A. Zwick, "The Growth of Vapor Bubbles in Superheated Liquids", *Journal of Applied Physics*, (1954): 25, 493.
91. Lee, K., and D. J. Ryley, "The Evaporation of Water Droplets in Superheated Steam", *Transactions of the ASME, Journal of Heat Transfer*, (1968): pp. 445-451.
92. Aumiller, D.L., “The Effect of Nodalization on the Accuracy of the Finite-Difference Solution of the Transient Conduction Equation”, *2000 RELAP5 International Users Seminar*, Jackson Hole, Wyoming, September 12-14, 2000.
93. Electric Power Research Institute, "The Chexal-Lellouche Void Fraction Correlation for Generalized Applications," NSAC-139, April 1991.
94. Inayatov, A.Y., "Correlation of Data on Heat Transfer Flow Parallel to Tube Bundles at Relative Pitches of 1.1 < s/d < 1.6," *Heat Transfer-Soviet Research*, (1975): 7, 3, pp. 84-88.
95. {{

}}2(a),(c)

96. Van den Eynde, G., "Comments on “A Resolution of the Stiffness Problem of Reactor Kinetics”," *Nuclear Science and Engineering*, (2006): 153:200-202.

© Copyright 2016 by NuScale Power, LLC

97. Saha, P., and N. Zuber, "Point of Net Vapor Generation and Vapor Void Fraction in Subcooled Boiling," *Proceedings Fifth International Heat Transfer Conference*, September 3-7, 1974, Tokyo, Japan: 4:175-179.

98. Lahey, R.T., "A Mechanistic Subcooled Boiling Model," *Proceedings Sixth International Heat Transfer Conference*, August 7-11, 1978, Toronto, Canada: 1:293 - 297.

99. U.S. Nuclear Regulatory Commission, “An Integrated Structure and Scaling Methodology for Severe Accident Technical Issue Resolution,” NUREG/CR-5809, Appendix D, November 1991.

© Copyright 2016 by NuScale Power, LLC

Appendix A. Input for NuScale Power Module Loss-of-Coolant Accident Model

The purpose of this Appendix is to present inputs for initial and boundary conditions and other key parameters for the NPM LOCA input model. The core input parameters, plant initial conditions (i.e., operational conditions), safety-related system setpoints and delays, and the LOCA break spectrum parameters used for the calculations stated in this report are presented. The operational range is provided for several parameters along with the basis for selection of the upper or lower range value that conservatively bounds the LOCA response.

© Copyright 2016 by NuScale Power, LLC

A.1 Core Input Parameters

Table A-1. Core input parameters

{{

}}2(a),(c), ECI

© Copyright 2016 by NuScale Power, LLC

{{

}}2(a),(c) ECI

© Copyright 2016 by NuScale Power, LLC

A.2 Initial Plant Conditions

Table A-2. Initial conditions for loss-of-coolant accident analysis

{{

}}2(a),(c), ECI

© Copyright 2016 by NuScale Power, LLC

A.3 Safety-Related System Actuation Setpoints and Delays

Table A-3. Safety signal actuation setpoints and delays

{{

}}2(a),(c), ECI

© Copyright 2016 by NuScale Power, LLC

{{

}}2(a),(c), ECI

© Copyright 2016 by NuScale Power, LLC

A.4 Break Spectrum Parameters

Table A-4. Break spectrum parameters

{{

}}2(a),(c), ECI

© Copyright 2016 by NuScale Power, LLC